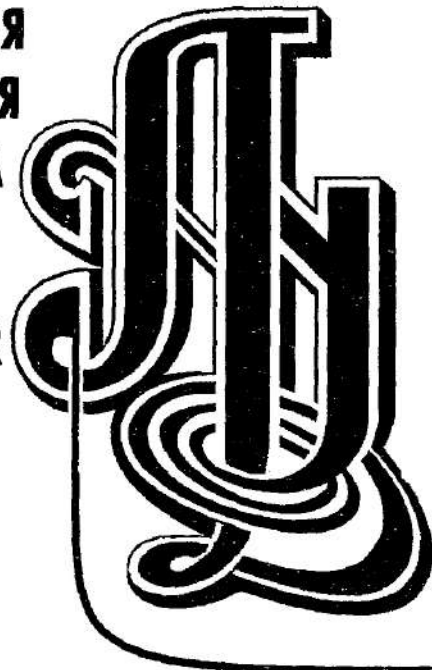
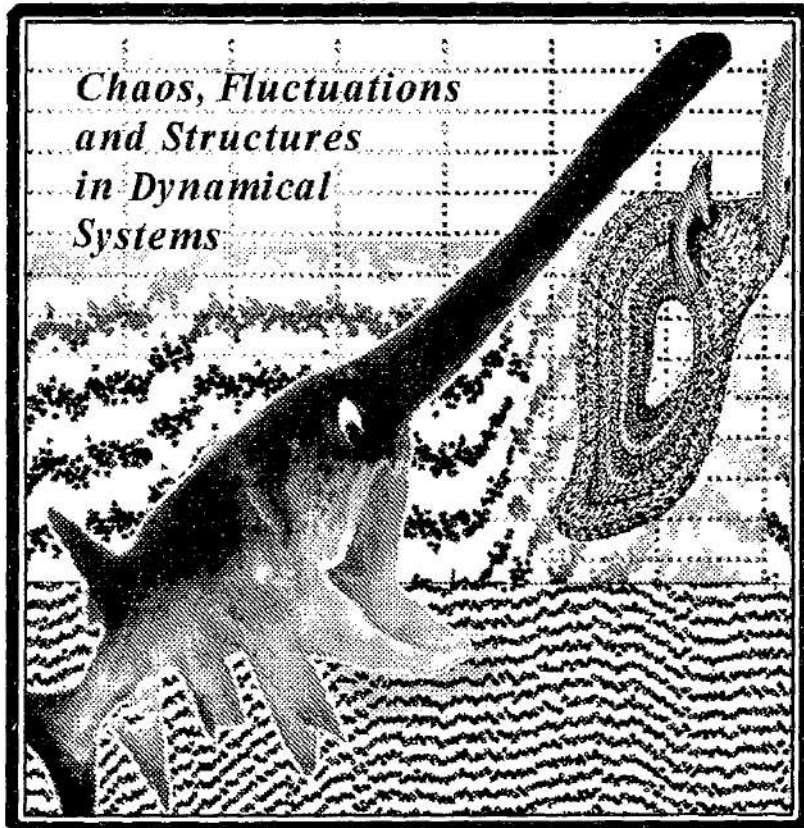


**ПРИКЛАДНАЯ
НЕЛИНЕЙНАЯ
ДИНАМИКА**

**APPLIED
NONLINEAR
DYNAMICS**



*Chaos, Fluctuations
and Structures
in Dynamical
Systems*



3
2003

In the cover design Figs 1,2 from the paper of A.Neiman et al. and Fig.4 from the paper of T.Dikanev et al. were used

МИНИСТЕРСТВО ОБРАЗОВАНИЯ РОССИЙСКОЙ ФЕДЕРАЦИИ

Известия высших учебных заведений

ПРИКЛАДНАЯ НЕЛИНЕЙНАЯ ДИНАМИКА

научно-технический журнал

издается с 1993 года

Выходит 6 раз в год

Том 11, № 3, 2003, Саратов

СОДЕРЖАНИЕ

Хаос, флуктуации и структуры в динамических системах

От редакционной группы	2
ОБЗОРЫ АКТУАЛЬНЫХ ПРОБЛЕМ НЕЛИНЕЙНОЙ ДИНАМИКИ	
<i>Анищенко В.С., Астахов В.В., Вадивасова Т.Е., Нейман А.Б., Стрелкова Г.И., Шиманский-Гайер Л.</i> Нелинейные эффекты в хаотических и стохастических системах	4
ДЕТЕРМИНИРОВАННЫЙ ХАОС	
<i>Thiel M., Romano M.C., Kurths J.</i> Аналитическое описание отображений последования для белого шума и хаотических процессов	20
<i>Шабунин А., Астахов В., Акопов А.</i> Эволюция бегущих волн к пространственно-временному хаосу: взаимодействие временной и пространственной динамики в кольце генераторов с удвоением периода	31
<i>Сильченко А.Н., Beri S., Лучинский Д.Г., McClintock P.V.E.</i> Флуктуационные переходы через локально-несвязанные и локально-связанные фрактальные границы бассейнов	38
<i>Хованов И.А., Хованова Н.А., McClintock P.V.E.</i> Оптимальный контроль флуктуаций в применении к подавлению индуцированных шумом нарушений стабилизации хаоса	46
<i>Пономаренко В.И., Прохоров М.Д., Караваев А.С., Селезнев Е.П., Диканев Т.В.</i> Восстановление динамических моделей систем с запаздыванием по временным рядам	56
<i>Белых В.Н., Белых И.В., Hasler Martin J.</i> Связанные системы типа «мир тесен»: динамические модели и синхронизация	67
ПРИКЛАДНЫЕ ЗАДАЧИ НЕЛИНЕЙНОЙ ТЕОРИИ КОЛЕБАНИЙ И ВОЛН	
<i>Braun H.A., Voigt K., Moss F.</i> Хаос в мозге и в сенсорных нейронах	77
<i>Нейман А., Russell D.F., Moss F., Schimansky-Geier L.</i> Синхронизация, шум и электрорецепторы	84
<i>Mosekilde E., Сосновцева О.В., Постнов Д.Э., Braun H.A., Huber M.T.</i> Нейронные генераторы ритма в присутствии шума	95
<i>Acebron J.A., Bulsara A.R., Rappel W.-J.</i> Динамика глобально связанных нейронных элементов ФитцХью - Нагумо в присутствии шума	110
<i>Янсон Н.Б., Игошева Н.Б., Баланов А.Г., Глушковская-Семячкина О.В., Анищенко Т.Г., McClintock P.V.E.</i> Индексы кардиореспираторной синхронизации из данных давления крови крыс	120
<i>Сосновцева О.В., Павлов А.Н., Mosekilde E., Holstein-Rathlou N.-H.</i> Эффекты синхронизации в многомодовой динамике связанных нефронов	133
<i>Шульгин Б.В., Charman S.C., Накаряков В.М.</i> Самосогласованная динамика частиц в развороте поля геомагнитного хвоста	148
<i>Дмитриев А.С., Касьян Г.А., Кузьмин Л.В.</i> Согласованная фильтрация хаотических сигналов	157
<i>Диканев Т., Смирнов Д., Пономаренко В., Безручко Б.</i> Три подзадачи реконструкции глобальной модели по временным рядам и их особенности.	165
БИФУРКАЦИИ В ДИНАМИЧЕСКИХ СИСТЕМАХ РАЗЛИЧНОЙ ПРИРОДЫ	
<i>Boccaletti S., Allaria E., Meucci R., Arcelli F.T.</i> Исследование переходов к фазовой синхронизации в экспериментальной нелинейной оптике	179
<i>Янчук С., Kapitaniak T.</i> Риддинг в присутствии малой расстройки по параметру	185
КНИЖНОЕ ОБОЗРЕНИЕ	
<i>Анищенко В.С., Астахов В.В., Вадивасова Т.Е., Нейман А.Б., Стрелкова Г.И., Шиманский-Гайер Л.</i> Нелинейные эффекты в хаотических и стохастических системах	190
КНИЖНАЯ ПОЛКА СТУДЕНТА	
<i>Пиковский А., Розенблюм М., Куртс Ю.</i> Синхронизация. Фундаментальный нелинейный эффект	195
ИЗ КНИГ И ЖУРНАЛОВ	
<i>Fluctuation and noise letters: Vadim S. Anishchenko and Igor A. Khovanov.</i> Synchronization of chaotic and stochastic oscillations and its applications	202
PERSONALIA	205

DEPARTMENT OF EDUCATION OF RUSSIAN FEDERATION

Izvestiya VUZ

APPLIED NONLINEAR DYNAMICS

scientific-technical journal

published since 1993

Published 6 times a year

Vol.11, № 3, 2003, Saratov

CONTENTS

Chaos, fluctuations and structures in dynamical systems

Editorial preface	3
REVIEWS OF ACTUAL PROBLEMS OF NONLINEAR DYNAMICS	
Statistical properties of deterministic and noisy chaotic systems. <i>V.S. Anishchenko, T.E. Vadivasova, G. I. Strelkova, G.A. Okrokvetskikh</i>	4
DETERMINISTIC CHAOS	
Analytical description of recurrence plots of white noise and chaotic processes. <i>M. Thiel, M.C. Romano, J. Kurths</i>	20
Evolution of running waves to spatio-temporal chaos: interaction of temporal and spatial dynamics in a ring of period-doubling self-oscillators. <i>A. Shabunin, V. Astakhov, A. Akopov</i>	31
Fluctuational transitions across locally-disconnected and locally-connected fractal basin boundaries. <i>A.N. Silchenko, S. Beri, D.G. Luchinsky and P.V.E. McClintock</i>	38
Optimal control of fluctuations applied to the suppression of noise-induced failures of chaos stabilization. <i>I.A. Khovanov, N.A. Khovanova and P.V.E. McClintock</i>	46
Recovery of dynamical models of time-delay systems from time series. <i>V.I. Ponomarenko, M.D. Prokhorov, A.S. Karavaev, Ye.P. Seleznev, T.V. Dikanov</i>	56
Small-world networks: dynamical models and synchronization. <i>Vladimir N. Belykh, Igor V. Belykh and Martin J. Hasler</i>	67
APPLIED PROBLEMS OF NONLINEAR OSCILLATION AND WAVE THEORY	
Chaos in the brain and in sensory neurons. <i>H.A. Braun, K. Voigt and F. Moss</i>	77
Synchronization, noise and electroreceptors. <i>A. Neiman, D.F. Russell, F. Moss and L. Schimansky-Geier</i>	84
Noisy neural rhythm generators. <i>E. Mosekilde, O.V. Sosnovtseva, D. Postnov, H.A. Braun and M.T. Huber</i>	95
Dynamics of globally coupled noisy FitzHugh-Nagumo neuron elements. <i>J.A. Acebrón, A.R. Bulsara and W.-J. Rappel</i>	110
Indices of cardiorespiratory synchronization from rat blood pressure data. <i>N.B. Janson, N.B. Igosheva, A.G. Balanov, O. Glushkovskaya-Semyachkina, T.G. Anishchenko, P.V.E. McClintock</i>	120
Synchronization phenomena in multimode dynamics of coupled nephrons. <i>O.V. Sosnovtseva, A.N. Pavlov, E. Mosekilde, N.-H. Holstein-Rathlou</i>	133
Self-consistent particle dynamics in the geotail magnetic field reversal. <i>B.V. Shulgin, S.C. Chapman, V.M. Nakariakov</i>	148
Matched filtration of chaotic signals. <i>A.S. Dmitriev, G.A. Kassian, L.V. Kuzmin</i>	157
Three subproblems of global model reconstruction from time series and their peculiarities. <i>T. Dikanov, D. Smirnov, V. Ponomarenko and B. Bezruchko</i>	165
BIFURCATION IN DYNAMICAL SYSTEMS	
Investigating the transition to phase synchronization in experimental nonlinear optics. <i>S. Boccaletti, E. Allaria, R. Meucci, and F.T. Arecchi</i>	179
Riddling in the presence of small parameter mismatch. <i>S. Yanchuk and T. Kapitaniak</i>	185
BOOK REVIEW	
Nonlinear dynamics of chaotic and stochastic system. <i>V.S. Anishchenko, V.V. Astakhov, T.E. Vadivasova, A.B. Neiman, G.I. Strelkova, L. Schimansky-Geier</i>	190
STUDENT'S BOOKSHELF	
Synchronization. A universal concept in nonlinear sciences. <i>Arkady Pikovsky, Michael Rosenblum and Jürgen Kurths</i>	195
FROM BOOKS AND JOURNALS	
Fluctuation and noise letters: <i>Vadim S. Anishchenko and Igor A. Khovanov</i> . Synchronization of chaotic and stochastic oscillations and its applications.	202
PERSONALIA	205

От редакционной группы

Настоящий специальный выпуск журнала «Прикладная нелинейная динамика» посвящен замечательной дате - 60-летию известного ученого, одного из создателей саратовской школы нелинейной динамики, заслуженного деятеля науки РФ, лауреата премии им. А. Гумбольдта, академика РАН, заведующего кафедрой нелинейной динамики и радиофизики Саратовского государственного университета, доктора физико-математических наук, профессора Вадима Семеновича Анищенко. Научные достижения В.С. Анищенко и его школы получили широкую известность и признание как в России, так и далеко за ее пределами. Они внесли заметный вклад в развитие многих аспектов нелинейной теории колебаний. Ученые многих стран хорошо знают и на протяжении многих лет сотрудничают с В.С. Анищенко и созданной им лабораторией нелинейной динамики, которая в этом году преобразована в Международный институт нелинейной динамики, объединяющий и координирующий работу шести международных научных коллективов из России, Германии, Дании и Великобритании.

К юбилею ученого его коллеги из ведущих университетов России, Европы и Америки представили в журнал свои научные работы. Тематика статей весьма разнообразна. Она охватывает многие фундаментальные и прикладные задачи нелинейной динамики, такие, например, как критерии динамического хаоса, бифуркационный анализ нелинейных систем различной природы, эффекты хаотической и стохастической синхронизации, применение методов нелинейной динамики и математического моделирования в биологии и медицине. А открывает выпуск обзор работ В.С. Анищенко с соавторами, посвященный исследованию статистических характеристик хаоса и анализу влияния шума на поведение хаотических систем. Таким образом, в журнале представлены последние достижения ряда ведущих научных коллективов в области нелинейной динамики и ее приложений. Надеемся, что собранный в этом юбилейном выпуске материал будет полезен для широкого круга читателей, интересующихся современными проблемами нелинейной динамики.

От имени всех авторов, приславших свои статьи в специальный выпуск, всех коллег, друзей и учеников мы желаем Вадиму Семеновичу всего самого наилучшего в день его юбилея, долгих лет жизни, новых ярких и фундаментальных открытий.

Саратов, октябрь 2003

*В.В. Астахов
Т.Е. Вадивасова
Г.И. Стрелкова*

Редакционная коллегия журнала присоединяется к поздравлениям и искренне желает Вадиму Семеновичу здоровья и дальнейших успехов в развитии его научной школы.

Editorial Preface

This special issue of the Journal Applied Nonlinear Dynamics is dedicated to the 60th birthday of Vadim Anishchenko. Vadim Anishchenko is one of the founders of School of Nonlinear Dynamics at Saratov State University. He is scientific coordinator and principal investigator of the Laboratory of Nonlinear Dynamics at Saratov State University. Professor Anishchenko is the Honored Man of Science of the Russian Federation, the Humboldt Prize Winner, the academician of the Russian Academy of Natural Sciences. He is the Head of the Radiophysics and Nonlinear Dynamics Chair. Fundamental scientific contribution of Vadim Anishchenko and his pupils and students to development of physics of nonlinear oscillations are widely known and highly recognized both in Russia and world-wide. Many of Vadim's former students became professors in physics both in Russia and abroad.

The highest standards of research in Vadim Anishchenko's laboratory have gained him, his students and coworkers world-wide international recognition. This year the Laboratory was reorganized into the International Institute of Nonlinear Dynamics that unites and coordinates the work of six international research groups from Russia, Germany, Denmark and the United Kingdom.

On the occasion of Vadim Anishchenko's 60th birthday his colleagues from leading Universities of Russia, Europe and the US and his former PhD students submitted their scientific papers to this special issue «Chaos, Fluctuations and Structures in Dynamical Systems». The presented papers cover many fundamental and applied aspects of nonlinear dynamics, such as criteria of dynamical chaos, bifurcational analysis of nonlinear systems of different nature, effects of chaotic and stochastic synchronization, application of the nonlinear dynamics and mathematical modeling methods in biology and medicine. This issue also includes a survey of the recent papers of Vadim Anishchenko and his collaborators, that is devoted to the study of statistical characteristics of chaos and effects of noise on the behavior of chaotic systems. Many of the authors benefited from discussions with Vadim Anishchenko, his original ideas, his outstanding personality.

We hope that this collection of papers will be helpful for students, lecturers and scientists who are interested in modern problems of nonlinear science.

On behalf of all the contributors to this special issue, all colleagues and friends, we wish Vadim Anishchenko very well on his 60th birthday and we look forward to his new inspiring and fundamental research during many many years.

Saratov, October 2003

*Vladimir Astakhov
Tatjana Vadivasova
Galina Strelkova*

The Editorial Board of the Journal «Izvestiya VUZ. Applied Nonlinear Dynamics» joins the congratulations and sincerely wishes Vadim S. Anishchenko a great health and further big success in the development of his Scientific School.



Izv. VUZ «AND», vol. 11, № 3, 2003

STATISTICAL PROPERTIES OF DETERMINISTIC AND NOISY CHAOTIC SYSTEMS

*Vadim S. Anishchenko, Tatjana E. Vadivasova, Galina I. Strelkova,
George A. Okrokovskhov*

This work represents a survey of the results that were recently obtained in the research group supervised by Prof. Dr. Vadim S. Anishchenko and published in a series of scientific papers. The presented results are referred to statistical description of dynamical chaos and to the effect of noise on different types of chaotic attractors. We consider peculiarities of the relaxation of an invariant probability measure in systems with chaotic attractors of different types and perform the correlation and spectral analysis of chaotic self-sustained oscillations.

1. Introduction

Dynamical chaos, like a random process, requires a statistical description. When chaotic systems are studied in computer or physical experiments, probability characteristics, such as a stationary probability distribution on an attractor, correlation functions, power spectra and others, are usually calculated or measured. Chaotic oscillations that correspond to different types of chaotic attractors in the phase space of dynamical systems are characterized by various statistical properties as well as by a different degree of sensitivity of the statistical characteristics to the influence of noise.

From a viewpoint of the rigorous theory, hyperbolic chaos is often called «true» chaos and is characterized by a homogeneous and topologically stable structure [1-4]. However, strange chaotic attractors of dissipative systems are not, as a rule, robust hyperbolic sets. They are rather referred to as a nearly hyperbolic attractors, e.g., the Lorenz attractor. Nearly hyperbolic (quasi-hyperbolic) attractors include some nonrobust orbits, e.g. separatrix loops, but their appearances and disappearances often do not affect the observed characteristics of chaos, such as a phase portrait, the power spectrum, Lyapunov exponents and others. Dynamical systems in a chaotic regime may give rise to an invariant measure which does not depend on an initial distribution and fully reflects the statistical properties of the attractor. The existence of an invariant measure has been theoretically proven for hyperbolic and nearly hyperbolic systems [5-10].

However, the most of chaotic attractors which we deal with in numeric simulation and real experiments are nonhyperbolic [11-13]. The problem of the existence of an invariant measure on a nonhyperbolic chaotic attractor involves serious difficulties because it is generally impossible to obtain a stationary probability distribution being independent of an initial distribution. A nonhyperbolic attractor is a maximal attractor of the dynamical system and encloses a countable set of both regular and chaotic attracting

subsets [11,12]. When δ -correlated Gaussian noise is added to the system, an invariant measure on such attractors exists too [14]. In the nonhyperbolic case the behavior of phase trajectories is significantly affected by noise [15-18] while it changes only slightly in systems with hyperbolic and nearly hyperbolic chaos [15,16,19,20].

A statistical description of noisy nonhyperbolic chaotic attractors is an important and still unsolved problem of the dynamical systems theory. One of the topical problems in this direction is to study the relaxation to stationary distributions in time. There are a number of fundamental questions which have as yet unclear answers. What is a real relaxation time of the system to a stationary distribution? Which factors define this time? Which characteristics can quantify the relaxation time to the stationary measure? What is the role of the noise statistics and the noise intensity in regularities of the relaxation to the stationary distribution? Is there any connection between the relaxation process and the system dynamics? These problems are studied in [21,22] with the methods of computer simulation.

The relaxation to a stationary distribution is described by the evolutionary operator that can be represented by the Fokker-Planck operator or the Frobenius-Perron operator. The eigenvalues and eigenfunctions of the evolutionary operator determine the rate and character of the relaxation process and characteristics of mixing, which are related to the relaxation to an invariant probability measure. However, if the dynamical system is high-dimensional ($N \geq 3$), the nonstationary solution of the Fokker-Planck equation is difficult enough to find even numerically. Therefore, the method of stochastic differential equations was used in the studies described in [21,22].

The presence of mixing causes autocorrelation functions to decay to zero for large times (correlation splitting). This means that the system states separated by a sufficiently large time interval become statistically independent [6,8,23-25]. From the property of mixing it follows that a dynamical system is ergodic. Additionally, for chaotic dynamical systems the splitting of correlations in time is connected with an instability of chaotic trajectories and with the system property to produce entropy [6,8,23-27]. In spite of their significant importance, correlation properties of chaotic processes have been studied insufficiently. It is widely believed that autocorrelation functions of chaotic systems exponentially decrease at a rate being defined by the Kolmogorov entropy [23]. The Kolmogorov entropy, H_K , in turn is bounded from above by the sum of positive Lyapunov exponents [8,27,28]. But this estimation is true only for some special cases.

It has been proven for some classes of discrete maps (expanding and Anosov ones), which exhibit a mixing invariant measure, that the decay of correlations with time is bounded from above by an exponential function [9,29-31]. There are different estimations of the rate of this exponential decay which are not always connected with Lyapunov exponents [32-34]. For continuous-time systems, there are no theoretical results at all for estimating the rate of correlation splitting [35].

The studies of specific chaotic systems testify to a complicated behavior of correlation functions, which is defined not only by positive Lyapunov exponents but also by different characteristics and peculiarities of the system chaotic dynamics [32,34,36].

In the papers [37-39] the correlation and spectral properties of chaotic oscillations are studied for several types of chaotic attractors which can be observed in autonomous differential systems with three-dimensional phase space. Classical models of nonlinear dynamics such as the Rössler oscillator [40], the Lorenz system [41], and the Anishchenko-Astakhov oscillator that represents a mathematical model of a real radiotechnical device [42] were chosen for the studies. In the cited papers an attempt was taken to answer several fundamental questions. Which peculiarities of the system's chaotic dynamics can define the rate of correlation splitting and the basic spectral line width? How does noise affect the spectral and correlation characteristics of chaos? Basing on the results of numerical simulation, we would like to show that in the context

of correlation properties, different types of chaotic self-sustained oscillations can be associated with basic models of stochastic processes such as harmonic noise and a telegraph signal.

The aim of this work is to present a brief review of the recent results reported in [21,22,37-39]. The presented results concern some probabilistic aspects of chaotic dynamics such as peculiarities of the relaxation to a stationary probability distribution, the rate of mixing and the correlation and spectral analysis of chaotic regimes of different types. A special attention is paid to the effect of noise on the statistical properties of chaotic dynamics.

2. Relaxation to a stationary probability distribution of chaotic attractors in the presence of noise

2.1. Models and numerical methods. We will study chaotic attractors of well-known model systems such as the Rössler oscillator [40]

$$\begin{aligned}\dot{x} &= -y - z + (2D)^{1/2}\xi(t), \\ \dot{y} &= x + ay, \\ \dot{z} &= b - z(m-x),\end{aligned}\tag{1}$$

and the Lorenz system [41]

$$\begin{aligned}\dot{x} &= -\sigma(x-y) + (2D)^{1/2}\xi(t), \\ \dot{y} &= rx - y - xz, \\ \dot{z} &= -\beta z + xy.\end{aligned}\tag{2}$$

In both models $\xi(t)$ is a normal white noise source with the mean value $\langle \xi(t) \rangle = 0$ and correlation $\langle \xi(t)\xi(t+\tau) \rangle = \delta(\tau)$, where $\delta()$ is Dirac's function. The parameter D denotes the noise intensity. For the Rössler system we fix $a=0.2$ and $b=0.2$ and vary the control parameter m in the interval $[4.25, 13.0]$. In the Lorenz system we choose two different regimes, namely, a quasi-hyperbolic attractor ($\sigma=10$, $\beta=8/3$, and $r=28$) and a nonhyperbolic attractor ($\sigma=10$, $\beta=8/3$, and $r=210$).

We integrate Eqs (1) and (2) using a fourth-order Runge-Kutta routine with noise sources taken into account. Chaotic attractors of systems (1) and (2) have been studied in detail and are typical examples of quasi-hyperbolic and nonhyperbolic chaos [43,44]. Thus, results obtained for Eqs (1) and (2) can be generalized to a wide class of dynamical systems.

To examine the relaxation to a stationary distribution in these systems, we analyze how points situated at an initial time in a cube of small size δ around an arbitrary point of the trajectory belonging to an attractor of the system evolve with time. We take $\delta=0.09$ for the size of this cube and fill it uniformly with $n=9000$ points. As time goes on, these points in the phase space are distributed throughout the whole attractor. To characterize the convergence to the stationary distribution we follow the temporal evolution of this set of points and calculate the ensemble average

$$\bar{x}(t) = \int p(x,t)xdx \approx 1/n \sum_{i=1}^n x_i(t).\tag{3}$$

Here, x is one of the system dynamical variables, and $p(x,t)$ is the probability density of

the variable x at the time t which corresponds to the chosen initial distribution. It is known that the phase trajectory of system (2) visits neighborhoods of two saddle-foci. In this case, when calculating $\bar{x}(t)$ one may first sum separately over points having fallen in the neighborhood of each saddle-focus, and then combine the obtained results. However, the mean value appears to approach zero in a short time interval and its further evolution is badly detected. To follow the relaxation in (2) we compute the mean value when points in the neighborhood of only one saddle-focus are taken into account. In this case the relaxation to this quantity goes more slowly in time. Then we calculate the function $\gamma(t_k)$:

$$\gamma(t_k) = |\bar{x}_m(t_{k+1}) - \bar{x}_m(t_k)|, \quad (4)$$

where $\bar{x}_m(t_k)$ and $\bar{x}_m(t_{k+1})$ are successive extrema of $\bar{x}(t)$. Thus, $\gamma(t_k)$ characterizes the amplitude of the mean value oscillations. In the expression (4) t_k and t_{k+1} are successive time moments corresponding to the extrema of \bar{x} . The temporal behavior of $\gamma(t_k)$ allows to judge the character and the rate of relaxation to the probability measure on the attractor.

We also calculate the maximal Lyapunov exponent (LE) λ_1 of a chaotic trajectory on an attractor. Besides, we also compute the normalized autocorrelation function (ACF) of steady-state oscillations $x(t)$:

$$\Psi(\tau) = \psi(\tau)/\psi(0), \quad \psi(\tau) = \langle x(t)x(t+\tau) \rangle - \langle x(t) \rangle \langle x(t+\tau) \rangle. \quad (5)$$

The brackets $\langle \dots \rangle$ denote time averaging.

To make some figures more informative and compact, instead of $\gamma(t_k)$ and $\Psi(\tau)$ we plot (where it is necessary) their envelopes $\gamma_0(t_k)$ and $\Psi_0(\tau)$, respectively.

2.2. Relaxation to a stationary distribution in the Rössler system: Mechanism of the effect of noise on the rate of mixing. A chaotic attractor realizing in the Rössler system (1) at fixed $a=b=0.2$ and in the parameter m interval $[4.25, 8.5]$ serves as a well-known example of a spiral attractor. The phase trajectory on the spiral attractor rotates with a high regularity around one or several saddle-foci. The autocorrelation function is oscillating and the power spectrum exhibits narrow-band peaks corresponding to the mean rotation frequency, its harmonics and subharmonics. By virtue of these properties spiral chaos is called phase-coherent [43,45-47].

The chaotic attractor of system (1) is qualitatively changing as the parameter m increases. In the interval $8.5 < m < 13.0$ there occurs a nonhyperbolic attractor of noncoherent type, called funnel attractor [42,46]. Phase trajectories on the funnel attractor make complicated loops around a saddle-focus and thus, demonstrate a nonregular rotation behavior. Consequently, the autocorrelation function of noncoherent chaos decreases much rapidly than that in the coherent case, and the power spectrum does not already contain sharp peaks.

The calculations performed for $m \in [4.25, 7.5]$ (spiral chaos) and for $m \in [8.5, 13.0]$ (noncoherent chaos) allow to assume that an invariant probability measure exists for the parameter values considered. All the effects being observed for each type of attractor in the system (1) are qualitatively preserved when the parameter m is varied. In our numeric simulation we fix $m=6.1$ for the spiral attractor and $m=13.0$ for the funnel attractor.

Figure 1 shows the typical behavior of $\gamma_0(t)$ for both the spiral and the funnel attractor of the Rössler system. We find that the noise significantly influences the rate of mixing in the regime of spiral attractor in the Rössler system. The relaxation time is strongly decreasing for increasing noise intensity (see Fig. 1, a).

We find a quite different situation for the funnel attractor. Noncoherent chaos is

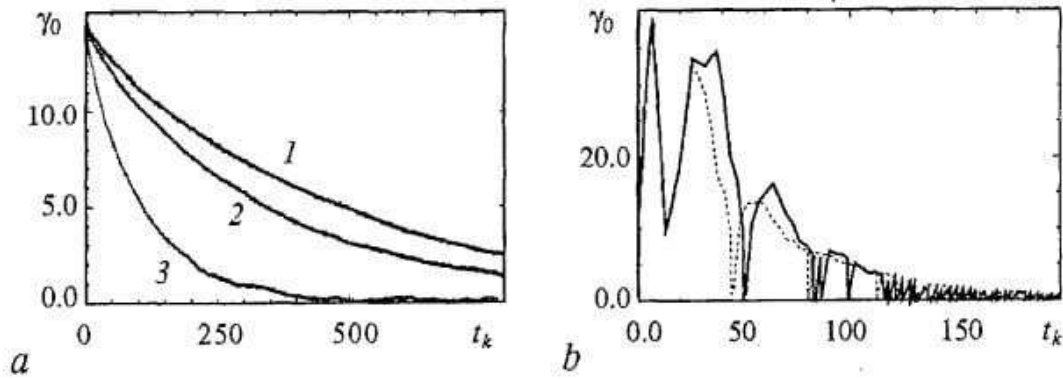


Fig. 1. $\gamma_0(t_k)$ for attractors in the Rössler system (1). (a) For the spiral attractor ($a=b=0.2, m=6.1$) at $D=0$ (curve 1), $D=0.001$ (curve 2), and $D=0.1$ (curve 3); (b) for the funnel attractor ($a=b=0.2, m=13$) at $D=0$ (solid line) and $D=0.01$ (dotted line)

practically insensitive to noise perturbations. Behavior of $\gamma_0(t_k)$ does not significantly change when noise is added to Eqs (1) (see Fig. 1, b). At the same time, it is well known that noncoherent chaos exhibits a close similarity to random processes. This fact can be verified, e.g. by means of the autocorrelation function $\Psi(\tau)$ for the spiral and the funnel

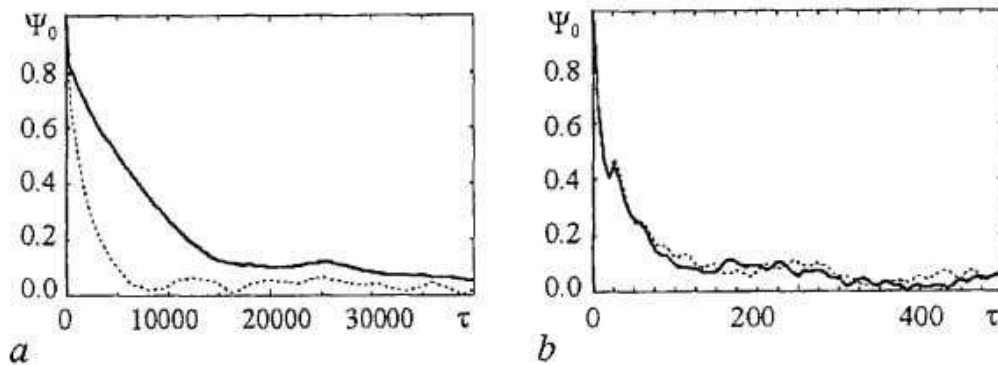


Fig. 2. Envelopes of the normalized autocorrelation function $\Psi_0(\tau)$ for attractors in (1). (a) At $m=6.1$ and for $D=0$ (solid line) and $D=0.01$ (dotted line); (b) at $m=13$ for $D=0$ (solid line) and $D=0.01$ (dotted line)

attractors in system (1) (Fig. 2). Our numerical experiments show that the correlation times are essentially different for these two chaotic regimes: without noise they differ by two orders. On the one hand, in the case of coherent chaos the correlation time decreases dramatically in the presence of noise (Fig. 2, a). On the other hand, the autocorrelation

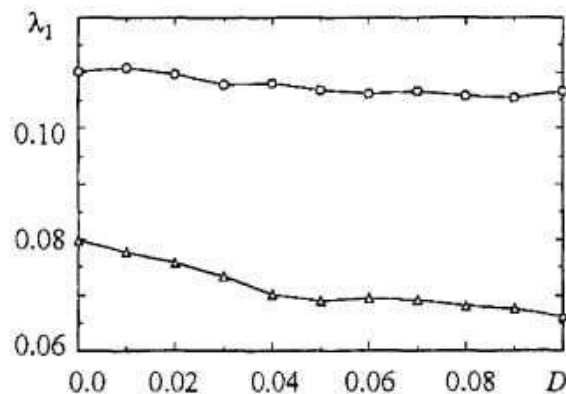


Fig. 3. For the Rössler system, λ_1 on the spiral (triangles) and the funnel (circles) attractor as functions of the noise intensity D

function for the funnel attractor in the deterministic case practically coincides with that in the presence of noise (Fig. 2, b). Hence, noncoherent chaos, which is nonhyperbolic, demonstrates some property of hyperbolic chaos, i.e. «dynamical stochasticity» turns out to be much stronger than that imposed from an external (additive) one [6]. This experimental result is interesting and requires a more detailed consideration. It is also worth noting another finding of our simulations. We have found that the positive LE for both the spiral chaos and the funnel chaos is weakly sensitive to fluctuations (see Fig. 3), and

rather grows not much with increasing noise intensity, whereas in certain cases the correlation time changes considerably under the influence of noise. Thus, in the regime of spiral chaos the rate of mixing is not uniquely determined by the largest LE but depends strongly on the noise intensity.

We suppose that the essential effect of noise on relaxation to the stationary distribution in the regime of spiral chaos may be associated with peculiarities of the phase trajectory dynamics in the neighborhood of an unstable equilibrium state. Since the trajectory rotates almost regularly on the spiral attractor, the relaxation process appears to be very long. The addition of noise to the system destroys the relative regularity of the trajectory and, consequently, the rate of mixing significantly increases.

It is known that for chaotic oscillations one can introduce the notion of instantaneous amplitude and phase [47]. The instantaneous phase characterizes the rotation of a trajectory around a saddle-focus. System (1) is of such type because the trajectory in the $(x-y)$ projection rotates around the unique saddle-focus located very near to the origin. Let us introduce the substitution of variables

$$x(t) = A(t)\cos\Phi(t), \quad y(t) = A(t)\sin\Phi(t), \quad (6)$$

that defines the amplitude $A(t)$ and the total phase $\Phi(t)$ of the chaotic oscillations. Then the instantaneous phase $\Phi(t)$ can be calculated as follows:

$$\Phi(t) = \arctan(y(t)/x(t)) + \pi n(t), \quad (7)$$

where $n(t)=0,1,2,\dots$ is the number of intersections of the phase trajectory with the plane $x=0$.

The component of mixing along the flow of trajectories is related with the divergence of the instantaneous phase values and thus, is determined by the temporal behavior of the phases. The instantaneous phase of an ensemble of initially close trajectories on the spiral attractors remain very close to each other over a long period of time, although the points in the secant plane are spread over the whole attractor section. In this case the relaxation to a stationary probability distribution on the whole attractor of a flow system will be much longer than that in the Poincaré map. The violation of regular rotation of trajectories is characteristic for the funnel attractor and leads to a nonmonotonic dependence of the instantaneous phase on time. The phase trajectory creates complicated loops at nonequal time intervals that causes the value of the current phase to slightly decrease. This results in a rapid divergence of the phase values of neighboring trajectories. The influence of noise on spiral chaos leads to similar effects. Figure 4, *a* shows the temporal dependences of the variance σ_Φ^2 of the instantaneous

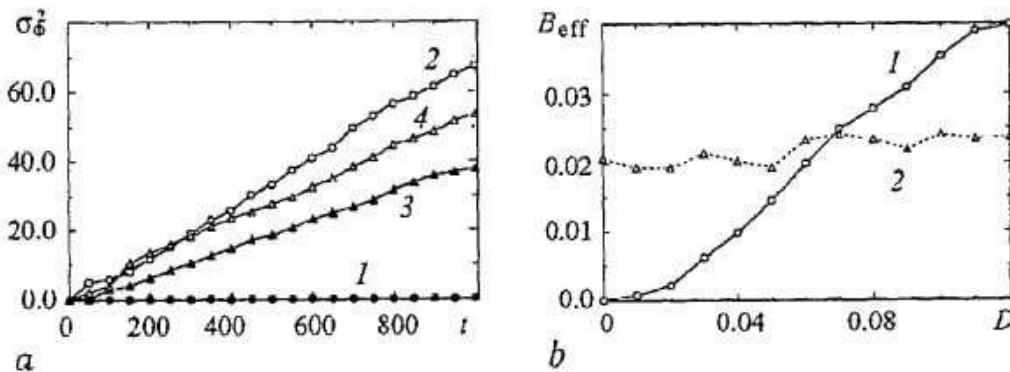


Fig. 4. Characteristics of the instantaneous phase divergence of neighboring trajectories for spiral chaos ($m=6.1$) and funnel chaos ($m=13$) in Eqs (1). (a) Temporal dependences of the variance of the instantaneous phase σ_Φ^2 for spiral chaos at $D=0$ (curve 1), $D=0.1$ (curve 2), and for noncoherent chaos at $D=0$ (curve 3), $D=0.1$ (curve 4). (b) The effective diffusion coefficient B_{eff} as a function of the noise intensity D for spiral (curve 1) and noncoherent (curve 2) chaos

phase on an ensemble of initially close trajectories for both the spiral and the funnel attractor of system (1). We observe that in both the noisy and the noise-free case the variation grows almost linearly on the time intervals being considered. The fact that the temporal dependence of the instantaneous phase variance of the chaotic oscillations in the Rössler system is a linear function was assumed in $[-\pi;\pi]$. Nevertheless, this suggestion was confirmed neither theoretically nor numerically or experimentally. In the case of spiral chaos without noise (curve 1), the value of σ_ϕ^2 is small (on the given time interval it does not exceed the variation of the uniform phase distribution on the interval $[-\pi;\pi]$) and increases much slower than in the other cases considered. The linear growth of the variation allows to estimate the divergence of the instantaneous phases by using the effective diffusion coefficient:

$$B_{\text{eff}} = 1/2 d\sigma_\phi^2(t)/dt. \quad (8)$$

Figure 4, *b* illustrates the dependences of B_{eff} of the instantaneous phase of chaotic oscillations on the noise intensity for both the spiral and the funnel attractor in the Rössler system (1). It is seen that in both cases B_{eff} grows with increasing D but for spiral chaos this growth is more significant. This result strongly testifies that B_{eff} is a very effective characteristic for diagnosing the statistical properties of a chaotic attractor in the presence of fluctuations.

2.3. Relaxation to a probability measure in the Lorenz systems. Well-known quasi-hyperbolic attractors in three-dimensional continuous-time systems, such as the Lorenz attractor, the Morioka-Shimizu attractor [48], are attractors of the switching type. The phase trajectory switches chaotically from the neighborhood of one saddle equilibrium state to the neighborhood of another one. Such switchings are accompanied by chaotic phase changes even without noise. In this case the addition of noise does not change considerably the phase dynamics and, consequently, does not influence the rate of relaxation to the stationary distribution.

Figure 5 shows the behavior of $\gamma_0(t_k)$ for both quasi-hyperbolic and nonhyperbolic chaotic attractors of the system (2) with and without noise added. We find that noise does not significantly influence the relaxation rate for the Lorenz attractor (Fig. 5, *a*). However, we observe a quite different situation for the nonhyperbolic attractor. There the rate of relaxation is strongly affected by noise (Fig. 5, *b*).

Now we are going to check whether the other characteristics of the mixing rate, such as the LE and the correlation time, will also depend on noise perturbations. For the same chaotic attractors in the Lorenz system we compute the largest LE λ_1 and estimate the normalized autocorrelation function $\Psi(\tau)$, $\tau=t_2-t_1$, of the dynamical variable $x(t)$ for different noise intensities D . We find that for both types of chaotic attractors the LE does

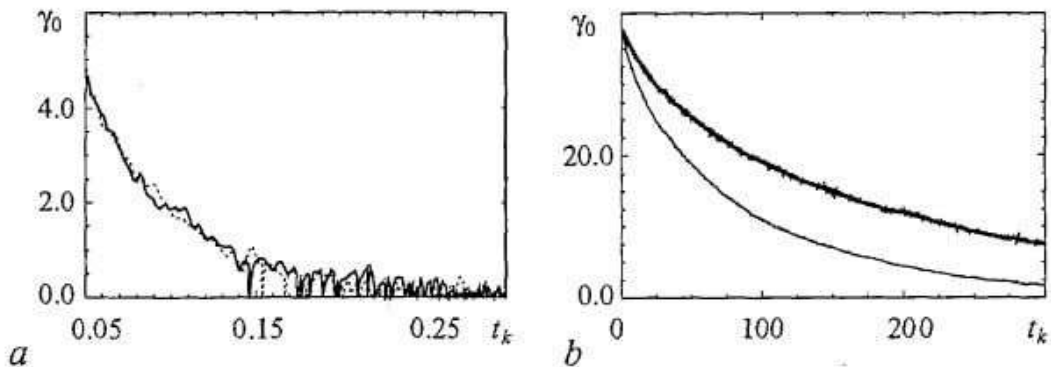


Fig. 5. $\gamma_0(t_k)$ for chaotic attractors in the Lorenz system (2). (a) For $r=28$ and $D=0$ (solid line), and $D=0.01$ (dotted line); (b) for $r=210$ and $D=0$ (thick line), and for $r=210$ and $D=0.01$ (thin line). Other parameters are $\sigma=10$, $\beta=8/3$

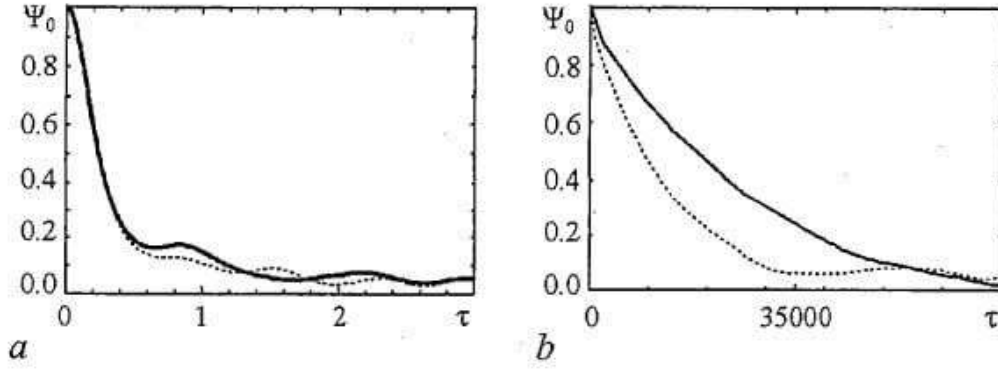


Fig. 6. Envelopes of the normalized autocorrelation function $\Psi_0(\tau)$ for attractors in system (2). (a) $r=28$ and $D=0$ (solid line), and $D=0.01$ (dotted line); (b) $r=210$, $D=0$ (solid line), and $D=0.01$ (dotted line)

not depend within the calculation accuracy on the noise intensity. The autocorrelation function of the quasi-hyperbolic attractor is practically not affected by noise (see curves 1 and 2 in Fig. 6, a). However, in the regime of a nonhyperbolic attractor it decreases more rapidly in the presence of noise (see curves in Fig. 6, b).

3. Correlation and spectral analysis of dynamical chaos

Let us now examine correlation and spectral properties of different types of chaotic oscillations in more details. Experience of the studies of dynamical chaos in three-dimensional differential systems shows that two classical models of random processes can be used to describe the correlation and spectral properties of a certain class of chaotic systems. They are the models of harmonic noise and a telegraph signal.

As we will demonstrate below, the model of harmonic noise represents sufficiently well correlation characteristics of spiral chaos, while the model of telegraph signal is quite suitable for studying statistical properties of attractors of the switching type, such as attractors in the Lorenz system [41] and in the Chua circuit [49].

In the following we summarize the main characteristics of the above mentioned classical models of random processes.

Harmonic noise is a stationary random process with zero mean. It is represented as follows [50-52]:

$$x(t) = R_0[1+\alpha(t)]\cos[\omega_0 t + \phi(t)], \quad (9)$$

where R_0 and ω_0 are constant (average) values of the amplitude and frequency of oscillations, respectively; $\alpha(t)$ and $\phi(t)$ are random functions that characterize amplitude and phase fluctuations, respectively. The process $\alpha(t)$ is assumed to be stationary.

Several simplifying assumptions which are most often used are as follows: (i) the amplitude and phase fluctuations are statistically independent, and (ii) the phase fluctuations $\phi(t)$ represent a Wiener process with a diffusion coefficient B . Under the assumptions made, the ACF of the process (9) can be written as follows [50-52]:

$$\psi(\tau) = 1/2 R_0^2 [1+K_\alpha(\tau)] \exp(-B|\tau|) \cos \omega_0 \tau, \quad (10)$$

where $K_\alpha(\tau)$ is the covariation function of reduced amplitude functions $\alpha(t)$ ¹. Using the Wiener-Khinchin theorem one can derive the corresponding expressions for the spectral power density.

¹Prefactor $R_0^2[1+K_\alpha(\tau)]$ is the covariation function $K_A(\tau)$ of the random amplitude $A(t)=R_0[1+\alpha(t)]$. This notion is most convenient to use in our further studies.

Generalized telegraph signal. This process describes random switchings between two possible states $x(t)=\pm a$. Two main kinds of telegraph signal are usually considered, namely, random and quasi-random telegraph signals [52,53]. A random telegraph signal is characterized by a Poissonian distribution of switching moments t_x . The latter leads to the fact that the impulse duration θ has the exponential distribution:

$$\rho(\theta) = n_1 \exp(-n_1 \theta), \quad \theta \geq 0, \quad (11)$$

where n_1 is the mean switching frequency. The ACF of such a process can be represented as follows:

$$\psi(\tau) = a^2 \exp(-2n_1 |\tau|). \quad (12)$$

Another type of telegraph signal (a quasi-random telegraph signal) corresponds to random switchings between the two states $x(t)=\pm a$, which can occur only in discrete time moments $t_n = n\xi_0 + \alpha$, $n=1,2,3,\dots$, where $\xi_0 = \text{const}$ and α is a random quantity. If the probability of switching events is equal to $1/2$, then the ACF of this process is given by the following expression:

$$\begin{aligned} \psi(\tau) &= a^2(1-|\tau|/\xi_0), & \text{if } |\tau| < \xi_0; \\ \psi(\tau) &= 0, & \text{if } |\tau| \geq \xi_0. \end{aligned} \quad (13)$$

3.1. Correlation and spectral analysis of spiral chaos. From a physical viewpoint, chaotic attractors of the spiral type possess the properties of a noisy limit cycle. However, spiral attractors are realized in fully deterministic systems, i.e., without external fluctuations. Consider the regime of spiral chaos in the Rössler system (1) for $a=b=0.2$ and $m=6.5$. Let us introduce the instantaneous amplitude $A(t)$ and phase $\Phi(t)$ according to the relations (6). We calculate the normalized autocorrelation function of the chaotic oscillations $x(t)$ (grey dots region 1, Fig. 7), the covariance function of the amplitude $K_A(t)$ and the effective phase diffusion coefficient B_{eff} . Figure 7 shows the results for $\Psi_x(\tau)$ in the system (1) both without noise and in the presence of noise. The ACF decays almost exponentially both without noise (Fig. 7, a) and in the presence of

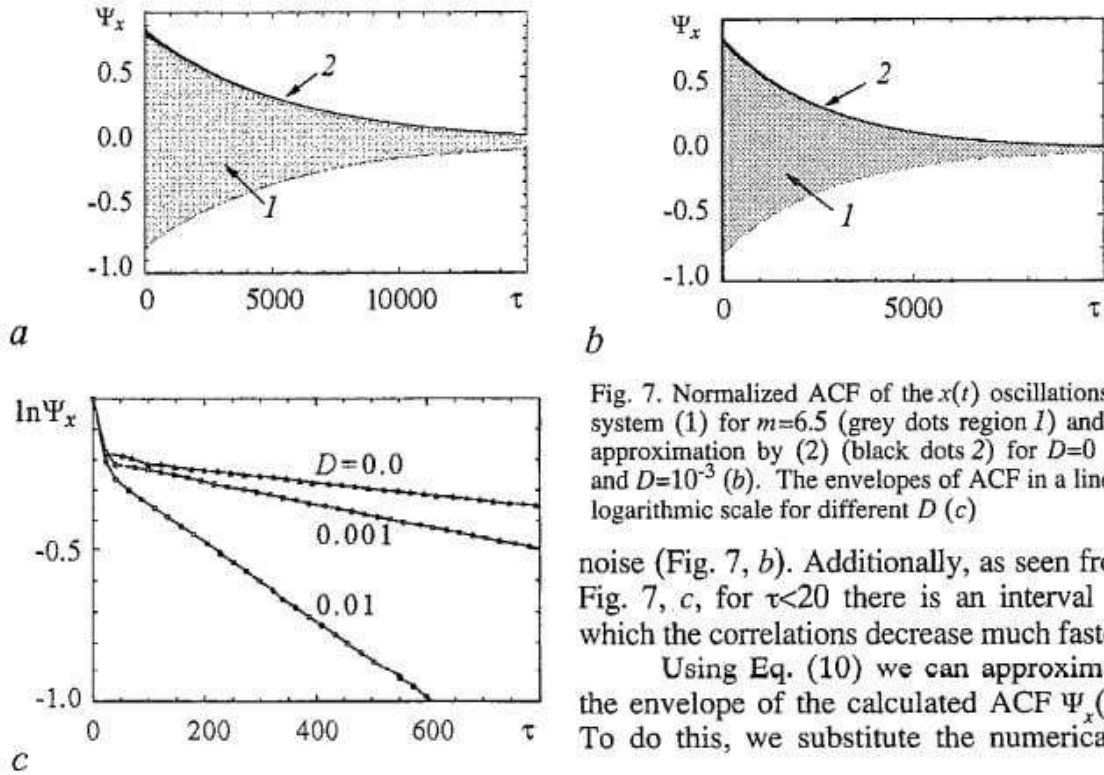


Fig. 7. Normalized ACF of the $x(t)$ oscillations in system (1) for $m=6.5$ (grey dots region 1) and its approximation by (2) (black dots 2) for $D=0$ (a) and $D=10^{-3}$ (b). The envelopes of ACF in a linear-logarithmic scale for different D (c)

noise (Fig. 7, b). Additionally, as seen from Fig. 7, c, for $\tau < 20$ there is an interval on which the correlations decrease much faster.

Using Eq. (10) we can approximate the envelope of the calculated ACF $\Psi_x(\tau)$. To do this, we substitute the numerically

computed characteristics $K_A(\tau)$ and $B=B_{\text{eff}}$ into an expression for the normalized envelope $\Gamma(\tau)$:

$$\Gamma(\tau) = K_A(\tau)/K_A(0)\exp(-B_{\text{eff}}|\tau|). \quad (14)$$

The calculation results for $\Gamma(\tau)$ are shown in Fig. 7, *a, b* by black dots (curves 2). It is seen that the behavior of the envelope of $\Psi(\tau)$ is described well by Eq. (14). Note that taking into account the multiplier $K_A(\tau)/K_A(0)$ enables us to obtain a good approximation for all times τ . This means that the amplitude fluctuations play a significant role on short time intervals, while the slow process of the correlation decay is mainly determined by the phase diffusion. Thus, we can observe a surprisingly good agreement between the numerical results for the spiral chaos and the data for the classical model of harmonic noise. At the same time, it is quite difficult to explain rigorously the reason of such a good agreement. Firstly, the relationship (10) was obtained by assuming the amplitude and phase values to be statistically independent. However, this approach cannot be applied to a chaotic regime. Secondly, when deriving (10) we used the fact that the phase fluctuations are described by a Wiener process. In the case of chaotic oscillations, $\Phi(t)$ is a more complicated process and its statistical properties are unknown. It is especially important to note that the findings presented in Fig. 7, *a* were obtained in the regime of purely deterministic chaos, i.e. without noise in the system.

We have shown that for $\tau > \tau_{\text{cor}}$ the envelope of the ACF for the chaotic oscillations can be approximated by the exponential law $\exp(-B_{\text{eff}}|\tau|)$. Then according to the Wiener-Khinchin theorem, the spectral peak at the average frequency ω_0 must have a Lorentzian shape and its width is defined by the effective phase diffusion coefficient B_{eff} :

$$S(\omega) = CB_{\text{eff}}/[B_{\text{eff}}^2 + (\omega - \omega_0)^2], \quad C = \text{const.} \quad (15)$$

The calculation results presented in Fig. 8 justify this statement. The basic spectral peak is approximated by using (15) and this fits quite well with the numerical results for the power spectrum of the $x(t)$ oscillations. We note that the findings shown in Figs 7 and 8 for the noise intensity $D=10^{-3}$ have also been verified for different values of D , $0 < D < 10^{-2}$, as well as for the range of parameter m values which correspond to the regime of spiral chaos. Our findings for the approximation of the ACF and the shape of the basic spectral peak are completely confirmed by our investigations of spiral attractors in other dynamical systems.

The spectral and correlation properties of spiral chaos were also explored in a physical experiment with the Anishchenko-Astakhov oscillator [42,43]. The performance of such kind of experiment is important as the stochastic equations of the oscillator are approximate only and cannot take into account all sources of natural fluctuations that are really operating in the electronic scheme of the oscillator. Experimental results are presented in Fig. 9 and completely confirm all the data obtained numerically.

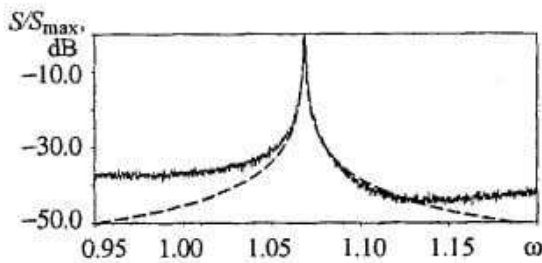


Fig. 8. A part of the normalized power spectrum of $x(t)$ oscillations in system (1) for $a=b=0.2$, and $m=6.5$ (solid line) and its approximation by Eq. (15) (dashed line) for the noise intensity $D=10^{-3}$

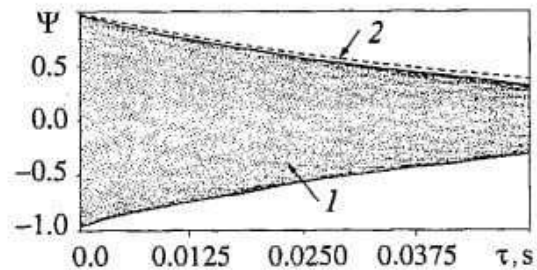


Fig. 9. Normalized ACF of the $x(t)$ oscillations in the Anishchenko-Astakhov oscillator (region 1) and its exponential approximation $\exp(-B_{\text{eff}}|\tau|)$ (curve 2) (physical experiment). The phase diffusion coefficient B_{eff} was calculated from experimental data independently on the ACF

3.2. Correlation characteristics of the Lorenz attractor. In the previous section we have used the effective phase diffusion coefficient to describe the correlation properties of the Rössler system and the Anishchenko-Astakhov oscillator. However, such an approach cannot be applied to approximate autocorrelation functions of chaotic oscillations of a switching type. Some chaotic attractors demonstrating a rather complex structure can contain certain regions which are separated by manifolds of saddle points and cycles. Transitions (switchings) between these regions can occur provided that certain conditions are fulfilled [54]. Such oscillations can be observed, for example, in the Lorenz system [41]. Let us consider the Lorenz system in the regime of the quasi-hyperbolic attractor for $r=28$, $\sigma=10$, and $b=8/3$.

In the phase space of the Lorenz system there are two saddle-foci that are symmetrical about the z -axis and are separated by the stable manifold of a saddle point in the origin. This stable manifold has a complex structure that allows the trajectories to switch between the saddle-foci in specific paths [11,54] (see Fig. 10). Unwinding about

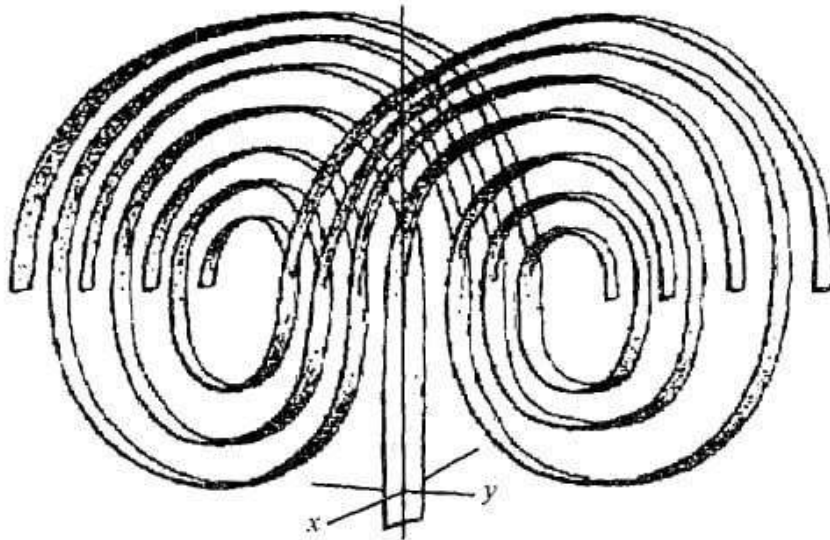


Fig. 10. Qualitative illustration of the structure of manifolds in the Lorenz system

one of the saddle-foci the trajectory approaches the stable manifold and then can jump to the other saddle-focus with a certain probability. The rotation about the saddle-foci does not contribute considerably to the decay of the ACF, while the frequency of «random» switchings essentially affects the rate of the ACF decay. Consider the time series of the x

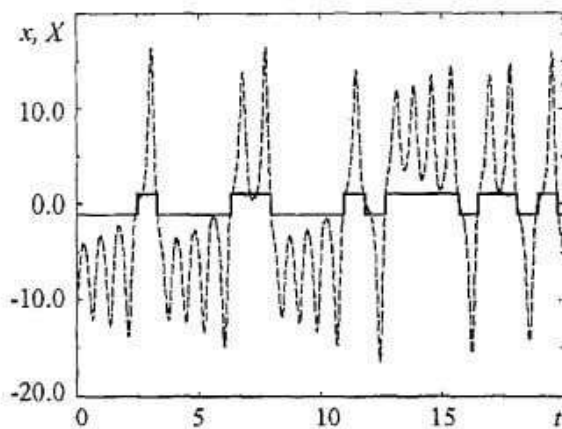


Fig. 11. Telegraph signal (solid curve) obtained for the $x(t)$ oscillations (dashed curve) of the Lorenz system at $\sigma=10$, $\beta=8/3$, and $r=28$

coordinate of the Lorenz system, that is shown in Fig. 11. If one introduces a symbolic dynamics, i.e., one excludes the rotation about the saddle-foci, one obtains a telegraph-like signal. Figure 12 shows the ACF of the $x(t)$ oscillations for the Lorenz attractor and the ACF of the corresponding telegraph signal. Comparing these two figures we can state that the time of the correlation decay and the behavior of the ACF on this time scale are predominantly determined by switchings, whereas the rotation about the saddle-foci makes a minor contribution to the ACF decay on large times. It is worth noting that the ACF decreases linearly on short times. This fact

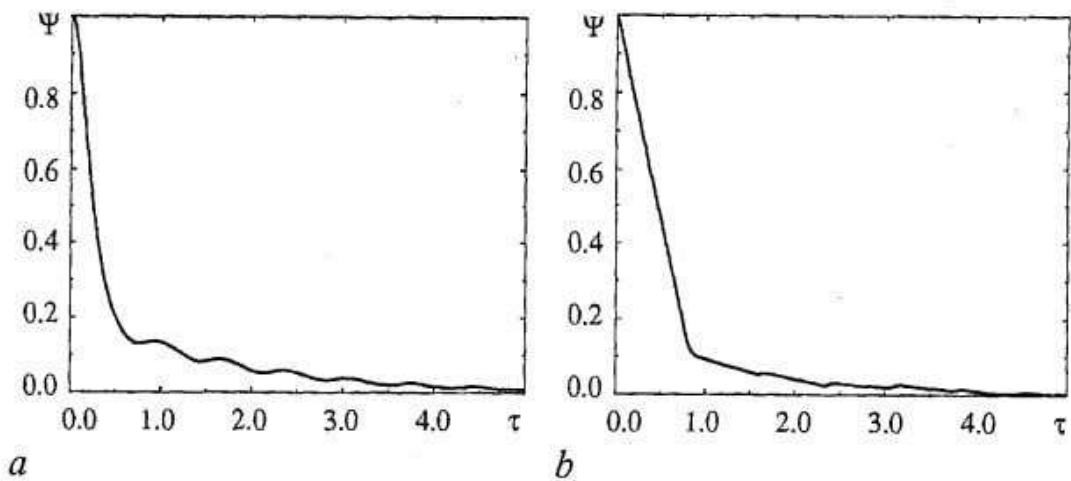


Fig. 12. The ACF of the $x(t)$ oscillations (a) and of the telegraph signal (b)

is remarkable as the linear decaying of the ACF corresponds to a discrete equidistant residence time probability distribution in the form of δ -peaks. Additionally, the probability of switchings between the two states is equal to $1/2$ [52,53].

Figure 13 shows the residence time distribution calculated for the telegraph signal resulting from switchings in the Lorenz system. As can be seen from Fig. 13, a, the residence time distribution in the two attractor regions really has a structure that is quite similar to an equidistant discrete distribution. At the same time the peaks are characterized by a finite width. Figure 13, b represents the probability distribution of switchings which occur at multiples of ξ_0 , where ξ_0 is the minimal residence time in one of the states. This dependence shows that the probability of transition at time ξ_0 is close to $1/2$. The discrete character of switchings can be explained by peculiarities of the structure of the manifolds of the Lorenz system (see Fig. 10). In the vicinity of the origin $x=0, y=0$ the manifolds split into two leaves. This leads to the fact that probability of switchings between two states in one revolution about the fixed point is approximately equal to $1/2$. This particular aspect of the dynamics ensures that the ACF of the $x(t)$ and $y(t)$ oscillations on the Lorenz attractor has the form defined by expression (13). However, the finite width of the peaks in the distribution and deviations from the probability $1/2$ can lead to an ACF that decays to a certain finite, nonvanishing value.

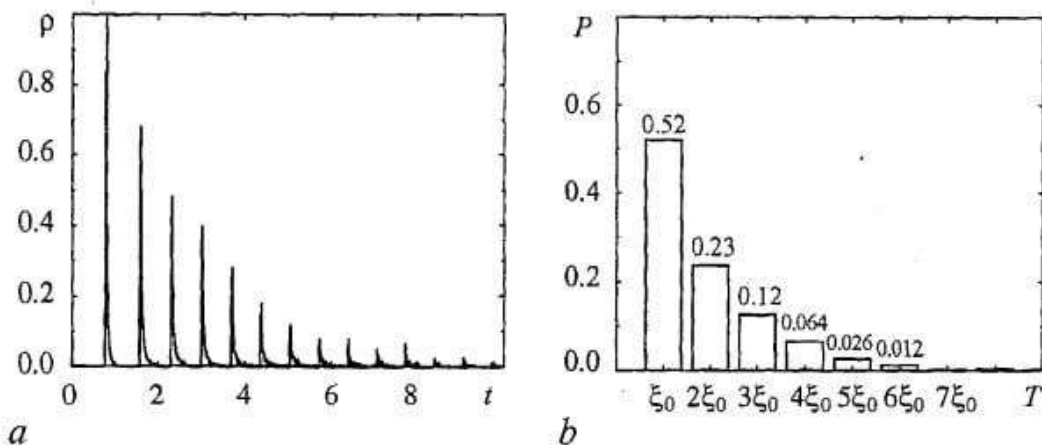


Fig. 13. The distribution of impulse durations of the telegraph signal (a) and probabilities of transitions at times multiple to ξ_0 (b)

4. Conclusion

In our studies we have shown that there is a group of nonhyperbolic attractors of spiral type for which noise strongly influences the characteristics of the relaxation to a stationary distribution as well as the correlation time and practically does not change the positive Lyapunov exponent.

The rate of mixing on nonhyperbolic attractors in R^3 is determined not only by the positive Lyapunov exponent but also depends on the instantaneous phase dynamics of chaotic oscillations. In the regime of spiral chaos noise causing phase changes can essentially accelerate the relaxation to a stationary distribution.

For chaotic attractors with a nonregular behavior of the instantaneous phase the rate of mixing cannot be considerably affected by noise. This statement is true for nonhyperbolic attractors of funnel type and for the attractors of switching type, for example, for the quasi-hyperbolic Lorenz attractor.

We have shown in our numerical simulation that the spiral chaos retains to a great extent the spectral and correlation properties of quasi-harmonic oscillations. With this, the rate of correlation splitting in a differential system depends on short times on both the instantaneous amplitude and the instantaneous phase diffusion. The width of the basic peak in the power spectrum of the spiral chaos is correspondingly defined by B_{eff} and oscillations of the instantaneous amplitude determine the level of the spectrum background. The effective phase diffusion coefficient in a noise-free system is defined by its chaotic dynamics but is not directly related to the positive Lyapunov exponent.

Our studies of statistical properties of the Lorenz attractor have demonstrated that the properties of the ACF is mainly defined by a random switching process and slightly depends on the rotation about the saddle-foci. The classical model of telegraph signal enables one to describe the behavior of $\psi(\tau)$ for the Lorenz attractor by using the expression (13). In particular, this expression approximates quite well a linear decay of the ACF from 1.0 to 0.2 that allows to estimate theoretically the correlation time. The power spectrum of the Lorenz attractor both in a flow and in the Poincaré map was studied in [36] by applying the symbolic dynamics methods. Already in this paper it has been established that the power spectrum is not a Lorenzian. Our results obtained by using the model of telegraph signal are in a good agreement with the findings presented in [36].

We are grateful to Prof. P. Talkner for valuable discussions. This work was partially supported by Award № REC-006 of the U.S. Civilian Research and Development Foundation and the Russian Ministry of Education (grant № E02-3.2-345). G.S. acknowledges support from INTAS (grant № YSF 2002-3).

References

1. Anosov D.V. // Proc. Steklov Math. Inst. 1967. Vol. 90, 3.
2. Smale S. // Bull. Amer. Math. Soc. 1967. Vol. 73, 747.
3. Ruelle D. and Takens F. // Commun. Math. Phys. Vol. 20, 167 (1971).
4. Guckenheimer J. and Holmes P. Nonlinear Oscillations, Dynamical Systems, and Bifurcations of Vector Fields. Springer, New York, 1983.
5. Sinai Ya.G. // Russian Math. Survey. 1970. Vol. 25, 141.
6. Sinai Ya.G. // Nonlinear Waves / edited by A.V. Gaponov-Grekhov. Nauka, Moscow, 1979, p. 192 (in Russian).
7. Bunimovich L.A. and Sinai Ya.G. // Nonlinear Waves / Edited by A.V. Gaponov-Grekhov. Nauka, Moscow, 1980, p. 212 (in Russian).
8. Eckmann J.-P., Ruelle D. // Rev. Mod. Phys. 1985. Vol. 57, 617.
9. Ruelle D. // Am. J. Math. 1976. Vol. 98, 619.

10. *Ruelle D.* // *Bol. Soc. Bras. Math.* 1978. Vol. 9, 83.
11. *Shilnikov L.P.* // *Int. J. of Bif. and Chaos.* 1997. Vol. 7, 1953; *Shilnikov L.P.* Strange attractors and dynamical models // *J. of Circuits, Systems, and Computers.* 1993. Vol. 3, 1.
12. *Afraimovich V.S. and Shilnikov L.P.* // *Nonlinear Dynamics and Turbulence/* edited by G.I. Barenblatt, G. Iooss, and D.D. Joseph. Pitman, Boston, London, Melbourne, 1983, p. 1.
13. *Anishchenko V.S. and Strelkova G.I.* // *Discrete Dyn. Nat. Soc.* 1998. Vol. 2, 53.
14. *Graham R., Ebeling W.* (private communications); *Graham R., Hamm A., and Tel T.* Nonequilibrium potentials for dynamical systems with fractal attractors or repellers // *Phys. Rev. Lett.* 1991. Vol. 66. P. 3089.
15. *Ott E., Yorke E.D., and Yorke J.A.* // *Physica D.* 1985. Vol. 16, 62.
16. *Schroer Ch.G., Ott E., and Yorke J.A.* Effect of noise on nonhyperbolic chaotic attractors // *Phys. Rev. Lett.* 1989. Vol. 81. P. 1397.
17. *Sauer T., Grebogi C., and Yorke J.A.* // *Phys. Rev. Lett.* 1997. Vol. 79. P. 59.
18. *Jaeger L. and Kantz H.* // *Physica D.* 1997. Vol. 105, 79.
19. *Kifer Yu.* // *Commun. Math. Phys.* Vol. 121, 445 (1989); *Kifer Yu.I.* // *Izv. Akad. Nauk SSSR. Ser. Math.* Vol. 38, 1091 (1974).
20. *Grebogi C., Hammel S., and Yorke J.* // *J. Complexity.* 1987. Vol. 3, 136; *Grebogi C., Hammel S., and Yorke J.* // *Bull. Am. Math. Soc.* 1988. Vol. 19, 465.
21. *Anishchenko V.S., Vadivasova T.E., Kopeikin A.S., Kurths J., and Strelkova G.I.* // *Phys. Rev. Lett.* 2001. Vol. 87, 054101.
22. *Anishchenko V.S., Vadivasova T.E., Kopeikin A.S., Kurths J., and Strelkova G.I.* // *Phys. Rev. E.* 2002. Vol. 65, 036206.
23. *Zaslavsky G.M.* *Chaos in Dynamical Systems.* Harwood Acad. Publishers, New York, 1985.
24. *Billingsley P.* *Ergodic Theory and Information.* John Wiley and Sons, Inc., New York, 1965.
25. *Cornfeld I.P., Fomin S.V., Sinai Ya.* *Ergodic Theory.* Springer, New York, 1982.
26. *Kolmogorov A.N.* *Dokl. Acad. Nauk SSSR* // 1959. Vol. 124(4). P. 754 (in Russian).
27. *Sinai Ya.* // *Dokl. Acad. Nauk SSSR.* 1959. Vol. 124(4). P. 768 (in Russian).
28. *Pesin Ya.* // *Russian Math. Surveys.* 1977. 32(4) 55.
29. *Bowen R.* *Equilibrium States and the Ergodic theory of Anosov Diffeomorphisms* // *Lect. Notes in Mathematics.* Springer, Berlin, Heidelberg, 1975.
30. *Blank M.L.* *Stability and Localization in Chaotic Dynamics.* Moscow Center for Cont. Math. Educ., Moscow, 2001 (in Russian).
31. *Ruelle D.* The thermodynamic formalism for expanding maps // *Math. Phys.* 1989. 125. 239.
32. *Christiansen F., Paladin G., Rugh H.H.* Determination of correlation spectra in chaotic systems // *Phys. Rev. Lett.* 1990. Vol. 65. 2087.
33. *Liverani C.* Decay of correlations. // *Ann. Math.* 1995. Vol. 142. 239.
34. *Froyland G.* Computer-assisted bounds for the rate of decay of correlations // *Comm. Math. Phys.* 1997. Vol. 189. 237.
35. *Bowen R., Ruelle D.* The ergodic theory of axiom a flows // *Inventiones Math.* 1975. Vol. 29. 181.
36. *Badii R., Finardi M., Broggi G., Sepúlveda M.A.* // *Physica D.* 1992. Vol. 58. 304.
37. *Anishchenko V.S., Vadivasova T.E., Okrokvetskikh G.A., Strelkova G.I.* Correlation analysis of dynamical chaos // *Physica A.* 2003. Vol. 325. 199.
38. *Anishchenko V.S., Vadivasova T.E., Kopeikin A.S., Kurths J., Strelkova G.I.* // *Fluct. Noise Lett.* 2003. Vol. 3.

39. *Anishchenko V.S., Vadivasova T.E., Okrokvertskhov G.A., Strelkova G.I.* // J. Comm. Techn. Electr. 2003. Vol. 48.
40. *Rössler O.E.* An equation for continuous chaos // Phys. Lett. A. 1976. Vol. 57. 397.
41. *Lorenz E.N.* Deterministic non-periodic flow // J. Atmos. Sci. 1963. Vol. 20. 130.
42. *Anishchenko V.S.* Complex Oscillations in Simple Systems. Moscow: Nauka, 1990 (in Russian).
43. *Anishchenko V.S.* Dynamical Chaos - Models and Experiments. World Scientific, Singapore 1995.
44. *Anishchenko V.S. et al.* Dynamics of Chaotic and Stochastic Systems. Springer, Berlin, Heidelberg 2002.
45. *Farmer J.D. et al.* // Ann. N.Y. Acad. Sci. 1980. Vol. 357, 45.
46. *Arneodo A., Collet P., and Tresser C.* Possible new strange attractors with spiral structure // Commun. Math. Phys. 1981. Vol. 79. P. 573.
47. *Rosenblum M., Pikovsky A., Kurths J.* Phase synchronization of chaotic oscillations // Phys. Rev. Lett. 1996. Vol. 76. 1804.
48. *Shilnikov L.P.* Methods Qual. Theory of Differential Equations. Gorky State University, Gorky, 1989, p. 130 (in Russian).
49. Chua's circuit: A paradigm for chaos / Ed. by R.N. Madan. World Scientific, Singapore, 1993.
50. *Stratonovich R.L.* Selected Problems of the Theory of Fluctuations in Radiotechnics. Moscow: Sov. Radio, 1961 (in Russian).
51. *Malakhov A.N.* Fluctuations in Auto-Oscillating Systems. Moscow: Nauka, 1968 (in Russian).
52. *Rytov S.M.* Introduction in Statistical Radiophysics. Moscow: Nauka, 1966 (in Russian).
53. *Tikhonov V.I., Mironov M.A.* Markovian Processes. Moscow: Sov. Radio, 1977 (in Russian).
54. *Jackson E.A.* Perspectives of Nonlinear Dynamics. Cambridge University Press. Vol. 1 (1989), 2(1991).

*International Institute of Nonlinear Dynamics,
Department of Physics, Saratov
State University, Saratov, Russia*

Received 17.09.03

УДК 537.86

СТАТИСТИЧЕСКИЕ СВОЙСТВА ДЕТЕРМИНИРОВАННЫХ И ЗАШУМЛЕННЫХ ХАОТИЧЕСКИХ СИСТЕМ

В.С. Анищенко, Т.Е. Вадивасова, Г.И. Стрелкова, Г.А. Окрокверцхов

Данная работа представляет собой обзор результатов, недавно полученных в группе исследователей, возглавляемой профессором В.С. Анищенко, и опубликованных в ряде научных статей. Представляемые результаты относятся к статистическому описанию динамического хаоса и влиянию шума на различные типы хаотических аттракторов. Рассматриваются особенности релаксации инвариантной вероятностной меры в системах с хаотическими аттракторами различных типов, проводится корреляционный и спектральный анализ хаотических автоколебаний.



Anishchenko Vadim Semenovich is the full Professor, Doctor of Sciences in Physics and Mathematics, the Honored Man of Science of Russia (1995), academician of the Russian Academy of Natural Sciences (2002), the Humboldt Prize Awarded on Physics (1999), Head of Radiophysics and Nonlinear Dynamics Chair. He is the author of 9 scientific monographs and more than 300 scientific papers. Since 2000 he is Director of the Scientific and Educational Center on Nonlinear Dynamics and Biophysics. He is a leading and well-known specialist in the field of oscillation theory and statistical radiophysics. He is a scientific supervisor of the International Institute of Nonlinear Dynamics of SSU.

E-mail: wadim@chaos.cas.ssu.runnet.ru



Vadivasova Tatyana Evgenevna is the full Professor of Radiophysics and Nonlinear Dynamics Chair of SSU. Her scientific interests are related with nonlinear oscillation theory, theory of deterministic chaos and theory of stochastic processes. She has about 60 scientific publications including 3 monographs.

E-mail: tanya@chaos.cas.ssu.runnet.ru



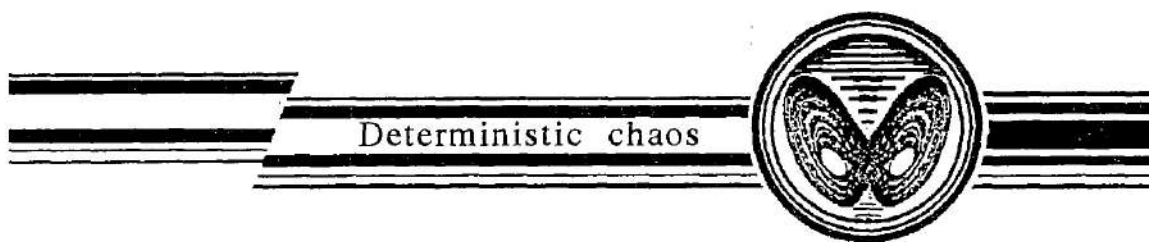
Strelkova Galina Ivanovna graduated from Saratov State University in 1993 on the specialty «radiophysics». In 1998 she defended her PhD thesis on the topic of properties and characteristics of nonhyperbolic chaos. Since 1994 she has been working as a leading engineer and a senior researcher at the Laboratory of Nonlinear Dynamics of SSU. Her scientific interests include nonlinear dynamics, deterministic chaos, statistical radiophysics, synchronization, noise-induced transitions. She published 25 scientific papers in leading Russian and foreign journals.

E-mail: galya@chaos.cas.ssu.runnet.ru



Okrokvertskhov Georgiy Aleksandrovich graduated from Saratov State University in 2002 on the speciality «biophysics». He is working as the assistant professor and continues his studies as a post-graduate student of Radiophysics and Nonlinear Dynamics Chair. His scientific interests are connected with nonlinear dynamics, the properties of nonhyperbolic chaos, statistical radiophysics. He has 6 scientific publications in Russian and foreign journals.

E-mail: george@chaos.cas.ssu.runnet.ru



Izv. VUZ. «AND», vol.11, № 3, 2003

ANALYTICAL DESCRIPTION OF RECURRENCE PLOTS OF WHITE NOISE AND CHAOTIC PROCESSES

M. Thiel, M.C. Romano, J. Kurths

We present an analytical description of the distribution of diagonal lines in Recurrence Plots for white noise and chaotic systems, and find that the latter one is linked to the correlation entropy. Further we identify two scaling regions in the distribution of diagonals for oscillatory chaotic systems that are hinged to two prediction horizons and to the geometry of the attractor. These scaling regions cannot be observed with the Grassberger-Procaccia algorithm. Finally, we propose methods to estimate dynamical invariants from RPs.

Dedicated to the 60th Birthday of Prof. Dr. Vadim Anishchenko

1. Introduction

Recurrence constitutes a fundamental property of dissipative chaotic systems. As Poincaré showed in his recurrence theorem in 1890 [1], if a system restricts its dynamics to a bounded subset of the phase space, the system will almost certainly, i.e. with probability one with respect to the natural measure, return arbitrarily close to any given initial condition.

Recurrence Plots (RPs) visualize in a two-dimensional binary matrix the recurrences of the system in phase space. The Recurrence Quantification Analysis (RQA) quantifies structures found in RPs to yield a deeper understanding of the underlying process from a given time series [2,3]. However, this method is widely applied [4 - 10] but in a rather pragmatic way. First steps in the direction of an analytical description were made by Faure et al. [11], Gao and Cai [3] and Casdagli [12].

In this contribution we give an analytical expression for the distribution of diagonals in RP in the case of stochastic processes and extend the results of [11,3] to chaotic flows. Further we compare our approach with the well-known Grassberger-Procaccia (G-P) algorithm [13] and show some advantages of the RP method for the estimation of some invariants of the dynamics, such as the correlation entropy. One of the most remarkable differences between our approach and the G-P algorithm is that we find two different scaling regions for oscillating chaotic flows, such as the Rössler system, instead of the single one obtained with the G-P algorithm. This new scaling region can be linked to the geometry of the attractor and defines another characteristic time scale of the system. Beyond we propose optimized measures for the identification of relevant structures in the RP.

The outline of this paper is as follows. In Sec. 2 we briefly introduce RPs. After considering in Sec. 3 the RPs of white noise, we proceed to general chaotic system (Sec. 4). Then, we exemplify our theoretical results for the Rössler system (Sec. 5) and present the two different scaling regions that characterize the system. Finally, we propose to estimate main characteristics of nonlinear systems from RPs which extends the importance of the RQA (Sec. 6).

2. Recurrence Plots and Recurrence Quantification Analysis

RPs were introduced to simply visualize the behavior of trajectories in phase space [2]. Suppose we have a dynamical system represented by the trajectory $\{\vec{x}_i\}$ for $i=1, \dots, N$ in a d -dimensional phase space. Then we compute the matrix

$$R_{ij} = \Theta(\varepsilon - \|\vec{x}_i - \vec{x}_j\|), \quad i, j = 1 \dots N, \quad (1)$$

where ε is a predefined threshold and $\Theta(\cdot)$ is the Heaviside function¹. The graphical representation of R_{ij} , called Recurrence Plot, is obtained encoding the value one as «black» and zero as «white» point. A homogeneous plot with mainly single points may indicate a mainly stochastic system. Paling away from the main diagonal may indicate a drift i.e. non-stationarity of the time series. A main advantage of this method is that it allows to apply it to nonstationary data [4].

To quantify the structures that are found in RPs, the Recurrence Quantification Analysis (RQA) was proposed [6]. There are different measures that can be considered in the RQA. One crucial point for these measures is the distribution of the lengths of the diagonal lines $P_\varepsilon(l)$ that are found in the plot. In the case of deterministic systems the diagonal lines mean that trajectories in the phase space are close to each other on time scales that correspond to the lengths of the diagonals. In the next sections we show that there is a relationship between $P_\varepsilon(l)$ and the correlation entropy. On the other hand we compute the distribution of diagonals for random processes to see that even in this case, there are some diagonals which can lead to pitfalls in the interpretation of the RQA because noise is inevitable in experimental systems. A more detailed discussion of this problem is given in [14].

3. Results for white noise

In this section we compute analytically the probability to find a black or recurrence point and the distribution of diagonals of length l in the RP in the case of independent noise. The probability to find a recurrence point in the RP is given by

$$P_b(\varepsilon) = \lim_{N \rightarrow \infty} 1/N^2 \sum_{i,j=1}^N R_{ij}, \quad (2)$$

and the probability to find a diagonal of at least length l in the RP is defined as

$$P_\varepsilon^c(l) = \lim_{N \rightarrow \infty} 1/N^2 \sum_{i,j=1}^N \prod_{m=0}^{l-1} R_{i+m, j+m}, \quad (3)$$

where c stands for cumulative. Note that $P_b(\varepsilon) = P_\varepsilon^c(1)$.

¹The norm used in Eq. 1 is in principle arbitrary. For theoretical reasons, that we will present later, it is preferable to use the maximum norm. However the numerical simulations of this paper are based on the Euclidian norm to make the results comparable with the literature. The theoretical results of this paper hold for both choices of the norm.

We consider a random variable X with probability density $\rho(x)$. Suppose that $\{x_i\}$ for $i=1, \dots, N$ is a realization of X and we are interested in the distribution of the distances of each point to all other points of the time series. This can be done by computing the convolution of the density $\rho(\cdot)$

$$R(x) = \rho(x) * \rho(x). \quad (4)$$

$P_b(\epsilon)$ is then gained by integrating $R(x)$ over $[-\epsilon, \epsilon]$

$$P_b(\epsilon) = \int_{-\epsilon}^{\epsilon} R(x) dx = 2 \int_0^{\epsilon} R(x) dx. \quad (5)$$

Note that $P_b(\epsilon)$ is invariant against shuffling of the data. For $[0,1]$ uniformly distributed noise, $R(x)$ is given by

$$R(x) = \begin{cases} 1 - |x| & \text{if } |x| < 1 \\ 0 & \text{else} \end{cases} \quad (6)$$

and hence the probability $P_b(\epsilon)$ for RPs and CRPs is given by

$$P_b(\epsilon) = 2\epsilon - \epsilon^2 + \Theta(\epsilon-1)[1-2\epsilon+\epsilon^2]. \quad (7)$$

For Gaussian white noise one finds $P_b(\epsilon) = \text{erf}(\epsilon/(2\sigma))$, where σ is the standard deviation.

Now it is straightforward to compute $P_\epsilon^c(l)$ in the CRPs (in RPs only asymptotically). As the noise is independent, we obtain

$$P_\epsilon^c(l) = P_b(\epsilon)^l. \quad (8)$$

The probability to find a recurrence point $P_b(\epsilon)$ is in both RPs and CRPs independent of the preceding point on the diagonal (except in the main diagonal). Eq. (8) shows that the probability to find a line of length l decreases exponentially with l .

For our example of uniformly distributed noise we get

$$P_\epsilon^c(l) = (2\epsilon - \epsilon^2 + \Theta(\epsilon-1)[1-2\epsilon+\epsilon^2])^l. \quad (9)$$

Note that in this case the exponential decay depends on ϵ . Hence the larger ϵ , the longer are the diagonal lines that one obtains. Usually one analyses the RP computed with only one threshold ϵ . As long diagonals are interpreted as a deterministic feature of the system (good predictability), using only one ϵ can lead to a misinterpretation of the dynamics of the system.

In the next sections we will show that the distribution of diagonals decays also exponentially for chaotic systems, but the decay is - at least in some region - independent of the threshold ϵ .

4. Results for chaotic systems

We present in this section an approach for chaotic systems. It is an extension of the results presented in [11] for chaotic maps and also covers general chaotic flows. To estimate the distribution of the diagonals in the RP, we start with the correlation integral [15]

$$C(\epsilon) = \lim_{N \rightarrow \infty} 1/N^2 \times \{\text{number of pairs } (i,j) \text{ with } |\vec{x}_i - \vec{x}_j| < \epsilon\}. \quad (10)$$

Note that the definition of $P_b(\epsilon)$ coincides with the definition of the correlation integral

$$C(\varepsilon) = \lim_{N \rightarrow \infty} 1/N^2 \sum_{i=1}^N \Theta(|x_i - x_j| - \varepsilon) \stackrel{\text{Eq. 1}}{=} \lim_{N \rightarrow \infty} 1/N^2 \sum_{i,j=1}^N R_{i,j} = P_b(\varepsilon). \quad (11)$$

This fact allows to link the known results about the correlation integral to the structures in RPs.

We consider a trajectory $\vec{x}(t)$ in the basin of an attractor in the d -dimensional phase space and the state of the system is measured at time intervals τ . Let $\{1, 2, \dots, M(\varepsilon)\}$ be a partition of the attractor in boxes of size ε . Then $p(i_1, \dots, i_l)$ denotes the joint probability that $\vec{x}(t=\tau)$ is in the box i_1 , $\vec{x}(t=2\tau)$ is in the box i_2, \dots , and $\vec{x}(t=l\tau)$ is in the box i_l . The order-2 Rényi entropy [16,17] is then defined as

$$K_2 = -\lim_{\tau \rightarrow 0} \lim_{\varepsilon \rightarrow 0} \lim_{l \rightarrow \infty} 1/(l\tau) \ln \sum_{i_1, \dots, i_l} p^2(i_1, \dots, i_l). \quad (12)$$

We can approximate $p(i_1, \dots, i_l)$ by the probability $P_{t,l}(\vec{x}, \varepsilon)$ of finding a sequence of points in boxes of length ε about $\vec{x}(t=\tau), \vec{x}(t=2\tau), \dots, \vec{x}(t=l\tau)$. Assuming that the system is ergodic, which is always the case for chaotic systems as they are mixing, we obtain

$$\sum_{i_1, \dots, i_l} p^2(i_1, \dots, i_l) = 1/N \sum_{i=1}^N p_i(i_1, \dots, i_l) \sim 1/N \sum_{i=1}^N P_{t,l}(\vec{x}, \varepsilon), \quad (13)$$

where $p_i(i_1, \dots, i_l)$ represents the probability of being in the box i_1 at time $t=\tau$, in the box i_2 at time $t=2\tau, \dots$ and in the box i_l at time $t=l\tau$. Further we can express $P_{t,l}(\vec{x}, \varepsilon)$ by means of the recurrence matrix

$$P_{t,l}(\vec{x}, \varepsilon) = 1/N \sum_{s=1}^N \prod_{m=0}^{l-1} \Theta(\varepsilon - |x_{t+m} - x_{s+m}|) = 1/N \sum_{s=1}^N \prod_{m=0}^{l-1} R_{t+m, s+m}. \quad (14)$$

Hence we obtain an estimator for the order-2 Rényi entropy by means of the RP

$$\hat{K}_2(\varepsilon, l) = 1/(l\tau) \ln \left(\underbrace{1/N^2 \sum_{t,s=1}^N \prod_{m=0}^{l-1} R_{t+m, s+m}}_{(*)} \right). \quad (15)$$

Note that (*) is the cumulative distribution of diagonal lines $P_\varepsilon^c(l)$ (Eq. (3)). Therefore, if we represent $P_\varepsilon^c(l)$ in a logarithmic scale versus l we should obtain a straight line with slope $-\hat{K}_2(\varepsilon)\tau$ for large l 's.

On the other hand, in the G-P algorithm the l -dimensional correlation integral is defined as

$$C_l(\varepsilon) = \lim_{N \rightarrow \infty} 1/N^2 \sum_{t,s=1}^N \Theta(\varepsilon - (\sum_{k=0}^{l-1} |x_{t+k} - x_{s+k}|^2)^{1/2}). \quad (16)$$

Grassberger and Procaccia [18] state that due to the exponential divergence of the trajectories, requiring

$$\sum_{k=0}^{l-1} |x_{t+k} - x_{s+k}|^2 \leq \varepsilon^2 \quad (17)$$

is essentially equivalent to

$$|x_{t+k} - x_{s+k}| < \varepsilon \quad \text{for } k = 1, \dots, l \quad (18)$$

which leads to the ansatz:

$$C_l(\varepsilon) \sim \varepsilon^\nu \exp(-l\tau K_2). \quad (19)$$

Further they make use of Takens embedding theorem [19] and reconstruct the whole trajectory from l measurements of any single coordinate. Hence they consider

$$\tilde{C}_l(\varepsilon) = \lim_{N \rightarrow \infty} 1/N^2 \sum_{t,s=1}^N \Theta(\varepsilon - (\sum_{k=0}^{l-1} |x_{t+k} - x_{s+k}|^2)^{1/2}) \quad (20)$$

and use the same ansatz Eq. (19) for $\tilde{C}_l(\epsilon)$. Then, the G-P algorithm obtains an estimator of K_2 considering

$$\tilde{K}_2(\epsilon, l) = 1/\tau \ln(\tilde{C}_l(\epsilon)/\tilde{C}_{l+1}(\epsilon)). \quad (21)$$

Due to the similarity of the RP approach to the G-P one, we state

$$P_\epsilon^c(l) \simeq \sum_{i_1, \dots, i_l} p^2(i_1, \dots, i_l) \simeq \tilde{C}_l(\epsilon) \sim \epsilon^\nu \exp(-l\tau K_2). \quad (22)$$

The difference between both approaches is that in $P_\epsilon^c(l)$ we further consider information about l vectors, whereas in $\tilde{C}_l(\epsilon)$ we have just information about l coordinates. Besides this, in the RP approach l is a length in the plot, whereas in the G-P algorithm it means the embedding dimension. As K_2 is defined for $l \rightarrow \infty$, the RP approach seems to be more appropriate than the G-P one, as it is always problematic to use very high embedding dimensions [20].

A further advantage of the RP method is that it does not make use of the approximation that Eq. (17) is essentially equivalent to Eq. (18). The quantity that enters the RPs is directly linked to the conditions Eq. (18) and hence uses one approximation less than the G-P method.

One open question for both methods is the identification of the scaling regions. It is somewhat subjective and makes a rigorous error estimation problematic. For the cases considered in this paper we have found that 10,000 data points assure reliable results for both methods. Even 5,000 data points allow for a reasonable estimation, whereas 3,000 data points or less yield small scaling regions that are difficult to identify. However, the RP method is advantageous for the estimation of K_2 as the representation is more direct. The most important advantage is presented in the next section: RPs allow to detect another scaling region in the Rössler attractor that cannot be observed with the G-P algorithm.

5. The Rössler System

We analyze the Rössler system with standard parameters $a=b=0.2$, $c=5.7$ [21]. We generate 15,000 data points based on the Runge-Kutta method of fourth order and neglect the first 5,000. The integration step is $h=0.01$ and the sampling rate is 20.

First, we estimate K_2 by means of the G-P algorithm. Fig. 1 shows the results for the correlation integral in dependence on ϵ . There is one well-expressed scaling region for each embedding dimension $l > 3$. Then we get from the vertical distances between the

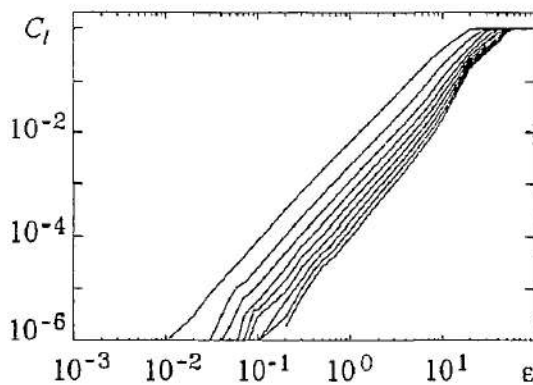


Fig. 1. G-P algorithm for the Rössler system; l varies from 3 (top) to 27 (bottom) in steps of 3

lines an estimate of \tilde{K}_2 (Fig. 2), $K_2=0.070 \pm 0.003$. Next, we calculate the cumulative distribution of the diagonal lines of the RP in dependence on the length of the lines l . We then represent the number of diagonals of length l , i.e. $N^c(l) = N^2 \times P_\epsilon^c(l)$, where N is the length of the time series (Fig. 3). For large l and small ϵ the scaling breaks down as there are not enough lines in the RP. The most remarkable fact obtained here is the existence of two well differentiated scaling regions. The first one is found for $1 \leq l \leq 84$ and the second one for $l \geq 85$. The existence of two scaling regions

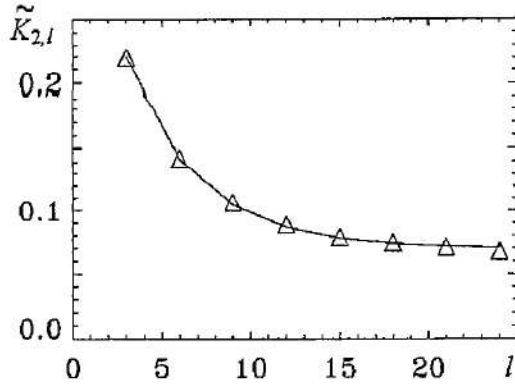


Fig. 2. Estimation of $\tilde{K}_{2,l}$ for the Rössler system with the G-P algorithm. The line is plotted to guide the eye

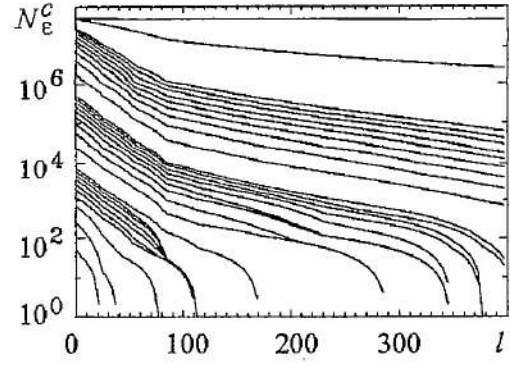


Fig. 3. Number of diagonal lines of at least length l in the RP of the Rössler system ($N^c(l) = N^2 \times P_{\epsilon}^c(l)$, where N is the length of the time series); ϵ varies logarithmically from 10^{-2} to 10.0 (bottom to top)

is a new and striking point obtained from this analysis and is not observed with the G-P method. The estimate of K_2^f from the slope of the first part of the lines is $K_2^f \approx 0.225 \pm 0.03$ (Fig. 4) and the one from the second part is $K_2^f \approx 0.0675 \pm 0.004$ (Fig. 5). Hence, K_2^f is

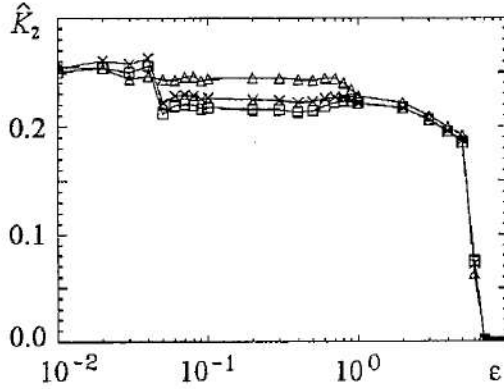


Fig. 4. RP method for the Rössler system: slope of the curves $N_{\epsilon}^c(l)$ in the first region for three different choices ($\times: l \in [1,84]$, $\Delta: l \in [1,40]$, $\square: l \in [16,80]$) of the scaling region in l

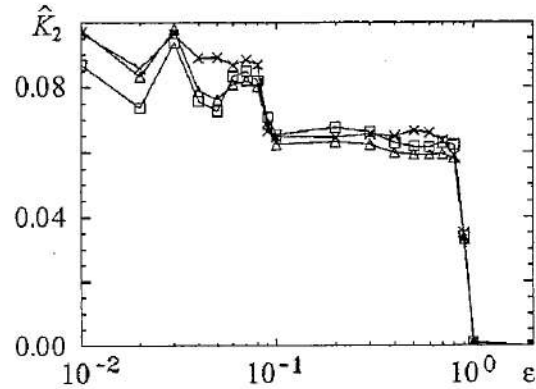


Fig. 5. RP method for the Rössler system: slope of the curves $N_{\epsilon}^c(l)$ in the second region for three different choices ($\times: l \in [88,108]$, $\Delta: l \in [88,200]$, $\square: l \in [108,160]$) of the scaling region in l

between 3-4 times higher than K_2 . As K_2 is defined for $l \rightarrow \infty$, the second slope yields the estimation of the entropy.

However, the first part of the curve is interesting too, as it is also independent of ϵ . The region $1 \leq l \leq 84$ characterizes the short term dynamics of the system up to three cycles around the fix point and corresponds in absolute units to a time of $t=16.8$, as we use a sampling rate of $\delta t=0.2$. These three cycles reflect a characteristic period of the system that we will call *recurrence period* T_{rec} . It is different from the dominant «phase period» T_{ph} , which is given by the dominant frequency of the power density spectrum. T_{rec} however, is given by recurrences to almost the same state in phase space.

Recurrences are represented in the plot by vertical (or horizontal, as the plot is symmetric) lines. Such a line occurs at the coordinates i, j if

$$R_{i,j+m} = \begin{cases} 1 & \text{if } m=-1 \\ 0 & \text{for } m \in \{0, \dots, l-1\} \\ 1 & \text{if } m=l. \end{cases} \quad (23)$$

The trajectory \vec{x}_n for times $n=j-1, \dots, j+l$ is compared to the point \vec{x}_j . Then the structure given by Eq. (23) can be interpreted as follows. At time $n=j-1$ the trajectory falls within an ε -box of \vec{x}_j . Then for $n=j, \dots, j+l-1$ it moves outside of the box, until at $n=j+l$ it recurs to the ε -box of \vec{x}_j . Hence, the length of the line is proportional to the time that the trajectory needs to recur close to \vec{x}_j .

In Fig. 6 we represent the distribution of vertical lines in the RP. The period of about 28 points corresponds to T_{ph} . However, the highest peak is found at a lag of about 87 points (the second scaling region begins at $l=85$). This means that after this time most of the points recur close to their initial state. This time also defines the recurrence period T_{rec} . For the Rössler attractor with standard parameters we find $T_{\text{rec}} \approx 3T_{\text{ph}}$.

For predictions on time scales below the recurrence period, $\tau^f = 1/K_2^f$ is a better estimate of the prediction horizon than $\tau = 1/K_2$. This interesting result means that the possibility to predict the next value within an ε -range is in the first part by a factor of more than 3 times worse than it is in the second part, i.e. there exist two time scales that characterize the attractor. The first slope is greater than the second one because it is more difficult to predict the next step if we have only information about a piece the trajectory for less than one recurrence period. Once we have scanned the trajectory for more than T_{rec} , the predictability increases and the slope of $P_\varepsilon^c(l)$ in the logarithmic plot decreases. Hence the first slope, as well as the time scale at which the second slope begins, reveal important characteristics of the attractor.

To investigate how the length of the first scaling region depends on the form of the attractor, we have varied the parameter c of the Rössler system with fixed $a=b=0.1$, so that different types of attractors appear [22]. Especially we have studied the cases $c=9$, which yields $T_{\text{rec}}=2T_{\text{ph}}$, and $c=30$, which gives $T_{\text{rec}}=4T_{\text{ph}}$. In both cases the length of the first scaling region corresponds as expected to T_{rec} .

On the other hand, the existence of the two scalings may be linked to the amplitude fluctuations and the phase diffusion of the Rössler system, because the same two time scales have been also recently found by Anishchenko et al. based on a rather subtle method [23 - 25]. There, the first scaling region was linked to the amplitude fluctuations and the second one to the phase diffusion.

The effect of the two scaling regions in the distribution of diagonal lines is also detectable in other oscillating nonhyperbolic systems like the Lorenz system and our simulations suggest a connection to the conclusions presented in [23]. We will report our results in more detail in a forthcoming paper.

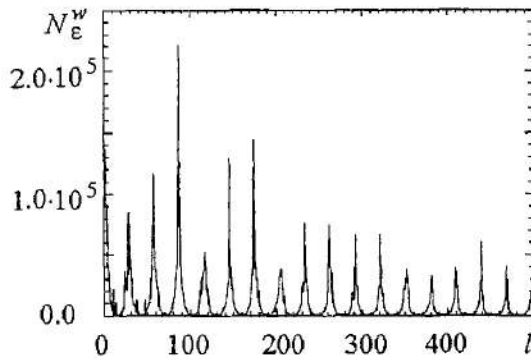


Fig. 6. Number of vertical lines in the Recurrence Plot of the Rössler system with standard parameters, $\varepsilon=0.05$ and based on 60,000 data points

6. Dynamical invariants for the RQA

With regard to our theoretical findings in Sec. 4 we have to assess the quality of the possible results of the RQA.

The measures considered in the RQA [6] are not invariants of the dynamical system, i.e. they usually change under coordinate transformations, and especially, they are in general modified by embedding [26]. Hence, we propose new measures to quantify the structures in the RP, that are invariants of the dynamical system.

The first measure we propose, is the slope of the cumulative distribution of the diagonals for large l . We have seen that it is (after dividing by τ) an estimator of the Rényi entropy of second order K_2 , which is a known invariant of the dynamics [27]. On the other hand, we also can consider the slope of the distribution for small l 's, as this slope shows a clear scaling region, too. The inverse of these two quantities, is then related to the forecasting time at different horizons. Especially the transition point from the first to the second scaling region is an interesting characteristic of the system.

The second measure we introduce, is the vertical distance between $P_\epsilon^c(l)$ for different ϵ 's. From Eq. (22) one can derive

$$\hat{D}_2(\epsilon) = \ln(P_\epsilon^c(l)/P_{\epsilon+\Delta\epsilon}^c(l))(\ln(\epsilon/(\epsilon+\Delta\epsilon)))^{-1}. \quad (24)$$

This is an estimator of the correlation dimension D_2 [17]. The result for the Rössler system is represented in Fig. 7. The mean value of $\hat{D}_2(\epsilon)$ is in this case 1.86 ± 0.04 . This result is in good accordance with the estimation of D_2 by the G-P algorithm given in [28], where the value 1.81 is obtained. With a modified G-P algorithm a value of 1.89 was reported [28].

The third measure we suggest, is an estimator of the generalized mutual information of order 2,

$$I_2(\tau) = 2H_2 - H_2(\tau) \quad (25)$$

where

$$H_2 = -\ln \sum_i p_i^2, \quad H_2(\tau) = -\ln \sum_i p_{i,j}^2(\tau) \quad (26)$$

are the generalized Rényi's second order entropy (also correlation entropy) and its corresponding joint second order entropy [29]. This measure can be estimated using the G-P algorithm as follows [30]

$$\tilde{I}_2(\epsilon, \tau) = \ln(C_2(\epsilon, \tau)) - 2\ln(C_1(\epsilon)). \quad (27)$$

Instead, we can estimate $I_2(\tau)$ using the recurrence matrix. As discussed in the preceding sections, one can estimate H_2 as

$$\hat{H}_2 = -\ln[1/N^2 \sum_{i,j=1}^N R_{i,j}]. \quad (28)$$

Analogously we can estimate the joint second order entropy by means of the recurrence matrix

$$\hat{H}_2(\tau) = -\ln[1/N^2 \sum_{i,j=1}^N R_{i,j} R_{i+\tau, j+\tau}]. \quad (29)$$

We compare the estimation of $I_2(\tau)$ based on the G-P algorithm with the one obtained by the RP method in Fig. 8. We see, that the RP method yields systematically higher estimates of the mutual information, as in the case of the estimation of the correlation entropy. However, the structure of the curves is qualitatively the same (it is just shifted to higher values by about 0.2). A more exhaustive inspection shows, that the difference is due to the use of the Euclidean norm. The estimate based on the RP method

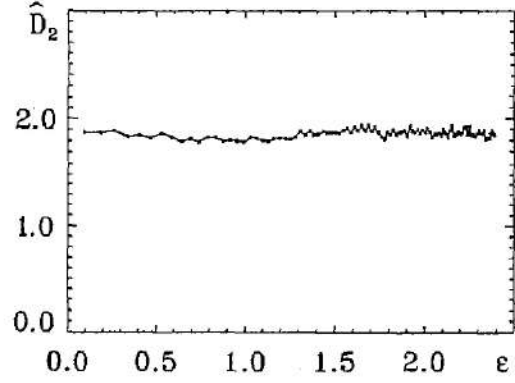


Fig. 7. Estimation of the correlation dimension D_2 for the Rössler attractor by the RP method. The parameters used for the Rössler system and the integration step are the same as in Sec. 5

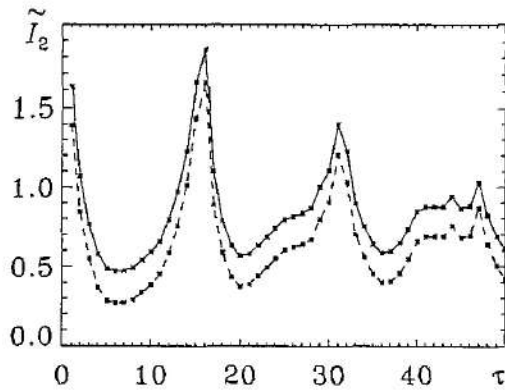


Fig. 8. Comparison of the estimators of the mutual information for the x -component of the Rössler system computed by the RP method (solid line) and the G-P algorithm (dashed line). The parameters used for the Rössler system and the integration step are the same as in Sec. 5

is almost independent of the norm, whereas the estimate based on the G-P algorithm clearly depends on the special choice. If the maximum norm is used (in G-P and RP) both curves coincide.

Note that the estimators for the invariants we propose are different from the ones of the G-P algorithm.

The three measures that we have proposed, are not only applicable for chaotic systems but also for stochastic ones, as the invariants are equally defined for both kinds of systems.

7. Conclusions

In this paper we have presented an analytical expression for the distribution of diagonals $P_\epsilon(l)$ for stochastic systems and chaotic flows, extending the results presented in [11]. We have shown that $P_\epsilon(l)$ is linked to the second order Rényi entropy rather than to the Lyapunov exponent. Further we have found in the logarithmic plot of $P_\epsilon(l)$ two different scaling regions with respect to ϵ , that characterize the dynamical system and are also related to the geometry of the attractor. This is a new insight provided by RPs that cannot be seen by the G-P algorithm and will be studied in more detail in a forthcoming paper. The first scaling region defines a new time horizon for the description of the system for short time scales. Beyond the RP method does not make use of high embedding dimensions, and the computational effort compared with the G-P algorithm is decreased. Therefore the RP method is rather advantageous than the G-P one for the analysis of rather small and/or noisy data sets. Besides this, we have proposed different measures for the RQA, like estimators of the second order Rényi entropy K_2 , the correlation dimension D_2 and the mutual information, that are, in contrast to the other often used RQA measures, invariants of the dynamics [26].

We thank Vadim Anishchenko very much for the long-standing and very exciting discussions and his suggestions on this work. Moreover we thank Dieter Armbruster, Annette Witt, Udo Schwarz and Norbert Marwan for the fruitful discussions. The project was supported by the «DFG Priority Program 1114».

References

1. Poincaré H. Sur le problème des trois corps et les équations de la dynamique // Acta Math. 13 (1890) 1-270.
2. Eckmann J.-P., Kamphorst S.O. and Ruelle D. Recurrence Plots of Dynamical Systems // Europhysics Letters.4 (1987) 973-977.
3. Gao J. and Cai H. On the structures and quantification of recurrence plots // Physics Letters.A 270 (1999) 75-87.
4. Marwan N., Wessel N., Meyerfeldt U., Schirdewan A. and Kurths J. Recurrence Plot Based Measures of Complexity and its Application to Heart Rate Variability Data // Phys. Rev. E.66 (2002) 026702.
5. Marwan N., Kurths J. Nonlinear analysis of bivariate data with cross recurrence plots // Phys. Lett. A.302(5-6) (2002) 299-307.

6. *Webber C.L. Jr. and Zbilut J.P.* Dynamical assessment of physiological systems and states using recurrence plot strategies // *J. Appl. Physiol.* 76 (1994) 965-973.
7. *Zbilut J.P., Giuliani A. and Webber C.L. Jr.* Recurrence quantification analysis and principal components in the detection of short complex signals // *Physics Letters A* 237 (1998) 131-135.
8. *Zbilut J.P., Giuliani A. and Webber C.L. Jr.* Detecting deterministic signals in exceptionally noisy environments using cross-recurrence quantification // *Physics Letters A* 246 (1998) 122-128.
9. *Holyst J.A., Zebrowska M. and Urbanowicz K.* Observations of deterministic chaos in financial time series by recurrence plots, can one control chaotic economy? // *Eur. Phys. J. B* 20 (2001) 531-535.
10. *Kurths J., Schwarz U., Sonett C.P. and Parlitz U.* Testing for nonlinearity in radiocarbon data // *Nonlinear Processes in Geophysics* 1 (1994) 72-75.
11. *Faure P. and Korn H.* A new method to estimate the Kolmogorov entropy from recurrence plots: its applications to neuronal signals // *Physica D.* 122 (1998) 265-279.
12. *Casdagli M.C.* Recurrence plots revisited // *Physica D.* 108 (1997), 12-44.
13. *Grassberger P. and Procaccia I.* Characterization of strange attractors // *Phys. Rev. Lett.* 50, number 5 (1983) 346-349.
14. *Thiel M., Romano M.C., Kurths J., Meucci R., Allaria E. and Arecchi T.* Influence of observational noise in recurrence quantification analysis // *Physica D* 171, number 3 (2002) 138-152.
15. *Grassberger P. and Procaccia I.* Measuring the strangeness of strange attractors // *Physica D* 9 (1983) 189-208.
16. *Rényi A.* Probability theory. North-Holland, (1970) (appendix).
17. *Grassberger P.* Generalized dimensions of strange attractors // *Physics Letters* 97 A, № 6 (1983) 227-230.
18. *Grassberger P. and Procaccia I.* Dimensions and entropies of strange attractors from a fluctuating dynamics approach // *Physica D* 13 (1984) 34-54.
19. *Takens F.* Detecting strange attractors in turbulence, in: *Dynamical Systems and Turbulence* / Eds. D.A. Rand and L.-S. Young // *Lecture Notes in Mathematics*, Vol. 898 (Springer, Berlin, 1980).
20. *Ruelle D.* Deterministic chaos: the science and the fiction // *Proc. R. Soc. Lond. A*, 427 (1990) 241-248.
21. *Rössler O.E.* An equation for continuous chaos // *Phys. Lett.* 57A, (1976) 397-398.
22. *Alligood K.T., Sauer T.D. and Yorke J.A.* Chaos an introduction to dynamical systems. Springer (1996).
23. *Anishchenko V.S., Vadivasova T.E., Kopeikin A.S., Strelkova G.I. and Kurths J.* Spectral and correlation analysis of spiral chaos // *Fluctuation and Noise Letters*, 3 (2003), L213-L221.
24. *Anishchenko V.S., Vadivasova T.E., Okrokvetskikh G.A. and Strelkova G.I.* Correlation analysis of dynamical chaos // *Physica A* 325 (2003), 199-212.
25. *Anishchenko V.S., Astakhov V., Neiman A., Vadivasova T. and Schimansky-Geier L.* *Nonlinear Dynamics of Chaotic and Stochastic Systems.* Springer (2001).
26. *Thiel M., Romano M.C. and Kurths J.* Spurious structures in Recurrence Plots induced by embedding // *Chaos* (submitted for publication).
27. *Schuster H.G.* *Deterministic Chaos.* Wiley VCH, (1984).
28. *Raab C. and Kurths J.* Estimations of large-scale dimensions densities // *Phys. Rev. E* 64 (2001) 0162161-0162165.
29. *Pompe B.* Measuring Statistical Dependences in a Time Series // *J. Stat. Phys.* 73 (1993), 587-610.
30. *Kantz H. and Schreiber T.* *Nonlinear Time Series Analysis.* University Press, Cambridge, (1997).

University of Potsdam, Germany

Received 28.08.2003

АНАЛИТИЧЕСКОЕ ОПИСАНИЕ ОТОБРАЖЕНИЙ ПОСЛЕДОВАНИЯ ДЛЯ БЕЛОГО ШУМА И ХАОТИЧЕСКИХ ПРОЦЕССОВ

M. Thiel, M.C. Romano, J. Kurths

Дано аналитическое описание распределения диагональных линий в отображениях последования для белого шума и систем с хаотической динамикой; показано, что это распределение связано с корреляционной энтропией. Идентифицированы две области скейлинга в распределении диагоналей для колебательных систем с хаотической динамикой, которые тесно связаны с двумя горизонтами предсказуемости и с геометрией аттрактора. Эти области скейлинга не могут быть получены с помощью алгоритма Грассбергера - Прокаччиа. В заключение предложены методы определения динамических инвариантов из отображений последования.



Marco Thiel was born in 1974 in Paderborn (Germany). After finishing his diploma degree he started his PhD studies at the Nonlinear Dynamics group of Prof. Kurths at the University of Potsdam. E-mail: thiel@agnld.uni-potsdam.de



Maria Carmen Romano was born in 1975 in Tudela (Spain). She studied physics in the Universities of Zaragoza (Spain) and Paderborn (Germany). After finishing her diploma degree she started in 1999 her PhD studies at the Nonlinear Dynamics group of Prof. Kurths at the University of Potsdam. E-mail: romano@agnld.uni-potsdam.de



Jürgen Kurths was born in GDR (1953). He graduated the University of Rostok (1975) in Mathematics and has got his PhD (1981). Now he is Director of the Interdisciplinary Center Dynamics of Complex Systems at the University of Potsdam, Full Professor (C4) for Theoretical Physics/Nonlinear Dynamics at University of Potsdam, Vice speaker of Sonderforschungsbereich Komplexe Nichtlineare Prozesse (Deutsche Forschungs-gemeinschaft), Vice President of the European Geophysical Society, Coordinator EU Network «Control, Synchronization and Characterization of Spatially Extended Nonlinear Systems». He is the member of the Editorial Board of Int. J. Bifurcation and Chaos, Visiting Fellow Muroran Institute of Technology (2001, Japan). J. Kurths is the Fellow of Fraunhofer Society, Guest Fellow of Max-Planck-Society, Fellow of the American Physical Society. E-mail: JKurths@agnld.uni-potsdam.de



Izv. VUZ «AND», vol. 11, № 3, 2003

**EVOLUTION OF RUNNING WAVES TO SPATIO-TEMPORAL CHAOS:
INTERACTION OF TEMPORAL AND SPATIAL DYNAMICS
IN A RING OF PERIOD-DOUBLING SELF-OSCILLATORS**

A. Shabunin, V. Astakhov, A. Akopov

In the work we consider transition from regular running waves to developed spatio-temporal chaos in a chain of period-doubling oscillators. We investigate typical bifurcations which take place on the base of the chosen running wave regime from the period-one cycle to developed temporal chaos. We found that oscillations remain spatially periodic until transition to temporal chaos. The exact spatial periodicity is changed by the periodicity in the average in the chaotic region. Destroying of the averaged spatio-periodic structure is connected with losing of coherence on main frequencies in the temporal spectra of neighbor oscillators in the chain.

To V. Anishchenko, on the occasion of his sixtieth birthday

In recent years a problems of collective dynamics of interacting oscillators attracts a great interests. A series of works was devoted to consideration of coupled maps arrays modeling different physical phenomena [1-4]. The maps with chaotic behavior have rich dynamics and they allow to research formation of regular and chaotic spatio-temporal structures resulted from synchronization of oscillations. Another base models are arrays of phase oscillators which can be applied for investigation of phenomena of phase synchronization and of formation of phase structures. Most of studies was devoted to the global mean-field coupling systems [5-10]. It was demonstrated that the very simple periodic oscillators can demonstrate complex macroscopic behavior: periodic, quasi-periodic and even chaotic through quasi-periodic and period-doubling routes [6]. The mean-field approach allowing to consider the behavior of the system as a whole, does not take into account local connections between elements, which can lead to formation of local spatial structures. Locally coupled limit-cycle oscillators was intensively investigated in the works [11-13]. The phase regularities in nearest-neighbor coupled oscillators were also considered on the example of the circle maps [14]. The work [15] investigated spatial synchronization in the chain of unidirectionally coupled period-doubling self-oscillators and developing of the dynamics along the array.

It has been known that chains of the simplest limit-cycle oscillators with periodic boundary conditions exhibit running waves regimes when oscillations in nearest sites differ from each other on constant phase shifts. In the work [11] a more complex oscillators chain was considered. It was demonstrated that taking into account the second harmonics in the spectrum of oscillations can lead to spatially chaotic behavior. Hence the transition to more realistic models lead to dynamics which can't be realized in the simplest phase oscillators arrays. The works [16-19] demonstrate that running waves regimes are possible for rings of chaotic oscillators. Nevertheless, until now a lot of

questions about the developing and destroying of the chaotic running waves remain unresolved. How does complicating of the temporal dynamics influence on the spatial structures? How the destroying of spatial structures is connected with the synchronization between nearest-neighbor oscillators? In our investigation we are focusing on these questions. We have chosen a chain of period-doubling self-oscillators (Chua's oscillators) with diffusion symmetric coupling

$$\begin{aligned}\dot{x}_i &= \alpha(y_i - x_i - f(x_i)), \\ \dot{y}_i &= x_i - y_i + z_i + \gamma(y_{i-1} + y_{i+1} - 2y_i), \\ \dot{z}_i &= -\beta y_i,\end{aligned}\tag{1}$$

where

$$f(x) = \begin{cases} bx + a - b & \text{if } x > 1 \\ ax & \text{if } |x| \leq 1 \\ bx - a + b & \text{if } x < -1, \end{cases} \quad i=1,2,\dots,N,$$

with periodic boundary conditions:

$$x_1 = x_N, \quad y_1 = y_N, \quad z_1 = z_N.$$

All oscillators are identical. The behavior of the single oscillator is widely described in the literature (see, for example, [20]). It is characterized by period-doubling bifurcations cascade and bistability, when two symmetric attractors formed near two non-trivial equilibria P_1 and P_2 coexist in the phase space. With parameter α increasing these attractors merge and as a result double scroll chaotic attractor appears.

We investigated the system (1) with changing of the parameter α and of coupling coefficient γ . Other parameters were fixed in the values: $a=-8/7$, $b=-5/7$, $\beta=-22$. The number of oscillators in the chain was $N=30$ and $N=1024$. At the value of α is more than $\alpha \approx 8.78$ period-one cycle temporal regimes with different spatial structures coexist in the system. Choosing spatially-periodic initial values one can obtain attractors characterized by exact space periodicity. These attractors can be considered as running waves rotating along the ring with constant phase velocity because oscillations in the every site has equal amplitude and equal phase shift relatively to the neighbor oscillator. We investigated the waves with spatial periods of 6, 10, 15 oscillators (for the 30-sites chain). With increasing of the parameter α these waves undergo bifurcations which lead to complicating of their temporal behavior. At small coupling we observed period-doubling bifurcations cascades of finite length. The number of the bifurcations increases with decreasing of the coupling and tends to infinity at zero coupling. The every cascade is ended by the tori birth bifurcation which is followed by the destroying of the torus and the transition to chaos. At larger coupling the period-doubling bifurcations do not take place and the torus appears on the base of the period-one cycle. The fig. 1 demonstrates a diagram of typical regimes on the plane of parameters γ - α for the family of regimes originated from the running wave with spatial period $\Lambda=15$. The region of stability of this family is bounded by lines marked by «o» (lines 1, 5). The line 1 bounds this region from the right. With crossing the line the regimes with wavelength $\Lambda=15$ lose their stability by sudden way and the system transits to waves with larger spatial periods. The line 5 marks destroying of periodic spatial structure by soft way. Near this line the spatial structure begins to change its form and over it the regime awfully «forgets» its original spatial structure. Over the line 1 and before the line 2 the stable period-one cycle is observed. On the line 2 the system transits to quasi-periodic behavior. This is the line of the torus 1T

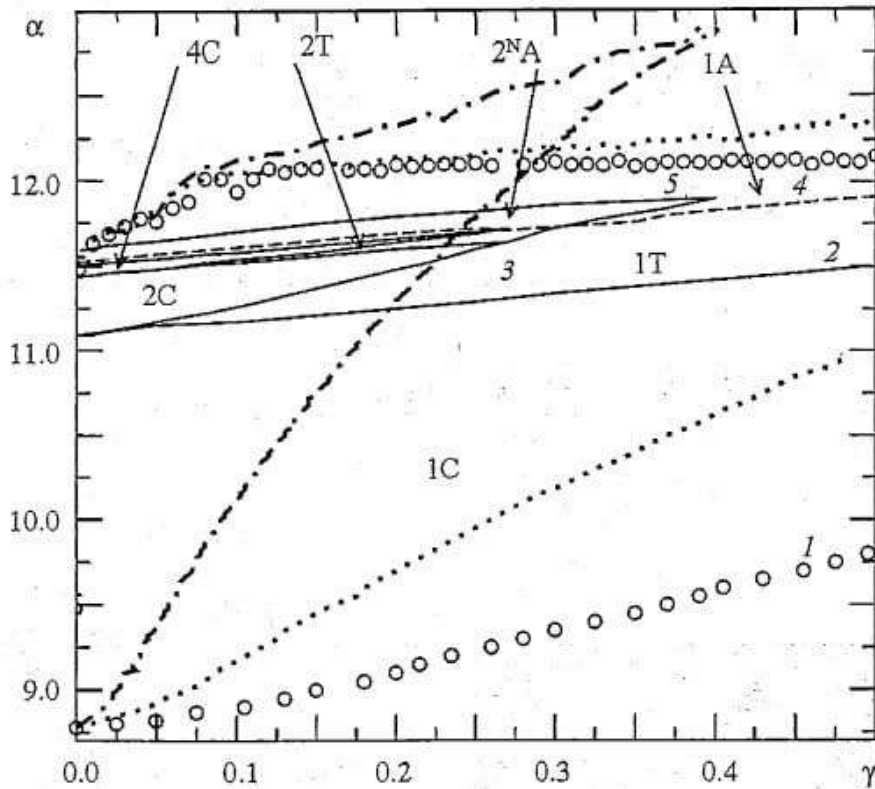


Fig. 1. Diagram of regular and chaotic regimes originated from the wave with spatial period $\Lambda=15$ (\circ); $\Lambda=10$ (dot lines); $\Lambda=6$ (dot-dashed line)

birth. At large coupling the system evaluates on the base of this torus and demonstrates transition to chaos through the torus breaking (dashed line 4 in the fig.1). Over this line a one-band chaotic attractor exists. At small coupling the transition to chaos occurs through the period-doubling bifurcations and quasi-periodic behavior originated from cycles with double periods. This region of smaller coupling is bounded by the line 3. In the fig. 1 we also built lines which bound regions of existence of regimes originated from running waves with spatial periods $\Lambda=10$ (dot lines) and $\Lambda=6$ (dot-dashed lines). It is seen that regimes with longer wavelengths occupy larger regions on the parameters plane. The short-lengths waves exist only at rather small coupling. The waves with minimal possible spatial period $\Lambda=2$ (π -waves) were not found in the system possibly because of very narrow region of existence. The bottom boundaries for regimes with different wavelengths coincide at the values of parameters $\alpha=8.78$, $\gamma=0$. Hence, the all mentioned period-one running waves originated from the same equilibrium. The upper boundaries coincide at the values $\alpha\approx 11.65$, $\gamma=0$ that corresponds to transition to one-band chaotic attractor in the uncoupled oscillator.

All bifurcations of regular regimes do not change their space periodicity. Oscillations remain exactly spatially periodic with the same periods until the transition to temporal chaos. In the chaotic region the spatial behavior changes its character. The exact space-periodicity destroys immediately after the transition to temporal chaos, but chaotic regimes preserve the space-periodicity in the average. Spatio-temporal diagrams and spatial spectra for these regimes are presented in the fig. 2. They are built for the one-band chaotic regime with averaged spatial period of $\Lambda=16$ for the chain of 1024 elements. The abscissa axis of the spatio-temporal diagram denotes the sites in the chain, the ordinate axis denotes the Poincare section of the variable x_i in the every oscillators observed for the long interval of time. Three parts of the figure demonstrate serial destroying of spatial structure with decreasing of coupling: at $\gamma=0.15$ (a), $\gamma=0.05$ (b), and

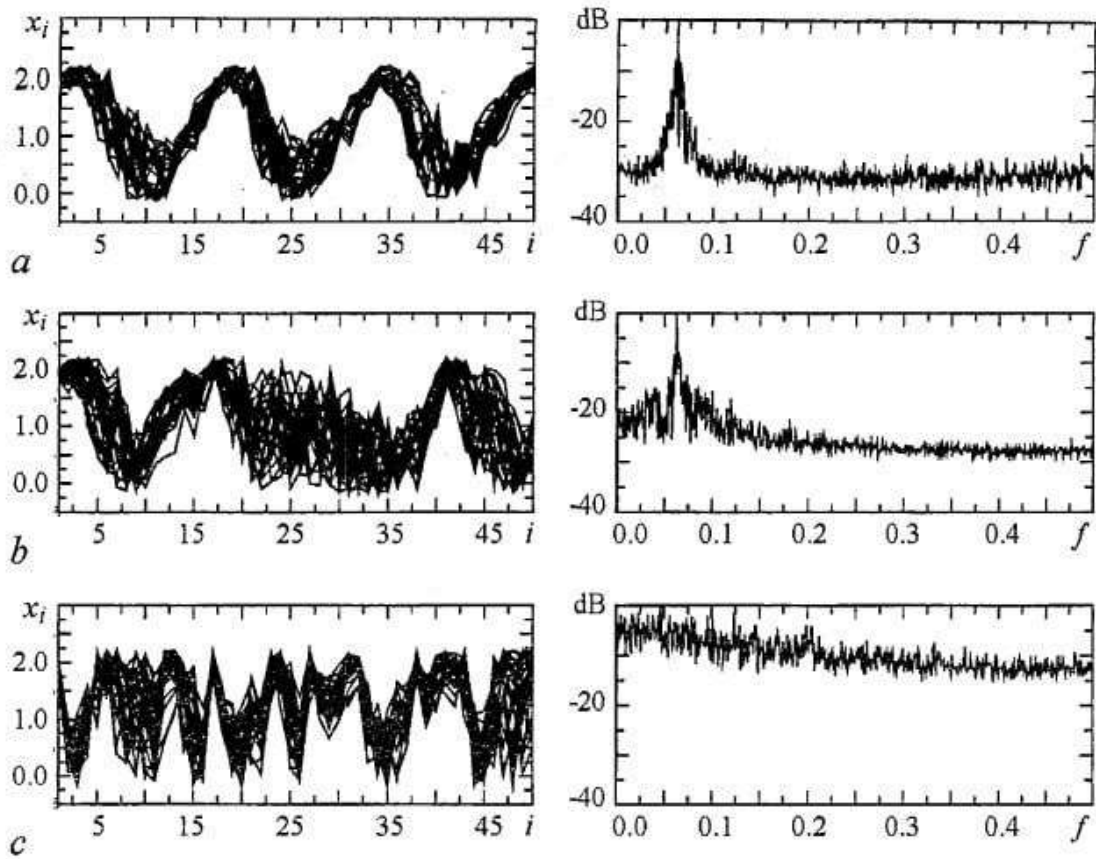


Fig. 2. Destroying of the averaged spatial structure of the wave at $\alpha=11.78$, with decrease of coupling: $\gamma=0.15$ (a); 0.05 (b); 0.02 (c)

$\gamma=0.02$ (c). The first case corresponds to averaged spatial periodicity with sharp peak in the spatial spectrum (fig. 2, a). Then, with decreasing of coupling the spatial diagram begins to lose its periodic structure that is accompany by widening of the peak in the spatial spectrum (fig. 2, b) and as a result at small coupling the periodic spatial structure awfully disappears and the spectrum becomes plate (fig. 2, c). It is interesting that the destroying of periodic spatial structure with decreasing of coupling takes place only for one-band temporal chaos. If we chose α correspondent to many-band attractor regimes the averaged space-periodicity exists until neglect small couplings.

The periodic spatial structure in the chain is connected with coherence of oscillations on main peaks in the temporal spectra of neighbor oscillators. The structure is preserved until the coherence function on the main peaks is equal to 1. The fig. 3 demonstrates changing in the power spectrum and in the correspondent coherent function for the cases described in the fig. 2. When main harmonics in the spectra are coherent the chaotic regime is almost spatially periodic. Decreasing of coupling leads to decreasing of the coherence function except main frequencies (fig. 3, b). This is accompany by gradual destroying of spatial periodicity. Then if the coherence for main peaks becomes smaller than 1 (fig. 3, c) the periodic spatial structure awfully breaks.

Summarizing the contents of our research we can conclude that the developing of temporal dynamics in the ring of identical period-doubling oscillators with diffusing coupling does not lead to changing of spatial periodicity until the transition to temporal chaos. In the chaotic region exact spatial periodicity is changed by the periodicity in the averaged. The destroying of the averaged periodic structure takes place only for developed one-band chaotic attractor. It occurs both with developing of chaos and with decreasing of coupling coefficient and is accompanied by the loss of coherence on main

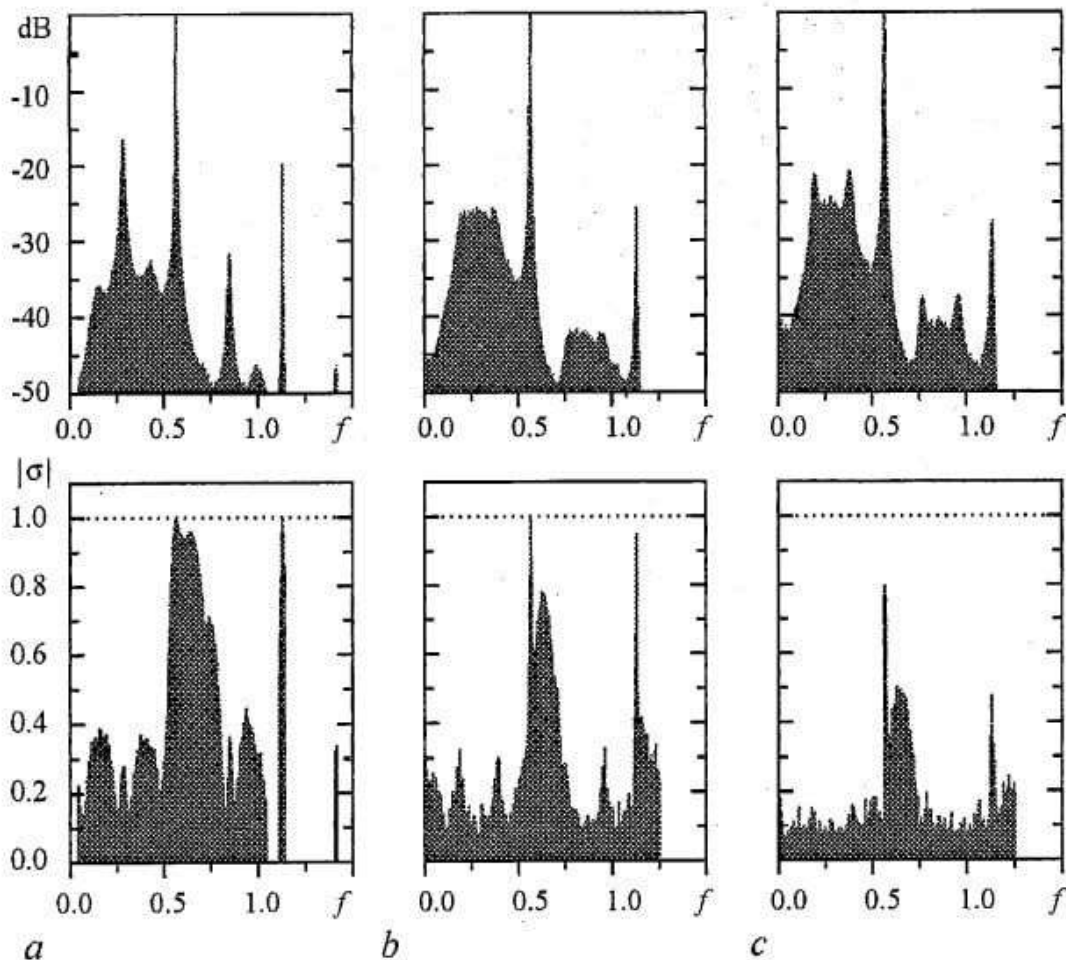


Fig. 3. Loss of the coherence between dynamics of the neighbor oscillators at $\alpha=11.78$, with the coupling decrease $\gamma=0.15$ (a); 0.05 (b); 0.02 (c)

peaks in the temporal spectra of neighbor oscillators. The family of regimes with determine spatial period exists in the limited range of the coupling. If the coupling is increased over the determine maximal values the system transits to a regime with larger spatial period.

The authors thanks to the Fond of Civil Research Development (Grant REC 006) for partial financial support.

References

1. Kaneko K. Simulating physics with coupled map lattices // Formation, dynamics and statistics of patterns. Singapore. World Scientific. 1989. Vol. 1. Pp. 1-54.
2. Kaneko K. Lyapunov analysis and information flow in coupled map lattices // Physica D. 1986. Vol. 23. Pp. 436-447.
3. Kaneko K. Towards thermodynamics of spatiotemporal chaos // Progr. of Theor. Physics. 1989, № 99. Pp. 263-287.
4. Kuznetsov A.P., Kuznetsov S.P. Spatial structures in dissipative media near the chaos threshold // Radiophysics. 1990. Vol. 34, № 2. Pp. 142-146.
5. Matthews P.C., Strogatz S.H. Phase diagram for the collective behavior of limit-cycle oscillators // Phys. Rev. Lett. 1990. Vol. 65, № 14. Pp. 1701-1704.
6. Matthews P.C., Mirollo R.E., Strogatz S.H. Dynamics of a large system of coupled nonlinear oscillators // Physica D. 1990. Vol. 52. Pp. 293-331.

7. *Daido H.* Onset of cooperative entrainment in limit-cycle oscillators with uniform all-to-all interactions: bifurcation of the order function // *Physica D.* 1996. Vol. 91. Pp. 24-66.

8. *Tass P.* Phase and frequency shifts in a population of phase oscillators // *Phys. Rev. E.* 1997. Vol. 56, № 2. Pp. 2043-2060.

9. *Bonilla L.L., Vicente C.J. P., Spigler R.* Time-periodic phases in populations of nonlinearly coupled oscillators with bimodal frequency distributions // *Physica D.* 1998. Vol. 113. Pp. 79-97.

10. *Yeung M.K.S., Strogatz S.H.* Time delay model of coupled oscillator // *Phys. Rev. Lett.* 1999. Vol. 82, № 3. Pp. 648-651.

11. *Daido N.* Strange waves in coupled-oscillator arrays: mapping approach // *Phys. Rev. Lett.* 1997. Vol. 78, № 9. Pp. 1683-1684.

12. *Bressloff P.C., Coombes S., Souza B.* Dynamics of a ring of pulse-coupled oscillators: group theoretical approach // *Phys. Rev. Lett.* 1997. Vol. 79, № 15. Pp. 2791-2794.

13. *Bressloff P.C., Coombes S.* Running waves in a chain of pulse-coupled oscillators // *Phys. Rev. Lett.* 1998. Vol. 80, № 21. Pp. 4815-4818.

14. *Pando C.L.* Effects of a periodic perturbation on a discrete-time model of coupled oscillators // *Phys. Lett. A.* 2000. Vol. 273. Pp. 70-79.

15. *Anishchenko V.S., Aranson I.S., Postnov D.E., Rabinovich M.I.* Spatial synchronization and bifurcations of chaos developing in a chain of coupled self-oscillators // *Dokl. Akad. Nauk SSSR.* 1986. Vol. 28, № 5. Pp. 1120-1124.

16. *Matias M.A., Perez-Munuzuri V., Marino I.P., Lorenzo M.N., Perez-Villar V.* Size instabilities in ring of chaotic synchronized systems // *Europhys. Lett.* 1997. Vol. 37, № 6. Pp. 379-384.

17. *Matias M.A., Guemez J., Perez-Munuzuri V., Marino I.P., Lorenzo M.N., Perez-Villar V.* Observation of a fast rotating wave in rings of coupled chaotic oscillators // *Phys. Rev. Lett.* 1997. Vol. 78, № 2. Pp. 219-222.

18. *Marino I.P., Perez-Munuzuri V., Perez-Villar V., Sanchez E., Mat M.A.* Interaction of chaotic rotating waves in coupled rings of chaotic cells // *Physica D.* 2000. Vol. 128. Pp. 224-235.

19. *Hu G., Zhang Y., Cerdeira H.A., Chen S.* From low-dimensional synchronous chaos to high-dimensional desynchronous spatiotemporal chaos in coupled systems // *Phys. Rev. Lett.* 2000. Vol. 85, № 16. Pp. 3377-3380.

20. *Komuro M., Tokunaga R., Matsumoto T., Chua L.O., Hotta A.* Global bifurcation analysis of the double scroll circuit // *Int. J. of Bifurcation and Chaos.* 1991. Vol. 1, № 1. Pp. 139-182.

Saratov State University, Russia

Recievd 28.08.2003

УДК 517.9

**ЭВОЛЮЦИЯ БЕГУЩИХ ВОЛН
К ПРОСТРАНСТВЕННО-ВРЕМЕННОМУ ХАОСУ: ВЗАИМОДЕЙСТВИЕ
ВРЕМЕННОЙ И ПРОСТРАНСТВЕННОЙ ДИНАМИКИ В КОЛЬЦЕ
ГЕНЕРАТОРОВ С УДВОЕНИЕМ ПЕРИОДА**

А. Шабунин, В. Астахов, А. Акопов

В данной работе рассматривается переход от регулярных бегущих волн к развитому пространственно-временному хаосу в цепочке осцилляторов с

удвоением периода. Исследуются типичные бифуркации, которые происходят на основе выбранного режима бегущей волны от цикла периода один до развитого временного хаоса. Обнаружено, что до перехода к временному хаосу колебания остаются пространственно периодическими. В области хаоса точная пространственная периодичность сменяется периодичностью в среднем. Разрушение усредненной пространственно-периодичной структуры связано с потерей когерентности на основных частотах во временных спектрах соседних генераторов в цепочке.



Shabunin Alexey Vladimirovich graduated from Saratov State University in 1990. He is an associate professor of Radiophysics and Nonlinear Dynamics Department of the Saratov State University, Ph.D. in Physics and Mathematics since 1998. His scientific interests include nonlinear dynamics, theory of oscillations, synchronization and chaos control. He is an author of more than 50 scientific publications. E-mail: alexey@chaos.ssu.runnet.ru



Astakhov Vladimir Vladimirovich graduated from Saratov State University in 1980. He is a Doctor of Science in Physics and Mathematics since 1999. He works as a professor of Radiophysics and Nonlinear Dynamics Department of the Saratov State University. His scientific interests are: nonlinear dynamics, theory of oscillations, synchronization and chaos control. He is an author of more than 80 scientific publications. E-mail: astakhov@chaos.ssu.runnet.ru



Akopov Artem Alexandrovich was born Sochi (1973). He graduated from Physical faculty of the Saratov State University (2000). Now he is a postgraduate student of Radiophysics and Nonlinear Dynamics Department of SSU. He is an author of 6 scientific publications.



Izv. VUZ «AND», vol. 11, № 3, 2003

FLUCTUATIONAL TRANSITIONS ACROSS LOCALLY-DISCONNECTED AND LOCALLY-CONNECTED FRACTAL BASIN BOUNDARIES

A.N. Silchenko, S.Beri, D.G. Luchinsky and P.V.E. McClintock

We study fluctuational transitions in a discrete dynamical system that has two coexisting attractors in phase space, separated by a fractal basin boundary which may be either locally-disconnected or locally-connected. It is shown that, in each case, transitions occur via an accessible point on the boundary. The complicated structure of paths inside the locally-disconnected fractal boundary is determined by a hierarchy of homoclinic original saddles. The most probable escape path from a regular attractor to the fractal boundary is found for the each type of boundary using both statistical analyses of fluctuational trajectories and the Hamiltonian theory of fluctuations.

1. Introduction

The stability of nonlinear multistable systems in the presence of noise is of great importance for practical applications [1,2]. It is well known that nonlinear dynamical systems can demonstrate sensitivity to initial conditions, even in the absence of limit sets with complex geometrical structure in their phase space. The reason lies in the complex structure of the basins of attraction, which may be fractal [3-8], thus raising some challenging and difficult problems. For example, how does a fluctuational transition take place across a fractal basin boundary (FBB)? What is the difference, if any, in the transition mechanism for the different types of FBB? If transitions across FBBs are characterised by general features, a knowledge of them could considerably simplify investigations of stability and control for chaotic dynamical systems, both of which are topical problems of broad interdisciplinary interest [9-11].

A promising approach to this problem is based on the analysis of fluctuations in the limit of small noise intensity: the system fluctuates to remote states along most probable deterministic paths [12-14] that correspond to rays in the WKB-like asymptotic solution of the Fokker-Planck equation [15]. The approach has been extended to chaotic systems, both continuous and discrete, [16-19]. It was shown recently that the homoclinic tangencies responsible for fractalization of the basins cause a decrease in the activation energy [20]. However, there are still no theoretical predictions about the mechanism of escape in the case of an FBB. Unsolved problems include the uniqueness of the escape path, the form of the boundary conditions on the FBB and, as already mentioned, whether or not the mechanism of escape depends on the type of FBB under consideration.

In this paper, we describe the mechanisms of fluctuational transition for two different types of FBB, namely, locally-disconnected (LD) and locally-connected (LC)

FBBs. We show below that in spite of the large qualitative differences between these types of FBB, their mechanisms of fluctuational transition are characterised by a universal common feature.

2. Transitions across a locally-disconnected FBB

There are known to be several types of FBB in different dynamical systems [4-8]. The LD FBB represents the simplest and commonest, and it is the only type of FBB to have been observed in experiments [4,5]. As we will show below, the mechanism of fluctuational transition across it is determined primarily by its deterministic structure, which enables us to infer that the mechanism must be generic to all systems with FBBs of this kind. To reveal the transition mechanism across an LD FBB, we take as our model the two-dimensional map introduced by Holmes [21]

$$\begin{aligned} x_{n+1} &= f_1(x_n, y_n) = y_n \\ y_{n+1} &= f_2(x_n, y_n, \xi_n) = -bx_n + dy_n - y_n^3 + \xi_n, \end{aligned} \quad (1)$$

where ξ_n is white Gaussian noise with $\langle \xi_n \rangle = 0$, and $\langle \xi_n \xi_m \rangle = 2D\delta_{nm}$. In what follows we will adopt the notation $\mathbf{x}_n = \{x_n, y_n\}$, $\mathbf{f} = \{f_1, f_2\}$ and $\xi_n = \{0, \xi_n\}$. Due to symmetry, the system (1) has pairs of coexisting attractors for $b=0.2$ and $2.0 \leq d \leq 2.745$. Their basins are separated by a boundary that may be either smooth or fractal depending on the chosen parameter values. We choose for our studies $b=0.2$ and $d=2.65$, which corresponds to there being two coexisting stable points of period 4 whose basins are separated by an LD FBB (see Fig.1). The fractal dimension of the boundary is equal to 1.8451.

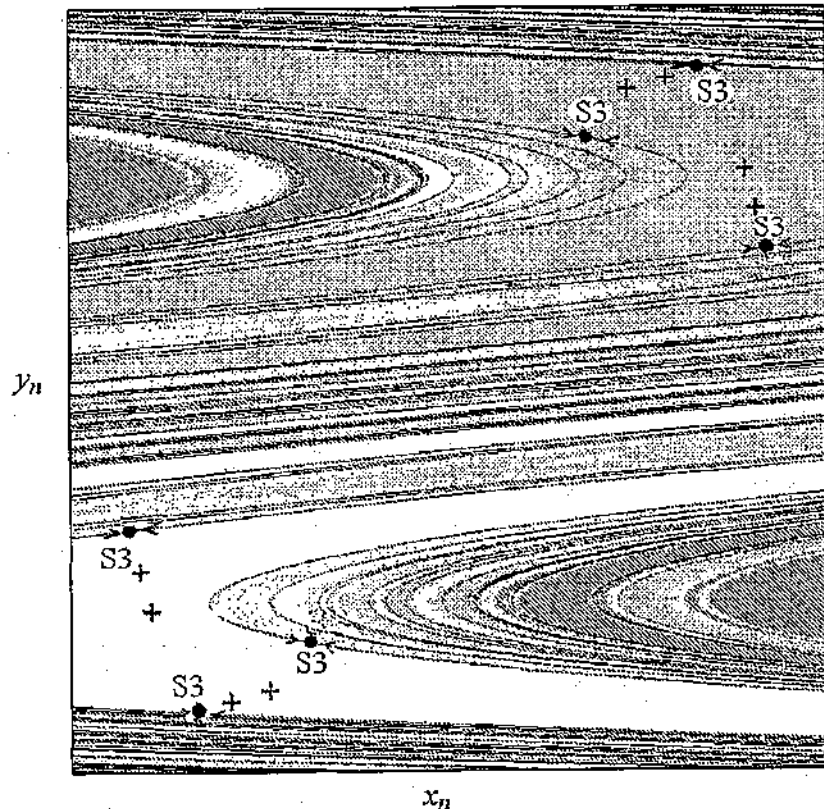


Fig. 1. The coexisting stable points of period 4 (black crosses) and their basins of attraction, shown in grey and white respectively. The accessible boundary saddle points of period 3 are indicated by the small filled circles S3. Their stable manifolds are drawn as solid black lines

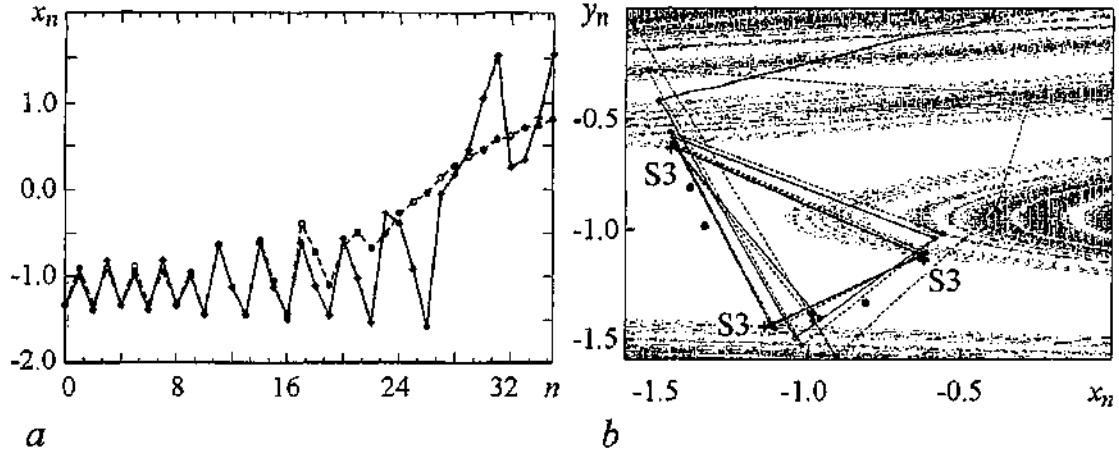


Fig. 2. (a) The most probable escape path (dashed line) connecting the stable point of period 4 with the period-3 saddle cycle lying on the fractal boundary obtained from the numerical simulations with $D=10^{-5}$. The optimal path found by the solution of the boundary-value problem is shown as a solid line. (b) Two-dimensional plot of the paths presented in (a)

To find the boundary conditions on the LD FBB, and the optimal fluctuational force steering the system (1) from one coexisting attractor to another, we will make use of an analogy between energy-optimal control and noise-induced escape from a basin of attraction. We have modelled (1) numerically, exciting the system with weak noise and collecting both the escape trajectories between the attractors and also the corresponding noise realisations inducing the transitions. By ensemble-averaging a few hundred such escape trajectories and noise realisations, we have obtained the optimal escape path (see Fig. 2) and corresponding optimal force shown in Fig. 3. In the case of the LD FBB, these results allow us both to determine the boundary conditions near the boundary, and to demonstrate the uniqueness of the most probable escape path (MPEP). A typical optimal escape path is shown in Fig. 2, a. A simple analysis of the optimal path shows that the system (1) leaves the stable point of period 4 and moves to the LD FBB, crossing it at a point of period 3 located near, or directly on, the LD FBB (see Fig. 2, a). Simple calculations have shown that a saddle point of period 3, S3, in Fig. 1 and Fig. 2, b (with multipliers $\rho_1=0.001218$ and $\rho_2=6.566269$) does exist for the chosen parameter values and that it lies on the boundary. Moreover, its stable manifold (solid black line in Fig. 1) is dense in the boundary and detaches the open neighborhood including the attractor from the LD FBB itself, allowing us to classify it as an accessible boundary point [22]. It is

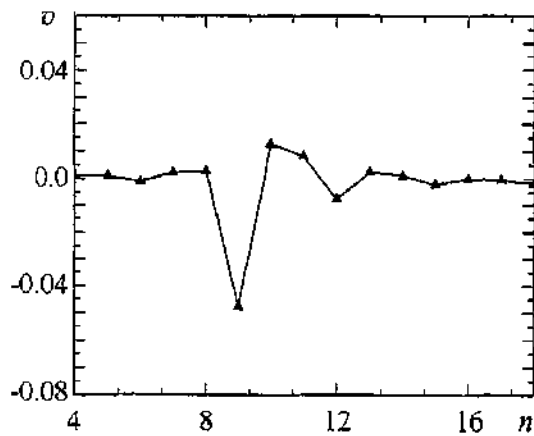


Fig. 3. The optimal fluctuational force v obtained from the Monte-Carlo simulations

well known that the energy-optimal path is given by that path which minimises the sum $S = 1/2 \sum_{n=1}^N \xi_n^2$, where ξ_n is the noise realization moving the system from one attractor to the other. The extremal problem can easily be solved by taking (1) into account by means of Lagrangian multipliers λ_n [18], yielding the following Lagrangian for minimization:

$$L = 1/2 \sum_{n=1}^N \xi_n^T \xi_n + \sum_{n=1}^N \lambda_n^T (x_{n+1} - f(x_n) - \xi_n),$$

where x_{n+1} , $f(x_n)$ and ξ_n are the two-dimensional vectors defined in (1). Further, varying L with respect to ξ_n and x_n we get the following two-dimensional map:

$$\begin{aligned}
x_{n+1} &= y_n, \\
y_{n+1} &= -bx_n + dy_n - y_n^3 + \lambda_n^y, \\
\lambda_{n+1}^x &= (d-3x_{n+1}^2)\lambda_n^x/b - \lambda_n^y/b, \\
\lambda_{n+1}^y &= \lambda_n^x.
\end{aligned} \tag{2}$$

Equations (2) are supplemented by the following boundary conditions

$$\lim_{n \rightarrow \infty} \lambda_n = 0, \quad \mathbf{x}_n^0 \in \text{attractor}, \quad \mathbf{x}_n^1 \in \text{LD FBB}. \tag{3}$$

In fact, the unique energy-optimal trajectory along which S takes its minimal value is a heteroclinic trajectory in the four-dimensional phase space of the system (2), connecting the stable point of period 4 with a point on the boundary. At this stage, we are ready to solve the corresponding boundary-value problem for (2) numerically. This can be done via a procedure involving shooting from a very small neighbourhood of the chosen saddle point, parametrizing the initial conditions as points lying on a two-dimensional unstable manifold of this saddle point, characterized by the appropriate radius r and angle ϕ , and with subsequent selection of the trajectory minimizing S . Initial values for the coordinates can be parametrised by the distance from the initial state and angular position; the initial values for the λ_n are obtained by using the equations for the linearised manifold. During the evolution of the system (2) far from its initial state, we collect the values $S_{n+1} = S_n + 1/2 \lambda_n^T \lambda_n$ and plot S_n as a function of the two parameters. Thus, the global minimum of the activation energy gives us the parameters corresponding to the optimal escape path. We emphasise that the optimal trajectory is physically real, and not just a mathematical abstraction. In fact, when the system (1) is driven by noise whose intensity tends to zero, the escape events become exponentially rare, but they take place in an almost deterministic way following very closely the deterministic trajectory of (2). As clearly seen from Fig. 2, the phase trajectory in (2) along which S takes its minimal value coincides with the MPEP obtained by taking an ensemble average of successful trajectories. Note that no action is required to bring the system to the other attractor after it has hit the FBB, and neither is there any possibility of controlling the motion inside the LD FBB.

Analysis of the structure of escape paths inside the LD FBB has shown that homoclinic saddle points play a key role. In the system (1), we observe an infinite sequence of saddle-node bifurcations of period 3,4,5,6..., occurring at parameter values $d_3 < d_4 < d_5 < d_6 \dots$ and caused by sequential tangencies of the stable and unstable manifolds of the saddle point O at (0,0). The homoclinic orbits appearing as the result of these bifurcations were classified earlier as *original saddles* and it was also shown that their stable and unstable manifolds cross each other in hierarchical sequence [22]. To characterize this hierarchical relationship between original saddles it is reasonable to use the ratio

$$\mu = |\lambda_{st}(S)|/|\lambda_{un}(S)|,$$

where $\lambda_{st}(S)$ and $\lambda_{un}(S)$ are the stable and unstable eigenvalues of the Jacobian matrix of (1) at the saddle point S. Simple calculations have shown that, for the original saddles of period 3,4,5,6... in (1), the following hierarchical sequence of index μ values occurs: $\mu_3=3.566$, $\mu_4=3.301$, $\mu_5=3.249$, $\mu_6=3.142$. It is known that unstable periodic orbits embedded within a chaotic saddle define a distribution of the natural measure on it both for hyperbolic and nonhyperbolic dynamical systems [23,24]. In particular, the natural measure η on a two-dimensional chaotic nonattracting set is concentrated along its unstable manifold and can be represented via unstable eigenvalues of unstable orbits: $\eta(C) = \sum 1/\lambda_{un}(x_i)$, where C is the region of phase space containing the chaotic saddle,

$\lambda_{un}(x_i)$ is the eigenvalue corresponding to the unstable manifold and the summation is over all the unstable orbits x_i in C [24] (cf. [23]). A statistical analysis of escape trajectories has shown that these probabilities demonstrate a hierarchical interrelation [25], which is in a good agreement with the distribution of the natural measure on the chaotic saddle O forming the LD FBB.

3. Transitions across a locally-connected FBB

We now consider the same escape problem, but in a system possessing an LC FBB. This type of FBB is generally observed in two-dimensional noninvertible analytic and nonanalytic maps [4,26]. We take as our model a typical quadratic conformal map:

$$\begin{aligned}x_{n+1} &= x_n^2 - y_n^2 + 0.7x_n + \xi_n^1, \\y_{n+1} &= 2x_n y_n + 0.7x_n + 0.5y_n + \xi_n^2,\end{aligned}\tag{4}$$

where ξ_n^1, ξ_n^2 are statistically independent sources of white, Gaussian, noise of zero mean that are of the same intensity D as each other. This map has stable points at the origin and at infinity, separated by the LC FBB. The boundary contains an infinite set of repelling points and, in this case, no stable or saddle points. Note that noise-induced escape from the attractor surrounded by the LC FBB in (4) was considered earlier in the pioneering work of Grassberger [18], who succeeded in calculating the optimal escape path, albeit without finding the boundary condition on the LC FBB or the mechanism of escape.

To find the boundary condition on the LC FBB and the optimal escape path, we use exactly the same technique as in the case of the LD FBB, above. The results of our calculations are presented in Fig. 4. As clearly seen from this figure, the system (4) leaves the stable point O at the origin along the unique optimal escape path and approaches the LC FBB at the unique point shown in Fig. 4, *a*. Moreover, our calculations have shown that the optimal fluctuational force (see Fig. 4, *b*) becomes equal to zero at this moment. According to our previous results, this means that the system (4) reached the boundary at this point, and its further relaxation to infinity is noise-free and completely specified by the deterministic structure of the FBB. Our calculations have shown that the boundary point A corresponds exactly to the repelling boundary point of period 9, which plays the role of the unique boundary condition on this LC FBB. These

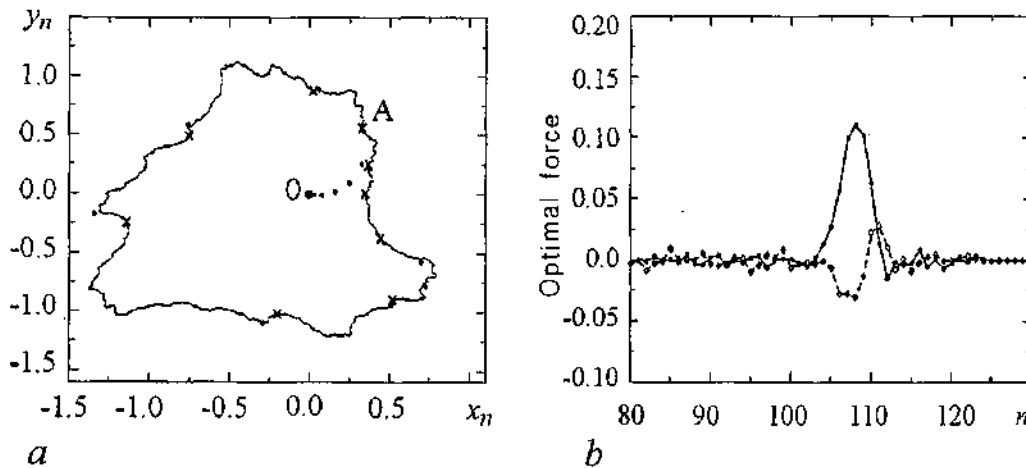


Fig. 4. (a) The locally-connected FBB (solid closed curve), unstable nodes of period 9 (crosses) and points of the optimal escape path obtained from the Monte-Carlo simulations (filled circles) with $D=5 \cdot 10^{-3}$. (b) Components of the optimal fluctuational force: x (solid line) and y (dashed line)

the corresponding four-dimensional extended map. To approach an understanding of why this repelling point should play the role of the boundary condition, it is necessary to look more closely at the structure of the LC FBB, which is the Julia set $J(\mathbf{x})$. It is well known that the Julia set contains a dense set of repelling points [27]. However, these points are not all the same, and they may be classified in terms of their local instability. Indeed, there are two types of repelling points forming the LC FBB in (4), namely, unstable nodes and unstable focuses. Every unstable node on the LC FBB has a part of its unstable manifold connecting it to the stable point O and lying fully inside its basin of attraction, whereas this is not true of a focus. By definition, a point \mathbf{x} is accessible if there is a continuous curve $\gamma: [0, \infty) \rightarrow C$ for which $\gamma(n)$ lies in the basin of attraction of \mathbf{x} for all n and $\lim_{n \rightarrow \infty} \gamma(n) = \mathbf{x}$. This fact enable us to conclude that unstable nodes form a countable set of accessible points on the LC FBB. The presence of a countable set of accessible points was rigorously proven [28] quite recently. Our calculations have shown that accessible boundary points are distributed nonuniformly on the boundary, and that their multipliers, have different values which, in turn, may lead to a hierarchal interrelationship between them. The quest for such a hierarchy, and further generalizations of our approach presented above, represent goals of our future investigations.

4. Conclusions

In conclusion, we have studied fluctuational transitions between coexisting regular attractors separated by both the LD and LC FBB. We have shown that an accessible point on the FBB plays the role of a unique boundary condition for both types of FBB. Our statistical analyses of fluctuational trajectories have yielded solutions of the boundary-value problem for both types of FBB, and have revealed the optimal fluctuational forces moving the systems (1) and (4) from one attractor to the other. We were also able to find the unique optimal escape path in both cases. The original saddles forming the homoclinic structure of the system (1) play a key role in the formation of the escape paths inside the LD FBB, and the difference in their local stability defines the hierarchical relationship between them. The results obtained can be applied directly to the other maps and flows having the same type of FBB.

The research has been supported by the Engineering and Physical Sciences Research Council (UK) and INTAS.

References

1. *Stratonovich R.L.* Topics in the Theory of Random Noise (Mathematics and its Applications). Taylor and Francis, 1967.
2. *Anishchenko V. S., Neiman A.B., Vadivasova T.E., Shimansky-Geier L., Astakhov V.V.* Nonlinear dynamics of Chaotic and Stochastic Systems. Springer Verlag, 2001.
3. *Ott E.* Chaos in Dynamical Systems. Cambridge University Press, 2002.
4. *McDonald S.W., Grebogi C., Ott E., and Yorke J.A.* Fractal basin boundaries // *Physica D.* 1985. Vol. 17. P. 125.
5. *Cartwright M.L. and Littlewood J.E.* // *Ann. Math.* 1951. Vol. 54. P. 1; *Moon F.C. and Li G.-X.* // *Phys. Rev. Lett.* 1985. Vol. 55. P. 1439.
6. *Sommerer J.C., and Ott E.* A physical system with qualitatively uncertain dynamics // *Nature.* 1993. Vol. 365. P. 135.
7. *Nusse H.E., and Yorke J.A.* Basins of attraction // *Science.* 1996. Vol. 271. P. 1376.
8. *Hunt B.R., Ott E., Rosa E.* Sporadically fractal basin boundaries of chaotic systems // *Phys. Rev. Lett.* 1999. Vol. 82. 3597.

9. *Fradkov A.L. and Pogromsky A.Y.* Introduction to control of oscillations and chaos // Series on Nonlinear Science A. 1998. Vol. 35. World Scientific, Singapore.
10. *Boccaletti S., Grebogi C., Lai Y.C., Mancini H., Maza D.* The control of chaos: theory and applications // Phys. Rep. 2000. Vol. 39. P. 103.
11. *Shinbrot T., Grebogi C., Ott E. and Yorke J.A.* Using small perturbations to control chaos // Nature (London). 1993. Vol. 363. P. 411; *Auerbach D., Grebogi C., Ott E. and Yorke J.A.* Controlling chaos in high dimensional systems // Phys. Rev. Lett. 1992. Vol. 69. P. 3479.
12. *Onsager L., and Machlup S.* Fluctuations and irreversible processes // Phys. Rev. 1953. Vol. 91. P. 1505.
13. *Dykman M.I., McClintock P.V.E., Smelyanskiy V.N., Stein N.D., and Stocks N.G.* Optimal paths and the prehistory problem for large fluctuations in noise driven systems // Phys. Rev. Lett. 1992. Vol. 68. P. 2718.
14. *Luchinsky D.G., Maier R.S., Mannella R., McClintock P.V.E., Stein D.L.* Experiments on critical phenomena in a noisy exit problem // Phys. Rev. Lett. 1997. Vol. 79. P. 3117; *Luchinsky D.G.* On the nature of large fluctuations in equilibrium systems: observation of an optimal force // J. Phys. A. 1997. Vol. 30. P. L577; *Luchinsky D.G. and McClintock P.V.E.* Irreversibility of classical fluctuations studied in analogue electrical circuits // Nature. 1997. Vol. 389. P. 463.
15. *Freidlin M.I. and Wentzel A.D.* Random Perturbations in Dynamical Systems. Springer, New York, 1984.
16. *Kautz R.L.* Activation energy for thermally induced escape from a basin of attraction // Phys. Lett. A. 1987. Vol. 125. P. 315.
17. *Beale P.D.* Noise-induced escape from attractor in one-dimensional maps // Phys. Rev. A. 1989. Vol. 40. P. 3998.
18. *Grassberger P.* Noise-induced escape from attractors // J. Phys. A: Math. Gen. 1989. Vol. 22. P. 3283.
19. *Graham R., Hamm A., and Tel T.* Nonequilibrium potentials for dynamical systems with fractal attractors or repellers // Phys. Rev. Lett. 1991. Vol. 66. P. 3089.
20. *Soskin S.M., Arrayás M., Mannella R., and Silchenko A.N.* Strong enhancement of noise-induced escape by nonadiabatic periodic driving due to transient chaos // Phys. Rev. E. 2001. Vol. 63. P. 051111.
21. *Holmes P.* A nonlinear oscillator with a strange attractor // Phil. Trans. R. Soc. 1979. Vol. A292. P. 419.
22. *Grebogi C., Ott E., and Yorke J. A.* Basin boundaries metamorphoses - changes in accessible boundary orbits // Physica D. 1987. Vol. 24. P. 243.
23. *Grebogi C., Ott E., and Yorke J. A.* Unstable periodic orbits and the dimensions of multifractal chaotic attractors // Phys. Rev. A. 1988. Vol. 37. P. 1711.
24. *Dhamala M. and Lai Y.-C.* The natural measure of nonattracting chaotic sets and its representation by unstable periodic orbits // Int. J. Bif. Chaos. 2002. Vol. 12. P. 2991.
25. *Silchenko A.N., Luchinsky D.G., and McClintock P.V.E.* Noise-induced escape through a fractal basin boundaries // Physica A, to be published.
26. *Gardini L., Mira C., Barugola J., Cathala J.C.* Chaotic Dynamics in Two-Dimensional Noninvertible Maps. World Scientific Publishing, 1996.
27. *Devaney R.L.* Introduction to Chaotic Dynamical Systems. Addison-Wesley, New-York, 1989.
28. *Bhattacharjee R., and Devaney R.L.* Tying hairs for the structurally stable exponentials // Ergodic Theory and Dynamical Systems. 2000. Vol. 20. P. 1603.

Department of Physics,
Lancaster University, USA
Saratov State University, Russia

Received 01.08.03

ФЛУКТУАЦИОННЫЕ ПЕРЕХОДЫ ЧЕРЕЗ ЛОКАЛЬНО-НЕСВЯЗАННЫЕ И ЛОКАЛЬНО-СВЯЗАННЫЕ ФРАКТАЛЬНЫЕ ГРАНИЦЫ БАССЕЙНОВ

A. N. Silchenko, S. Veri, D. G. Luchinsky, P. V. E. McClintock

Мы изучаем флуктуационные переходы в дискретной динамической системе, которая имеет два сосуществующих аттрактора в фазовом пространстве, разделенных фрактальными границами бассейнов, которые могут быть или локально-несвязанными или локально-связанными. В каждом случае переходы осуществляются через общедоступную точку на границе. Сложная структура путей внутри локально-несвязанных фрактальных границ определяется иерархией гомоклинических первоначальных седел. Наиболее вероятная траектория выхода с регулярного аттрактора к фрактальной границе найдена для каждого типа границы с использованием как статистического анализа флуктуационных траекторий, так и Гамильтоновой теории флуктуаций.



Silchenko Alexander Nikolaevich was born on 18 May 1972 in Saratov. He gained his undergraduate degree in physics from Saratov State University in 1994. In 1998 he got a degree of Candidate of Physical and Mathematical Sciences (PhD) from Saratov State University. In 2000-2001 he was working at the Institute of Physics, Academia Sinica, Taipei, Taiwan as a Postdoctoral Research Associate. He is currently an EPSRC Research Associate at Lancaster University. Current research interests are fluctuational transitions in complex nonlinear systems, bifurcational analysis, synchronization, stochastic resonance.

E-mail: a.silchenko@landcaster.ac.uk

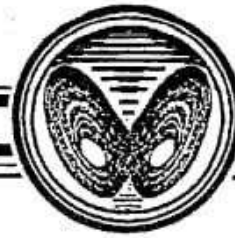


Beri Stefano graduated in Physics in both Pisa University (Italy) and Scuola Normale Superiore (Italy) in 2001. He is currently PhD student in Lancaster University. His main research areas concern the investigation of the stochastic dynamics of non-linear, non-equilibrium systems and the nonlinear dynamics of vertical cavity surface emitting lasers. He is author or coauthor of 6 papers.



Luchinsky Dmitrii G. was born in Moscow on 18 October 1959. He was educated in Moscow, gaining his undergraduate degree in physics from Moscow State University (Radiophysics Division) in 1983. He obtained his Candidate of Physical and Mathematical Sciences (PhD) degree from the All-Russian Institute for Metrological Service (VNIIMS) in 1990. His research in nonlinear optics has included the invention of a new optically bistable device, the discovery of a new form of optical hysteresis, and the first observation of optical heterodyning noise-protected with stochastic resonance. He has made numerous contributions to the understanding of topics in stochastic nonlinear dynamics, including stochastic resonance, large rare fluctuations and solution of the problem of escape from chaotic attractors and energy-optimal control of chaotic systems. He has been a Royal Society Visiting Fellow at Lancaster University on three occasions and a visiting consultant in the NASA Ames research centre in USA on two occasions. Currently

he is an EPSRC Research Associate on leave of absence from his permanent position as Senior Scientific Researcher in VNIIMS. His current research interests are focused on the modelling, controlling and inferencing complex stochastic dynamical systems including applications to semiconductor lasers, open ionic channels in biological membranes and physiology of the cardiovascular system.



OPTIMAL CONTROL OF FLUCTUATIONS APPLIED TO THE SUPPRESSION OF NOISE-INDUCED FAILURES OF CHAOS STABILIZATION

I.A. Khovanov, N.A. Khovanova and P.V.E. McClintock

Double strategy of chaos and fluctuation controls is developed. Noise-induced failures in the stabilization of an unstable orbit in the one-dimensional logistic map are considered as large fluctuations from a stable state. The properties of the large fluctuations are examined by determination and analysis of the optimal path and the optimal fluctuational force corresponding to the stabilization failure. The problem of controlling noise-induced large fluctuations is discussed, and methods of control have been developed.

Introduction

The control of chaos represents a very real and important problem in a wide variety of applications, ranging from neuron assemblies to lasers and hydrodynamic systems [1]. The procedure used consists of stabilizing an unstable periodic orbit by the application of precisely designed small perturbations to a parameter and/or a trajectory of the chaotic system. Different methods of chaos control have been suggested and applied in many different physical contexts, as well as numerically to model systems [1]. For practical applications of these control methods, it is important to understand how noise influences the stabilization process, because fluctuations are inherent and inevitably present in dissipative systems. The problem has not been well studied. Typically, a method is developed for stabilization of the orbit without initially taking any account of fluctuations. Only then the authors do check the robustness of their method by introducing weak noise into the system [1]. Thus, in the celebrated pioneering work of Ott, Grebogi and York, «Controlling chaos» [2], the authors just noted that noise can induce failures of stabilization.

In this work we consider noise-induced failures in the stabilization of an unstable orbit and the problem of controlling these failures. The method of Ott, Grebogi and Yorke (OGY) [2] and a modification of the adaptive method (ADP) [1] are used to stabilize an unstable point of the logistic map. We consider the small noise limit where stabilization failures are very rare and therefore they can be considered as large fluctuations (deviations) from a stable state. We study the properties of large deviations by determining the optimal paths and the optimal fluctuational forces corresponding to the failures. We employ two methods to determine the optimal paths and forces. The first of these builds and analyzes the prehistory probability distribution to determine the optimal path and optimal force [3]. The second method considers an extended map (relative to the

initial one) which defines fluctuational paths and forces in the zero-noise limit [4,5]. Furthermore we use the optimal paths and forces to develop methods of controlling the large deviations, i.e. the noise-induced failures of stabilization. In the literature, methods for stabilization are often referred to as a control methods too. To differentiate controlling large fluctuations from controlling chaos, we therefore use the term «stabilization» to indicate the control of chaos.

In section 1 we describe the procedures for stabilization of an unstable orbit of the logistic map. The general approach to the control of a large deviation is presented in section 2. Noise-induced failures of stabilization are considered in section 3. The results obtained are discussed in the conclusion.

1. Chaos stabilization

For simplicity we will stabilize an unstable fixed point x^* of the logistic map:

$$x_{n+1} = rx_n(1-x_n), \quad (1)$$

where x_n is a coordinate, n is discrete time and r is the control parameter that determines different regimes of the map's behavior (1). The coordinate of the fixed point x^* is defined by the condition: $x_{n+1}=x_n$, and consequently its location depends on the parameter r :

$$x^* = 1 - 1/r. \quad (2)$$

We set the parameter $r=3.8$, a value for which an aperiodic (chaotic) regime is observed in (1), and the point x^* is embedded in the chaotic attractor.

From the range of existing stabilization methods, we chose to work with just two: the OGY and ADP methods mentioned above.

To stabilize a fixed point by the OGY method, perturbations Δr are applied to the parameter r , leading to the map being modified (1) in the following manner:

$$x_{n+1} = (r+\Delta r_n)x_n(1-x_n), \quad \Delta r_n = r(2x^*-1)(x_n-x^*)/[x^*(1-x^*)]. \quad (3)$$

To stabilize a fixed point by the ADP method, perturbations Δx are applied to the map's coordinate. The value of the perturbation Δx is defined by the distance between the current system coordinate and the coordinate of the stabilized state:

$$x_{n+1} = rx_n(1-x_n) + \Delta x_n, \quad \Delta x_n = (x_n-x^*). \quad (4)$$

We consider local stabilization procedure. During local stabilization, the perturbations Δr and Δx differ from zero only if the following condition is satisfied:

$$|x_n-x^*| < \epsilon. \quad (5)$$

Here ϵ is a small value: we fixed $\epsilon=0.01$. If the condition (5) is not satisfied then stabilization is absent, i.e. $\Delta r=0$ or $\Delta x=0$.

So, stabilization involve modifications of the initial map (1), and thus we use another map in the form (3) or (4). The fixed point x^* is an attractor of the new map. After the stabilization is switched on, a trajectory of the map tends to the fixed point x^* , and subsequently remains there.

In the presence of noise the trajectory fluctuates in the vicinity of the stabilized state, i.e. noise-induced dynamics appears. In addition, noise can induce stabilization failures, i.e. breakdown in the condition (5).

Our aim is to study these noise-induced stabilization failures and analyze the problem of how to suppress them. We therefore consider the maps (3) and (4) in the presence of additive Gaussian fluctuations:

$$x_{n+1} = (r + \Delta r_n)x_n(1-x_n) + D\xi_n, \quad \Delta r_n = r(2x^* - 1)(x_n - x^*)/[x^*(1-x^*)], \quad (6)$$

$$x_{n+1} = rx_n(1-x_n) + \Delta x_n + D\xi_n, \quad \Delta x_n = (x_n - x^*). \quad (7)$$

Here D is the noise intensity; ξ_n is a Gaussian random process with zero-average $\langle \xi \rangle = 0$, δ -correlation function $\langle \xi_n \xi_{n+k} \rangle = \delta(k)$ and dispersion $\langle \xi^2 \rangle = 1$.

2. Control of large fluctuations

Large fluctuations manifest themselves as large deviations from the stable state of the system under the action of fluctuational forces. Large fluctuations play a key role in many phenomena, ranging from mutations in DNA to failures of electrical devices. In recent years significant progress has been achieved both in understanding the physical nature of large fluctuations and in developing approaches for describing them. The latter are based on the concept of optimal paths - the paths along which the system moves during large fluctuations. Large fluctuations are very rare events during which the system moves from the vicinity of a stable state to a state remote from it, at a distance significantly larger than the amplitude of the noise. Such deviations can correspond to a transition of the system to another state, or to an excursion along some trajectory away from the stable state and then back again. During such deviations the system is moved with overwhelming probability along the optimal path under the action of a specific (optimal) fluctuational force. The probability of motion along any other (non-optimal) path is exponentially smaller. In practice, therefore large fluctuations must of necessity occur along deterministic trajectories. The problem of controlling large fluctuations can thus be reduced to the task of controlling motion along a deterministic trajectory. Consequently, the control problem can be solved through application of the control methods developed for deterministic systems [6].

Let us consider the control problem. We will follow the work [7] and consider the control of large fluctuations by a weak additive deterministic control force. Weakness means here that the energy of the control force is comparable with the energy (dispersion) of the fluctuations (see [8] for details). In this case, the extremal value of the functional R for optimal control, which moves the system from an initial state x^i to a target state x^f , takes the form [7]:

$$R_{\text{opt}}(x^f, F) = S^{(0)}(x^f) \pm \Delta S, \quad \Delta S = (2F)^{1/2} [\sum_{k=N_i}^{N_f} (\xi_k^{\text{opt}})^2]^{1/2}, \quad (8)$$

where ξ_k^{opt} is the optimal fluctuational force that induces the transition from x^i to x^f in the absence of the control force; $S^{(0)}$ is an energy of the transition, N_i and N_f are the times at which the fluctuational force ξ_k^{opt} starts and stops, and F is a parameter defining the energy of the control force.

The optimal control force u_n^{opt} for the given functional (8) is defined [7] by:

$$u_n^{\text{opt}} = \mp (2F)^{1/2} \xi_n^{\text{opt}} [\sum_{k=N_i}^{k=N_f} (\xi_k^{\text{opt}})^2]^{1/2} \times \delta(x_n - x_n^{(0)\text{opt}}), \quad (9)$$

where $x_n^{(0)\text{opt}}$ is the optimal fluctuational path in the absence of the control force. The minus sign in the expression (9) decreases the probability of a transition to the state x^f , and the plus sign increases the probability. It can be seen that the optimal control force u_n^{opt} is completely defined by the optimal fluctuational force ξ_k^{opt} , and the optimal fluctuational path $x_n^{(0)\text{opt}}$, corresponds to the large fluctuation. Therefore to solve the control problem it is necessary, first, to determine the optimal path $x_n^{(0)\text{opt}}$ leading from the state x^i to the state x^f under the action of the optimal fluctuational force ξ_k^{opt} . Thus, a solution of the control problem depends on the existence of an optimal path: it is obvious

that the approach described should be straightforward to apply, provided that the optimal path exists and is unique.

We consider below an application of the approach described to suppress large fluctuations in the one-dimensional map. The large fluctuations in question are considered here to correspond to failures in the stabilization of an unstable orbit.

The control procedure depends on the determination of the optimal path and optimal fluctuational force and, to define them, we will use two different methods. The first method is based on an analysis of the prehistory probability distribution (PPD) and the second one consists of solving a boundary problem for an extended map which defines fluctuational trajectories.

The PPD was introduced in [3] to analyze optimal paths experimentally in flow systems. We will use the distribution to analyze fluctuational paths in maps. Note, that in [9,10] it was shown that analysis of the PPD allows one to determine both the optimal path and the optimal fluctuational force. The essence of this first method consists of a determination of the fluctuational trajectories corresponding to large fluctuations for extremely small (but finite) noise intensity, followed by a statistical analysis of the trajectories. In this experimental method the behaviour of the dynamical variables x_n and of the random force ξ_n are tracked continuously until the system makes its transition from an initial state x^i to a small vicinity of the target state x^f . Escape trajectories x_n^{esc} reaching this state, and the corresponding noise realizations ξ_n^{esc} of the same duration, are then stored. The system is then reset to the initial state x^i and the procedure is repeated. Thus, an ensemble of trajectories is collected and then the fluctuational PPD p_n^h is constructed for the time interval during which the system is monitored. This distribution contains all information about the temporal evolution of the system immediately before the trajectory arrives at the final state x^f . The existence of an optimal escape path is diagnosed by the form of the PPD p_n^h : if there is an optimal escape trajectory, then the distribution p_n^h at a given time n has a sharp peak at optimal trajectory x_n^{opt} . Therefore, to find an optimal path it is necessary to build the PPD and, for each moment of time n , to check for the presence of a distinct narrow peak in the PPD. The width of the peak defines the dispersion σ_n^h of the distribution and it has to be of the order of the mean-square noise amplitude $D^{1/2}$ [3]. The optimal fluctuational force that moves the system trajectory along the optimal path can be estimated by averaging the corresponding noise realizations ξ_n^{esc} over the ensemble. Note, that investigation of the fluctuational prehistory also allows us to determine the range of system parameters for which optimal paths exist.

To determine the optimal path and force by means of the second method we analyze extended maps [4,5] using the principle of least action [5]. Such extended maps are analogous to the Hamilton-Jacobi equation in the theory of large fluctuations for flow systems. For the one-dimensional map $x_{n+1}=f(x_n)+D\xi_n$, the corresponding extended map in the zero-noise limit takes the form:

$$\begin{aligned}x_{n+1} &= f(x_n) + y_n/g(x_n), \\ y_{n+1} &= y_n/g(x_n), \\ g(x_n) &= \partial f(x_n)/\partial x_n.\end{aligned}\tag{10}$$

The map is area-preserving, and it defines the dynamics of the noise-free map $x_{n+1}=f(x_n)$, if $y_n=0$. If $y_n \neq 0$ then the coordinate x_n corresponds to a fluctuational path, and the coordinate y_n to a fluctuational force. Stable and unstable states of the initial map become saddle states of the extended map. So, the fixed point x^* of the ADP (7) and OGY (6) maps becomes a saddle point of the corresponding extended map. Fluctuational trajectories (including the optimal one) starting from x^* belong to unstable manifolds of the fixed point $(x^*, 0)$ of the extended map.

The procedure for determination of the optimal paths consists of solving the boundary problem for the extended map (10):

$$x_{-\infty} = x^*, \quad y_{-\infty} = 0, \quad (11)$$

$$x_{\infty} = x^f, \quad y_{\infty} = 0, \quad (12)$$

where x^* is the initial state and x^f is a target state.

To solve the boundary problem different methods can be used. For the one-dimensional maps under consideration, a simple shooting method is enough [11]. We choose an initial perturbation l along the linearized unstable manifolds in a vicinity of the point $(x^*, 0)$ of the map (10). The procedure to determine a solution can be as follows: looking over all possible values l , we determine a trajectory which tends to the point $(x^f, 0)$. Note that, because these maps are irreversible there exists, in general, an infinite number of solutions of the boundary problem. The optimal trajectory (path) has minimal action (energy) $S = \sum_{n=-\infty}^{\infty} y_n^2$; here y_n is calculated along the trajectory, corresponding a solution of the boundary task.

3. Noise-induced failures in stabilization

A breakdown of the condition (5) corresponds to a failure of stabilization, i.e. to the noise-induced escape of the trajectory from an ε -vicinity of the fixed point x^* . The target state x^f corresponds to the boundaries of the stabilization region: $x^f = x^* \pm \varepsilon$.

Instead of analyzing the maps (6) and (7) in the ε -vicinity of the fixed point x^* we can investigate linearized maps of the following form: (path) has minimal

$$x_{n+1} = ax_n + D\xi_n, \quad (13)$$

here a is a value of derivative $\partial f(x_n)/\partial x_n$ in the fixed point x^* . For the map (6) the derivative is equal to zero $a_{\text{OGY}} = 0$, and for the map (7) $a_{\text{ADP}} = -0.8$.

Let us investigate stabilization failure by considering the most probable (optimal) fluctuational paths, which lead from the point x^* to boundaries $x^* \pm \varepsilon$. For linearized maps (13) the extended map (10) can be reduced to the form:

$$x_{n+1} = ax_n + y_n/a, \quad (14)$$

$$y_{n+1} = y_n/a$$

with the initial condition $(x_0 = x^*, y_0 = 0)$ and the final condition $x^f = x^* \pm \varepsilon$. It can be seen that a solution of the map (14) increases proportionally to $y_n = \text{const}/a^n$ [12]. This means that, for the ADP map (7), the amplitude of the fluctuational force increases slowly but that, for the OGY map (6), the failure arises as the result of only one fluctuation (iteration). Because equation (14) is linear, the boundary problem will have a unique solution [11]. Thus, analysis of the linearized extended map (14) shows that there is an optimal path, and it gives a qualitative picture of exit through the boundary $x^* \pm \varepsilon$.

Let us check the existence of the optimal paths through an analysis of the prehistory of fluctuations. To obtain exit trajectories and noise realizations we use the following procedure. At the initial moment of time, a trajectory of the map is located at point x^* . The subsequent behaviour of the trajectory is monitored until the moment at which it exits from the ε -region of the point x^* . The relevant parts of the trajectory, just before and after its exit, are stored. The time at which the exit occurs is set to zero. Thus ensembles of exit trajectories and of the corresponding noise realizations are collected and PPDs are built.

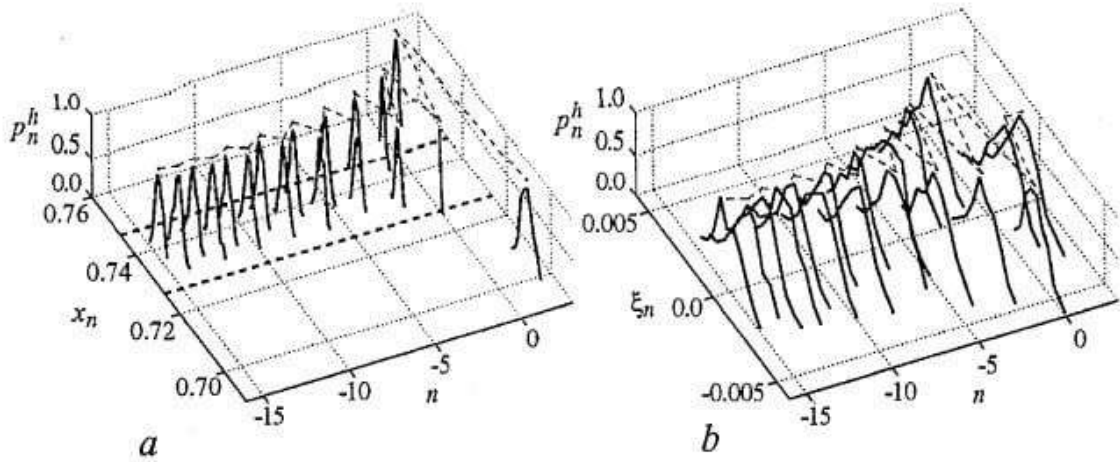


Fig. 1. PPDs p_n^h of the exit trajectories (a) and noise realizations (b) of ADP map for the boundary $(x^* - \epsilon)$. The thick dashed lines indicate ϵ -region of stabilization. The thin dashed lines connect maxima of PPDs. The noise intensity is $D=0.0011$

To start with, we will discuss these ideas in the context of the ADP map. Fig. 1, a shows PPDs of the escape trajectories of the ADP map, and the corresponding noise realizations for the exit through the boundary $(x^* - \epsilon)$ are shown in Fig. 1, b. The picture of exit through the other boundary $(x^* + \epsilon)$ is symmetrical, so we present results for one boundary only. It is evident (Fig. 1) that there is the only one exit path. Note, that the path to the boundary $(x^* - \epsilon)$ is approximately 2.8 more probable than the path to the boundary $(x^* + \epsilon)$. This difference arises from an asymmetry of the map in respect of the boundaries.

Because for each boundary there is the only one exit path, the optimal path and the optimal fluctuational force can be determined by simple averaging of escape trajectories and noise realizations respectively. In Fig. 2 the optimal exit paths and the optimal fluctuational forces are shown for the boundaries $(x^* - \epsilon)$ and $(x^* + \epsilon)$. The paths and the forces coincide with a solution of the boundary problem (circles in the Fig. 2) of the extended linear map (14). As can be seen the optimal path is long, and the amplitude of the fluctuational force increases slowly, in agreement with analysis of the linearized map (14).

The optimal fluctuational force obtained (Fig. 2, b) must correspond [10] to the energy-optimal deterministic force that induced the stabilization failure. We have

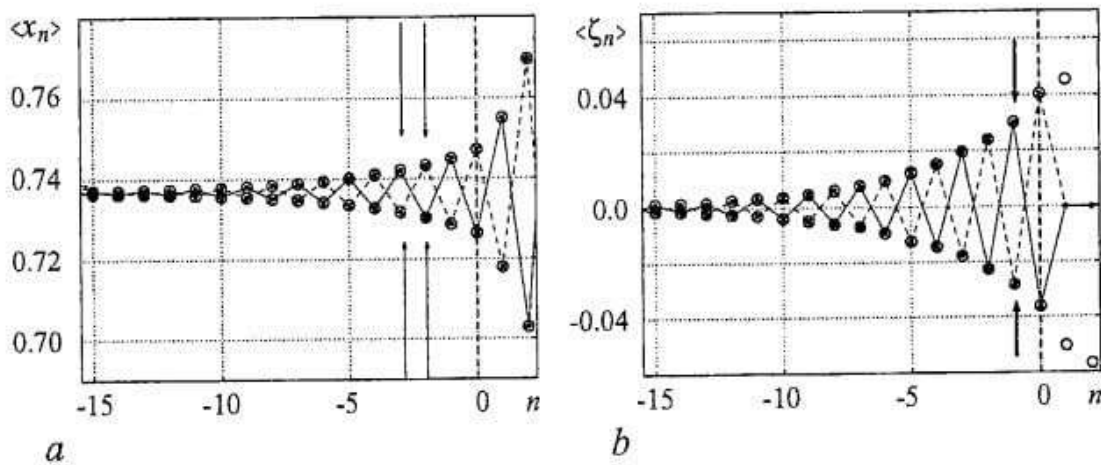


Fig. 2. The optimal paths (a) and the optimal forces (b) for exit through the boundary $(x^* - \epsilon)$ (solid line) and the boundary $(x^* + \epsilon)$ (dashed line) for ADP map. Circles indicate the optimal paths and forces obtained by solving the boundary problem for the linearized extended map (14). The optimal paths and forces used in the control procedure are marked by arrows

checked this prediction and found that the optimal force induces the exit from an ε -region of the point x^* : we selected an initial condition at the point x^* and included the optimal fluctuational force additively; as a result we observed the stabilization failure. If we decrease the amplitude of the force by 5-10%, then the failure does not occur. It appears, therefore, the deduced force allows us to induce the stabilization failure with minimal energy (see [10] for details).

Using the optimal path and the force we can solve the opposite task [7,8] - to decrease the probability of the stabilization failures. Indeed, if during the motion along the optimal path we will apply a control force with the same amplitude but with the opposite sign as the optimal fluctuational force has, then, obviously, the failure will not occur. Because we know the optimal force then, in accordance with the algorithm [7] described above, it is necessary to determine the time moment when system is moving along the optimal path. For the ADP method the optimal path is long enough to identify that a trajectory is moving along the optimal path, and then to apply a control force.

In the presence of control the map (7) is modified:

$$\begin{aligned} x_{n+1} &= rx_n(1-x_n) + \Delta x_n + D\xi_n + u_n, \\ \Delta x_n &= (x_n - x^*), \end{aligned} \quad (15)$$

here u_n is the deterministic control force.

We use the following scheme to suppress the stabilization failures. Initially the control force is equal to zero ($u_n=0$) and the map is located in the point x^* ; we continuously monitor a trajectory of the map (15) and define the time moment when the system starts motion along the optimal path $\langle x_n \rangle$. We assume that the system moves along the optimal path $\langle x_n \rangle$ if it passes within a small vicinity of the coordinate $\langle x_2 \rangle$ and then within a small vicinity of $\langle x_3 \rangle$ (see arrows in Fig. 2, *a*). Then on the following iteration we add the control force $u_n = -\text{sign}(\xi_n)\langle \xi_n \rangle$, $n=-1$ (see Fig. 2, *b*).

In Fig. 3, *a* dependences of the mean time $\langle \tau \rangle$ between the failures on the noise intensity D are plotted in the absence, and in the presence, of the control procedure. It is clear that the mean time $\langle \tau \rangle$ is substantially increased by the addition of the control, i.e. stability in the face of fluctuations is significantly improved by the addition of the control scheme. The efficiency of the control procedure depends exponentially [7] on the amplitude of the control force (Fig. 3, *b*), and there is an optimal value of the control force, which is very close to the value (arrow in Fig. 3, *b*) of the optimal fluctuational force.

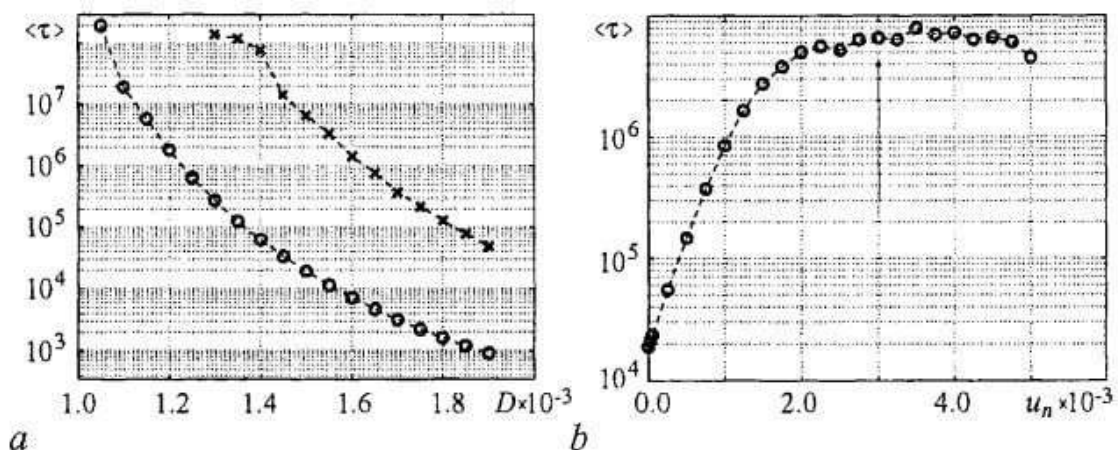


Fig. 3. (a) The dependences of mean time $\langle \tau \rangle$ between stabilization failures on noise intensity D in the absence (circles) and in the presence (crosses) of the control. The size of the stabilization region is $\varepsilon=0.01$. (b) The dependence of the mean time $\langle \tau \rangle$ on the amplitude of the control force u_n is presented for the ADP method. The value of $\langle \tau \rangle$ corresponding to the optimal fluctuational force is marked by the arrow

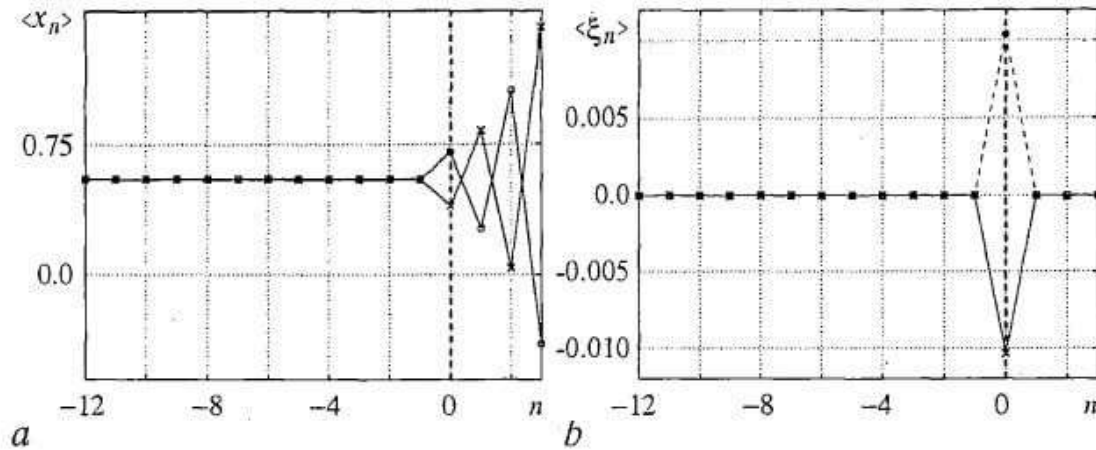


Fig. 4. For the OGY map, the optimal path (a) and the optimal force (b) are shown for exit through the boundary $(x^* - \epsilon)$ (crosses) and the boundary $(x^* + \epsilon)$ (circles)

Now consider noise-induced stabilization failures for OGY map (6). An analysis of the linearized map has shown that the failure occurs as the result of a single fluctuation. We have checked the conclusion by an analysis of the fluctuational trajectories of the map (6), much as we did for the ADP map. The optimal path and optimal force are shown in Fig. 4 for both boundaries, $(x^* + \epsilon)$ and $(x^* - \epsilon)$. An exit occurs during one iteration and there is no a prehistory before this iteration. It means that we cannot determine the moment at which the large fluctuation starts and, consequently, that we cannot control the stabilization failures. The existence of a long prehistory is thus a key requirement in the control the large fluctuations.

Conclusion

We have considered noise-induced failures in the stabilization of an unstable orbit, and the problem of how to control such failures. In our investigations, they correspond to large deviations from stable points. We have shown that noise-induced failures can be analyzed effectively in terms of linearized noisy maps.

Large noise-induced deviations from the fixed point in one-dimensional maps have been analyzed within the framework of the theory of large fluctuations. The key point of our consideration is that the dynamics of the optimal path, and the optimal fluctuational force, correspond directly to stabilization failures. We have applied two approaches - experimental analysis of the prehistory probability distribution and the solution of the boundary problem for extended maps - to determine the optimal path and the optimal fluctuational force, and we have compared their results. The two approaches give the same results.

A procedure for the control of large fluctuations in one-dimensional maps has been demonstrated. It is based on the control concept developed in [7] for continuous systems. We have introduced an additional control scheme which significantly improves the stabilization of an unstable orbit in the presence of noise. It was successful for the ADP method of stabilization, and problematic for the OGY method. We have shown that the control procedure has limitations connected with the presence of long time prehistory of large fluctuation.

Our consideration of the control problem is relevant to a continuous system which has a one-dimensional curve in its Poincaré section, e.g. the Rössler system. For such systems we can formulate the control task as that of control at discrete moments of time (the moments of intersection of the Poincaré section) by using impulsive forces. The

intervals between these moments were used to calculate and to form the necessary control force. Note that a similar approach is widely used in control technology.

The main limitation of our present control approach lies in the necessity of studying the fluctuational dynamics of a given system prior to consideration of its control. Such a study can be carried out by use of an extended map of the system, if model equations are known, and/or experimentally by analysis of the fluctuational prehistory distribution. A system model can be easily written down by determination of the eigenvalue of a stabilized unstable point: there are many effective methods of doing so [13].

We thank D.G. Luchinsky and V. Smelyansky for useful and stimulating discussions and help. The research was supported by the Engineering and Physical Sciences Research Council (UK) and INTAS (grant 01-867).

References

1. Boccaletti S., Grebogi C., Lai Y.C., Mancini H., and Maza D. // Phys. Rep. Vol. 329, 103 (2000).
2. Ott E., Grebogi C., and Yorke J. // Phys. Rev. Lett. Vol. 64, 1196 (1990).
3. Dykman M.I., McClintock P.V.E., Smelyanski V.N., Stein N.D., and Stocks N.G. // Phys. Rev. Lett. Vol. 68, 2718 (1992).
4. Graham R. and Tel T. // Phys. Rev. Lett. Vol. 66, 3089 (1991).
5. Grassberger P. // J. Phys. A. Vol. 22, 3283 (1989).
6. Pontryagin L.S. The Mathematical Theory of Optimal Processes (Macmillan, 1964).
7. Smelyanskiy V.N., and Dykman M.I. // Phys. Rev. E. Vol. 55, 2516 (1997).
8. Whittle P. Optimal Control: Basics and Beyond (Wiley, 1996).
9. Luchinsky D.G. // J. Phys. A. Vol. 30, L577 (1997).
10. Khovanov I.A., Luchinsky D.G., Mannella R., and McClintock P.V.E. // Phys. Rev. Lett. Vol. 85, 2100 (2000).
11. Press W.H. et al. Numerical recipes: the art of scientific computing (Cambridge University Press, Cambridge, 1989).
12. Reimann P., and Talkner P. // Phys. Rev. E. Vol. 44, 6348 (1991).
13. Badii R., Brun E., Finardi M., Flepp L., Holzner R., Parisi J., Reyl C., and Simonet J. // Rev. Mod. Phys. Vol. 66, 1389 (1994).

*Physics Department, Saratov
State University, Russia
Department of Physics, Lancaster
University, LA1 4YB, UK*

Received 12.09.2003

УДК 519.6: 537.86:519.2

ОПТИМАЛЬНЫЙ КОНТРОЛЬ ФЛУКТУАЦИЙ В ПРИМЕНЕНИИ К ПОДАВЛЕНИЮ ИНДУЦИРОВАННЫХ ШУМОМ НАРУШЕНИЙ СТАБИЛИЗАЦИИ ХАОСА

И.А. Хованов, Н.А. Хованова, P.V.E. McClintock

Разрабатывается двойная стратегия управления хаосом и флуктуациями. Индуцированные шумом нарушения стабилизации неустойчивых орбит в одномерном логистическом отображении рассматриваются как большие флуктуации

от устойчивого состояния. Свойства больших флуктуаций проверяются путем определения и анализа оптимального пути и оптимального флуктуационного воздействия, соответствующего нарушению стабилизации. Обсуждается проблема управления индуцированных шумом больших флуктуаций, и разрабатываются методы управления.



Khovanov Igor Aleksandrovich was born on October 1971. He was educated in Physics Department of Saratov State University, gaining his undergraduate degree in «radiophysics» in 1993. He got a degree of Candidate of Physical and Mathematical Sciences (PhD) in 1997 from Saratov University. Since 1996 he worked Assistant of nonlinear dynamics and radiophysics chair of Saratov University and from 1999 he is Assistant Professor of this chair. Scientific interests: stochastic processes and nonlinear dynamics.

E-mail: igor@chaos.ssu.runnet.ru

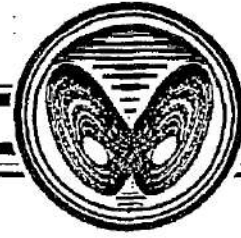


Khovanova Natalia Aleksandrovna was born on June 1972. She was educated in Physics Department of Saratov State University, gaining his undergraduate degree in «radiophysics» in 1994. She gained a degree of Candidate of Physical and Mathematical Sciences (PhD) from Saratov University in 1997. Since 1996 she worked Assistant of general physics chair of Saratov University and from 1997 she is Assistant Professor of this chair. Scientific interests: stochastic processes and nonlinear dynamics.

E-mail: khovanova@chaos.ssu.runnet.ru



Peter Vaughan Elsmere McClintock was born in Omagh, N.Ireland, on 17 October 1940. After being educated in Ireland, N. Rhodesia, W.Germany and England, he read physics at Queen's University Belfast, gaining his BSc in 1962. His doctoral research in Oxford, under H.M. Rosenberg, was on spin-phonon interactions in paramagnetic crystals at very low temperatures, leading to a DPhil in 1966. During his subsequent postdoctoral appointment (1966-1968) at Duke University, N. Carolina, Henry Fairbank and Horst Meyer introduced him to the superfluidity and other fascinating properties of liquid helium. Since 1968, when he came to Lancaster University, where he is now Professor of Physics, he has investigated several topics related to liquid helium, including a measurement of the Landau critical velocity, studies of the creation and decay of quantized vortices, and helium isotopic separation. He has also contributed to the exploration of a range of fundamental problems in stochastic nonlinear dynamics and applications to the cardiovascular system. He holds a DSc from Queen's University, Belfast, and is a Fellow of the Institute of Physics. E-mail: p.v.e.mcclintock@lancaster.ac.uk



RECOVERY OF DYNAMICAL MODELS OF TIME-DELAY SYSTEMS FROM TIME SERIES

*V.I. Ponomarenko, M.D. Prokhorov, A.S. Karavaev,
Ye.P. Seleznev, T.V. Dikanev*

We develop the method for the estimation of the parameters of time-delay systems from time series. The method is based on the statistical analysis of time intervals between extrema in the time series and the projection of the infinite-dimensional phase space of a time-delay system to suitably chosen low-dimensional subspaces. We verify our method by using it for the reconstruction of different time-delay differential equations from their chaotic solutions.

Introduction

The present paper deals with the problem of reconstruction of nonlinear dynamical models of time-delay systems from time series. The importance of this problem is determined by the fact that time-delay systems are wide spread in nature. The behavior of such systems is affected not only by the present state, but also by past states. These systems are usually modeled by delay-differential equations. Such models are successfully used in many scientific disciplines, such as physics, physiology, biology, economic, and cognitive sciences. Typical examples include population dynamics [1], where individuals participate in the reproduction of a species only after maturation, or spatially extended systems, where signals have to cover distances with finite velocities. Within this rather broad class of systems, one can find the Ikeda equation [2] modeling the passive optical resonator system, the Lang-Kobayashi equations [3] describing semiconductor lasers with optical feedback, the Mackey-Glass equation [4] modeling the production of red blood cells, and various models describing different phenomena from glucose metabolism to infectious diseases. The advantage of methods proposed in the paper is that they can be applied to the systems of different nature if these systems have similar structure of model equations.

In the most general case the time-delay systems are described by the following equation

$$x^{(n)}(t) + \varepsilon_{n-1}x^{(n-1)}(t) + \dots + \varepsilon_1x^{(1)}(t) = F(x(t), x(t-\tau_1), \dots, x(t-\tau_k)), \quad (1)$$

where $x^{(n)}(t)$ is the derivative of order n ; $\varepsilon_1, \dots, \varepsilon_{n-1}$ are the coefficients; and τ_1, \dots, τ_k are the delay times. To uniquely define the system (1) state it is necessary to prescribe the initial conditions in the entire time interval $[-\tau_k, 0]$. Therefore, the phase space of the system has

to be considered as infinite-dimensional. In fact, for large delay times even scalar delay-differential equations can possess high-dimensional chaotic dynamics. Thus, the direct reconstruction of the system by the time-delay embedding techniques runs into severe problems. For a successful recovery of the time-delay systems one has to use special methods. The most of them are based on the projection of the infinite-dimensional phase space of time-delay systems onto low-dimensional subspaces. These methods use different criteria of quality for the reconstructed equations, for example, the minimal forecast error of constructed model [5-8], the minimal value of information entropy [9], or various measures of complexity of the projected time series [10-14]. Several methods of time-delay system analysis exploit regression analysis [15,16] and correlation function construction [17,18]. In this paper we further develop the methods proposed by us recently [19,20] for the estimation of the parameters of time-delay systems from time series for a more wide class of time-delay systems.

Reconstruction of scalar time-delay systems

Let us consider one of the most popular first-order delay-differential equation

$$\varepsilon_0 \dot{x}(t) = -x(t) + f(x(t-\tau_0)), \quad (2)$$

where $x(t)$ is the system state at time t , function f defines nonlocal correlations in time, τ_0 is the delay time, and parameter ε_0 characterizes the inertial properties of the system. In general case Eq. (2) is a mathematical model of an oscillating system composed of a ring with three ideal elements: nonlinear, delay, and inertial ones (Fig. 1). In the present paper we develop a technique for estimating τ_0 , f , and ε_0 from the time series.

It should be noted that available for measurement dynamical variable could be obtained from different points of the time-delay system (2), indicated in Fig. 1 by the numerals 1-3. Let us consider first the case when the observed dynamical variable is $x(t)$ measured at the point 1. To estimate the delay time τ_0 we exploits the features of extrema shape and location in the system (2) temporal realization $x(t)$. The peculiarities of extrema location in time are clearly illustrated by $N(\tau)$ plot in Fig. 2. To construct it one has to define for different τ values the number N of pairs of extrema in $x(t)$, that are separated in time by τ . If N is normalized to the total number of extrema, then for sufficiently large extrema number it can be used as an estimation of probability to find a pair of extrema in $x(t)$ separated by the interval τ . Let us explain the qualitative features of $N(\tau)$ for various values of parameter ε_0 .

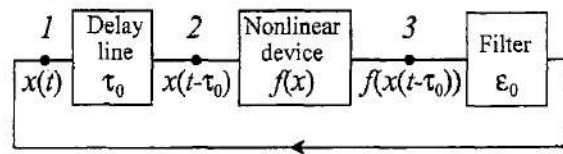


Fig. 1. Delayed nonlinear feedback system. Arabic numerals designate points where a dynamical variable is measured

In the absence of inertial properties ($\varepsilon_0=0$) time differentiation of Eq. (2) gives

$$\dot{x}(t) = \dot{x}(t-\tau_0) df(x(t-\tau_0))/dx(t-\tau_0). \quad (3)$$

From Eq. (3) it follows that if $\dot{x}(t-\tau_0)=0$, then $\dot{x}(t)=0$. Thus, for $\varepsilon_0=0$ every extremum of $x(t)$ is followed within the time τ_0 by the extremum¹. As the result, $N(\tau)$ shows a maximum for $\tau=\tau_0$ in Fig. 2, a.

In the presence of inertial properties ($\varepsilon_0>0$), which corresponds to real situations,

¹ For chaotic temporal realizations of the systems under investigation practically all critical points with $\dot{x}(t)=0$ are the extremal ones, and therefore we call the points with $\dot{x}(t)=0$ the extremal points throughout this paper.

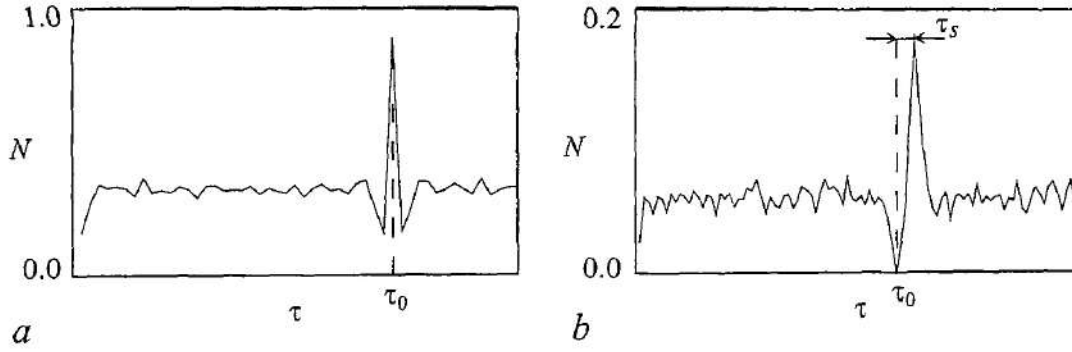


Fig. 2. Number N of pairs of extrema in a realization of Eq. (2) separated in time by τ , as a function of τ . $N(\tau)$ is normalized to the total number of extrema in time series. (a) $\varepsilon_0=0$. $N(\tau)$ has a sharp maximum at the level of the delay time of the system. (b) $\varepsilon_0>0$. $N(\tau)$ has a pronounced minimum at the level of the delay time of the system. The location of maximum is determined by the parameter ε_0

the most probable value of the time interval between extrema in $x(t)$ shifts from τ_0 to larger values. This effect can be explained using the ring system shown in Fig. 1: the filter introduces a certain additional delay in the system. As the result, the extrema in $x(t)$ can be found most often at the distance $\tau_0 + \tau_s$ apart (Fig. 2, b). For instance, the computational investigation of Eq. (2) with quadratic nonlinear function $f(x) = \lambda - x^2$ allows us to obtain an estimation $\tau_s \approx \varepsilon_0/2$ for large values of the parameter of nonlinearity λ .

For $\varepsilon_0 > 0$ the extrema in $x(t)$ are close to quadratic ones and therefore $\dot{x}(t) = 0$ and $x(t) \neq 0$ at the extremal points. It can be shown that in this case there are practically no extrema in $x(t)$ separated in time by τ_0 . To prove this let us differentiate Eq. (2) with respect to t :

$$\varepsilon_0 \ddot{x}(t) = -\dot{x}(t) + \dot{x}(t - \tau_0) df(x(t - \tau_0))/dx(t - \tau_0). \quad (4)$$

If for $\dot{x}(t) = 0$ in a typical case $\ddot{x}(t) \neq 0$, then, as it can be seen from Eq. (4), for $\varepsilon_0 \neq 0$ the condition $\dot{x}(t - \tau_0) \neq 0$ must be fulfilled. Thus, there must be no extremum separated in time by τ_0 from a quadratic extremum and hence $N(\tau_0) \rightarrow 0$. For $\tau \neq \tau_0$, the derivatives $\dot{x}(t)$ and $\dot{x}(t - \tau)$ can be simultaneously equal to zero, i.e., it is possible to find extrema separated in time by τ . The specific configuration presented in Fig. 2, b in the neighborhood of $\tau = \tau_0$ is duplicated at larger τ in the neighborhood of $\tau = 2\tau_0, 3\tau_0, \dots$

The procedure of the delay time estimation from the $N(\tau)$ plot considered with systems like (2) can be successfully applied to time series gained from a more general class of time-delay systems

$$\dot{x}(t) = F(x(t), x(t - \tau_0)). \quad (5)$$

Time differentiation of Eq. (5) gives

$$\ddot{x}(t) = \dot{x}(t) \partial F(x(t), x(t - \tau_0)) / \partial x(t) + \dot{x}(t - \tau_0) \partial F(x(t), x(t - \tau_0)) / \partial x(t - \tau_0). \quad (6)$$

Similarly to Eq. (4), Eq. (6) implies that in the case of quadratic extrema derivatives $\dot{x}(t)$ and $\dot{x}(t - \tau_0)$ do not vanish simultaneously, i.e., if $\dot{x}(t) = 0$, then $\dot{x}(t - \tau_0) \neq 0$.

Thus, for τ_0 definition one has to determine the extrema in the time series and after that to define for different values of time τ the number N of pairs of extrema separated in time by τ and to construct the $N(\tau)$ plot. The absolute minimum of $N(\tau)$ is observed at the delay time τ_0 .

To recover the parameter ε_0 and the nonlinear function f of system (2) from the chaotic time series let us rewrite Eq. (2) as

$$\varepsilon_0 \dot{x}(t) + x(t) = f(x(t-\tau_0)). \quad (7)$$

Thus, it is possible to reconstruct the nonlinear function by plotting in a plane a set of points with coordinates $(x(t-\tau_0), \varepsilon_0 \dot{x}(t) + x(t))$. According to Eq. (7), the constructed set of points reproduces the function f . Since the parameter ε_0 is a priori unknown, one needs to plot $\varepsilon \dot{x}(t) + x(t)$ versus $x(t-\tau_0)$ under variation of ε , searching for a single-valued dependence in the plane $(x(t-\tau_0), \varepsilon \dot{x}(t) + x(t))$, which is possible only for $\varepsilon = \varepsilon_0$. As a quantitative criterion of single-valuedness in searching for ε_0 we use the minimal length of a line $L(\varepsilon)$, connecting all points ordered with respect to $x(t-\tau_0)$ in the plane $(x(t-\tau_0), \varepsilon \dot{x}(t) + x(t))$. The minimum of $L(\varepsilon)$ is observed at $\varepsilon = \varepsilon_0$. The set of points constructed for the defined ε_0 in the plane $(x(t-\tau_0), \varepsilon_0 \dot{x}(t) + x(t))$ reproduces the nonlinear function, which can be approximated if necessary. In contrast to methods presented in [11,12] which use only extremal points or points selected according to a certain rule for the nonlinear function recovery, the proposed technique uses all points of the time series. It allows one to estimate the parameter ε_0 and to reconstruct the nonlinear function from short time series even in the regimes of weakly developed chaos.

To test the efficiency of the proposed technique we apply it to a time series produced by numerical integration of the passive optical resonator system of Ikeda [2]

$$\dot{x}(t) = -x(t) + \mu \sin(x(t-\tau_0) - x_0) \quad (8)$$

with $\mu=20$, $\tau_0=2$, $x_0=\pi/3$, $\varepsilon_0=1$. Note that the nonlinear function in the Ikeda equation is multimodal one. Part of the time series is shown in Fig. 3, *a*. The time series is sampled in such a way that 200 points in time series cover a period of time equal to the delay time

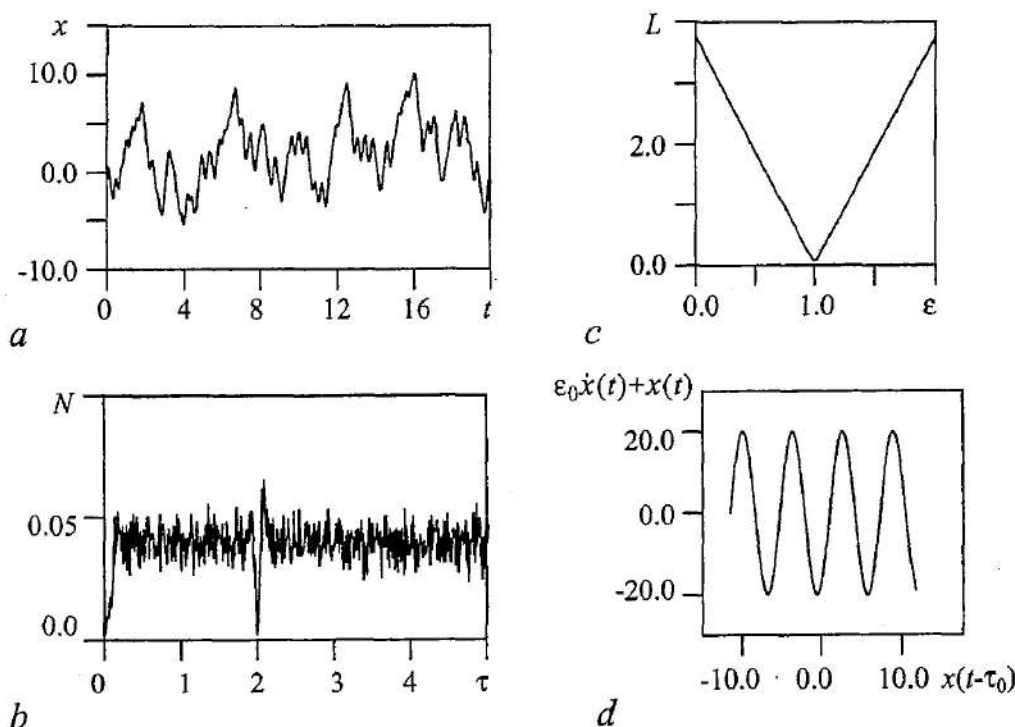


Fig. 3. (a) Time series of the Ikeda equation (8); (b) number N of pairs of extrema in the time series separated in time by τ , as a function of τ . $N(\tau)$ is normalized to the total number of extrema in the time series. $N_{\min}(\tau) = N(2.00)$; (c) - length L of a line connecting points ordered with respect to $x(t-\tau_0)$ in the plane $(x(t-\tau_0), \varepsilon_0 \dot{x}(t) + x(t))$ as a function of ε . $L(\varepsilon)$ is normalized to the number of points. $L_{\min}(\varepsilon) = L(1.00)$; (d) - the recovered nonlinear function

$\tau_0=2$. The data set consists of 25000 points and exhibits about 1000 extrema. Figure 3, *b* illustrates the τ -dependence of the number N of pairs of extrema separated in time by τ .

The time derivatives $\dot{x}(t)$ are estimated from the time series by applying a local parabolic approximation. The step of τ variation in Fig. 3, *a* is equal to the integration step $h=0.01$. The absolute minimum of $N(\tau)$ takes place exactly at $\tau=\tau_0=2.00$. To construct the $L(\epsilon)$ plot (Fig. 3, *c*) the step of ϵ variation was also set by 0.01. The minimum of $L(\epsilon)$ takes place accurately at $\epsilon=\epsilon_0=1.00$. In Fig. 3, *d* the nonlinear function is shown. This recovered function coincides practically with the true function of Eq. (8).

To investigate the robustness of the method to additional noise we analyze the data produced by adding to the time series of Eq. (8) zero-mean Gaussian white noise. The presence of noise in time series brings into existence spurious extrema. These extrema are not caused by the intrinsic dynamics of a system and temporal distances between them are random. With the extrema number increasing, a probability to find a pair of extrema in time series separated in time by τ has to increase in general. The extrema number increasing induced by noise is also followed by the increase of probability to find a pair of extrema separated by the interval τ_0 . However, for moderate noise levels this probability is still less than the probability to find a pair of extrema separated in time by $\tau \neq \tau_0$. Since the absolute minimum of $N(\tau)$ is very well pronounced in the absence of noise, it can be clearly distinguished even in the noise presence if the noise level is not very high. Hence, the qualitative features of the $N(\tau)$ plot specified by the delay-induced dynamics are retained for a moderate noise level. The presence of noise is more critical for the parameter ϵ_0 estimation and the nonlinear function recovery.

Figure 4 illustrates the results of the Ikeda equation reconstruction from the time series corrupted with zero-mean Gaussian white noise with a standard deviation of 20% of the standard deviation of the data without noise. The location of the absolute minimum of $N(\tau)$ (Fig. 4, *a*) allows one to estimate the delay time accurately, $\tau_0'=2.00$. The minimum of $L(\epsilon)$ (Fig. 4, *b*) takes place at $\epsilon_0'=0.98$. The nonlinear function recovered using the estimated τ_0' and ϵ_0' is shown in Fig. 4, *c*. In spite of sufficiently high noise level and inaccuracy of ϵ_0 estimation the recovery of the nonlinear function has a good quality which is significantly higher than that reported in [21] for the same parameter values of the Ikeda equation with noise.

In the second case, when the observed dynamical variable is $x(t-\tau_0)$ measured at the point 2 (Fig. 1), one can use the described above procedure for estimation of the system parameters since the observable is simply shifted in time by the delay time τ_0 . For the third possible case, when the observed variable is $f(x(t-\tau_0))$ which is measured at the point 3 (Fig. 1), one needs another technique for reconstruction of the time-delay system.

As well as in the time series of $x(t)$, there are also practically no extrema separated in time by τ_0 in the time series of the system (2) variable $f(x(t-\tau_0))$, since, $df(x(t-\tau_0))/dt=$

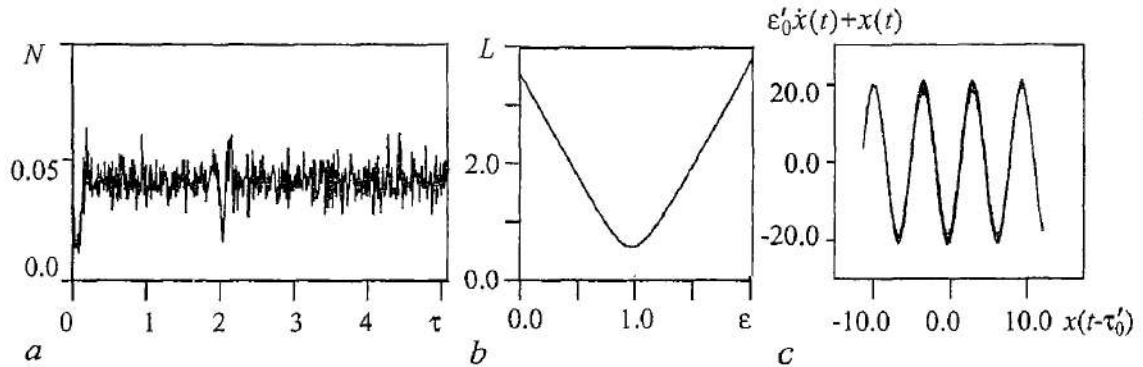


Fig. 4. Reconstruction of the Ikeda equation from its time series $x(t)$ with additive Gaussian white noise for noise level of 20%. (a) The $N(\tau)$ plot. $N_{\min}(\tau)=N(2.00)$. (b) The $L(\epsilon)$ plot. $L_{\min}(\epsilon)=L(0.98)$. (c) The recovered nonlinear function

$=\dot{x}(t-\tau_0)df(x(t-\tau_0))/dx$. Then, the delay time τ_0 can be estimated by the location of the absolute minimum in the $N(\tau)$ plot constructed from the variable $f(x(t-\tau_0))$.

To recover the parameter ε_0 and the function f we filter the chaotic signal $f(x(t-\tau_0))$ with a first-order low-pass filter and plot $f(x(t-\tau_0))$ versus $u(t-\tau_0)$, where $u(t-\tau_0)$ is the signal at the filter output, shifted by the time τ_0 defined earlier. If the filter inertial properties are characterized by the parameter $\varepsilon=\varepsilon_0$, then $u(t-\tau_0)=x(t-\tau_0)$ and the set of points constructed in the plane $(x(t-\tau_0), f(x(t-\tau_0)))$ reproduces the nonlinear function f . Since the parameter ε_0 is a priori unknown, one needs to plot $f(x(t-\tau_0))$ versus $u(t-\tau_0)$, under variation of the filter parameter ε , searching for a single-valued dependence in the plane $(u(t-\tau_0), f(x(t-\tau_0)))$, which is possible only for $\varepsilon=\varepsilon_0$. As a quantitative criterion of single-valuedness in searching for ε_0 we use the minimal length of a line $L(\varepsilon)$, connecting all points ordered with respect to $u(t-\tau_0)$ in the plane $(u(t-\tau_0), f(x(t-\tau_0)))$. The minimum of $L(\varepsilon)$ is observed at $\varepsilon=\varepsilon_0$. The set of points constructed for the defined ε_0 in the plane $(u(t-\tau_0), f(x(t-\tau_0)))$ reproduces the nonlinear function, which can be approximated if necessary.

We apply the method to a time series of the variable $f(x(t-\tau_0))$ of the Mackey-Glass equation [4]

$$\dot{x}(t) = -bx(t) + ax(t-\tau_0)/(1+x^c(t-\tau_0)), \quad (9)$$

which can be converted to Eq. (2) with $\varepsilon_0=1/b$ and the function

$$f(x(t-\tau_0)) = ax(t-\tau_0)/(b(1+x^c(t-\tau_0))). \quad (10)$$

The parameters of the system (10) are chosen to be $a=0.2$, $b=0.1$, $c=10$, $\tau_0=300$ to produce a dynamics on a high-dimensional chaotic attractor. The sampling time is set by 1.

Figure 5 illustrates the reconstruction of the Mackey-Glass system parameters. Figure 5, *a* shows the number N of pairs of extrema in the time series of $f(x(t-\tau_0))$, separated in time by τ . The step of τ variation in Fig. 5, *a* is equal to the integration step $h=1$. The location of the absolute minimum of $N(\tau)$ allows us to estimate the delay time, $\tau_0'=300$. To construct the $L(\varepsilon)$ plot (Fig. 5, *b*) we use the step of ε variation equal to 0.1. The minimum of $L(\varepsilon)$ takes place at $\varepsilon_0'=10.0$ ($\varepsilon_0=1/b=10$). The nonlinear function recovered using the estimated τ_0' and ε_0' is shown in Fig. 5, *c*. This recovered function coincides practically with the true function (10).

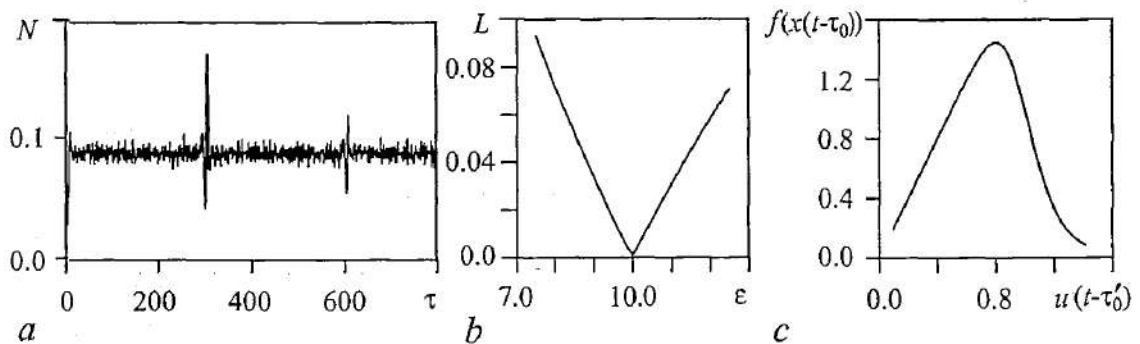


Fig. 5. Reconstruction of the Mackey-Glass system from the variable $f(x(t-\tau_0))$. (a) The $N(\tau)$ plot. $N_{\min}(\tau)=N(300)$. (b) The $L(\varepsilon)$ plot. $L_{\min}(\varepsilon)=L(10.0)$. (c) The recovered nonlinear function

Reconstruction of nonscalar time-delay systems

The method of τ_0 definition from time series described above for scalar time-delay systems can be extended to high-dimensional time-delay systems having the following form

$$x^{(n)}(t) + \varepsilon_{n-1}x^{(n-1)}(t) + \dots + \varepsilon_1\dot{x}(t) = F(x(t), x(t-\tau_0)), \quad (11)$$

Differentiation of Eq. (11) with respect to t gives

$$\begin{aligned} x^{(n+1)}(t) + \varepsilon_{n-1}x^{(n)}(t) + \dots + \varepsilon_1\ddot{x}(t) = \\ = \dot{x}(t)\partial F(x(t), x(t-\tau_0))/\partial x(t) + \dot{x}(t-\tau_0)\partial F(x(t), x(t-\tau_0))/\partial x(t-\tau_0). \end{aligned} \quad (12)$$

The condition $\dot{x}(t-\tau_0) \neq 0$ for $\dot{x}(t) = 0$ will be satisfied if the left-hand side of Eq. (12) does not vanish. In general, a probability to obtain zero in the left-hand side of Eq. (12) is very small and therefore, the $N(\tau)$ plot qualitatively must have a shape similar to that inherent in the case of first-order delay-differential equations like (2) and (5).

The proposed method of estimation of the parameter ε_0 and the nonlinear function can be also applied to a variety of time-delay systems of order higher than that of (2). For instance, if the dynamics of a time-delay system is governed by the second-order delay-differential equation

$$\varepsilon_2\ddot{x}(t) + \varepsilon_1\dot{x}(t) = -x(t) + f(x(t-\tau_0)), \quad (13)$$

the nonlinear function can be reconstructed by plotting in a plane a set of points with coordinates $(x(t-\tau_0), \varepsilon_2\ddot{x}(t) + \varepsilon_1\dot{x}(t) + x(t))$. The constructed set of points reproduces the function f . Since the parameters ε_1 and ε_2 are a priori unknown, one needs to plot $\hat{\varepsilon}_2\ddot{x}(t) + \hat{\varepsilon}_1\dot{x}(t) + x(t)$ versus $x(t-\tau_0)$ under variation of $\hat{\varepsilon}_1$ and $\hat{\varepsilon}_2$, searching for a single-valued dependence in the plane $(x(t-\tau_0), \hat{\varepsilon}_2\ddot{x}(t) + \hat{\varepsilon}_1\dot{x}(t) + x(t))$, which is possible only for $\hat{\varepsilon}_1 = \varepsilon_1$, $\hat{\varepsilon}_2 = \varepsilon_2$. As a quantitative criterion of single-valuedness in searching for ε_1 and ε_2 we use the minimal length of a line $L(\hat{\varepsilon}_1, \hat{\varepsilon}_2)$ connecting all points ordered with respect to $x(t-\tau_0)$ in this plane. The minimum of $L(\hat{\varepsilon}_1, \hat{\varepsilon}_2)$ is observed at $\hat{\varepsilon}_1 = \varepsilon_1$, $\hat{\varepsilon}_2 = \varepsilon_2$. The set of points constructed for the defined ε_1 and ε_2 in the plane $(x(t-\tau_0), \varepsilon_2\ddot{x}(t) + \varepsilon_1\dot{x}(t) + x(t))$ reproduces the nonlinear function. However, the quality of reconstruction deteriorates, since the procedure involves numerical calculation of the second derivative.

Recovery of the delay times for time-delay systems with two coexisting delays

Let us consider now a time-delay system with two different delay times τ_1 and τ_2

$$\dot{x}(t) = F(x(t), x(t-\tau_1), x(t-\tau_2)). \quad (14)$$

Time differentiation of Eq. (14) gives

$$\ddot{x}(t) = \dot{x}(t)\partial F/\partial x(t) + \dot{x}(t-\tau_1)\partial F/\partial x(t-\tau_1) + \dot{x}(t-\tau_2)\partial F/\partial x(t-\tau_2). \quad (15)$$

Similarly to temporal realization of Eq. (5), the realization $x(t)$ of Eq. (15) has mainly quadratic extrema and therefore $\dot{x}(t) = 0$ and $\ddot{x}(t) \neq 0$ at the extremal points. Hence, if $\dot{x}(t) = 0$, the condition must be fulfilled,

$$ax(t-\tau_1) + bx(t-\tau_2) \neq 0 \quad (16)$$

where $a = \partial F(x(t), x(t-\tau_1), x(t-\tau_2))/\partial x(t-\tau_1)$ and $b = \partial F(x(t), x(t-\tau_1), x(t-\tau_2))/\partial x(t-\tau_2)$. The condition (16) can be satisfied if $\dot{x}(t-\tau_1) \neq 0$ or/and $\dot{x}(t-\tau_2) \neq 0$. By this is meant that in the

case of quadratic extrema derivatives $\dot{x}(t)$ and $\dot{x}(t-\tau_1)$, or $\dot{x}(t)$ and $\dot{x}(t-\tau_2)$ do not vanish simultaneously. As the result, the number of extrema separated in time by τ_1 and τ_2 from a quadratic extremum must be appreciably less than the number of extrema separated in time by other values of τ and hence the $N(\tau)$ plot will demonstrate minima at $\tau=\tau_1$ and $\tau=\tau_2$. But these minima are not so pronounced as in the case of a single delay time, since only one of the terms of Eq. (16) is necessary not equal to zero.

As an example, we demonstrate the method efficiency with a generalization of the Mackey-Glass equation by introducing a further delay,

$$\dot{x}(t) = -bx(t) + \frac{1}{2} ax(t-\tau_1)/(1+x^c(t-\tau_1)) + \frac{1}{2} ax(t-\tau_2)/(1+x^c(t-\tau_2)) \quad (17)$$

with $a=0.2$, $b=0.1$, $c=10$, $\tau_1=70$, and $\tau_2=300$. The $N(\tau)$ plot is presented in Fig. 6. The most pronounced minima of $N(\tau)$ are observed at $\tau=70$ and $\tau=299$ providing a good estimation of both the delay times τ_1 and τ_2 .

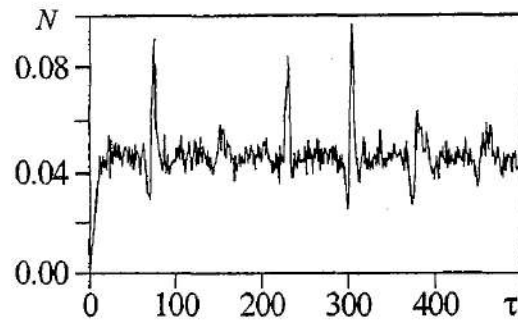


Fig. 6. Number N of pairs of extrema in a realization of Eq. (17) separated in time by τ , as a function of τ . $N(\tau)$ is normalized to the total number of extrema in time series. $N_{\min 1}(\tau)=N(70)$, $N_{\min 2}(\tau)=N(299)$

Conclusion

We have proposed the methods for reconstructing different time-delay systems from time series. These methods are based on the statistical analysis of time intervals between extrema in the time series and the projection of the infinite-dimensional phase space of a time-delay system to suitably chosen low-dimensional subspaces. The methods allow one to estimate the delay time, the parameter characterizing the inertial properties of the system, and the nonlinear function even in the presence of sufficiently high noise. The method of the delay time definition uses only operations of comparing and adding. It needs neither ordering of data, nor calculation of approximation error or certain measure of complexity of the trajectory and therefore it does not need significant time of computation. The proposed techniques of the nonlinear function recovery and estimation of the parameter characterizing the system inertial properties use all points of the time series what allows one to apply the method to short time series even in the regimes of weakly developed chaos.

The authors thank B.P. Bezruchko for stimulating discussions. This work was supported by the Russian Foundation of Fundamental Research, Grant № 03-02-17593, U.S. Civilian Research Development Foundation for the Independent States of the Former Soviet Union, Award № REC-006, State contract № 40.020.1.1.1168 with Minpromnauki RF, and FNP «Dynasty» and ICFFM, Grant № 245 662.

References

1. Kuang Y. Delay Differential Equations With Applications in Population Dynamics, Academic Press, Boston, 1993.
2. Ikeda K. Multiple-valued stationary state and its instability of the transmitted light by a ring cavity system // Opt. Commun. 1979. Vol. 30. P. 257-261.

3. Lang R., Kobayashi K. External optical feedback effects on semiconductor injection lasers // *IEEE J. Quantum Electron.* 1980. Vol. 16. P. 347-355.
4. Mackey M.C., Glass L. Oscillations and chaos in physiological control systems // *Science.* 1977. Vol. 197. P. 287-289.
5. Fowler A.C., Kember G. Delay recognition in chaotic time series // *Phys. Lett. A.* 1993. Vol. 175. P. 402-408.
6. Hegger R., Bunner M.J., Kantz H., Giaquinta A. Identifying and modeling delay feedback systems // *Phys. Rev. Lett.* 1998. Vol. 81. P. 558-561.
7. Zhou C., Lai C.-H. Extracting messages masked by chaotic signals of time-delay systems // *Phys. Rev. E.* 1999. Vol. 60. P. 320-323.
8. Udaltsov V.S., Goedgebuer J.-P., Larger L., Cuenot J.-B., Levy P., Rhodes W.T. Cracking chaos-based encryption systems ruled by nonlinear time delay differential equations // *Phys. Lett. A.* 2003. Vol. 308. P. 54-60.
9. Tian Y.-C., Gao F. Extraction of delay information from chaotic time series based on information entropy // *Physica D.* 1997. Vol. 108. P. 113-118.
10. Kaplan D.T., Glass L. Coarse-grained embeddings of time series: random walks, gaussian random process, and deterministic chaos // *Physica D.* 1993. Vol. 64. P. 431-454.
11. Bunner M.J., Popp M., Meyer Th., Kittel A., Rau U., Parisi J. Recovery of scalar time-delay systems from time series // *Phys. Lett. A.* 1996. Vol. 211. P. 345-349.
12. Bunner M.J., Popp M., Meyer Th., Kittel A., Parisi J. Tool to recover scalar time-delay systems from experimental time series // *Phys. Rev. E.* 1996. Vol. 54. P. 3082-3085.
13. Bunner M.J., Meyer Th., Kittel A., Parisi J. Recovery of the time-evolution equation of time-delay systems from time series // *Phys. Rev. E.* 1997. Vol. 56. P. 5083-5089.
14. Bunner M.J., Ciofini M., Giaquinta A., Hegger R., Kantz H., Meucci R., Politi A. Reconstruction of systems with delayed feedback: (I) Theory // *Eur. Phys. J. D.* 2000. Vol. 10. P. 165-176.
15. Voss H., Kurths J. Reconstruction of nonlinear time delay models from data by the use of optimal transformations // *Phys. Lett. A.* 1997. Vol. 234. P. 336-344.
16. Ellner S.P., Kendall B.E., Wood S.N., McCauley E., Briggs C.J. Inferring mechanism from time-series data: delay differential equations // *Physica D.* 1997. Vol. 110. P. 182-194.
17. Eurich C.W., Milton J.G. Noise-induced transitions in human postural sway // *Phys. Rev. E.* 1996. Vol. 54. P. 6681-6684.
18. Ohira T., Sawatari R. Delay estimation from noisy time series // *Phys. Rev. E.* 1997. Vol. 55. P. 2077-2080.
19. Bezruchko B.P., Karavaev A.S., Ponomarenko V.I., Prokhorov M.D. Reconstruction of time-delay systems from chaotic time series // *Phys. Rev. E.* 2001. Vol. 64. 056216.
20. Ponomarenko V.I., Prokhorov M.D. Extracting information masked by the chaotic signal of a time-delay system // *Phys. Rev. E.* 2002. Vol. 66. 026215.
21. Voss H., Kurths J. Reconstruction of nonlinear time-delayed feedback models from optical data // *Chaos, Solitons and Fractals.* 1999. Vol. 10. P. 805-809.

*Institute of RadioEngineering and
Electronics of RAS, Saratov Branch
Department of Nonlinear Processes,
Saratov State University*

Received 4.09.2003

ВОССТАНОВЛЕНИЕ ДИНАМИЧЕСКИХ МОДЕЛЕЙ СИСТЕМ С ЗАПАЗДЫВАНИЕМ ПО ВРЕМЕННЫМ РЯДАМ

*В.И. Пономаренко, М.Д. Прохоров, А.С. Караваяев,
Е.П. Селезнев, Т.В. Диканев*

Работа посвящена развитию метода оценки параметров систем с запаздыванием по временным рядам. Метод основан на статистическом анализе временных интервалов между экстремумами временного ряда и проецировании бесконечномерного фазового пространства системы с запаздыванием в соответствующим образом выбранные подпространства малой размерности. Работоспособность метода продемонстрирована при реконструкции различных дифференциальных уравнений с запаздыванием по их хаотическим решениям.



Ponomarenko Vladimir Ivanovich was born in Saratov (1960). He graduated from Saratov State University (1982). He defended a dissertation for the degree of Ph.D. on Physics and Mathematics (1992). Now, he is a senior researcher in Saratov Department of the Institute of RadioEngineering and Electronics of Russian Academy of Sciences. Fields of scientific activity: nonlinear dynamics, experimental modelling of complex systems, time series analysis. He is an author of about 60 publications.



Prokhorov Mikhail Dmitrievich was born in Saratov (1968). He graduated from Department of Physics, Saratov State University (1992). He defended a dissertation for the Ph.D. degree on Physics and Mathematics (1997). Now, he is a senior researcher in the Saratov Department of the Institute of RadioEngineering and Electronics of Russian Academy of Sciences. His fields of speciality are nonlinear dynamical modelling, time series analysis and time-delay systems. He is an author of about 50 publications.



Karavaev Anatoly Sergeevich was born in 1981 in Saratov. He has been studying in Saratov State University since 1999. Now he is fifth year student in Department of Nonlinear Processes. He was awarded grants from CRDF REC-006 (2001/2002) and Dynasty Foundation (2003) as a young scientist. His main scientific results are achieved in the field of proposing the methods of time-delay systems reconstruction from experimental time series. He is an author of 13 papers including 4 articles in Russian and foreign journals.



Seleznev Yevgeny Petrovich was born in Saratov (1960) and graduated from Saratov State University (1982). He defended a dissertation for the degree of Ph.D. on Physics and Mathematics (1990). Now, he is a senior researcher in Saratov Department of the Institute for RadioEngineering and Electronics of Russian Academy of Sciences and associated professor in Department of Nonlinear Processes of Saratov State University. Fields of scientific activity: experimental and numerical investigation of nonlinear dynamical systems. He is an author of about 90 publications.



Dikaney Taras Viktorovich was born in Saratov (1979). He graduated from Department of Nonlinear Processes, Saratov State University (2002). Now, he is a graduate student of Saratov State University. He was selected as Soros Student in 1997-2001 and received several Russian awards for young scientists. He was a research fellow in projects supported by RFFI and CRDF. Fields of scientific activity: nonstationary time series analysis, dynamical modelling from time series. He is an author of 20 publications.



Izv. VUZ «AND», vol.11, № 3, 2003

SMALL-WORLD NETWORKS: DYNAMICAL MODELS AND SYNCHRONIZATION

Vladimir N. Belykh, Igor V. Belykh, and Martin J. Hasler

This paper provides a short review of recent results on synchronization in small-world dynamical networks of coupled oscillators. We also propose a new model of small-world networks of cells with a time-varying coupling and study its synchronization properties. It is shown that such a time-varying structure of the network can ensure more reliable synchronization than the conventional small-worlds. The term «small world» refers to a network of locally connected nodes having a few additional long-range shortcuts chosen at random. The addition of the shortcuts sharply reduces the average distance between the nodes and therefore provides the so-called small-world effect. Discovered first in social networks, the small-world effect appeared to be a characteristic of many real-world structure both human-generated or of biological origin. For social networks, this property implies that almost any pair of people in the world can be connected to one another by a short chain of intermediate acquaintances, of typical length about six. However, the structure of social networks is not homogeneous, there are always key persons that provide distant out-local-world connections between people. This paper is written in honor of the 60th birthday of our friend and colleague, Wadim S. Anishchenko, who is one of such key persons in the Nonlinear Dynamics community.

1. Introduction

The study of networks pervades all of science, from physics and neurobiology to engineering and social sciences. From the perspective of nonlinear dynamics, we would like to understand how a huge network of interacting dynamical systems be they neurons, computers connected in Internet or power stations will behave collectively, given their individual dynamics and coupling structure [1]. This paper contributes to elucidate the relation between the network dynamics and graph theory and to apply mathematical theory of synchronization to networks of different nature. Ordinarily, the connection topology is assumed to be either completely regular or completely random. However, many biological, technological, and social networks lie somewhere between these extremes. In 1998, Watts and Strogatz found a simple model of networks that can be tuned through this middle ground: regular coupled networks with the addition of increasing amounts of disorder (a few additional randomly arising connections). These coupled systems were called «small-world» networks [2], by analogy with the small-world phenomenon.

This famous phenomenon was discovered in 1967 by the american social

psychologist Milgram [3]. He performed a simple experiment as follows. He sent roughly 300 letters to randomly selected people in Omaha, Nebraska with the instruction to get the letter to a single «target» person in Boston using only personal contacts. Milgram gave each «sender» some information about the target including name, location, and occupation, so that if the sender did not know the target (and it was extremely unlikely that they would), they could send the letter to someone they did know who they thought would be «closer» to the target. Thus began a chain of senders, each member of the chain attempting to zero in on the target by sending the letter to someone else: a friend, family member, business associate, or casual acquaintance. Milgram's surprising finding was that for the 60 chains that eventually reached the target, the average number of steps in a chain was around six, a result that has entered folklore as the phrase «Six degrees of separation». From this experiment, Milgram concluded that six was the average number of acquaintances separating any two people in the world. Given the form of Milgram's experiment, one could be forgiven for supposing that the figure six is probably not a very accurate one. The experiment certainly contained many possible sources for errors. However, the general result that two randomly chosen human beings can be connected by only short chain of intermediate acquaintances has been subsequently verified, and is now widely accepted. This small-world property of social networks, that the average distance between the nodes is relatively short, has been shown to be widespread in many other real-world structures including the WWW connections [4], scientific networks [5], epidemiological models [6], electrical power grid [7], electronic circuits [8] and neural and biochemical networks [9,10].

The semi-random model of Watts and Strogatz, that reproduces remarkably well main characteristic of many real-world networks, is the following. It starts from a ring lattice with n vertices (the pristine, original, world), each node is connected to its $2k$ nearest neighbors (periodic boundary conditions are applied just for convenience and not strictly necessary). Then shortcuts links are added between random pairs of nodes with probability p per link. Watts and Strogatz conjectured that dynamical systems coupled in this way would display enhanced propagation speed, synchronizability and computation power, as compared with regular lattices of the same size [1]. The intuition is that the short path could provide high-speed communication channels between distant parts of the system, thereby facilitating any dynamical process (like synchronization or computation) that requires global coordination and information flow.

This model has been the subject of significant recent interest within the physics, mathematics, and engineering community. Most theoretical studies were concerned with statistical and combinatoric properties of small-world networks (graphs) where the cells do not have the individual temporal dynamics [1]. Dynamical processes on small-world networks were studied relatively little and mainly by means of computer simulation [7,10-12]. In particular, it was numerically shown that small-world connections may essentially improve synchronization properties of networks of limit-cycle and chaotic oscillators. In turn, synchronization in networks of periodic and chaotic oscillators with different regular and random coupling configurations has been intensively studied [13-21].

More recently, significant progress in the study of the relation between the addition of random shortcuts and the synchronization properties of networks was made by Barahona and Pecora [22]. They applied the Master Stability function approach [18] to the study of local synchronization in small-world networks and showed, through numerics and analysis, how the addition of random shortcuts improves network synchronizability. The connectivity matrices G were once chosen at random and then fixed forever. This is the usual approach of defining the small-world networks. Within this approach, statistics of the connectivity matrices G was translated into statistics of the synchronization thresholds.

In this paper, we propose a new model of dynamical small-world networks where

the shortcuts change as a function of time [23]. Instead of randomly choosing the shortcuts and leaving them fixed, we randomly choose the shortcuts, leave them only for an interval of time τ fixed, then randomly choose another set of shortcuts, leave them again for a lapse of time τ fixed, etc. More precisely, our probabilistic model is the following. During each time interval of length τ , every possible shortcut is turned on with probability p , independently of the switching on and off of the other shortcuts, and independently of whether or not it has been turned on during the previous time interval. Furthermore, we assume that the switching time τ is small with respect to the intrinsic time constants of the dynamics of the individual cells.

This way of transforming a network with fixed couplings, the «pristine world», into a time-varying small-world network can always be applied. We call it the «blinking model» [23]. In this paper, we shall concentrate on global synchronization in the important example where the pristine world is a ring of $2k$ -nearest neighbor coupled chaotic oscillators. The methods developed here, however, are more generally applicable.

The blinking model is actually of practical importance. In practice, often collections of subsystems that are organized into a network actually interact only sporadically. This is true in biology as well as in technology. Neurons in the brain send out electrical signals in the form of spikes and most of the interaction with the other neurons takes place during the arrival of the spikes at the connection points, the synapses. Since the spike duration is usually small with respect to the interspike intervals, this is an important example of «blinking» interaction. Of course, here the occurrence of spikes of different neurons and at different times are not just independent random variables, and the spike durations are actually caused by the dynamics of the individual neurons. Nevertheless, the distant node interaction is of intermittent nature.

In technology, practical systems exist that can be modelled rather precisely by the blinking model. Packet switched networks such as the Internet are an important example. Dynamical processes in the computers that are networked through Internet interact by sending messages that are subdivided into packets and sent over the network. Both in the network links as in the computers themselves, they have to share the available communication time slots with many other packets that belong to communications between different computers and/or different processes. The occurrence of the other packets can be considered as independent, and the timeslots available for the communication between specific processes can also often be considered independent due to the congestion of the links by the other packets. Thus, the blinking model may be appropriate in many different situations.

The model of small-world networks, that we propose, consists of the pristine world (the regular locally coupled lattice of oscillators) and time-dependent on-off coupling between any other pair of cells. Hence we consider the network

$$\dot{x}_i = F(x_i) + \sum_{j=1}^n \varepsilon_{ij}(t/\mu) P x_j, \quad i = 1, \dots, n, \quad (1)$$

where $x_i = (x_i^1, \dots, x_i^d)$ is the d -vector of the coordinates of the i -th oscillator, and μ is a scalar parameter. The matrix P determines by which variables the oscillators are coupled. The $n \times n$ connectivity matrix $G = \varepsilon_{ij}(t)$ is symmetric and has vanishing row-sums and nonnegative off-diagonal elements such that $\varepsilon_{ij} = \varepsilon_{ji}$, $\varepsilon_{ij} \geq 0$ for $i \neq j$, and $\varepsilon_{ii} = -\sum_{j=1, j \neq i}^n \varepsilon_{ij}$, $i = 1, \dots, n$. The number of non-zero off-diagonal elements of the matrix G equals m .

As the pristine world, we take a conventional network, a ring of $2k$ -nearest neighbor coupled oscillators. In this case the connectivity matrix G_{blink} , corresponding to the blinking model, has the $2k$ adjacent diagonals with the coupling constants ε and on-off time-dependent small-world connections parameters $\varepsilon_{i,j_r}(t/\mu)$ standing in all remaining places of the matrix G_{blink} , where $r = 1, 2, \dots, n(n-2k-1)/2$.

We assume the functions $\varepsilon_{i,j_r}(t/\mu)$ to be binary signals that take the constant value ε

with probability p and the value 0 with probability $q=1-p$ in time interval of length τ . Therefore the random variables $\varepsilon_{i,j_r}(m\tau)$ are independent and identically distributed for different m and τ . We assume that $\mu=\tau/T \ll 1$, where T is a characteristic transient time of the individual oscillator, and τ can be also interpreted as a characteristic interval of the time-varying connectivity matrix G .

Typically, in networks of continuous time oscillators, synchronization becomes stable when the coupling strength between the oscillators exceeds a critical value. In this context, a central question is to know the bounds on the coupling strengths such that the stability of synchronization is guaranteed. In this paper, we obtain the conditions for the stability of the synchronous state in the blinking model and reveal their dependence on the coupling configuration, probability p of reswitchings, and properties of the individual oscillators.

2. Synchronization in the pristine world

We start off with the study of global synchronization in the blinking model by considering first synchronization in the pristine world.

To calculate analytical bounds for the synchronization threshold value of coupling in the ring of $2k$ nearest neighbor coupled oscillators, we apply our Connection Graph Stability method, developed in [24], to this network. This general synchronization method combines the Lyapunov function approach with graph theoretical reasonings and allows us to tackle the problem of global stability of synchronization in rather irregular complicated networks.

Hereafter, we omit the proofs [24] and describe only the main results. For the pristine world, sufficient conditions of global synchronization are:

$$\varepsilon > \varepsilon^* = (a/n)R(k,n), \quad (2)$$

where a is a parameter defined by the individual node dynamics and introduced similar to [19,21], and $R(k,n) \simeq (n/2k)^3 = L^3(0)$, where $L(0)$ is the average path length of the pristine world [2]. Consequently, we obtain the following bounds on the synchronization thresholds of global synchronization in the pristine world with the $2k$ diagonals:

$$\varepsilon > \varepsilon^* = an^2/(8k^3). \quad (3)$$

One can check the effectiveness and generality of the estimate (3) for different k . For one extreme case where $k=1$, the network is a ring of diffusively coupled oscillators and the estimate takes the form

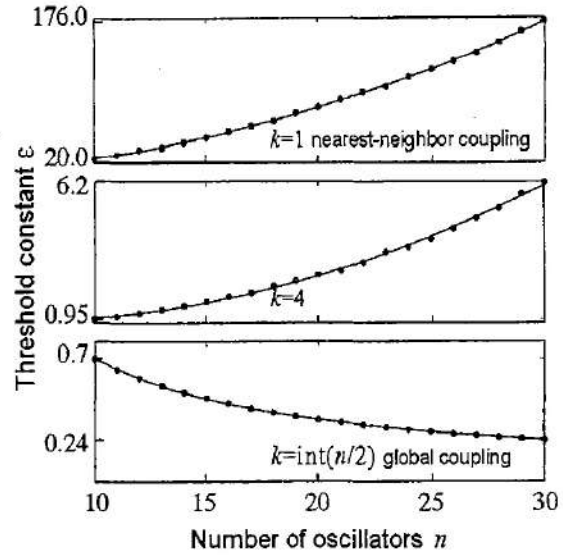
$$\varepsilon^* = \tilde{a}n^2,$$

where $\tilde{a}=a/8$. This estimate presents a quadratic law of the dependence of the synchronization threshold of global synchronization on the number of oscillators. For another extreme case where $k=\text{int}(n/2)$, all oscillators of the ensemble are globally coupled and the estimate presents the law $\varepsilon^*=b/n$ that is well-known for the oscillators with the mean field coupling. Here, b is a new constant. Note that between these extremes there is a case with $k_{\text{const}} \simeq n^{2/3}$, where the synchronization threshold is constant and does not depend on the number of oscillators.

We conjecture that the real threshold for complete synchronization follows closely the same law of dependence on n and k , but with a constant c lower than a which we obtained by stabilizing explicitly the individual oscillators. In support of this claim, we have determined numerically the thresholds for complete synchronization as functions of n for various values of k and we have fitted a curve of the form $cn^2/(8k^3)$ to the data, by

Fig. 1. Dependence of the synchronization thresholds ε^* on the number of oscillators n and on the depth of nearest-neighbor interaction k in the ring of $2k$ -nearest neighbor coupled Lorenz systems. The analytical curves $cn^2/(8k^3)$ (solid lines) for different k fit the numerical data (small circles) in a least-squares sense.

letting vary c (Fig. 1). It can be seen that the deviation of the data from the fitted curve is very small, indeed. Note that we consider only the networks of oscillators admitting global synchronization with increasing coupling. In fact, most known chaotic dynamical systems belong to this class of networks.



3. Auxiliary regular coupling scheme

Let us now consider a regular configuration by adding to the pristine world (with the coupling matrix G) an additional global coupling such that the coupling coefficient $v\varepsilon$ is added to all free places of the matrix G , $0 \leq v \leq 1$. In this extended matrix G_e , the main diagonal elements are such that they preserve vanishing null row-sums. Thus we obtain the all-to-all regular coupling configuration with two different coupling strengths ε and $v\varepsilon$. The rigorous bound of global synchronization threshold in the network with the extended matrix G_e is calculated as follows [23]:

$$\varepsilon^* = (an)R(k,n)/[1+v(R(k,n)-1)], \quad (4)$$

where $R(k,n) = (n/(2k))^3$.

In the context of introducing additional small-world connections with sn edges added at random to the pristine world, where $s > 0$ is rational, the parameter $v = 2s/(n-1-2k)$ may be considered as the mean frequency of the appearance of shortcuts. The added coupling parameter $v\varepsilon$ may be thought of the averaged coupling strength of the sn connections. One can observe that the dependence (4) of the threshold ε^* on the mean frequency of the shortcuts appearance v has a drastic diminution in the region of small v (see Fig. 2,a).

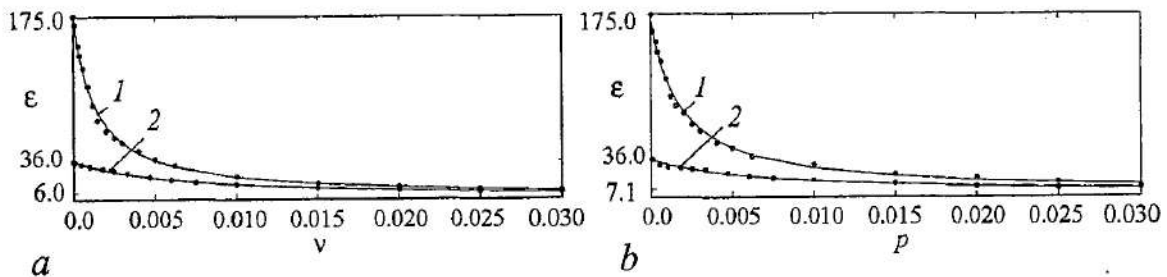


Fig. 2. Dependence of the synchronization thresholds on the parameter v in the all-to-all coupled network with the coupling matrix G_e (a) and on the probability p of the shortcut appearance in the blinking model (b). The pristine world is a ring of 30 nearest-neighbor coupled Lorenz systems. The time step of switchings in the blinking model $\tau = 0.1$. The analytical curves $\varepsilon^* = (an)L(0)/[1+v(L(0)-1)]$ and $\varepsilon^* = (an)L(0)/[1+p(L(0)-1)]$ fit the data remarkable well. $k = 1$ (1); $k = 2$ (2)

4. Synchronization in the blinking model

Let us now return to our blinking model of the small-world shortcut addition with the time-dependent connectivity matrix G_{blink} . Figure 3 shows the time-varying structure of shortcut connections in the blinking model of 30 coupled oscillators. Here, the pristine world is a ring of locally coupled systems ($k=1$).

Recall that the switching time τ is fast with respect to the characteristic transient time T of the individual oscillator such that the parameter μ in Eq. (1) is small. Under this assumption, the blinking model becomes a slow-fast system. Thus, applying the Averaging Theorem [25] to the slow-fast system (1) with the time dependent coupling matrix G_{blink} , we obtain the system (1) with the averaged graph matrix G_{mean} with the constant link strengths $\varepsilon_{i,j}(t)=p\varepsilon=\text{const}$, where p is the probability of shortcut switchings in this blinking model.

Therefore the synchronization problem within the small-world network with blinking on-off shortcuts is reduced by averaging to the network with the constant matrix G_0 that is similar to the matrix G_e , where the probability p stands for the additional all-to-all coupling multiplicative parameter v .

Hence for this case, the rigorous bound of global synchronization is calculated as follows:

$$\varepsilon^* = (a/n)L^3(0)/[1+p(L^3(0)-1)], \quad (5)$$

where $L^3(0)=(n/(2k))^3$. For $p=0$, the estimate (5) becomes the synchronization threshold for the pristine world, and for $p=1$, it gives the synchronization threshold for all-to-all coupling. For $0 < p < 1$, the dependence (5) of the synchronization threshold on p reveals the sharp reduction of the synchronization threshold such that the addition of a few small-world connections (p is small) significantly improves the synchronization properties of the network (see Fig. 2, *b*).

Let us now present the effective path length for our blinking model and its dependence on the probability p . Recall that for $p=0$, the threshold (5) becomes the threshold (5) for the pristine world. Rewriting the dependence (5) in the form similar to Eq. (2), we introduce the effective path length of the blinking model as follows: $L^3(p)=L^3(0)/(1+p(L^3(0)-1))$. Therefore the normalized effective path length has the following dependence on the probability p :

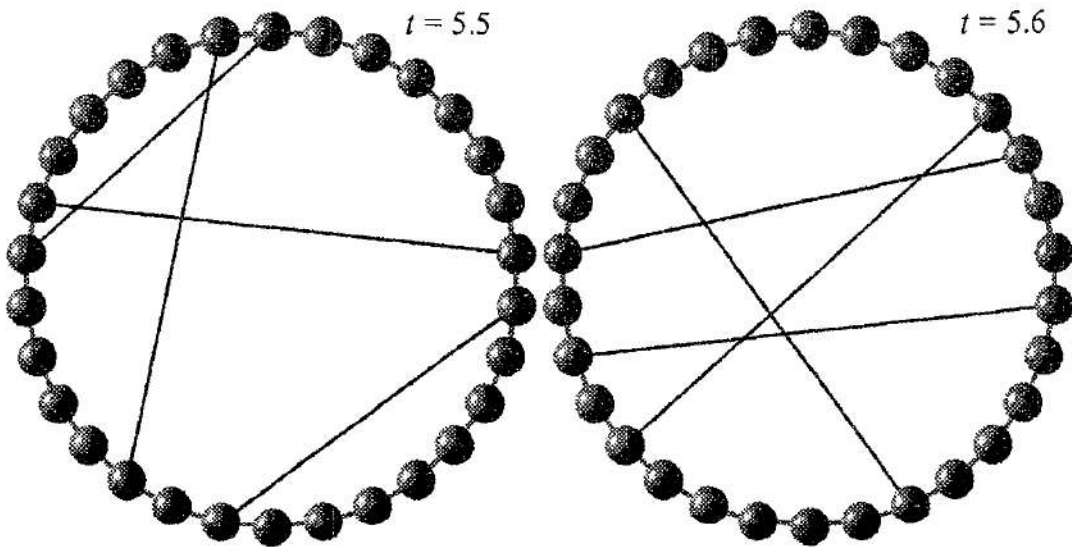


Fig. 3. The blinking model of shortcuts connections. Probability of switchings $p=0.01$, the time step of switchings $\tau=0.1$

$$L(p)/L(0) = 1/(1+(n^3/(8k^3-1)p)^{1/3}).$$

This formula clearly manifests the sharp decrease of the effective path length under a small increase of p from 0 in the blinking model.

5. Conclusions

A new type of dynamical small-world networks of chaotic cells has been proposed. For the first time for such networks with a time-varying coupling configuration, mathematically rigorous and tight bounds on the strength of coupling between the cells have been established that are necessary to achieve complete synchronization independently of the initial conditions. The synchronization thresholds have been explicitly linked with the average path length of the coupling graph and with the probability p .

In previous papers on synchronization in small-world networks a fraction of shortcuts are chosen at random at the beginning and they remain fixed for the rest of the time. In such an approach the synchronization threshold is the mean value of the thresholds for all possible shortcut combinations. However, these thresholds strongly depend on the particular choice of the shortcuts such that the addition of fixed in time small-world links does not necessarily guarantee synchronizability. It was stated in [11,12] that a sufficient amount of randomly chosen shortcuts will cause total synchronization. In other words, there exists a critical value for the probability p for which the small-world network, obtained by adding any given shortcuts, will synchronize completely. This statement is, in general, incorrect. In fact, the addition of fixed in time small-world links *does not* necessarily guarantee synchronizability. The addition of links filling out an entire row in the coupling matrix G does produce a tremendous increase of connectivity and a sharp reduction of the synchronization threshold. At the same time, the addition of coupling coefficients, located in the matrix G as a dense small «spot» and forming an all-to-all coupling within a small subgroup, does not reduce substantially the synchronization threshold. The latter case is not very likely to happen when there are many cells but it has nonetheless a nonzero probability for a finite number of cells.

On the contrary, when the critical probability p is reached in the blinking model, then almost surely the system will synchronize. In other words, the set of on-off shortcut switching sequences that fail to force total synchronization has probability zero. For this property to be true, necessarily the switching time τ must be much smaller than T , the typical time constant for the individual cell dynamics. In this context, for many technical applications and, probably, for the coordinating brain functioning, the blinking effect of the shortcut appearance provides more reliable synchronization and global coordinating properties than the networks with the small-world but fixed coupling structure.

Let us end this paper devoted to Wadim's anniversary by a somewhat frivolous conclusion. In the context of the blinking model of a scientific collaborating network, the distant short-time connections can be considered as telephone calls, personal visits to friends and colleagues, etc. The characteristic time of reswitching τ in the blinking model is a time interval between these desirable events, T is the time when the network studies a particular problem. As we have learned from the above study of the blinking model, to improve synchronization properties of the network, the time τ of coordinating phone calls and visits should be small with respect to T , but these desirable events should be frequent. Consequently, we wish Wadim at the occasion of his 60-th birthday a bright scientific future with many short and intensive interactions with his scientific friends to whom we belong.

I.B. and M.H. acknowledge the financial support of the Swiss National Science Foundation through Grant № 2100-065268. This work was also supported in part by INTAS (Grant № 01-2061) and RFFI (Grant № 02-01-00968).

References

1. *Strogatz S.H.* Exploring complex networks // *Nature*. 2001. Vol. 410. P. 268.
2. *Watts D.J. and Strogatz S.H.* Collective dynamics of «small-world» networks // *Nature*. 1998. Vol. 393. P. 440.
3. *Milgram S.* The small-world problem // *Psychol. Today*. 1961. Vol. 2. P. 60.
4. *Eckmann J.-P. and Moses E.* Curvature of co-links uncovers hidden thematic layers in the World Wide Web // *Proc. Natl. Acad. Sci. U.S.A.* 2002. Vol. 99. 5825.
5. *Newman M.E.J.* Scientific collaboration networks. I. Network construction and fundamental results // *Phys. Rev. E*. 2001. Vol. 64. 016131.
6. *Kuperman M. and Abramson G.* Small world effect in an epidemiological model // *Phys. Rev. Lett.* 2001. Vol. 86. P. 2909.
7. *Watts D.J.* Small worlds // Princeton Univ. Press, Princeton, 1999.
8. *i Cancho R.F., Janssen C., and Solé R.V.* Topology of technology graphs: small world patterns in electronic circuits // *Phys. Rev. E*. 2001. Vol. 64. 046119.
9. *Jeong H., Tombor B., Albert R., Oltvai Z.N., and Barabási A.-L. and Albert R.* The large-scale organization of metabolic networks// *Nature (London)*. 2000. Vol. 407. P. 651.
10. *Lago-Fernández L.F., Huerta R., Corbacho F., and Sigüenza J.A.* Fast response and temporal coherent oscillations in small-world networks // *Phys. Rev. Lett.* 2000. Vol.84. P. 2758.
11. *Gade P.M. and Hu C.K.* Synchronous chaos in coupled map lattices with small-world interactions // *Phys. Rev. E*. 2000. Vol. 62. P. 6409.
12. *Wang X. and Chen G.* Synchronization in small-world dynamical networks // *Int. J. Bifurc. and Chaos*. 2002. Vol. 12. P. 187.
13. *H. Fujisaka and T. Yamada.* Stability theory of synchronized motions in coupled oscillatory systems // *Prog. Theor. Phys.* 1983. Vol. 69. P. 32.
14. *Afraimovich V.S., Verichev N.N., and Rabinovich M.I.* Stochastic synchronization in dissipative systems // *Izv. Vuzov. Radiofiz.* 1986. Vol. 29. P. 795.
15. *Pecora L.M. and Carroll T.L.* Synchronization in chaotic systems // *Phys. Rev. Lett.* 1990. Vol. 64. P. 821.
16. *Anishchenko V.S., Vadivasova T.E., Postnov D.E., Safonova M.A.* Synchronization of chaos // *Int. J. Bifurc. and Chaos*. 1992. Vol. 2. 633.
17. *Wu C.W. and Chua L.O.* Synchronization in an array of linearly coupled dynamical systems // *IEEE Trans. Circuits Syst., I: Fundam. Theory Appl.* 1996. Vol. 43. 161.
18. *Pecora L.M. and Carroll T.L.* Master stability function for synchronized coupled systems // *Phys. Rev. Lett.* 1998. Vol. 80. 2109.
19. *Belykh V.N., Belykh I.V., and Hasler M.* Hierarchy and stability of partially synchronous oscillations of diffusively coupled dynamical systems // *Phys. Rev. E*. 2000. Vol. 62. 6332.
20. *Pikovsky A., Rosenblum M., and Kurths J.* Synchronization: a universal concept in nonlinear science // Cambridge University Press, Cambridge, 2001.
21. *Belykh I.V., Belykh V.N., Nevidin K.V., and Hasler M.* Persistent clusters in lattices of coupled nonidentical chaotic systems // *CHAOS*. 2003. Vol. 13. P. 165.
22. *Barahona M. and Pecora L.M.* Synchronization in small world systems // *Phys. Rev. Lett.* 2002. Vol. 89. 054101.
23. *Belykh I.V., Belykh V.N., and Hasler M.* Blinking model and synchronization

in small-world networks with a time-varying coupling // *Physica D*. 2004 (to be published).

24. *Belykh V.N., Belykh I.V., and Hasler M.* Connection graph stability method for synchronized coupled chaotic systems // *Physica D*. 2004 (to be published).

25. *Bogoljubov N.N., Mitropolski Yu.A.* Asymptotic methods in oscillation theory. Moscow: Nauka, 1974.

*Mathematics Department, Volga State Academy,
Nizhny Novgorod, Russia
Laboratory of Nonlinear Systems, Swiss Federal
Institute of Technology Lausanne (EPFL),
Switzerland*

Received 19.09.03

УДК 537.86

СВЯЗАННЫЕ СИСТЕМЫ ТИПА «МИР ТЕСЕН»: ДИНАМИЧЕСКИЕ МОДЕЛИ И СИНХРОНИЗАЦИЯ

В.Н. Белых, И.В. Белых, Martin J. Hasler

В работе представлен краткий обзор результатов исследования синхронизации взаимосвязанных динамических систем типа «мир тесен» (small-world). Предложена новая модель сетей типа «мир тесен» с изменяющейся во времени структурой связи. Показано, что такая структура связи обеспечивает более надежную синхронизацию, чем традиционные системы типа «мир тесен» с фиксированными связями. Термин «small world» (в прямом русском переводе «маленький мир» или, правильной, «мир тесен») относится к связанной системе, состоящей из локально связанных элементов и имеющей, в то же время, небольшое количество дальних вероятностных связей (shortcuts). Действительно, добавление нескольких дальних связей может существенно уменьшить среднее характеристическое расстояние между элементами даже очень большой локально связанной сети. Эффект типа «мир тесен», обнаруженный впервые социологами при исследовании структуры общества, является важной характеристикой многих других взаимодействующих систем, например, таких как ансамбли связанных нейронов в мозге, компьютерные сети и Интернет, взаимодействующие популяции и т.д. В применении к структуре общества это свойство означает, что два любых человека в мире связаны между собой через небольшое количество промежуточных знакомств. Считается, что среднее число звеньев такой цепи равно шести. Однако структура таких связей неоднородна, и всегда в обществе есть ключевые люди, обеспечивающие реальное взаимодействие между различными группами людей. Эта статья написана в честь 60-летия нашего друга и коллеги, Вадима Семеновича Анищенко, который является именно таким ключевым человеком в научном сообществе людей, занимающихся нелинейной динамикой.



Vladimir N. Belykh was born in N. Novgorod region (1943). He received the Diploma in 1966, the first PhD degree in 1972 from the University of Nizhny Novgorod, and the second Doctoral degree in 1985 from the University of St.-Petersburg, all in physics and mathematics. He became full professor in 1986. Nowadays he is currently the Head of Mathematics Department of Volga State Academy (Nizhny Novgorod and Professor at the Advanced School of General and Applied Physics of the University of Nizhny Novgorod). He received numerous Russian and international prizes, including Lenin's Komsomol prize (1974), Medal of Honored Scientist of the Russian Federation (1993), Prominent Scientist distinction of the Russian Federation (1994), Soros Professorship grant (1995), Distinguished Professor Scholarship (1996-2003). He held visiting Professor positions and gave lectures in different overseas universities including University of California, Berkeley; the Technical University of Denmark; University of Potsdam, Swiss Federal Institute of Technology; Eindhoven University of Technology, etc. His research interests include nonlinear dynamics and chaos, qualitative theory and bifurcation theory of concrete dynamical systems, mathematical modeling in electrical engineering, physics, biology and economics. A chaotic attractor of a two-dimensional map proposed by him in 1981, called the Belykh attractor, is now recognized as a classical object of ergodic theory.

E-mail: belykh@unn.ac.ru



Igor Belykh was born in Nizhny Novgorod (1973). He received the Diploma in 1995 and the PhD degree in 1999 from the University of Nizhny Novgorod, both in physics and mathematics. Nowadays he is a postdoctoral fellow at the Laboratory of Nonlinear Systems and a lecturer at the School of Computer and Communication Sciences of Swiss Federal Institute of Technology Lausanne (EPFL). He holds also a researcher position at the Department of Differential Equations, headed by L.P. Shilnikov, at the Institute of Applied Mathematics and Cybernetics, Nizhny Novgorod (on leave). He received several Russian and international prizes, including the Soros Student Award (1996), Razuvaev Award (1998), Soros PhD student Award (1997,1998), and Research Scholarship from Swiss Government (1998). He held visiting researcher positions at the Department of Physics of the Technical University of Denmark in 1997, 1999, 2000, and at the Department of Electrical Engineering of Swiss Federal Institute of Technology Lausanne (1998-1999). His present interests include nonlinear dynamics of biological neurons and neural systems, coupled dynamical systems, synchronization and cooperative behavior, modeling of nonlinear circuits and systems, and applications of nonlinear dynamics in physics, biology, and engineering.



Martin Hasler was born in Wetzikon canton Zurich (1945). He received the Diploma in 1969 and the PhD degree in 1973 from the Swiss Federal Institute of Technology, Zurich, both in physics. He continued research in mathematical physics at Bedford College, University of London, from 1973 to 1974. At the end of 1974 he joined the Circuits and Systems group of the Swiss Federal Institute of Technology Lausanne (EPFL), where he was given the title of a Professor in 1984. He became associate and full professor, respectively, in 1996 and 1999. In 2002, he was acting Dean of the newly created School of Computer and Communication Sciences of EPFL. During the 70's, his research was concentrated on filter theory and design, in particular active and switched capacitor filters. Since 1980 his research is centered on nonlinear circuits and systems, including the qualitative analysis of resistive and dynamic circuits, the modeling and identification of nonlinear circuits and systems, neural networks and the engineering applications of complicated nonlinear dynamics, in particular chaos. Chaos is applied to the transmission of information and to signal processing. Among the applications of the modeling and identification of nonlinear systems is the modeling of high-temperature superconductors for energy applications. Very recently, he is interested in the information processing in the brain.

He is a Fellow of the IEEE. He was the chairman of the Technical Committee on Nonlinear Circuits and Systems IEEE CAS Society from 1990 to 1993. From 1993 to 1995 he was the Editor of the IEEE Transactions on Circuits and Systems, Part I. He was the Chairman of ISCAS 2000, Geneva, Switzerland. He was a member of the Board of Governors of the IEEE CAS Society and currently he is its Vice-President for Technical Activities.

He is a member of the Scientific Council of the Swiss National Science Foundation since Jan. 2000.



Izv. VUZ «AND», vol. 11, № 3, 2003

CHAOS IN THE BRAIN AND IN SENSORY NEURONS

Hans A. Braun, Karlheinz Voigt, and Frank Moss

The brain is a complex organ, possibly among the most complex in the universe. The possibility exists therefore that chaotic dynamics is one of its characteristics. But sensory neurons are also complex and such processes also may be found in them. Here we show some experimental data from electroreceptors of catfish and hypothalamic neurons from the paraventricular nucleus of rat brain slices. The data show the presence of unstable periodic orbits, one of the signatures of low dimensional chaotic dynamics. Professor Vadim S. Anishchenko was a very early pioneer of fundamental studies of chaos and continues to make innovative, inspiring and original contributions to the science of complexity in all fields.

1. Introduction

Studies of chaotic dynamics date to a time just prior to the turn of the last decade with Vadim S. Anishchenko having made early fundamental contributions [1]. Moreover, Anishchenko was an early pioneer in the essentially experimental technique of exploring chaos in electronic circuits specifically designed for that purpose [2,3]. And he continues today actively providing inspiration to young researchers in dynamical systems theory and experiment the world over [4]. On this, the occasion of his sixtieth birthday, it is an honor and pleasure to contribute the following modest paper devoted to experimental searches for chaotic signatures in two biological preparations.

Unstable Periodic Orbits (UPOs) are a characteristic signature of low dimensional dynamical chaos [5,6] and have been experimentally demonstrated and quantitatively measured originally in an electronic circuit [7]. UPOs are the quintessential instability evident in complex systems. A trajectory encounters a saddle-shaped potential, approaches its unstable fixed point along a stable manifold and departs along an unstable manifold. The speeds of approach and departure are governed by the Lyapunov exponents, a positive exponent being the hallmark of chaos. Chaotic systems show spectra of UPOs of various orders. Here we confine our discussions to those of the lowest order, that is period 1.

2. Data analysis: How Unstable Periodic Orbits are detected in neural spike trains

Biology is fraught with instabilities at all levels from single cells to systems of whole organs. Thus we might expect to find UPOs in biological preparations. The information flow in neurons is encoded in the sequences of time intervals between action

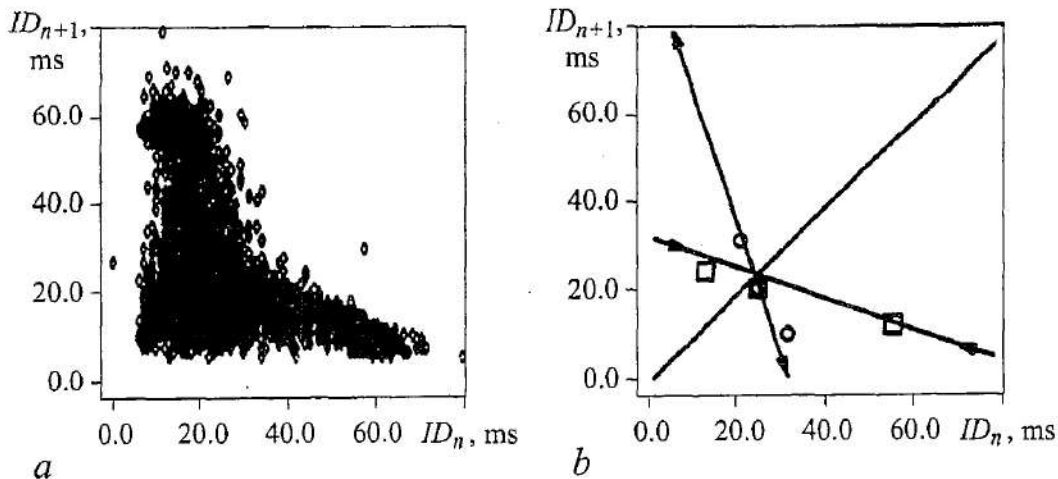


Fig. 1. (a) Complete record of time intervals called a scatter plot. (b) Single example encounter extracted from the record shown in (a). The 45-degree line shows all periodic orbits. The unstable fixed point is the intersection of stable (inward pointing arrows) and unstable (outward pointing arrows) manifolds

potential occurrences, or «spikes». These time series are called «spike trains». So it is in particular patterns of time interval sequences within the trains that we must seek the signatures of UPOs. Indeed, we seek to describe and detect an «encounter» with the unstable fixed point in the aforementioned saddle.

As we have shown previously for some sensory neurons, these encounters can be detected in 2-dimensional time interval plots, where a time interval between a pair of action potentials is plotted versus the immediately preceding time interval [8-10]. An example is shown in Fig. 1, a where a complete neural recording is plotted in this way. In Fig. 1, b we show an example encounter extracted by an appropriate algorithm as described below from all the data shown in Fig. 1, a. In Fig. 1, b, the squares show the approach to the unstable fixed point, marked by the crossing of the two straight lines that indicate the manifolds. Inward-pointing arrows mark the stable and outward-pointing arrows mark the unstable manifolds. As the points converge on the fixed point, they feel the instability and start to diverge along the unstable manifold as shown by the circles. Thus a particular sequence consisting of 3 points approaching followed immediately by 3 points departing identifies an encounter with a period 1 UPO. Of course, such systems often display more complex structures of higher order UPOs than detected here. These have been further investigated in Hodgkin-Huxley-type neuron models [11,12].

Moreover, biological systems are almost always contaminated with high-dimensional random processes, or «noise». Thus we must seek to find (and hopefully to count) the UPOs in the noisy chaotic systems that are usual for biology. In systems contaminated by some high dimensional noise, UPOs spend much of their time in high-dimensional phase space, but occasionally execute trajectories with detectable signatures on 2-dimensional projections. The number, N , of encounters with UPOs in the complete record measures the «strength» of the instability. The problem is that in systems contaminated with noise, there are also «false encounters» that happen just by chance even in completely random data sets. These are taken into account by analyzing «surrogate» data sets for the number N_s of false encounters. These are detected and counted in exactly the same way as for the actual data. In fact, the simplest surrogates are constructed by just randomly scrambling the locations of the time intervals in the actual data set. A statistical measure of the strength of the instability is the following:

$$K = (N - \langle N_s \rangle) / \sigma.$$

One must repeat the false positive count many times in order to get a good

statistical average $\langle N_s \rangle$, and the standard deviation of the determinations of N_s in the surrogates is σ . Thus in Eq. 1 K has units of standard deviations. For $K \geq 3$, the statistical precision of the determination, that is the presence of UPOs in the data set, is at the 95% confidence level.

3. Results

We will not repeat here the details of the experimental preparations as those have been presented previously [10]. Figure 2 shows results for a catfish electroreceptor

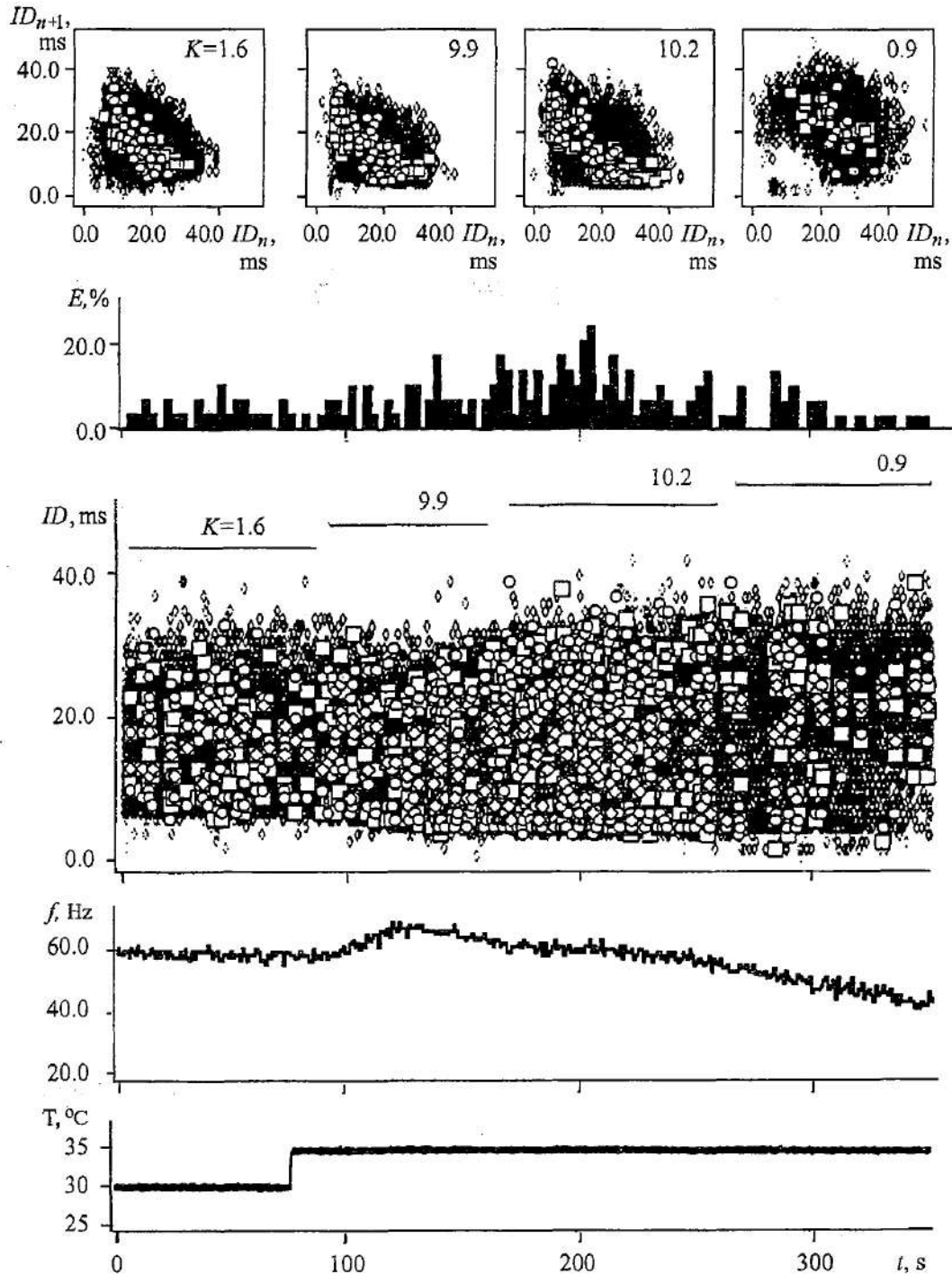


Fig. 2. Scatter plots, histograms of UPO counts, the complete time interval record, mean firing rate and temperature step recorded for the electroreceptor of a catfish

subject to a temperature step at a certain time. The top panel shows 4 scatter plots with the encounters indicated by squares (stable) and circles (unstable) movements along the manifolds. The K -values are shown, the maximum being around 10. The next panel down shows a histogram of the numbers of encounters counted in segments of the data set marked by the solid lines in the panel below. That panel shows the complete record of time intervals plotted against time. The mean firing rate and temperature step are shown in the bottom panels. Note that a bifurcation takes place about 75 s after the temperature step. The transition to period-2 is accompanied by a substantial increase of the UPO count. Note also that the appearance of large numbers of UPOs anticipates the bifurcation as shown by the bar marked with $K=9.9$ in the middle panel. These occurrences are called «precursors» and have been previously developed as tools for predicting the approach of bifurcations [13].

We turn now to the hypothalamus, a part of the brain involved in temperature regulation of the body. We have found that hypothalamic neurons from the

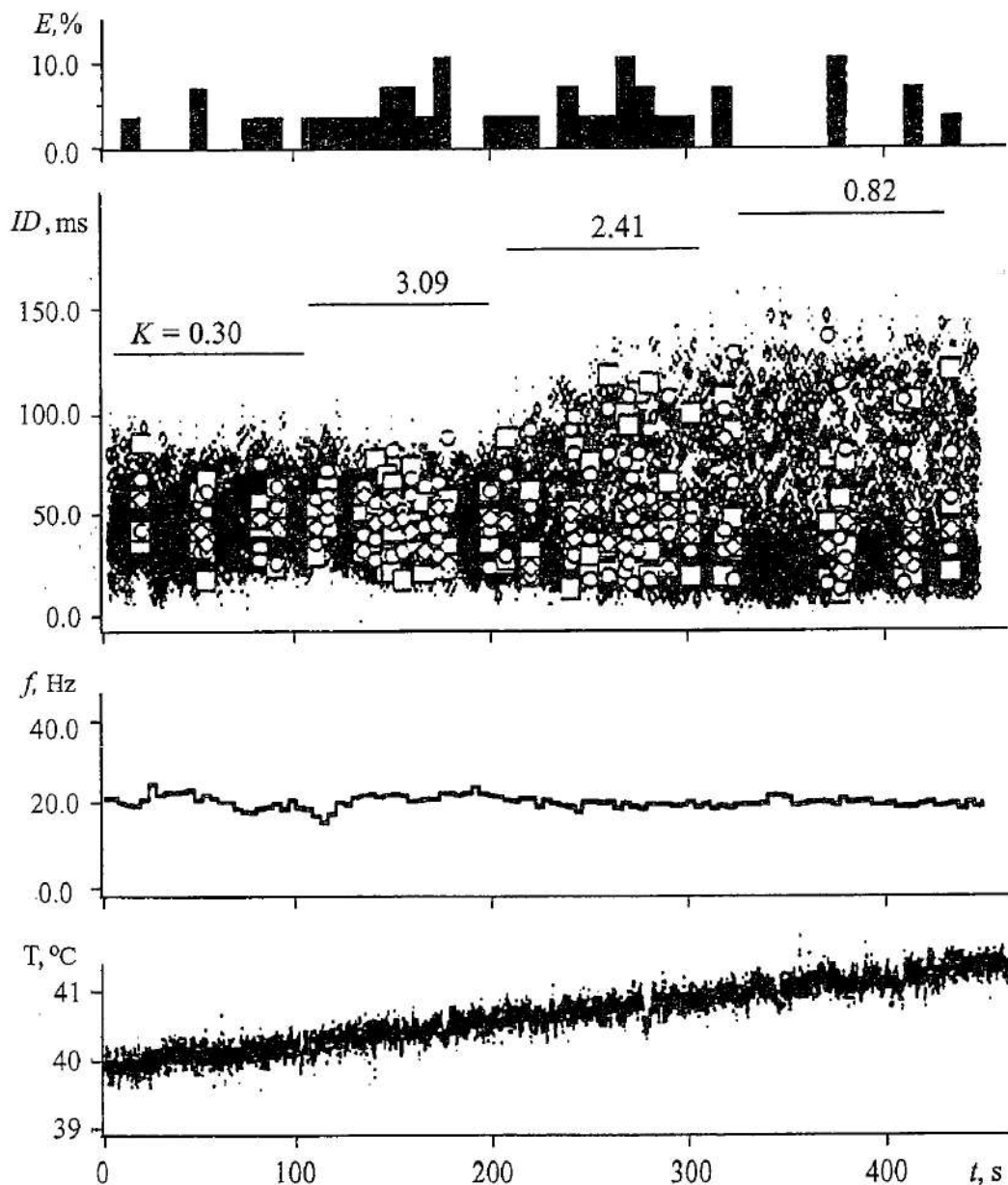


Fig. 3. Histograms of UPOs (top panel), the complete time interval record, mean firing rate and temperature scan (bottom panel) for a hypothalamic neuron in a rat brain slice

paraventricular nucleus in rat brain slices are indeed temperature sensitive, and that UPOs can track and anticipate the onset of bifurcations. Well-characterized rats were executed humanely, their brains extracted and slice preparations obtained following previously detailed procedures [10]. The neurons were then identified and extracellular recordings of their firings made while the temperature of the bath was slowly swept upward. The results are shown in Fig. 3. The upper panel shows histograms of the encounters for the recording segments shown by the solid bars below. The K -values are marked on the bars. The complete record of time intervals is shown in the second panel down. The mean firing rate and temperature sweep are shown in the bottom two panels. Encounters are again identified by squares (stable) and circles (unstable) in the complete record. The first part of the record (time <100 s) shows stable period-1 activity with no significant numbers of UPOs. Later, at around 150 s, we can easily see the precursors marked by $K=3.09$ just prior to the period doubling bifurcation. Just after the bifurcation at the beginning of the period-2 regime, large numbers of UPOs again occur with $K=2.41$. Note that in the fully developed period-2 regime after about 300 s, the neuron again becomes stable with $K=0.82$ indicating no detectable UPOs. Thus we can track the transitions from stable period-1 to unstable period-2 and back to stable period-2 again using our technique for detecting and counting UPOs.

All animals used in this study were treated humanely and in strict accordance with the appropriate German Federal Requirements in effect at the time of the experiments.

4. Summary

We have shown how UPOs can be detected and counted in biological preparations of sensory neurons. The two preparations used were electroreceptor neurons in the catfish and hypothalamic neurons in the paraventricular nucleus of a rat brain. In all cases the neurons sense temperature changes by first anticipating then executing period doubling bifurcations. The sudden increase of the density of UPOs can be used to anticipate these bifurcations. We have here addressed the general topic of instability and stability in biological electrosensory neurons and in the thalamus of the rat brain.

This work was supported by the INTAS grant 01-2061 and by the US Office of Naval Research. F.M. is grateful to the Alexander von Humboldt Foundation for continuing support.

References

1. *Anishchenko V.S.* Dynamical Chaos - Basic Concepts. Teubner-Texte zur Physik, Leipzig, 1987.
2. *Anishchenko V.S.* Dynamical Chaos in Physical Systems: Experimental Investigation of Self-Oscillating Circuits. Teubner-Texte zur Physik, Leipzig, 1989.
3. *Anishchenko V.S.* Dynamical Chaos - Models and Experiments. World Scientific, Singapore, 1995.
4. *Anishchenko V.S., Astakhov V.V., Neiman A.B., Vadivasova T.E., and Schimansky-Geier L.* Nonlinear Dynamics of Chaotic and Stochastic Systems. Springer Verlag, Berlin, 2002.
5. *Artuso R., Aurell E., and Cvitanovic P.* Recycling of strange sets I: cycle expansions // *Nonlinearity*. 1990. Vol. 3. Pp. 325-338.
6. *Artuso R., Aurell E., and Cvitanovic P.* Recycling of strange sets II: applications // *Nonlinearity*. 1990. Vol. 3. Pp. 361-375.
7. *Pierson D. and Moss F.* Detecting periodic unstable points in noisy chaotic and

limit cycle attractors with applications to biology // *Phys. Rev. Lett.* 1995. Vol. 75. Pp. 2124-2127.

8. *Braun H.A., Schfer K., Voigt K., Peters R., Bretschneider F., Pei X., Wilkens L. and Moss F.* Low-dimensional dynamics in sensory biology 1: thermally sensitive electroreceptors of the catfish // *J. Comp. Neurosci.* 1997. Vol. 4. Pp. 335-347.

9. *Braun H.A., Dewald M., Schfer K., Voigt K., Pei X., Dolan K., and Moss F.* Low-dimensional dynamics in sensory biology 2: facial cold receptors of the rat // *J. Comp. Neurosci.* 1999. Vol. 7. Pp. 17-32.

10. *Braun H.A., Dewald M., Voigt K., Huber M., Pei X., and Moss F.* Finding unstable periodic orbits in electroreceptors, cold receptors and hypothalamic neurons // *Neurocomputing.* 1999. Vol. 26-27. Pp. 79-86.

11. *Braun H.A., Huber M.T., Dewald M., Schfer K., Voigt K.* Computer simulations of neuronal signal transduction: The role of nonlinear dynamics and noise // *Int. J. Bifurc. and Chaos.* 1998. Vol. 8. Pp. 881-889.

12. *Braun W., Eckhardt B., Braun H.A., Huber M.* Phase space structure of a thermoreceptor // *Phys. Rev. E.* 2000. Vol. 62. Pp. 6352-6360.

13. *Omberg L., Dolan K., Neiman A., and Moss F.* Detecting the onset of bifurcations and their precursors from noisy data // *Phys. Rev. E.* 2000. Vol. 61. Pp. 4848-4853.

*Institute of Physiology, University
of Marburg, Germany
Center for Neurodynamics,
University of Missouri at St. Louis, USA*

Recieved 28.08.2003

УДК 577.359

ХАОС В МОЗГЕ И В СЕНСОРНЫХ НЕЙРОНАХ

H.A. Braun, K. Voigt, F. Moss

Мозг является сложным органом, относится к числу наиболее сложных объектов мироздания. Поэтому существует вероятность, что одной из его характеристик является хаотическая динамика. Однако сенсорные нейроны также являются сложными, и в них также могут быть найдены хаотические процессы. В данной работе мы демонстрируем некоторые экспериментальные данные, записанные с электрорецепторов полосатой зубатки и гипоталамических нейронов из паравентрикулярных ядер срезов мозга крысы. Данные демонстрируют наличие неустойчивых периодических орбит - одной из характерных черт маломерной хаотической динамики. Профессор В.С. Анищенко был среди самых первых инициаторов фундаментальных исследований хаоса и продолжает осуществлять новаторский, вдохновляющий и оригинальный вклад в науку сложности во всех ее областях.



Frank Moss holds degrees in both Physics (PhD) and Engineering (BS and MS) from the University of Virginia. He studied macroscopic quantum fluids at the University of Rome in Italy on a Postdoctoral Fellowship awarded by the National Science Foundation. Moss' early research centered on turbulence in superfluid liquid helium, for which he was later awarded Fellowship in the American Physical Society. Later he studied random fluctuations and noise in nonlinear physical systems, and in the early 90's broadened these studies to include applications in sensory biology. In 1995, he established the Center for Neurodynamics and continues as its Director. Research of the Center has attracted editorial commentary in numerous science journals, for example, *Nature*, *Science* and *Science News* as well as the popular press including *The Economist* and *The Financial Times* (London). Moss is the author of over 215 scientific publications including the editorship of several books and special issues of journals. He has given over 260 lectures at national and international conferences and institutes. He was awarded senior fellowships by the British government and by NATO and is a winner of the prestigious Humboldt Research Prize in Germany as well as numerous other awards for notable research. He currently serves on the editorial boards of two international journals and is a consulting editor for numerous others. He is a past chairperson of the Division of Biological Physics of the American Physical Society. He is currently Curators' Professor at the University of Missouri at St. Louis, USA. E-mail: mossf@umsl.edu

Hans Albert Braun is head of the Neurodynamics Group at the Institute of Physiology at the University of Marburg in Germany. He has been trained as electronic engineer at the Technical University in Karlsruhe where he obtained a degree in «Electrobiology». In course of a supplementary study of «Human Biology» he obtained his PhD at the Medical Faculty of the University of Marburg.

His research involves experiments and models of neuronal encoding and neuromodulatory processes in peripheral sensory receptors (thermo- and electroreceptors) and hypothalamic neurones (neuroendocrine functions) including computer modelling studies of affective disorders. The aim is the understanding of neuronal systems dynamics at different levels and to elucidate their functional principles.

Hans A. Braun is member of several scientific societies and has been honored with the fellowship of the Biophysics Division of the American Physical Society. E-mail: braun@mailier.uni-marburg.de

Karlheinz Voigh - Institute of Physiology, University of Marburg, 35037 Marburg, Germany.



SYNCHRONIZATION, NOISE AND ELECTRORECEPTORS

Alexander Neiman, David F. Russell, Frank Moss, and Lutz Schimansky-Geier

Classical notion of synchronization, introduced originally for periodical self-sustained oscillators, can be extended to stochastic systems. This can be done even in the case when the characteristic times of a system are fully controlled by noise. Stochastic synchronization is then defined by imposing certain conditions to various statistical measures of the process. We review various approaches to stochastic synchronization and apply them to study synchronization in the electrosensory system of paddlefish.

1. Introduction

Among other nonlinear effects, the phenomenon of synchronization is probably the most often observed in the great variety of systems of different origins. From a general point of view synchronization represents the relation between two objects that are oscillating in time. The oscillators are said to be synchronized, or in «synchrony», when there exists a fixed phase relation between them.

Besides man-made systems where synchronization is actually used [1], this phenomenon has been observed in biological systems [2] starting from microscopic level of cell populations [3] and single neurons [4 - 6] to large neural networks [7], human cardio-respiratory dynamics [8] as well as external synchronization of human cardio rhythm [9], and behavior of large populations of living objects [10]. We refer to a recent book [11] for a comprehensive review on modern theories and applications of synchronization.

Synchronization occurs when a nonlinear oscillator, possessing a stable periodic motion, is subjected to an external time-dependent force or is coupled with another oscillator. Classical theory of synchronization operates with so-called self-sustained periodic oscillators. The characteristics of stable periodic oscillations of such systems, represented by a stable limit cycle in the phase space, are determined by natural properties of the oscillator and do not depend upon initial conditions [12]. When a self-sustained oscillator is driven by an external periodic force of appropriate amplitude and frequency, the oscillations of the system occur in phase with the external signal. Synchronization is thus defined as phase locking and frequency entrainment. The same effect occurs when two (or more than two) self-sustained oscillators are coupled.

Recent studies have shown that the class of systems and driving signals which exhibit synchronization could be significantly extended. Different types of synchronization have been found in chaotic systems, including the classic type of phase synchronization in periodically driven and coupled chaotic systems [13 - 16].

In this paper, we are concerned with noisy synchronization. Though originally studied quite early [17], the theory of stochastic synchronization has only recently been applied to biological or medical systems. As intuitively expected, noise usually acts against synchronization. However, recently it has been shown that for a large class of stochastic systems the phenomenon of noise enhanced phase synchronization can be observed [18].

2. Stochastic synchronization

Synchronization of coupled periodic self-sustained oscillators is understood as adjustment of their phases and frequencies. If $\Phi(t)$ is the phase of one oscillator and $\Psi(t)$ is the phase of another oscillator (or the phase of periodic driving force), then the phase locking condition reads:

$$|\phi(t)| < \text{const}, \quad \phi(t) = n\Phi(t) - m\Psi(t), \quad (1)$$

where n and m are integer numbers. The phases $\Phi(t)$, $\Psi(t)$ are defined on a whole real line. In the regime of synchronization, the phase difference, $\phi(t)$, therefore, remains constant forever. In the simplest case of 1:1 synchronization the response of the oscillator is represented by one complete cycle per one period of driving force. More general case is $m:n$ synchronization, which means that during m complete cycles of driving signal there occur n complete cycles of the oscillator. For periodic oscillators the synchronization condition Eq. (1) is equivalent to the notion of frequency locking $n\omega = n\dot{\Phi} = m\Omega = m\dot{\Psi}$.

The concept of synchronization for stochastic systems is not trivial. As is well known [17] noise influence on a self-sustained oscillator results in the diffusion of its phase. That is why the properly defined phase difference ϕ is also diffuses so that the condition Eq. (1) never fulfills in the presence of Gaussian noise. The phase locking may occur only for random periods of time and is interrupted by so-called phase slips. Thus, the definition of synchronization in the presence of noise appears to be «blurred». That is why the conditions of synchronization should be defined in statistical way and we have to use the notion of «effective» or «stochastic» synchronization [19,20]. It can be defined by imposing restrictions on (i) signal-to-noise ratio, in the case of periodically driven self-sustained oscillator; (ii) frequency fluctuations; and (iii) phase fluctuations.

We use here the strongest definition of stochastic synchronization based on statistics of phase fluctuations. Statistical measures of synchronization can be based on the stationary probability density of the phase difference wrapped into $[0, 2\pi]$. A well-expressed maximum will correspond to a strong synchronization in statistical sense. This can be further quantified by the synchronization index [7] as the first Fourier mode of the stationary probability density of the phase difference: $\gamma^2 = \langle \sin\phi \rangle^2 + \langle \cos\phi \rangle^2$. The synchronization index changes from 0 (no synchronization, uniform distribution of the phase difference) to 1 (perfect synchronization, δ -type distribution of the phase difference).

Another way to characterize stochastic synchronization is to calculate the effective diffusion coefficient for the phase difference. The system is effectively synchronized by external periodic force if the mean time in course of which the instantaneous phase of the system is locked, is larger than some given value. The quantity related to this definition which can be used as a measure of phase coherence is the effective diffusion constant D_{eff} defined as $D_{\text{eff}} = 1/2 d/dt [\langle \phi^2(t) \rangle - \langle \phi(t) \rangle^2]$. The effective diffusion constant describes spreading of an initial distribution of the phase difference due to noise-induced diffusion. It can be shown that the effective diffusion constant D_{eff} is inverse proportional to the mean time interval of phase locking.

Phase synchronization in conventional oscillatory systems, for instance, the van der Pol oscillator, is usually destroyed by noise [17]. However, in systems exhibiting the

phenomenon of stochastic resonance noise can enhance synchronization [23,18]. Periodically driven bistable or excitable stochastic systems can be considered from the synchronization point of view. However, in order to study phase synchronization we need to introduce instantaneous phase of the system. The problem is that for aperiodic signals the definition of the phase becomes ambiguous.

Several approaches can be used. The formal but general definition of instantaneous phase is based on *the concept of analytic signal* [21], whereby the instantaneous phase is defined as the argument of the analytic signal. The analytic signal is a complex function of time with the real part being the original signal and the imaginary part being the Hilbert transform of the original signal. This approach was used to study phase synchronization of chaotic systems [16] and stochastic resonance systems [18].

In the case of bistable or excitable systems the phase can be associated with the moments of time t_n when a particle crosses a barrier [18] or with occurrences of spikes in the case of excitable systems. For such stochastic point processes the phase increases by 2π every time t_n and linearly interpolated between t_{n+1} and t_n [18,20]. Another approach was recently proposed in [22] where time t_n were associated with a level crossings. This approach allowed to calculate analytically so-called Rice frequency and to compare it with other approaches, for example with analytic signal approach [22].

As soon as the phase is defined we can pose synchronization problem: whether the instantaneous phase of the switching and the corresponding mean switching frequency can be locked by external periodic force. In [23,18] it was shown that the mean switching frequency in periodically driven bistable systems can be locked in a finite range of noise intensities, while the effective diffusion coefficient exhibits a minimum being plotted versus the noise intensity. In [24] mutual synchronization of two coupled stochastic bistable systems was studied. An analytical approach for calculations of the effective diffusion constant was developed in [25]. In this way the notion of synchronization can be extended to a wide class of systems whose characteristic time scales are completely controlled by noise.

3. Electrorceptors in paddlefish

The paddlefish *Polyodon spathula*, named for its long flattened spatula-like appendage extending in front of the head, the «rostrum» (see Fig. 1). The rostrum is covered with tens of thousands of sensory receptors, morphologically similar to the ampullae of Lorenzini of sharks and rays, well-known to be passive electroreceptors. These ampullary-type electroreceptors respond to the microvolt-scale electrical signals emitted by planktonic prey such as *Daphnia*, and are used by paddlefish to locate plankton during feeding behavior [26]. The location of the rostrum, out in front of the mouth, allows it to function as an «early warning system» for approaching prey, as the fish swims forward continuously. Hence the rostrum functions as an antenna, carrying arrays of electrosensors.

Electrorceptors in paddlefish form a passive sensory system, meaning that

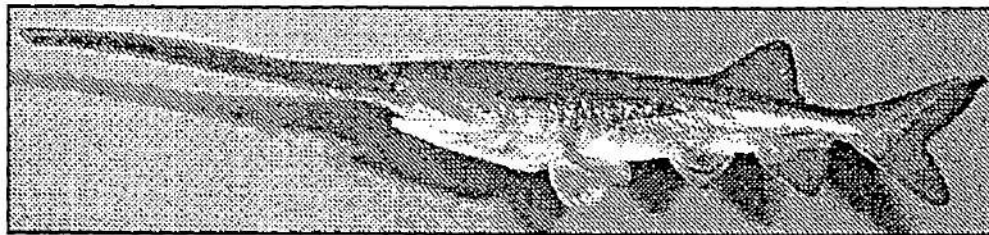


Fig. 1. Photo of a juvenile paddlefish

paddlefish only receive signals, from external sources. An external opening (pore) in the skin, 80-210 μ diameter, leads into a short canal $\approx 200 \mu$ long. The pores are organized into clusters of 5-20 on the rostrum, but there are much larger clusters on the head, gill covers, and near the mouth. The internal end of each canal is covered with a sensory epithelium. An epithelium is a layer of cells, one cell thick, typically lining a hollow organ. The epithelium contains two types of cells. It is the «hair cells» which are considered electrosensitive. The number of receptor cells per epithelium is ≤ 400 . The hair cells are interspersed among «support cells». The support and hair cells form «tight» intercellular junctions, or high-resistance seals, which block extracellular paths from the canal to the interior of the body, reducing the flow of electrical current. The term «electroreceptor» is thus refers to the entire structure of pore + canal + epithelium + primary afferent axon. Although the hair cells are the actual sensors, the spike-train coded output of the primary afferent is what is most often recorded, using a microelectrode placed in the sensory ganglion (collection of nerve cell bodies), located near but outside the brain. A key feature of the spike trains from the primary afferents of ampullary electroreceptor is their spontaneous quasi-periodic noisy firing patterns. It was recently discovered that the electroreceptors in paddlefish possess a novel type of organization of being composed from two distinct types of oscillators [27]. One oscillator resides in a population of epithelial cells and is synaptically and unidirectionally coupled with second oscillator, located in the afferent terminal. The fundamental frequency of epithelial oscillator is 25-27 Hz at 22°C for different electroreceptors, while the mean firing rate for different afferents varies in a wide range of 35-65 Hz. The unidirectional coupling of these oscillators results in a specific biperiodic firing patterns. However, only afferent oscillator is affected by external electrical stimuli [27].

Thus, the electroreceptor can be represented by a dynamical system of two unidirectionally coupled oscillators. Therefore, it is natural to expect that electroreceptor cells can be synchronized by a weak external periodic field.

In vivo electrophysiological experiments has been performed with juvenile paddlefish. A detailed description of the experimental setup can be found in [26,27].

4. Synchronization of electroreceptors by periodic electric field

We stimulated electroreceptors by a weak electric field generated by a dipole located near the rostrum of the fish. The electric field strengths were comparable in magnitude to those generated by zooplankton (a few tens of $\mu\text{V}/\text{cm}$). We recorded the spike train generated by a primary afferent and the periodic electric signal from the dipole simultaneously.

The frequency of stimulation was always significantly lower than the mean firing rate (mean frequency) of the electroreceptors, since electroreceptors respond best at low frequencies 4-10 Hz [26]. Thus we can expect higher order synchronization where there are several spikes per one stimulation period. A generic model for a periodically driven self-sustained oscillator is the circle map [2]. The circle map represents a stroboscopic Poincaré map of a quasi-periodic motion. It has a general form of

$$\phi_{n+1} = \phi_n + \rho + f(\phi_n) \text{ mod } 2\pi, \quad (2)$$

where the parameter ρ has the meaning of the ratio of fundamental frequencies of the oscillator and the driving force without coupling between them and $f(\phi)$ is a 2π periodic function. In our particular case we can strobe the phase of the periodic stimulus $2\pi f_s t$ at the moments of time t_n when the afferent spikes occur. In other words, we calculate the phase of a spike ϕ_n relative to the stimulus phase: $2\pi f_s t_n$ and then define ϕ_n on a unit circle:

$$\phi_n = f_s t_n \bmod 1, \quad (3)$$

where f_s is the stimulus frequency. In the case of perfect synchronization the circle map (2) possesses a periodic cycle, such that the dependence of ϕ_n versus n (time) will be represented by several horizontal lines. The number of lines is determined by a particular phase locking regime. For example, in the case 1:5 synchronization we will observe 5 horizontal lines. The results of calculations using Eq. (3) are presented in Fig. 2. Three different regimes can be clearly distinguished. At a low stimulus frequency (5 Hz) the high-order mode-locking of 1:17 is realized during some time segments. The pronounced 1:5 phase locking occurs at $f=17$ Hz. The five horizontal stripes correspond to phase locking segments, while the inclined lines correspond to phase slips. The phase locking occurs during a few hundreds of stimulus periods. Finally, at higher frequency $f=21$ Hz we observe quasi-periodic behavior with no synchronization. The synchrograms (see also [8]) shown in Fig. 2 has qualitatively the same structure as iteration sequences of stochastic circle map.

The statistical evidence of synchronization behavior is also presented in Fig. 2 as the probability density of the cyclic phase difference. In the case of strong 1:5 mode synchronization, the probability density consists of well expressed peaks corresponding to the phase-locking patterns.

In the examples shown above synchronization occurs without significant modulation of the firing rate of the afferent neurons, that is, spikes are uniformly distributed over the periods of external stimuli. We observed, however, different type of

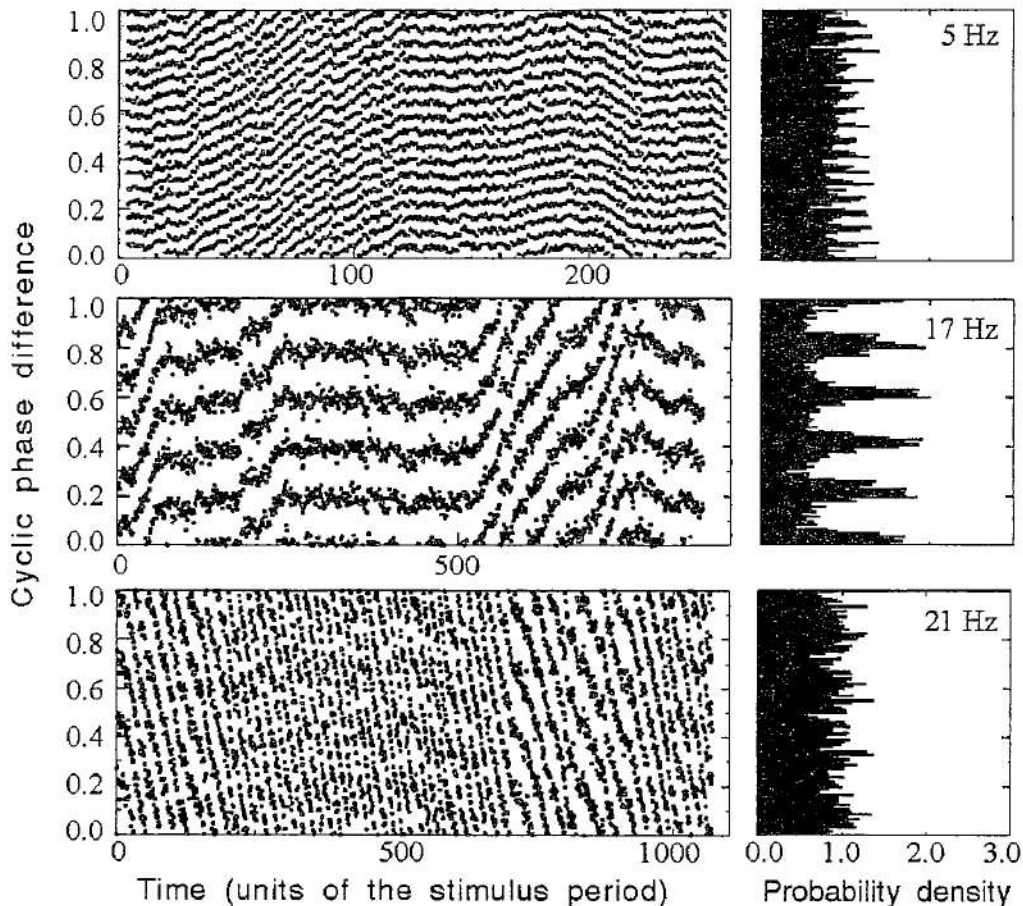


Fig. 2. The cyclic phase difference of spike trains, calculated using Eq. (3), for the indicated values of dipole electric field frequency. The corresponding probability densities of the cyclic phase difference are shown at the right sides

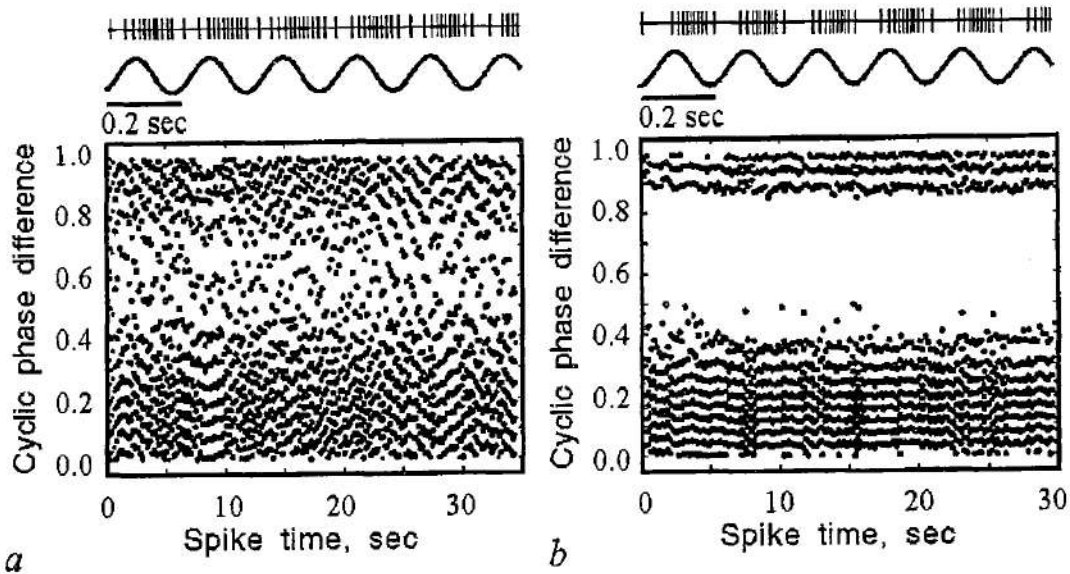


Fig. 3. Examples of recordings of spike train from an electroreceptor cell stimulated by a dipole electric field at 5 Hz with two different amplitudes. Corresponding calculation of the cyclic phase difference are shown below

primary afferents responses to external stimuli in terms of bursts [28]. In such a case external stimulus induces qualitative change in the firing patterns of afferent neurons: transition to bursting mode, when spikes concentrated in groups of bursts. With periodic stimuli we again observed synchronization, but now the firing rate is modulated significantly by the stimulus. An example of such synchronization is shown in Fig. 3, where an electroreceptor was stimulated by 5 Hz electric field. For a small amplitude (Fig. 3, *a*) the afferent already exhibits bursts, but synchronization is very poor: there is only one short phase locking segment. For a larger amplitude of periodic stimulus synchronization is clearly observed (Fig. 3, *b*): spike train is organized in bursts of 10-11 spikes. Moreover, individual spikes inside bursts are locked to specific positions on the stimulus period, which reflects phase synchronization.

5. Synchronization due to common noise

In paddlefish electroreceptors, the individual afferents usually possess different mean frequencies (mean firing rates) and different degrees of frequency variability [27]. Moreover, they are noncoupled. It appears, however, that all the electroreceptors have similar slow dynamics, which was revealed by synchronization of noise-induced bursts [28] in different receptors.

We simultaneously recorded the single-unit spikes from pairs of electroreceptor afferents *in vivo*, using metal microelectrodes. One receptive field was on the left side of the rostrum, the other on the right side. Their locations on opposite sides of the rostrum, which are innervated by different nerves, guaranteed that the pairs of afferent neurons were not coupled. We used uniform-field stimulation of all the electroreceptors: stimulus currents were passed between 15×5 cm chlorided silver plate electrodes at the ends of the experimental chamber (see [28] for experimental details). A computer-generated zero-mean Ornstein-Uhlenbeck (OU) noise process was used. The correlation time was set to be 0.002 sec, corresponding to a 500 Hz bandwidth. We generated a sequence of 30 segments of OU noise with incrementing intensities. Each noise segment was 180 sec long, and segments were separated by 5 sec of no stimulus. For comparison, we also used

computer generated white noise, high-pass filtered OU noise, or noise from a General Radio model 1390 B generator which was lowpass filtered by an 8-pole Bessel filter set to 50 Hz.

Stimulation with weak noise ($<2.5 \mu\text{V}/\text{cm}$ rms) did not change the firing mode of an electroreceptor afferent, but rather led to the well-known effect of widening the peak in the probability density of interspike intervals and, correspondingly, the power spectrum peak at the mean frequency of the afferent [27]. When noise of a certain intensity ($>2.5 \mu\text{V}/\text{cm}$ rms) was applied, the firing patterns of the afferents changed drastically such that afferents produced bursts: spikes were concentrated in clusters of bursts which were separated by quiescent epochs. The interspike intervals within a burst decreased towards the center of the burst [28], indicating a parabolic type of bursting [29].

A new slow time scale is introduced by the noise, and can be expressed as the mean interburst interval ($\langle\tau_b\rangle$). The mean interburst interval declined exponentially with increasing noise intensity, which was well fitted by the Arrhenius law, $\langle\tau_b\rangle = \nu \exp(\Delta^2/\sigma^2)$ [28]. This implies that burst generation is excitable, and has a well-defined threshold, Δ , estimated as $\approx 3 \mu\text{V}/\text{cm}$, which is only 3-fold higher than the limit of electroreceptor sensitivity [28].

One of the functional implications of bursting regimes is synchronization [30]. Indeed, the existence of bursts implies a slow time scale which makes synchronization of burst onsets easier in comparison with synchronization of individual spikes.

A representative example of data from two different afferents, recorded simultaneously, is shown in Fig. 4. In the absence of stimulation, the individual spikes in these neurons were not synchronized or correlated, since their mean firing rates were different: afferent #1 fired faster (45.1 Hz) than afferent #2 (33.4 Hz). With noise stimulation switched on, each burst started almost simultaneously in the two neurons, even though the number of spikes inside a burst was different for the two neurons.

We characterized the coincidence of bursts in pairs of neurons in terms of stochastic synchronization, measuring the phases $\phi_{1,2}(t)$ of burst onsets in each neuron, which increases by 2π every time a burst occurs, and interpolates linearly between two sequential burst onsets:

$$\phi_1(t) = 2\pi(t - \tau_k^{(1)}) / (\tau_{k+1}^{(1)} - \tau_k^{(1)}) + 2\pi k,$$

$$\phi_2(t) = 2\pi(t - \tau_m^{(2)}) / (\tau_{m+1}^{(2)} - \tau_m^{(2)}) + 2\pi m,$$

where $\tau_k^{(1)}$ and $\tau_m^{(2)}$ are bursts onsets in the first and the second neurons, respectively, and $\tau_k^{(1)} < t < \tau_{k+1}^{(1)}$, $\tau_m^{(2)} < t < \tau_{m+1}^{(2)}$. When stochastic synchronization occurs [17], constant segments of the phase difference $\Delta\phi(t) = \phi_1(t) - \phi_2(t)$ (phase locking) are interrupted by

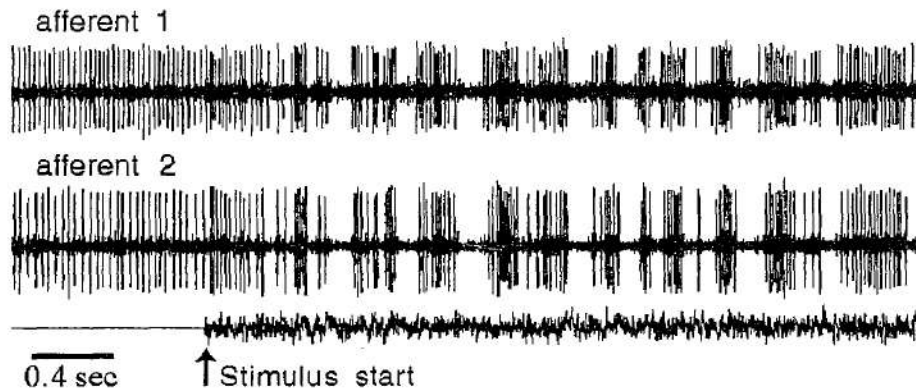


Fig. 4. Example of simultaneous recordings of spike trains from a pair of electroreceptor afferents. The onset of stimulation with computer-generated OU noise of $16.8 \mu\text{V}/\text{cm}$ rms amplitude is marked by the arrow

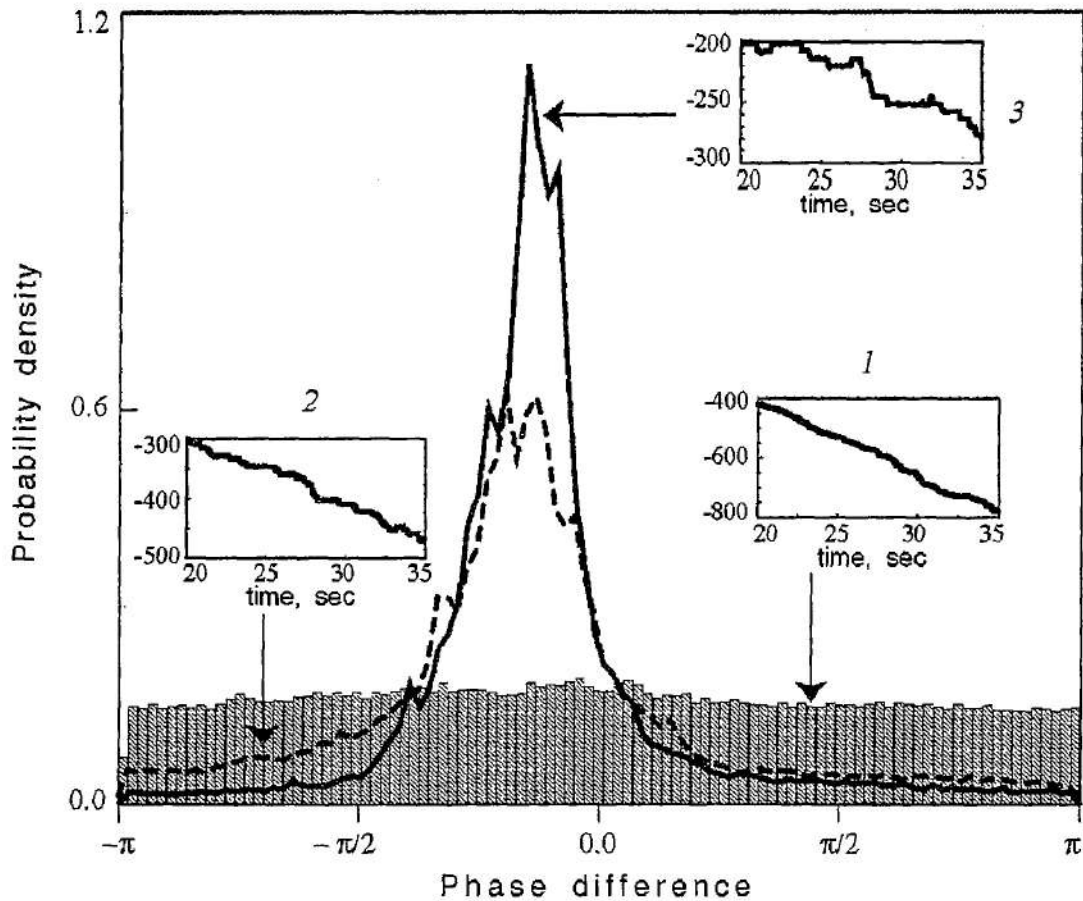


Fig. 5. Probability densities of the phase differences shown in the inset. Insets: Phase differences of burst onsets in a pair of afferents for the following noise rms amplitude: (1) $2 \mu\text{V}/\text{cm}$, (2) $8 \mu\text{V}/\text{cm}$, (3) $20 \mu\text{V}/\text{cm}$.

abrupt 2π phase slips. This is illustrated in Fig. 5 for noise-induced bursting, where the phase differences for three different noise intensities are presented. For a large noise intensity (curve 3), the burst onsets are synchronized, which is expressed in the existence of horizontal epochs of phase locking lasting several seconds. The probability density of the phase difference, $P(\Delta\phi)$ (see Fig. 5) characterizes the degree of synchronization: a well-expressed peak in $P(\Delta\phi)$ indicates synchronization, while a uniform distribution indicates its absence. The probability density is nearly uniform for weak noise, when bursts in the two neurons are not synchronized. With increased noise intensity, the probability density of the phase difference developed a well-defined peak, indicating strong synchronization between the bursting neurons.

6. Conclusion

In this paper we demonstrated the phenomenon of stochastic synchronization on a living «model», the electroreceptor system of paddlefish. Two types of synchronization were considered. The first, synchronization of a single electroreceptor by periodic stimuli. And the second, synchronization of two electroreceptors by a common noise field. Young paddlefish use electrosensitivity to feed zooplankton and synchronization mechanism might be responsible for extreme sensitivity of the paddlefish to weak periodic electric field generated by plankton and also for nearly 100 % successful prey capturing. Synchronous burst responses of a population of sensory neurons may be a neural mechanism for coincidence detection, and may substantially simplify the neural operations that a fish's brain must perform to detect prey and to calculate their position and velocity [31]. The impulse-like electrical signal emitted by an individual plankton

prey (e.g. *Daphnia*) moving along the rostrum, or the exponentially correlated Gaussian electrical noise generated by swarms of *Daphnia* [32], may be adequate stimuli for evoking synchronized bursting of different electroreceptors during feeding behavior.

This work was supported by the Office of Naval Research - Physics Division, the National Institutes of Health (R01DC004922-01), the National Science Foundation (INT-0128974) and DAAD (D/0104610). A.N., F.M. and L.S.-G. thank Prof. Vadim Anishchenko for numerous stimulating discussions on topics of stochastic synchronization.

References

1. *Blekhman I.* Synchronization in science and technology. ASME Press, New York, 1988.
2. *Glass L. and Mackey M.C.* From clocks to chaos. The Rhythms of life. Princeton University Press, Princeton, NJ, 1988.
3. *Soen Y., Cohen N., Lipson D., and Braun E.* Emergence of spontaneous rhythm disorders in self-assembled networks of heart cells // *Phys. Rev. Lett.* 1999. Vol. 82. Pp. 3556-3559.
4. *Elson R.C., Selverston, Huerta R., Rulkov N.F., Rabinovich M.I. and Abarbanel H.D.I.* Synchronous behavior of two coupled biological neurons // *Phys. Rev. Lett.* 1998. Vol. 81. Pp. 5692-5695.
5. *Neiman A., Pei X., Russell D.F., Wojtenek W., Wilkens L., Moss F., Braun H.A., Huber M.T., and Voigt K.* Synchronization of the electrosensitive cells in the paddlefish // *Phys. Rev. Lett.* 1999. Vol. 82. Pp. 660-663.
6. *Bahar S., Neiman A., Wilkens L., and Moss F.* Synchronization and stochastic resonance effects in the crayfish caudal photoreceptor // *Phys. Rev. E.* 2002 Vol. 65. 050901.
7. *Tass P., Rosenblum M., Weule J., Kurths J., Pikovsky A., Volkmann J., Schnitzler A., and Freund H.* Detection of n:m phase locking from noisy data: Application to magnetoencephalography // *Phys. Rev. Lett.* 1998. Vol. 81. Pp. 3291-3294.
8. *Schäfer C., Rosenblum M.G., Abel H. and Kurths J.* Synchronization in the human cardiorespiratory system // *Phys. Rev. E.* 1999. Vol. 60. Pp. 857-870.
9. *Anishchenko V.S., Balanov A.G., Janson N.B., Igosheva N.B., and Bordukov G.V.* Entrainment between heart rate and weak noninvasive forcing // *Int. J. of Bifurcation and Chaos.* 2000. Vol. 10. Pp. 2339-2348.
10. *Winfree A.T.* The Geometry of Biological Time. Springer, New York, 1980.
11. *Pikovsky A.S., Rosenblum M.G., and Kurths J.* Synchronization. A Universal Concept in Nonlinear Sciences. Cambridge University Press, Cambridge, 2001.
12. *Andronov A., Witt A., and Khaykin S.* Theory of Oscillations. Pergamon Press, Oxford, 1966.
13. *Pecora L.M., and Carroll T.L.* Synchronization in chaotic systems // *Phys. Rev. Lett.* 1990. Vol. 64. Pp. 821-824.
14. *Anishchenko V.S., Vadivasova T.E., Postnov D.E., Safonova M.A.* Forced and mutual chaos synchronization // *Radiotekhnika i Elektronika.* 1991. Vol. 36. Pp. 338-351 (in Russian).
15. *Anishchenko V.S., Vadivasova T.E., Postnov D.E., Safonova M.A.* Synchronization of chaos // *Int. J. of Bifurcation and Chaos.* 1992. Vol. 2. Pp. 633-644.
16. *Rosenblum M.G., Pikovsky A.S., and Kurths J.* Phase synchronization of chaotic oscillators // *Phys. Rev. Lett.* 1996. Vol. 76. Pp. 1804-1807.
17. *Stratonovich R.L.* Topics in the Theory of Random Noise. Gordon and Breach, New York, 1981.

18. *Neiman A., Silchenko A., Anishchenko V., and Schimansky-Geier L.* Stochastic resonance: noise-enhanced phase coherence // *Phys. Rev. E.* Vol. 58. Pp. 7118-7125.
19. *Malakhov A.N.* Fluctuations in Auto-oscillation Systems. Nauka, Moscow, 1968 (in Russian).
20. *Anishchenko V.S., Astakhov V.V., Neiman A.B., Vadivasova T.E., and Schimansky-Geier L.* Nonlinear Dynamics of Chaotic and Stochastic Systems. Springer, Berlin, 2002.
21. *Bendat J.S., and Piersol A.G.* Random Data. John Wiley and Sons, 1986.
22. *Callenbach L., Hänggi P., Linz S.J., Freund J.A. and Schimansky-Geier L.* Oscillatory systems driven by noise: Frequency and phase synchronization // *Phys. Rev. E.* 2002. Vol. 65. 051110.
23. *Shulgin B., Neiman A., and Anishchenko V.* Mean switching frequency locking in stochastic bistable systems driven by a periodic force // *Phys. Rev. Lett.* 1995. Vol. 75. Pp. 4157-4160.
24. *Neiman A.* Synchronizationlike phenomena in coupled stochastic bistable systems // *Phys. Rev. E.* 1994. Vol. 49. Pp. 3484-3488.
25. *Freund J., Neiman A., and Schimansky-Geier L.* Analytic description of noise-induced synchronization // *Europhysics Letters.* 2000. Vol. 50. Pp. 8-14.
26. *Wilkins L.A., Russell D.F., Pei X., and Gurgens C.* The paddlefish rostrum functions as an electrosensory antenna in plankton feeding // *Proc. Royal Soc. London B.* 1997. Vol. 264. Pp. 1723-1729.
27. *Neiman A., and Russell D.F.* Stochastic biperiodic oscillations in the electroreceptors of paddlefish // *Phys. Rev. Lett.* 2001. Vol. 86. Pp. 3443-3446.
28. *Neiman A. and Russell D.F.* Synchronization of noise-induced bursts in noncoupled sensory neurons // *Phys. Rev. Lett.* 2002. Vol. 88. 138103.
29. *Ermentrout G.B. and Kopell N.* Parabolic bursting in an excitable system coupled with a slow oscillation // *SIAM J. Appl. Math.* 1986. Vol. 46. Pp. 233-253.
30. *Izhikevich E.M.* Neuronal excitability, spiking and bursting // *Int. J. of Bifurcations and Chaos.* 2000. Vol. 10. Pp. 1171-1266.
31. *Naundorf B. and Freund J.A.* Signal detection by means of phase coherence induced through phase resetting // *Phys. Rev. E.* 2002. Vol. 66. 040901(R).
32. *Freund J., Schimansky-Geier L., Beisner B., Neiman A., Russell D., Yakusheva T., and Moss F.* Behavioral stochastic resonance: How the noise from a daphnia swarm enhances individual prey Capture by juvenile paddlefish // *Journal of Theoretical Biology.* 2002. Vol. 214. Pp. 71-83.

*Center for Neurodynamics, University
of Missouri at St. Louis, USA
Institute for Physics, Humboldt
University at Berlin, Germany*

Received 28.08.2003

УДК 537.86:519.2: 577.359

СИНХРОНИЗАЦИЯ, ШУМ И ЭЛЕКТРОРЕЦЕПТОРЫ

А. Нейман, D.F. Russell, F. Moss, L. Schimansky-Geier

Классическое понятие синхронизации, первоначально введенное для периодических автоколебаний, может быть расширено на стохастические систе-

мы. Это можно осуществить даже в том случае, когда характерные времена системы полностью управляются шумом. Стохастическая синхронизация при этом определяется как установление некоторых условий для различных статистических мер процесса. Мы проводим обзор разных подходов к стохастической синхронизации и применяем их для изучения синхронизации в электросенсорной системе веслоноса.



Neiman Alexander Borisovich - was born in Saratov in 1962. He has graduated Saratov State University in 1993. He received his PhD (1991) and Doctor Science Degree (1998). He is author more than 100 articles. Currently he is Professor at the Department of Physics and Astronomy of Ohio University, USA. Scientific interest nonlinear dynamics, stochastic dynamics of nonlinear systems, theory of information, applications in biology and medicine.
E-mail: neiman@helios.phy.ohiou.edu

Russell David - senior Research Investigation, Research Associate Professor (Biology), Center for Neurodynamics, University of Missouri at St. Louis, USA.
E-mail: drussell@admiral.umsl.edu



Frank Moss holds degrees in both Physics (PhD) and Engineering (BS and MS) from the University of Virginia. He studied macroscopic quantum fluids at the University of Rome in Italy on a Postdoctoral Fellowship awarded by the National Science Foundation. Moss' early research centered on turbulence in superfluid liquid helium, for which he was later awarded Fellowship in the American Physical Society. Later he studied random fluctuations and noise in nonlinear physical systems, and in the early 90's broadened these studies to include applications in sensory biology. In 1995, he established the Center for Neurodynamics and continues as its Director. Research of the Center has attracted editorial commentary in numerous science journals, for example, Nature, Science and Science News as well as the popular press including The Economist and The Financial Times (London). Moss is the author of over 215 scientific publications including the editorship of several books and special issues of journals. He has given over 260 lectures at national and international conferences and institutes. He was awarded senior fellowships by the British government and by NATO and is a winner of the prestigious Humboldt Research Prize in Germany as well as numerous other awards for notable research. He currently serves on the editorial boards of two international journals and is a consulting editor for numerous others. He is a past chairperson of the Division of Biological Physics of the American Physical Society. He is currently Curators' Professor at the University of Missouri at St. Louis, USA. E-mail: mossf@umsl.edu

L. Shimansky-Geier - was born in Germany (1950). Education: Diplom - State University of Yerevan (1974); Ph.D. - Humboldt-University at Berlin (1981); D.Sc.- Humboldt-University at Berlin (1986). Now he is the Professor, the Head of the Stochastic Processes Chaire, of Humboldt-University at Berlin. Fellowships and Activities: Moscow State University (1981-1982); University of Augsburg Speaker of the Collaborative Research Center «Nonlinear Complex Processes» (1991); Editor of «Fluctuation and Noise Letters» (2000); Associated Member of the Center of Neurodynamics, University of Missouri at St. Louis (2001). His research fields: stochastic resonance; stochastic ratchets; noise induced transitions. He published more than 150 scientific works, including 6 books.

E-mail: alsg@physik.hu-berlin.de



Izv. VUZ. «AND», vol. 11, № 3, 2003

NOISY NEURAL RHYTHM GENERATORS

E. Mosekilde, O.V. Sosnovtseva, D. Postnov, H.A. Braun, and M.T. Huber

The dynamical features of spike train generation in the presence of noise are investigated for three different models of neural rhythm generators: a single neuron model that simulates impulse pattern modulation for temperature encoding in mammalian cold receptors, a minimal neural network that describes transitions between beta and gamma rhythms in the brain and an electronic switching device that represents a simple breathing rhythm generator for a snail. We show that noise can explain a number of peculiarities in the observed spike trains, cause coherent switchings between different states, and induce new rhythms in small neural ensembles.

1. Introduction

Noise can introduce multivarious effects especially in nonlinear and chaotic systems and makes the dynamics of such systems still more difficult to understand. Vadim S. Anishchenko, together with his group, has made major contributions towards a better understanding of nonlinear and chaotic systems under the influence of noise [1,2]. Such approaches can become of particular value for the understanding of pattern generation in neuronal systems because neurons are inherently nonlinear, often chaotic and inevitably contaminated with noise.

The spatiotemporal characteristics of neural firing patterns in connection with brain function have received considerable interest, and many studies have been performed in order to understand the origin and role of various forms of synchronized neural activity (e.g., [3,4]). Even single functional units demonstrate flexible neuronal patterns, and experimental recordings of peripheral sensory receptors and central neurons show more or less continuous transitions between different types of oscillatory patterns as a function of physiologically relevant stimuli [5,6]. In accordance with experimental observations on mammalian cold receptors, the Huber/Braun model [7], for example, reproduces tonic activities or bursting discharges due to slow oscillation cycles each triggering a group of impulses during its suprathreshold phase. Moreover, there exist irregular patterns of apparently chaotic origin [8,9] while other patterns that can be explained only with essential contributions of noise are typical for thermosensitive neurons [6].

The complex and multifarious effects of noise on neural firing have not yet been fully understood. Neural activity is known to be noisy [10], and this stochastic feature is observed during both information transmission and spontaneous firing. At the same time, noise can play a constructive role in neural systems. In the presence of a subthreshold signal, the excitation threshold may be crossed when noise is superimposed onto the

signal. This happens with high probability when the signal has its maximum and, hence, allows the biological system to detect signals that without noise would remain subthreshold [11,12], demonstrating the effect of stochastic resonance [13]. An excitable neuronal system can exhibit the related phenomenon of coherence resonance [14]. In this case, there is no underlying periodic signal, and the resonance phenomenon is controlled by the noise intensity and the time of relaxation. Stochastic synchronization phenomena, i.e., the synchronization of noise-activated or noise-induced rhythms, have been studied in electrosensitive cells of the paddlefish by Neiman *et al.* [15]. Different types of noisy phase-locked regimes were observed.

Many neural systems can perform oscillations in different modes. Hence, the interesting questions arise: How is the dynamics of neural firing with *multimode* behavior affected by noise, and under what conditions can noise activate new rhythms? In this paper we focus on the following aspects:

(i) how can the presence of noise interfere with the spike generating mechanisms and the subthreshold oscillations in peripheral pattern generators, and under what conditions can it completely change the spiking pattern? The intrinsic dynamics is characterized by oscillatory changes in the membrane potential that are below or close to the spike threshold. In this situation naturally occurring stochastic influences due to membrane or synaptic noise can be an essential component in signal encoding. The reason is that the noise actually determines whether a spike is triggered during an oscillatory cycle or not. Hence, mixed patterns typically result, consisting of random sequences of spike-triggering and subthreshold oscillations;

(ii) how is the switching process between coexisting rhythmic activities in the brain influenced by noise? Brain oscillations are normally divided into different types based mainly on their frequency. Rhythms in the β (12-30 Hz) and the γ (30-80 Hz) ranges are found in many parts of the nervous system and are associated with attention, perception and cognition. Recently Kopell *et al.* [16] demonstrated that a model including both inhibitory interneurons and excitatory pyramidal cells can produce β as well as γ oscillations that employ different dynamical mechanisms to synchronize. The β mode is able to synchronize with long conduction delays corresponding to signals traveling over a significant distance in the brain. Similar distances can not be tolerated by the γ rhythms that are used more for local communication. It has been noted in electroencephalogram signals that rhythms of different frequencies can be found simultaneously [17]. In this connection we describe noise-induced activities in terms of regularized switching events;

(iii) how can noise control the appearance of additional time scales in small neuron ensembles? In contrast to previous studies we investigate *noise-induced* rather than noise-activated oscillatory modes, i.e., we focus on time scales that are produced and controlled by noise and that do not exist in the deterministic case. We provide experimental observation of such multimode behavior and investigate the conditions for generation and entrainment of the various modes.

2. Tuning cold-receptor discharges

2.1. The Huber/Braun model. Mammalian cold receptors are particularly interesting in connection with the present analysis, both because of the complicated impulse patterns that they generate and because of the clear influence of noise. The impulse patterns are generally characterized by regular and relatively frequent burst discharges at intermediate temperatures with irregular and less frequent bursting patterns occurring at lower temperatures and irregular single spike discharges observed at higher temperatures. The stationary frequency vs temperature characteristic typically displays a maximum at intermediate temperatures (25-30°C). This lack of monotonicity implies that

the temperature encoding must be associated with the firing pattern as such and not only with the average firing rate. The Huber/Braun model of mammalian cold receptor was described in detail in Refs [7,18]. In brief, it consists of two interacting minimal sets of ionic conductances, each including simplified de- and repolarizing Hodgkin-Huxley-type currents with sigmoidal steady state activation kinetics. For simplicity, inactivation is neglected. The two sets operate at different voltage levels and time scales. High threshold, fast activating currents are for spike generation (marked by indices d and r); low threshold, slow activating currents generate subthreshold potential oscillations (indices sd and sr). Including a leakage current I_l and the applied current I_{appl} , the membrane potential V is given by:

$$c\dot{V} = -I_l - I_d - I_r - I_{sd} - I_{sr} - I_{appl} \quad (1)$$

with c denoting the membrane capacitance. In our generalized approach we do not refer to specific ionic currents but to the de- and repolarizing components of the two subsystems, the spike generator and the subthreshold oscillator. I_d is the fast depolarizing current and I_r is the fast repolarizing current which reflect the classical Na^+ - and K^+ -currents in the spike generation. The physiological basis for the two other currents, I_{sd} and I_{sr} , may be different in different neurons.

The leakage current is given by

$$I_l = g_l(V - E_l) \quad (2)$$

and the voltage-dependent ionic currents are expressed in the form:

$$I_i = \rho g_i a_i (V - E_i), \quad (3)$$

$$a_{i\infty} = 1/(1 + \exp(s_i(V - V_{0i}))), \quad (4)$$

$$\dot{a}_i = \phi(a_{i\infty} - a_i)/\tau_i. \quad (5)$$

with $i=d, r, sd,$ and sr . Here, E_i are the equilibrium potentials, g_i the maximum conductances at the reference temperature T_0 , and a_i the voltage and time-dependent activation parameters. ρ allows for the temperature scaling of the ionic currents. V_{0i} and s_i are half-activation potentials and slopes, respectively, of the steady state activation curves.

Exceptions to the above formulations are the assumed instantaneous activation of the fast depolarizing current

$$a_d = a_{d\infty}, \quad (6)$$

and the direct coupling of the slow repolarizing current to the slow depolarizing current:

$$\dot{a} = \phi(\eta I_{sd} - k a_{sr})/\tau_{sr}. \quad (7)$$

Here, η denotes the coupling constant and k is a relaxation factor.

The temperature dependences are expressed in terms of the scaling parameters ρ and ϕ for the maximum conductances and the time constants, respectively:

$$\rho = 1.3^{(T-T_0)/\Delta}, \quad \phi = 3.0^{(T-T_0)/\Delta}. \quad (8)$$

Here, T is the temperature at which the receptor cells operate, $T_0=25^\circ\text{C}$ is the reference temperature, and $\Delta=10^\circ\text{C}$ is a scaling temperature. Each time T increases by Δ , the maximum conductance increases by a factor 1.3 and the time constants by a factor 3.

To account for the effect of random dynamics we have applied Gaussian white noise according to the Fox-Mueller algorithm [19]:

$$g_w = (-4Dh\ln a)^{1/2} \cos 2\pi b \quad (9)$$

with a and b being random numbers between 0 and 1; h denotes the integration step, and the noise intensity is adjusted by the dimensionless parameter D . The noise is directly added to the membrane potential.

With the above simple temperature scaling and with noise implemented in the model equations, the full variety of experimentally observed impulse pattern evolves almost naturally. Increasing the temperature speeds up the ionic kinetics and leads to a faster dynamics of the subthreshold oscillator. This is associated with a decrease in the number of spikes that can be triggered per oscillation cycle.

2.2. Role of noise in pattern formation. Fig. 1 reproduces some of the most characteristic patterns from experimental recordings for rat cold receptors [7] for direct comparison with the results of our modelling studies which are shown in the traces below. It can be seen that the model almost perfectly mimics all types of cold receptor discharges, but it also becomes evident that at least one type of pattern can be simulated only with the addition of noise. This is the pattern that consists of a mix of spike-generating and subthreshold oscillations (skippings) that typically occurs in the upper temperature range and can be seen in both experimental and modelling data (35°C, left diagrams) but not in the lowest diagram which is from a completely deterministic simulation ($D=0$). In this situation only the presence of noise allows the subthreshold oscillations to randomly exceed the threshold for spike-generation.

The second row shows the tonic firing patterns that typically can be seen in experimental recordings at normal skin temperatures around 30°C and which also occur in our simulations with the appropriate temperature scaling. Noise does not seem to have

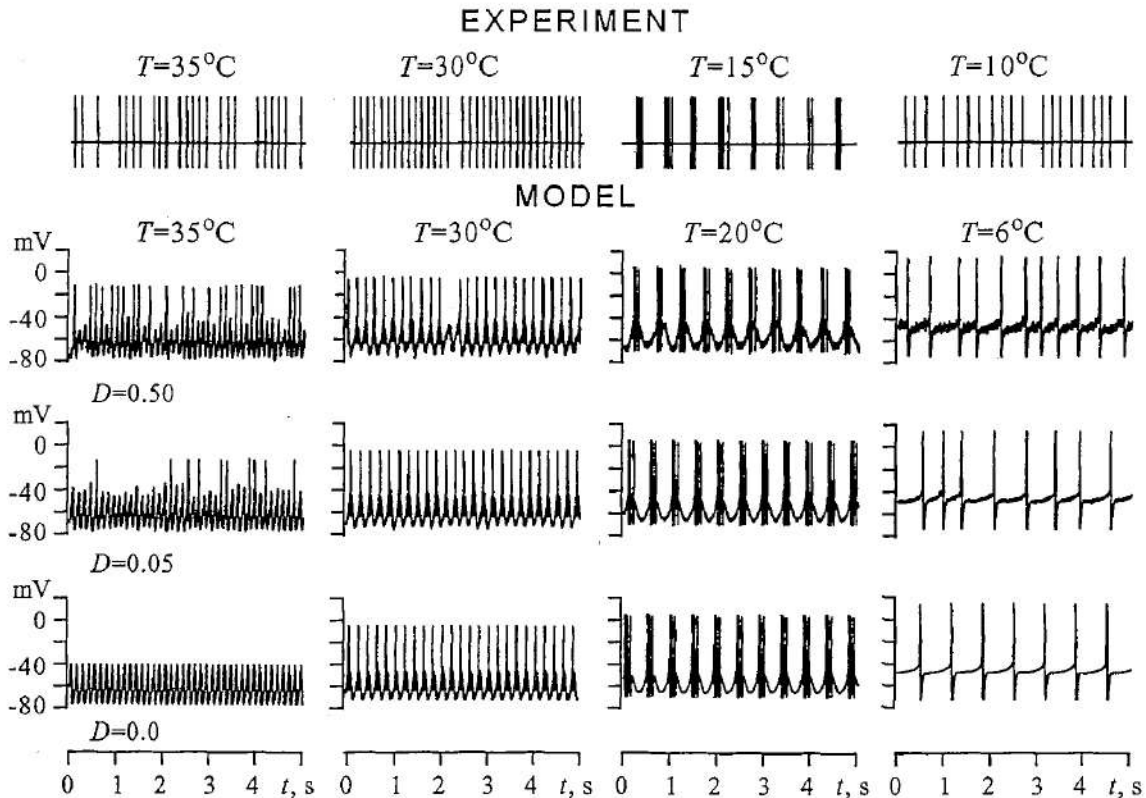


Fig. 1. Typical impulse patterns for cold receptors at different temperatures. Comparison of experimentally recorded spike trains (upper traces) and modelling results from deterministic simulations ($D=0$, lowest traces) and with addition of noise ($D=0.05$ and $D=0.5$, intermediate traces). The parameters of the numerical simulations are given in Ref. [20]

major influence on the pattern generation. There is a regular tonic discharge because each oscillation cycle succeeds to trigger a spike - with a single exception: at $D=0.5$ one of the oscillation cycles obviously fails to produce a spike. The upper trace indicates that a similar phenomenon may occur in the experimental recordings: a spike is missing within an otherwise regular tonic discharge. (Note that the simulation for $D=0.5$ and $T=30^\circ\text{C}$ has been shifted along the time axis for the missing spike to occur at the same time as the spike in the experimental sequence.) Although the missing spikes represent singular events, their occurrence suggests that noise cannot only induce spiking in otherwise completely subthreshold oscillations (as shown in the left traces) but can also prevent impulse generation in otherwise regularly spiking sequences. Such situations can cover a broad range of stimulus encodings.

In the third row of the figure we are comparing electrophysiological recordings and model simulations of different noise levels in the range of bursting discharges. More random input simply seems to induce more random fluctuations of spike-generation without any qualitative change of the pattern. This appears to also be the case at the lowest temperatures where the experimental recordings often exhibit irregular tonic discharges. The deterministic simulations generate completely regular discharges and the addition of noise is needed to produce the more realistically appearing irregular spike sequences.

With the addition of noise the model successfully reproduces the major types of experimentally recorded impulse patterns and it explains how these patterns can be related to the resonance behavior between slow subthreshold oscillations and spike generating mechanisms. The Huber/Braun is valuable not only because it successfully simulates stationary cold receptor discharges, but also as a generalized neuronal pattern generator of significant flexibility.

3. Transitions between β and γ rhythms

3.1. The Kopell model. In a neural system, the individual neuron is generally located in an excitatory or inhibitory network that provides a variety of inputs to the neuron, primarily via the synaptic currents. In the present section we consider a minimal model for a neural network capable of producing both β and γ oscillations. Developed by Kopell *et al.* [16], the model includes two excitatory pyramidal neurons and one inhibitory interneuron. The network architecture is illustrated in Fig. 2 where open and filled arrowheads represent excitatory and inhibitory connections, respectively. Solid lines indicate fixed connections, and dotted lines represent connections that are varied during the simulations. By contrast to the single neuron considered in Sec. 2, the interesting features of the present system are connected with the interaction of the different neurons. Many factors contribute to making the environment of the network noisy. All of these factors are regarded as random external fluctuations. As we have seen in the previous section it is likely that neurons can use such external fluctuations to process their input signals more

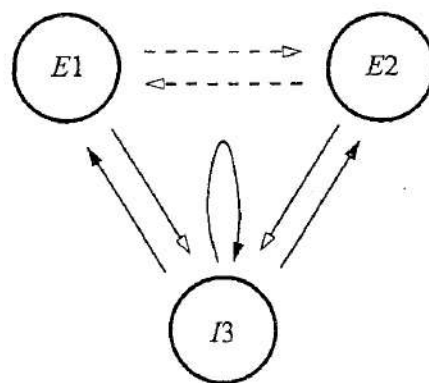


Fig. 2. Architecture of the Kopell oscillatory network. E1 and E2 are excitatory cells, and I3 is an inhibitory cell. Open and filled arrowheads represent excitatory and inhibitory connections, respectively. Solid lines indicate fixed connections, and dotted lines represent synapses whose efficacies are varied in the simulations

effectively. Here, we shall see how the presence of noise can generate transitions between different rhythmic modes in the network.

The Kopell model is based on Hodgkin-Huxley type neurons [21] which are modelled in accordance with the original formulation (rather than the simplified form used in the Huber/Braun model). There are no currents for subthreshold oscillations. Instead, there is an additional slow potassium current that accounts for after-hyperpolarization (ahp) in the excitatory neurons. The voltage of an excitatory neuron is controlled by the following differential equation:

$$c\dot{V} = -g_l(V-E_l) - g_{Na}m^3h(V-E_{Na}) - g_K n^4(V-E_K) - g_{ahp}w(V-E_K) - i_{syn}^e + i_{appl}^e \quad (10)$$

One recognizes the leak current $g_l(V-E_l)$, the sodium current $g_{Na}m^3h(V-E_{Na})$, the potassium current $g_K n^4(V-E_K)$, and the additional potassium current for after-hyperpolarization $g_{ahp}w(V-E_K)$. There is also a synaptic current input i_{syn}^e and a term for external current application i_{appl}^e . V is the membrane potential, E_j ($j=Na$ or K) is the Nernst (or reversal) potentials for the respective ions, and g_j the corresponding conductances; c is the membrane capacitance.

The gating variables are assumed to obey the standard dynamical equations:

$$\dot{m} = \alpha_m(V)(1-m) - \beta_m(V)m, \quad (11)$$

$$\dot{h} = \alpha_h(V)(1-h) - \beta_h(V)h, \quad (12)$$

$$\dot{n} = \alpha_n(V)(1-n) - \beta_n(V)n, \quad (13)$$

$$\dot{w} = \alpha_w(V)(1-w) - \beta_w(V)w, \quad (14)$$

where the α and β - functions describe the voltage-dependent opening and closing rates for the various channels. For each excitatory neuron, a single equation controls the state of the synapses going from this neuron to others:

$$\dot{s}_e = \alpha_{s_e}(V)(1-s_e) - \beta_{s_e}s_e. \quad (15)$$

Synaptic input to an excitatory neuron (here, E1) results in a current

$$i_{syn,E1}^e = g_{ee} s_{e,E2}(V-E_e) + g_{ie} s_{i,I3}(V-E_i). \quad (16)$$

In this expression, the s -variables refer to the presynaptic neurons (E2 and I3, respectively), whereas the voltage V refers to the postsynaptic neuron (E1). E_e and E_i denote the reversal potentials associated with excitatory and inhibitory synapses. A similar equation is used for the synaptic current of E2.

The inhibitory neuron I3 is very similar to E1 and E2, only the after-hyperpolarization-current is not included:

$$c\dot{V} = -g_l(V-E_l) - g_{Na}m^3h(V-E_{Na}) - g_K n^4(V-E_K) - i_{syn}^i + i_{appl}^e \quad (17)$$

Noting that w does not appear, the remaining gating variables for the inhibitory neuron I3 are controlled by Eqs (11-13).

Inhibitory synapses are governed by the equation:

$$\dot{s}_i = \alpha_{s_i}(V)(1-s_i) - \beta_{s_i}s_i. \quad (18)$$

The inhibitory neuron receives inputs from E1 and E2 as well as from a mechanism of self-inhibition:

$$i_{syn,I3}^i = (g_{ei} s_{e,E1} + g_{ei} s_{e,E2})(V - E_e) + g_{ii} s_{i,I3}(V - E_i). \quad (19)$$

The detailed description of the various functions and parameter values can be found in the original paper [16]. Two parameters are varied in the present study: g_{ee} , the strength of the connections between E1 and E2, and g_{ahp} , the maximal conductance for the slow potassium ion channels.

The Kopell model demonstrates three main network modes.

- For low values of the two parameters, the three neurons spike in synchrony with a frequency in the γ band;

- If g_{ahp} is increased, the E1 and E2 neurons start to miss every other spike, lowering their individual frequencies into the β band. However, since E1 and E2 are out of phase, the population of excitatory neurons as a whole continues to produce γ oscillations;

- Increasing the connection strengths between E1 and E2 makes the excitatory neurons spike simultaneously, thereby producing β oscillations.

The results of scanning over a two-dimensional parameter space are shown in Fig. 3. Here, one can distinguish four to five different oscillatory modes. For low values of g_{ahp} , the region denoted γ corresponds to parameter values that generate γ rhythms where all neurons (E1, E2, and I3) spike in every cycle. The « γ population» state γ_{pop} is located to the left with intermediate values of g_{ahp} . In this region, the neurons E1 and E2 both demonstrate β rhythms of 16-17 Hz, but their overall behavior is found to produce oscillations in the γ band. There is a large region β occupied by β oscillations where E1 and E2 are in full synchrony with half the frequency of the γ rhythm. With decreasing g_{ahp} , they evolve into the β population β_{pop} . This state produces a β rhythm, but only half as powerful as the β state described earlier since only one excitatory neuron (E1) spikes. Within a range of parameters one can observe high-order solutions with different combinations of spiking and silent states in the two excitatory neurons [22]. The dynamics seems to be limited in the g_{ahp} direction by the appearance of a silent-state, in which E1 and E2 never spike due to the effects of the after-hyperpolarization current in combination with the spontaneous spiking of the I3 neuron. In the gray region, the γ_{pop} and the β modes coexist. The observation of a large region with coexisting solutions may have important inferences with respect to brain function. The question is: Can the Kopell model switch between the coexisting states? Physiologically, the externally applied current i_{appl}^e , together with ionic and synaptic currents, could represent the influence of other neurons of the brain. As previously noted, this influence may be considered in many instances as stochastic. Let us, therefore, examine the influence of fluctuations on the switching process.

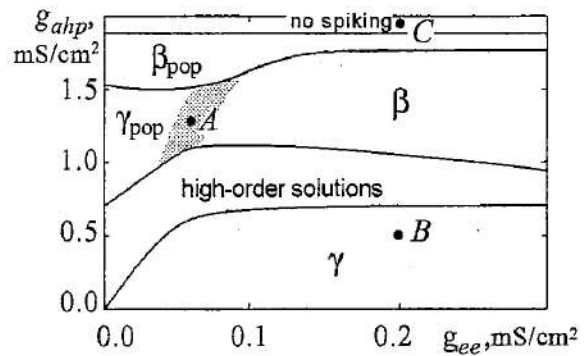


Fig. 3. Different oscillatory modes as functions of g_{ee} (the coupling between excitatory neurons) and g_{ahp} (the conductance for the slow K-channel in excitatory neurons). In the gray region the γ_{pop} and β modes coexist. In the region denoted high-order solutions we find a great variety of frequency-locked states

3.2. Stochastic dynamics. Since noise may have different origins and can contribute in different ways, we assume that our network operate in a noisy field (Fig. 2). We represent this as Gaussian noise $\xi(t)$ with intensity D added to the first equations of each neuron.

Switchings between coexisting γ_{pop} and β modes. With noise of sufficient intensity, the system switches between two states. This can be characterized in different ways. First, we can introduce a phase shift between the spiking events in E1 and E2 as $\Delta\phi=2\pi t/T$. In this case, the system can be considered as bistable where a trajectory alternates between $\Delta\phi=0$ and $\Delta\phi=\pi$. With increasing noise intensity, hopping becomes more frequent. Secondly, the system can be described via the overall dynamics of the excitatory neurons. Let us choose the parameters to be in the region where γ_{pop} and β oscillations coexist (point A in Fig. 3). In the noiseless case, with the applied initial conditions, the resulting output oscillations is a β rhythm. This corresponds to a sharp peak at $f_{\beta}=17$ Hz. With noise, an additional peak appears at $f_{\gamma}=34$ Hz. With increasing noise, the peak at f_{β} becomes broader and smaller in amplitude.

To describe the switching dynamics we can evaluate different characteristics. Fig. 4, *a* illustrates the behavior of the residence time (solid and dotted curves) in the bistable system with $\Delta\phi=0$ and $\Delta\phi=\pi$. With vanishing noise, the system remains in the $\Delta\phi=0$ state and the residence time tends to infinity. When noise is introduced, the system can switch to the other state. With increasing noise, the residence times in the two states tend to become equal.

A quantitative measure of coherence is the so-called regularity coefficient which can be calculated as [14]:

$$R = \langle\tau\rangle / (\langle\tau^2\rangle - \langle\tau\rangle^2)^{1/2}, \quad (20)$$

where τ is specified as the switching time between the states (Fig. 4, *a*, dashed curve) or as the interspike interval (Fig. 4, *b*). The time averaged duration identifies the mean period and, hence, the mean frequency $\langle f \rangle = 1/\langle\tau\rangle$ of the noise-activated oscillations. Figure 4, *a* illustrates how the coherence of the switching events (dashed curve) grows monotonically when the noise intensity is increased. Very strong noise causes fast switching. The residence time then becomes less than two interspike periods, and our two-state approach no longer applies. The spike train provides an efficient way to code a sequence of action potentials with nearly the same shape since the most important information in neuronal systems is widely believed to be coded in the time sequence of action potential generation [23]. The spike train is a binary time series with a value 1 at the time of action potential generations and 0 at other times. We analyzed the coherence properties for spike trains in the presence of noise. The results of a calculation of the regularity coefficient (20) as a function of noise intensity are shown in Fig. 4, *b*. The curve is seen to display a maximum for noise intensities around $D=0.4$. For weak noise, the contribution of γ_{pop} to the whole spike train is small. At the optimal noise intensity β and γ_{pop} contribute equally to the spiking train. Strong noise destroys the β rhythm, and the regularity decreases. This represents an example of coherence resonance in the noise-induced switching between different modes of the neural system.

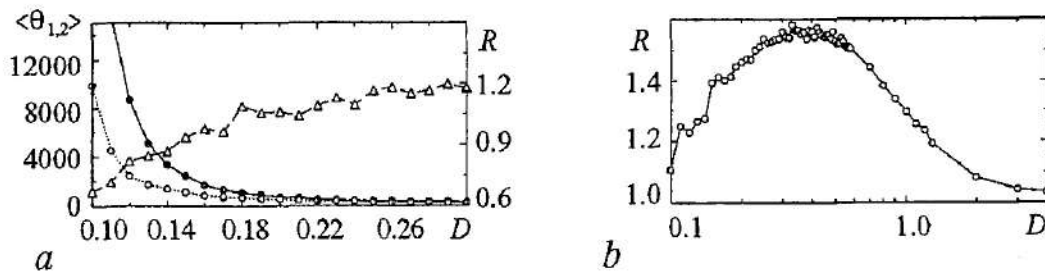


Fig. 4. (a) Residence time $\langle\theta_{1,2}\rangle$ for $\Delta\phi=0$ (solid curve) and $\Delta\phi=\pi$ (dotted curve) and regularity coefficient R of the switching time (dashed curve) as functions of the noise amplitude; (b) regularity coefficient R calculated from the interspike intervals; $g_{ahp}=1.25$ mS/cm², $g_{ee}=0.05$ mS/cm². $\Delta\phi$ represents the phase shift between the spiking events in the excitatory neurons E1 and E2

Hopping between γ and β regimes. In the diagram presented in Fig. 3, regions of γ and β rhythms are separated by the region of high-periodic solutions. Fixing the parameters at the point B of the diagram, when adding noise we observe a *direct* transition between the main rhythms. The residence time in the β regime now grows with increasing noise intensity. Our measure of coherence calculated over the interspike intervals indicates a well-pronounced maximum at some optimal noise intensity at which β and γ spike trains alternate in a regular way (Fig. 5). Here, we observe another example of regularized hopping events induced by applied noise, but now with one of the involved states being unstable for the considered parameters.

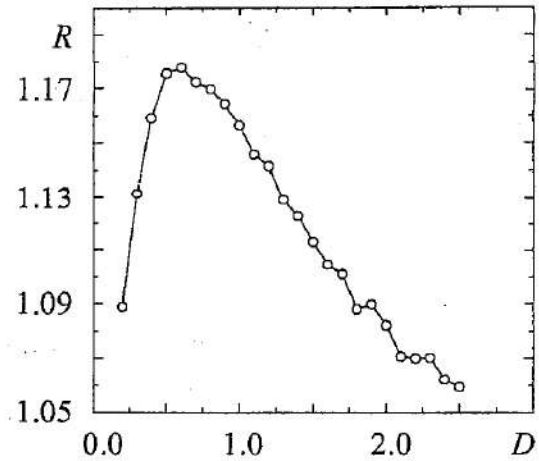


Fig. 5. Coherence dynamics of interspike intervals in the Kopell model for $g_{ahp}=0.5$ mS/cm² and $g_{ee}=-0.2$ mS/cm². As before, D represents the noise amplitude

Onset of spiking dynamics. Let us hereafter see how noise can cause firing events in this local network. (Parameter values corresponding to point C in Fig. 3.) It is known that the behavior of spike trains can exhibit coherence resonance at an optimal noise intensity, as described for a single Hodgkin-Huxley model by Lee *et al.* [24]. In this case, noise affects the dynamics of the system in two ways: (i) increasing the noise intensity decreases the silence (activation) time so that the contribution of the spiking dynamics increases. This enhances the regularization of spiking dynamics of the membrane potential. (ii) noise also produces amplitude and phase fluctuations of the firing dynamics, destroying the periodicity in spiking events. The competition of these two mechanisms produces the phenomenon of coherence resonance, i.e. a maximal degree of coherence for an optimal noise level. This phenomenon is responsible for the first peak of coherence for E1 (Fig. 6). With vanishing connection between the excitatory cells ($g_{ee}=0.0$), E2 demonstrates coherence of spiking events at a higher noise intensity because of its different internal parameters. Due to inhibitory synapses (controlled directly in the Kopell model by varying g_{ii} and g_{ie}), the first neuron adjusts its spiking train and demonstrates a secondary coherence resonance at higher noise intensity (Fig.6, a).

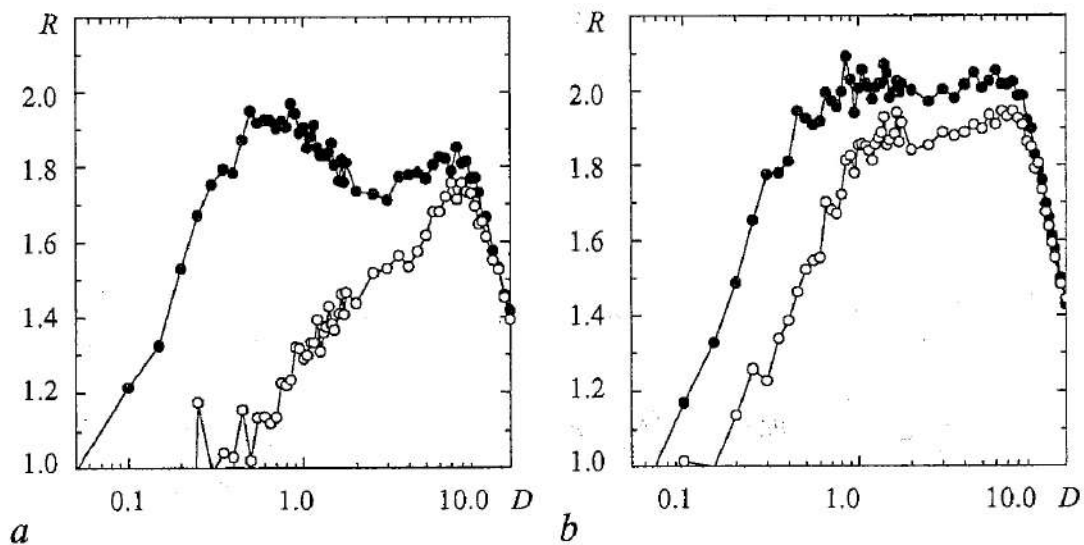


Fig. 6. Regularity for (a) $g_{ahp}=2.0$ mS/cm², $g_{ee}=0.0$ mS/cm² and (b) $g_{ahp}=2.0$ mS/cm², $g_{ee}=0.2$ mS/cm². Note, how the two peaks observed in (a) are closer to one another in (b)

When the E1-E2 connection is introduced ($g_{ee} = 0.2 \text{ mS/cm}^2$), the two peaks approach one another and the excitable units demonstrate a well-pronounced peak of coherence at the same noise intensity. This is illustrated in Fig. 6, *b*. Because of the synchronization effects, the maximal value of R is higher than in the previous case [25].

4. Noise-induced rhythms

Let us hereafter focus on *noise-induced* rather than on noise-activated oscillatory modes. This implies that we focus on time scales that are generated and controlled by noise and do not exist in the deterministic case. We provide experimental observation of such multimode behavior and investigate the conditions of generation and entrainment of the specified modes.

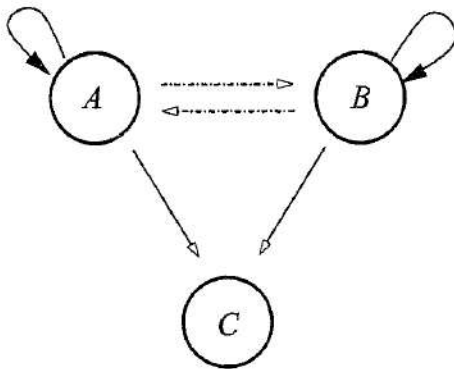


Fig. 7. Schematic presentation of a breathing rhythm generator for a snail

mutually inhibitory coupling chains that can increase the threshold voltages of the first (V_{th1}) and second (V_{th2}) units. Each coupling chain contains a rectifier and a low-pass filter with coupling strength g_{ij} and time constant τ_{ij} , where i, j denote the unit numbers. Note that the self-inhibitory time constants were chosen to be equal and to be greater than the mutually inhibitory time constants, i.e., $\tau_{11} = \tau_{22} > \tau_{12} = \tau_{21}$.

With a small noise intensity D (which is the same for the two units), both excitable units keep silent most of the time, and their threshold voltages remain equal ($V_{th1} \approx V_{th2}$). For intermediate noise levels, the coupling influence on the threshold voltages becomes

The purpose of this section is to describe the two-mode stochastic behavior of an electronic system that has been constructed as a hard-wired version of the simplest breathing rhythm generator for a snail (Fig. 7) [26]. A single monovibrator circuit [27], being the functional unit in our electronic experiment, captures the essential aspects of excitable systems generating a single electric impulse whenever the input voltage exceeds the threshold level. The implementation of interacting excitable units shown in Fig. 8, *a* contains self- and

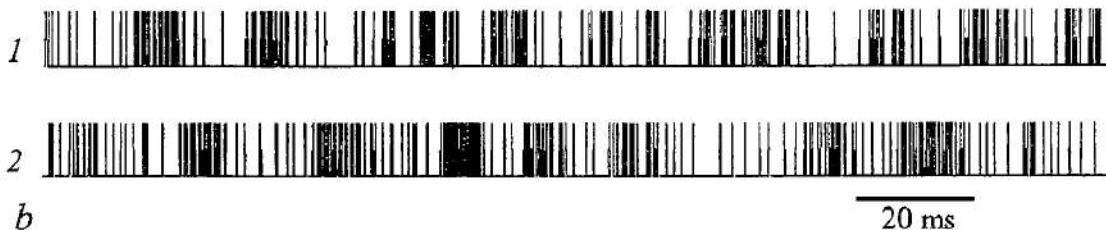
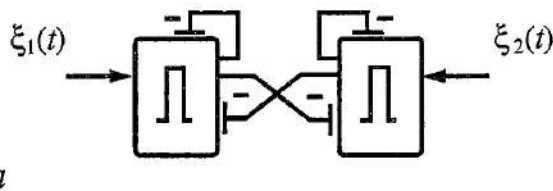


Fig. 8. (*a*) Two monovibrators with delayed inhibitory couplings imitate the simple neural circuit. (*b*) Stochastic spike trains generated by the first and second excitable units. Antiphase behavior is indicated on the average

significant. At the same time, since mutual inhibition makes the in-phase regime unstable, one of the two units gets the upper hand with respect to its ability to suppress the firings of the other. However, with intensive firing, the slow self-inhibitory chain with rate τ_{11} (or τ_{22}) comes into operation and suppresses the activity of the stronger unit. This creates better conditions for excitation of the other unit, and the process continues in an alternating manner, producing a behavior with time-varying firing rates for the two excitable units (Fig. 8, *b*).

In this operating regime, two peaks in the power spectrum are clearly distinguished (Fig. 9, *a*). The high frequency peak corresponds to noise-induced oscillations in the single system while the low frequency peak reveals a new noise-induced oscillatory mode. Hence, the system of coupled excitable units generates a new oscillatory mode that is characterized by the values of τ_{ij} and by the relation between the noise intensity and the initial threshold voltages (V_{th1}, V_{th2}). Fig. 9, *b* demonstrates how the frequencies of these oscillations (open circles) depend on the noise intensity. Inspection of the figure clearly shows that with increasing noise strength, both frequencies grow (i.e., they are noise-controlled), but the growth rates are different (i.e., they operate independently of each other). For strong noise, an excitable system can be immediately pushed out from the equilibrium state in spite of the threshold voltage. The low frequency peak in the power spectrum disappears, and the additional time scale no longer exists.

The regularity of the low-frequency stochastic oscillations is related to the process of pulse generation in the state of each excitable unit. Hence it is determined by the effect of coherence resonance [27]. Fig. 9, *b* illustrates how the output regularity R (filled circles) is suddenly increased when low frequency oscillations appear, but the peak at the noise-induced eigenfrequency f_2 becomes washed out because of the threshold modulation.

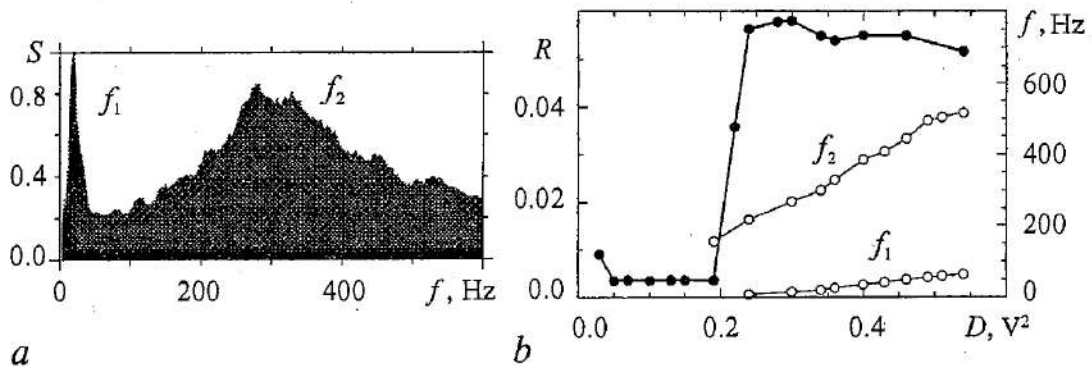


Fig. 9. Two-mode dynamics in the excitable system presented in Fig. 8*a*. (*a*) Power spectrum with well-pronounced peaks ($D=0.34V^2$) and (*b*) peak frequencies (open circles) and measure of regularity R (filled circles) vs noise intensity D

5. Discussion

We considered noise-activated and noise-induced rhythms in models representing three different neural systems: (i) a single-neuron model of a peripheral pattern generator (a mammalian cold receptor); (ii) a small neural network (the Kopell model) that can account for the coexistence of β and γ rhythms in the brain, and (iii) a coupled monovibrator system that can serve as a model of a simple breathing rhythm generator. Our results indicate that the interaction between stochastic phenomena and complex deterministic dynamics may lead to a variety of different phenomena of importance for neural rhythm generation.

The single neuron model mimics the discharge pattern of peripheral cold receptors where impulse generation is determined by slow-wave oscillations which trigger one or

more impulses during their depolarizing phases. This holds true for both deterministic and stochastic simulations with the exception that noise can induce spiking as well as skipping around the onset of period-one activity. In the regular bursting range noise does not produce any qualitative effects on the pattern but mainly smoothens the deterministically abrupt transitions. In the chaotic regime noise destroys the fine structure of the bifurcations. Thus, noise is assumed to play an essential role in sensory neurons: spike generation is clearly phase-locked to the underlying oscillations but noise determines the threshold crossings and hence the times at which spikes are generated. In addition to serving as cellular substates for synchronization in neuronal networks, subthreshold oscillations can also serve as cellular substates for a sensitive and differential neuromodulatory control based on the intrinsic oscillatory dynamics as optimized by naturally occurring noise sources. Further studies on subthreshold oscillating neurons should encompass the interesting neuromodulatory and encoding properties which arise from cooperative effects of oscillations with noise.

The neuronal network model also displays spiking patterns that are modified in an essential manner by the presence of noise. Especially in the area with coexisting solutions, noise causes the network to jump from one state to the other. There is a sharp transition between the oscillatory mode and a hopping state between the coexisting solutions, and this transition is controlled by the noise intensity. The output signal demonstrates quite «regular» switchings for a certain noise intensity. Moreover, noise can initiate switchings in the region where the main β and γ oscillations are separated by high-periodic solutions in the parameter space. In this case, we again observe an optimal noise intensity at which the jumping behavior becomes coherent. A particularly interesting finding is that, due to synaptic inhibitory interaction, the excitatory cells can demonstrate double coherence resonance [28]. With the introduction of a coupling between these neurons, the two peaks of regularity merge together, giving rise to further gain of regularity by virtue of synchronization.

We also showed that a simple system of coupled excitable functional units can generate a few oscillatory modes that are induced and controlled by noise [29]. Possible advantages of multimode dynamics may include: (i) increased sensitivity via coherence resonance; we have found multiple coherence resonance phenomenon related to different frequency entrainments and to the appearance of additional time scales; (ii) expanded flexibility. The presence and interaction of two distinct oscillatory modes enrich the dynamical patterns. The electronic approach involving excitable stochastic units with self- and mutually inhibitory couplings can be applied to simulate neuron systems with a priori given phase relations.

This work was partly supported by INTAS grant 01-2061 and RFBR grant 01-02-16709. O.S. acknowledges INTAS (Grant YSF 01/1-0023) and the Lundbeck Foundation.

References

1. *Anishchenko V.S.* Dynamical Chaos: Models and Experiments. World Scientific, Singapore, 1995.
2. *Anishchenko V.S., Astakhov V.V., Neiman A.B., Vadivasova T.E., and Schimansky-Geier L.* Nonlinear Dynamics of Chaotic and Stochastic Systems. Springer Verlag, Berlin, 2002.
3. *Eckhorn R., Bauer R., Jordan W., Brosch M., Kruse W., Munk W., and Reitboeck H.J.* Coherent oscillations: A mechanism of feature linking in the visual cortex? *Biol. Cybern.* 60 (1988), 121-130.
4. *Gray C.M., König P., Engel A.K., and Singer W.* Oscillatory responses in cat

- visual cortex exhibit inter-columnar synchronization which reflects global stimulus properties, *Nature* 338 (1989), 334-337.
5. Braun H.A., Bade H., and Hensel H. Static and dynamic discharge patterns of bursting cold fibers related to hypothetical receptor mechanisms. *Pflügers Arch.* 386 (1980), 1-9.
 6. Braun H.A., Schäfer K., Wissing H., and Hensel H. Periodic transduction processes in thermosensitive receptors // *Sensory Receptor Mechanisms* (eds W. Hamann, A. Iggo), World Scientific, Singapore, (1984), 147-156.
 7. Braun H.A., Huber M.T., Dewald M., Schäfer K., and Voigt K. Computer simulations of neuronal signal transduction: The role of nonlinear dynamics and noise // *Int. J. Bifurcation & Chaos*. 1998. Vol. 8. Pp. 881-889.
 8. Braun W., Eckhardt B., Braun H.A., and Huber M.T. Phase space structure of a thermoreceptor // *Phys. Rev. E*. 2000. Vol. 62. Pp. 6352-6360.
 9. Feudel U., Neiman A., Pei X., Wojtenek W., Braun H.A., and Huber M.T. Homoclinic bifurcations in a Hodgkin-Huxley model of thermally sensitive neurons // *Chaos*. 2000. Vol. 10. Pp. 231-239.
 10. Tuckwell H.C. *Stochastic Processes in the Neurosciences*. SIAM, Philadelphia, 1989; Taylor J.G., *Neurodynamics*, (eds F. Fasman and H.D. Doebner), World Scientific, Singapore (1991), 129-164.
 11. Braun H.A., Wissing H., Schäfer K., and Hirsch M.C. Oscillation and noise determine signal transduction in shark multimodal sensory cells // *Nature*. 1994. Vol. 367. Pp. 270-273.
 12. Russell D.F., Wilkens L.A., and Moss F. Use of behavioural stochastic resonance by paddle fish for feeding // *Nature*. 1999. Vol. 402. Pp. 291-294.
 13. Nakamura K. Stochastic Resonance in the FitzHugh-Nagumo Neuron Model // *Proc. Inst. Natural Sci.* 2000. Vol. 35. Pp. 179-185.
 14. Pikovsky A.S. and Kurth J. Coherence resonance in a noise-driven excitable system // *Phys. Rev. Lett.* 1997. Vol. 78. Pp. 775-778.
 15. Neiman A., Pei X., Russell D., Wojtenek W., Wilkens L., Moss F., Braun H.A., Huber M.T., and Voigt K. Synchronization of the noise electrosensitive cells in the paddlefish // *Phys. Rev. Lett.* 1999. Vol. 82. Pp. 660-663.
 16. Kopell N., Ermentrout G.B., Whittington M.A., and Traub R.D. Gamma rhythms and beta rhythms have different synchronization properties // *Proc. Nat. Acad. Sci. USA*. 2000. Vol. 97. Pp. 1867-1872.
 17. Bressler S.L., Coppola R., and Nakamura R. Episodic multiregional cortical coherence at multiple frequencies during visual task performance // *Nature*. 1993. Vol. 366. Pp. 153-156.
 18. Braun H.A., Huber M.T., Anthes N., Voigt K., Neiman A., Pei X., and Moss F. Interaction between slow and fast conductances in the Huber/Braun model of cold-receptor discharges // *Neurocomputing*. 2000. Vol. 32-33. Pp. 51-59.
 19. Fox R.F., Gatland I.R., Roy R., and Vemuri G. Fast accurate algorithm for numerical simulation of exponentially correlated colored noise // *Phys. Rev. A*. 1988. Vol. 38. Pp. 5938-5940.
 20. 1) Equilibrium potentials: $E_{sd}=E_d=50$, $V_{sr}=V_r=-90$, $V_l=-60$ (mV); 2) ionic conductances: $g_l=0.1$, $g_d=1.5$, $g_r=2.0$, $g_{sd}=0.25$, $g_{sr}=0.4$ (mS/cm²); 3) membrane capacitance: $C=1$ (μF/cm²) gives a passive time constant $\tau_M=C/g_l=10$ (ms); 4) activation time constants: $\tau_r=2$, $\tau_{sd}=2$, $\tau_{sr}=2$ (ms); 5) slope of steady state activation: $s_d=s_r=0.25$, $s_{sd}=0.09$; 6) half activation potentials: $V_{0d}=V_{0r}=-25$, $V_{0ds}=-40$ (mV); 7) coupling and relaxation constants for I_{sr} : $\eta=0.012$, $k=0.17$; 8) reference temperature: $T_0=25^\circ(\text{C})$.
 21. Hodgkin A.L. and Huxley A.F. A quantitative description of membrane current and its application to conduction and excitation in nerve // *J. Physiol.* 1952. Vol. 117. Pp. 500-544.
 22. Fausboll A. Analysis of a Minimal Network of Cortical Neurons. MSc. Thesis, DTU, Denmark, 2001.

23. Moore G.P., Perkel D.H., and Segundo J.P. Statistical analysis and functional interpretation of neuronal spike data // *Ann. Rev. Physiol.* 1966. Vol. 28. Pp. 493-522.
24. Lee S.-G., Neiman A., and Kim S. Coherence resonance in a Hodgkin-Huxley neuron // *Phys. Rev. E.* 1998. Vol. 57. Pp. 3292-3297.
25. Postnov D.E., Setskinsky D.V., and Sosnovtseva O.V. Stochastic synchronization and the growth in regularity of the noise-induced oscillations // *Tech. Phys. Lett.* 2001. Vol. 27. Pp. 49-55.
26. Rosenzweig M.R., Leiman A.L., Breedlove S.M. *Biological Psychology*. Sinaur Associated, Inc. Sunderland, Massachusetts, 1996.
27. Postnov D.E., Han S.K., Yim T., and Sosnovtseva O.V. Experimental observation of coherence resonance in cascaded excitable systems // *Phys. Rev. E.* 1999. Vol. 59. 3791-3794; Han S.K., Yim T., Postnov D.E., and Sosnovtseva O.V. Interacting coherence resonance oscillators // *Phys. Rev. Lett.* 1999. Vol. 83. Pp. 1771-1774.
28. Sosnovtseva O.V., Setskinsky D., Fausboll A., Mosekilde E. Transitions between beta and gamma rhythms in neural systems // *Phys. Rev. E.* 2002. Vol. 66. 041901(6).
29. Postnov D.E., Sosnovtseva O.V., Han S.K., and Kim W.S. Noise-induced multimode behavior in excitable systems // *Phys. Rev. E.* 2002. Vol. 66. 016203(5).

*Department of Physics, The Technical
University of Denmark,
Physics Department, Saratov
State University, Russia
Institute of Physiology, University
of Marburg, Germany*

Received 31.07.03

УДК 532.517, 517.9, 621.373

НЕЙРОННЫЕ ГЕНЕРАТОРЫ РИТМА В ПРИСУТСТВИИ ШУМА

E. Mosekilde, O.V. Sosnovtseva, Д.Э. Постнов, Н.А. Браун, М.Т. Хубер

Исследуются динамические особенности генерации последовательности спайков в присутствии шума для трех различных моделей нейронных генераторов ритма: простой нейронной модели, которая воспроизводит импульсную модуляцию для кодирования температуры в холодовых рецепторах млекопитающих, минимальной нейронной сети, описывающей переходы между бета- и гамма-ритмами в мозге, и электронного переключательного устройства, представляющего собой простой генератор дыхательного ритма улитки. Мы показываем, что шум может объяснить множество особенностей в наблюдаемой последовательности спайков, вызывать когерентные переключения между различными состояниями, и индуцировать новые ритмы в малых нейронных ансамблях.



Erik Mosekilde received the M.Sc. in electrical engineering from the Technical University of Denmark (DTU) in 1966, the Ph.D. in solid state physics from DTU in 1968, and the Dr.Sc. in semiconductor instabilities from the University of Copenhagen in 1977. In 1970 he was a postdoctoral fellow at IBM Watson Research Center in Yorktown Heights, New York. He has been a visiting scientist at a number of different universities in Europe and North America. He is a co-author of 190 scientific papers and of several books, including two recent books on «Topics in Nonlinear Dynamics» and «Chaotic Synchronization». His main interests are modeling of complex systems and applications of nonlinear dynamics. He is a Professor in nonlinear dynamics and a Head of the Department of Physics at DTU, Denmark.



Olga Sosnovtseva received the M.Sc. from Saratov State University, Russia in 1989, and the Ph.D. degree in Physics and Mathematics in 1996, also from Saratov State University. Since 2001 she has been a postdoctoral fellow at The Technical University of Denmark. She is co-author of 40 scientific papers. Her current interests are within the field of nonlinear dynamics and modelling of biological systems. E-mail: olga@fysik.dtu.dk



Dmitry Postnov is a professor of the Chair of Radiophysics and Nonlinear Dynamics of Saratov State University, Candidate of Science in Physics and Mathematics since 1990, Doctor of Science in Physics and Mathematics since 2001. He is an author of 56 papers in scientific journals and of book «Chaotic Synchronization. Applications to living systems» (World Scientific, 2002). E-mail: postnov@chaos.cas.ssu.runnet.ru

Hans Albert Braun is head of the Neurodynamics Group at the Institute of Physiology at the University of Marburg in Germany. He has been trained as electronic engineer at the Technical University in Karlsruhe where he obtained a degree in «Electrobiology». In course of a supplementary study of «Human Biology» he obtained his PhD at the Medical Faculty of the University of Marburg.

His research involves experiments and models of neuronal encoding and neuromodulatory processes in peripheral sensory receptors (thermo- and electroreceptors) and hypothalamic neurones (neuroendocrine functions) including computer modelling studies of affective disorders. The aim is the understanding of neuronal systems dynamics at different levels and to elucidate their functional principles.

Hans A. Braun is member of several scientific societies and has been honored with the fellowship of the Biophysics Division of the American Physical Society. E-mail: braun@mail.uni-marburg.de



Martin Tobias Huber is university lecturer of biological psychiatry and neuroinformatics at the Department of Psychiatry and Psychotherapy of the University of Marburg. His research interests include clinical and modelling studies of disease-relevant features of short- and longterm changes in biological systems such as neuromodulation, sensitivity adjustment, sensitization and adaptation. The aim of these studies is the characterization of normal and pathological systems biology with particular emphasis on the biological psychiatry of affective disorders and schizophrenia.



Izv. VUZ «AND», vol. 11, № 3, 2003

DYNAMICS OF GLOBALLY COUPLED NOISY FITZHUGH-NAGUMO NEURON ELEMENTS

J.A. Acebrón, A.R. Bulsara, and W.-J. Rappel

We study the noisy FitzHugh-Nagumo model in the presence of an external sinusoidal driving force. We derive a Fokker-Planck equation for both the single element and for the globally coupled system. We introduce an efficient way to numerically solve this Fokker-Planck equation and show that the external driving force leads to a classical resonance when its frequency matches the underlying systems frequency. This resonance is also investigated analytically by exploiting the different timescales in the problem. Agreement between the analytical results and numerical results is excellent and reveals the existence of a stochastic bifurcation.

To Vadim Anishchenko, on the occasion of his sixtieth birthday

1. Introduction

The FitzHugh-Nagumo model (FHN) is a simplified version of the celebrated Hodgkin-Huxley model [1], which describes the firing mechanism in a excitable nerve cell. In the FHN, the dynamics of the nerve cell has been reduced to two variables: a fast, activation, variable and a slow, recovery, variable [2]. Due to its relative simplicity, the FHN and its extensions has been studied extensively. Both single neurons and populations of diffusively coupled neurons have been investigated. In addition, the periodically driven FHN, where either the slow or the fast equation contains a time-periodic driving term, has received considerable attention [3-7]. Moreover, as the FHN displays a rich phase diagram that includes excitable, oscillatory and bistable regimes, it has become a «workhorse» in the field of pattern formation (see e.g. [8,9]).

In this paper, we investigate the FHN in the presence of noise and a probe signal. In addition to studying the single element, we examine the effect of coupling the FHN elements in a global fashion. Particular attention is paid to the classical resonance effect that can arise when a system with an underlying frequency is driven by a probe signal [4,10].

2. Model equations

Let us start with the most general form of the FHN model:

$$dx/dt = Ax^3 + Bx^2 + Cx + Hy + I + \xi, \quad (1)$$

$$dy/dt = Ex + Fy + G,$$

where ξ 's are Gaussian white noises, with $\langle \xi(t) \rangle = 0$, $\langle \xi(t)\xi(t') \rangle = 2D\delta(t-t')$ and where A through G are parameters that determine the dynamics of the system. To make the treatment in this paper as general as possible all relevant expressions will be derived using the above set of equations. However, when presenting the results of numerical calculations, we have chosen to limit ourselves here to the investigation of the FHN in its more conventional notation:

$$\alpha dx/dt = x(x-a)(1-x) - y + \xi, \quad (2)$$

$$dy/dt = x - py - b,$$

where α is typically taken to be small.

In order to study the properties of the stochastic differential equation in (1), we start by deriving the Fokker-Planck equation (FPE) for the density probability, which is given by:

$$\begin{aligned} \partial\rho/\partial t = D\partial^2\rho/\partial x^2 - \partial/\partial x[(Ax^3 + Bx^2 + Cx + Hy + I)\rho] - \\ - \partial/\partial y[(Ex + Fy + G)\rho], \end{aligned} \quad (3)$$

which has to be accompanied by initial and boundary data (decay to zero as $x \rightarrow \pm\infty$, $y \rightarrow \pm\infty$, with sufficiently high rate), and the normalization condition

$$\int_{-\infty}^{\infty} \int_{-\infty}^{\infty} dx dy \rho(x, y, t) = 1. \quad (4)$$

In the following, we are interested in finding solutions of the FPE for large time. This search is greatly facilitated by the fact that the FPE has a unique stationary solution. This can be seen by noting that there exists a Lyapunov function (see [11] and references therein). It then follows that such a stationary solution is unique and globally stable. For parameters values for which analytical progress is difficult to achieve one has to resort to numerics. Direct simulation of the Langevin equations (1), as has been commonly done in the FHN repertoire, can be computationally intensive. For reasonably accurate results one typically has to average over many realizations. This is particularly the case for systems close to a bifurcation point where one has to distinguish between different stable solutions and for systems where the noise is large. Numerical solutions of the FPE, on the other hand, can be obtained much faster. Rather than using a finite difference scheme we have used an efficient spectral method for which we expand the density probability ρ using a basis of Hermite polynomials

$$\rho(x, y, t) = \sum_{n=0}^{\infty} r_n^m(t) H_n(x) H_m(y) e^{-x^2} e^{-y^2}. \quad (5)$$

Note that this expansion satisfies the boundary conditions, and the normalization condition with $r_0^0 = 1/\pi$.

Let us insert Eq. (5) into the FPE (3). We then obtain the following hierarchy of coupled ordinary differential equations for $r_n^m(t)$.

$$\begin{aligned} \dot{r}_n^m = [\frac{3}{2} An^2 + Cn + Fm] r_n^m + [B(n - \frac{1}{2}) + I] r_{n-1}^m + \\ + [D + \frac{3}{4} A(n-1) + \frac{1}{2} C] r_{n-2}^m + (B/4) r_{n-3}^m + (A/8) r_{n-4}^m + Bn(m+1) r_{n+1}^m + \\ + An(n+1)(n+2) r_{n+2}^m + Gr_n^{m-1} + (F/2) r_n^{m-2} + \frac{1}{2} (H+E) r_{n-1}^{m+1} + E(n+1) r_{n+1}^{m-1}, \end{aligned} \quad (6)$$

$$n = 0, 1, \dots, \infty, \quad m = 0, 1, \dots, \infty,$$

where $\langle x \rangle$, and $\langle y \rangle$ are given by

$$\langle x \rangle = \int_{-\infty}^{\infty} \int_{-\infty}^{\infty} dx dy x \rho(x, y, t) = \pi r_1^0, \quad (7)$$

$$\langle y \rangle = \int_{-\infty}^{\infty} \int_{-\infty}^{\infty} dx dy y \rho(x, y, t) = \pi r_0^1. \quad (8)$$

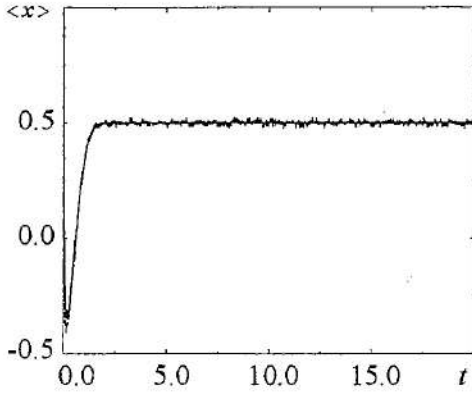


Fig. 1. Comparison between the numerical solution of the Langevin equations (dashed line; averaged over $m=500$ realizations) and the solution of the Fokker-Planck equation (solid line) by the spectral method with $N=M=7$ coefficients. Parameters are $D=0.01, b=0.5, p=1, \alpha=0.05$

The numerical method consists of truncating the infinite hierarchy of first-order, coupled nonlinear differential equations, for a reasonable number of modes $n=0, \dots, N$, and $m=0, \dots, M$, setting $r_{N+1}^{M+1}=0$. We have compared the numerical solution obtained via the Fokker-Planck approach, to the solution of the Langevin equations, obtained by averaging over a large number of realizations. In Fig. 1, we plot the first moment $\langle x \rangle$ as a function of time, obtained numerically by solving the Langevin equations (1) and by solving the FPE using the above-described spectral method. The spectral method (with $N=M=7$ moments) is seen to provide excellent agreement with the more conventional and time-consuming technique based on numerically integrating

the coupled stochastic differential equations (1).

Following this preamble, we start with an extension of the model equations (1) to describe a system of globally linearly coupled FitzHugh-Nagumo elements. Global coupling is also most amenable (of all the possible coupling schemes) to theoretical treatment. We will couple the elements in the following global fashion:

$$dx_i/dt = Ax_i^3 + Bx_i^2 + Cx_i + Hy_i + I + K/N \sum_{j=1}^N (x_j - x_i) + \xi_i, \quad (9)$$

$$dy_i/dt = Ex_i + Fy_i + G, \quad i = 1, \dots, N. \quad (10)$$

With this type of coupling, the FPE for the perfectly synchronized system is identical to the FPE of a single element.

We are interested in the analytical investigation of the Langevin dynamics above, for the case of very large N . A neat picture of such a case can be given by the limiting-model obtained when $N \rightarrow \infty$ (thermodynamic limit). In this limit, it is well known [12,13] that models with mean-field coupling are described by an evolution equation for the one-particle probability density. This can be seen by noting that the hierarchy of equations for all the multiparticle probability densities can be closed by assuming molecular chaos. In such a way, the one-system probability density $\rho(x, y, t)$ is asymptotically in the limit, $N \rightarrow \infty$, the solution of the following nonlinear Fokker-Planck equation:

$$\partial \rho / \partial t = D \partial^2 \rho / \partial x^2 - \partial / \partial x [(Ax^3 + Bx^2 + Cx + Hy + K(\bar{x} - x) + I)\rho] - \partial / \partial y [(Ex + Fy + G)\rho], \quad (11)$$

where

$$\bar{x} = \int_{-\infty}^{\infty} \int_{-\infty}^{\infty} dx dy x \rho(x, y, t). \quad (12)$$

The hierarchy (6) now becomes:

$$\begin{aligned}
\dot{r}_n^m = & \left(\frac{3}{2}An^2 + Cn + Fm - Kn\right)r_n^m + [B(n - \frac{1}{2}) + I + \pi Kr_1^0]r_{n-1}^m + \\
& + [D + \frac{3}{4}A(n-1) + \frac{1}{2}C - K/2]r_{n-2}^m + (B/4)r_{n-3}^m + (A/8)r_{n-4}^m + Bn(m+1)r_{n+1}^m + \\
& + An(n+1)(n+2)r_{n+2}^m + Gr_n^{m-1} + (F/2)r_n^{m-2} + \frac{1}{2}(H+E)r_{n-1}^{m+1} + E(n+1)r_{n+1}^{m-1},
\end{aligned} \tag{13}$$

$$n = 0, \dots, \infty, \quad m = 0, \dots, \infty.$$

Note that now the hierarchy consists of a system of coupled first-order nonlinear differential equations.

In Fig. 2, we have compared the numerical solution obtained via the nonlinear Fokker-Planck approach to the solution of the Langevin equations for a large number of FHN oscillators ($N=5000$). The solution of the FPE, corresponding to $N \rightarrow \infty$, provides excellent agreement with the finite N case and shows that $N=5000$ is already close to infinity for all practical purposes.

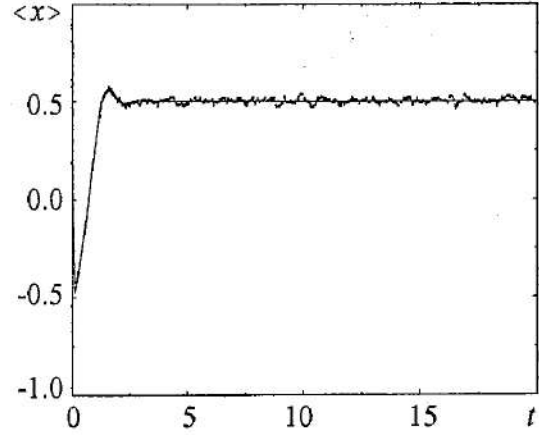


Fig. 2. Comparison between solution obtained by means of FPE (solid line), and direct numerical simulation of the Langevin equations (dashed line) for $N=5000$ oscillators. Parameters are as in Fig. 1, and $K=1$

3. Bifurcation analysis

To investigate the bifurcations in the noisy case it is worthwhile to determine the underlying frequency of the system. One way of determining this frequency is to compute $\langle x \rangle$ from the Langevin equations and evaluate its time dependence. Unfortunately, this is computationally very costly. On the other hand, $\langle x \rangle$ calculated from the FPE, which offers a computationally superior way to characterize the system, does not display a time-dependent behavior for a single FHN oscillator. Therefore, an alternative way of finding the frequency needs to be employed. Fortunately, as we will see below, including an external time-sinusoidal «probe» signal leads to a classical resonance which can be used to determine the underlying frequency [4]. We will consider an external signal that has a time-sinusoidal component $G=G_0+q\sin(\omega_p t)$ in (1) (or, equivalently, $b=b_0+q\sin(\omega_p t)$ in (2)).

To illustrate the effect of the probe signal, we first performed Langevin simulations and calculated $\langle y \rangle$. In Fig. 3 we have plotted the power spectrum of this quantity, for three different probe signals; two of them with frequencies ω_p that differs significantly from and one that is very close to the underlying frequency. The power spectrum was obtained by averaging 100 timeseries of 2^{23} timesteps each. The figure illustrates clearly that for a probe signal frequency that matches the broad peak (corresponding to the, in general, non-sinusoidal running oscillations) in the power spectrum of the unprobed system, the signal is amplified. Thus, adding a probe signal gives us a tool to investigate the dynamics of the noisy system. On the other hand, it is worthwhile to exploit such a result to study the bifurcations in our noisy system. In Fig. 3, *a*, and *b*, we show the results for two different values of the noise strength. For small noise strength (Fig. 3, *a*), the peak in the powerspectrum reaches a maximum for non-zero values of the probing frequency while for larger noise strengths (Fig. 3, *b*) this peak is reached for $\omega_p=0$. Thus, there is a

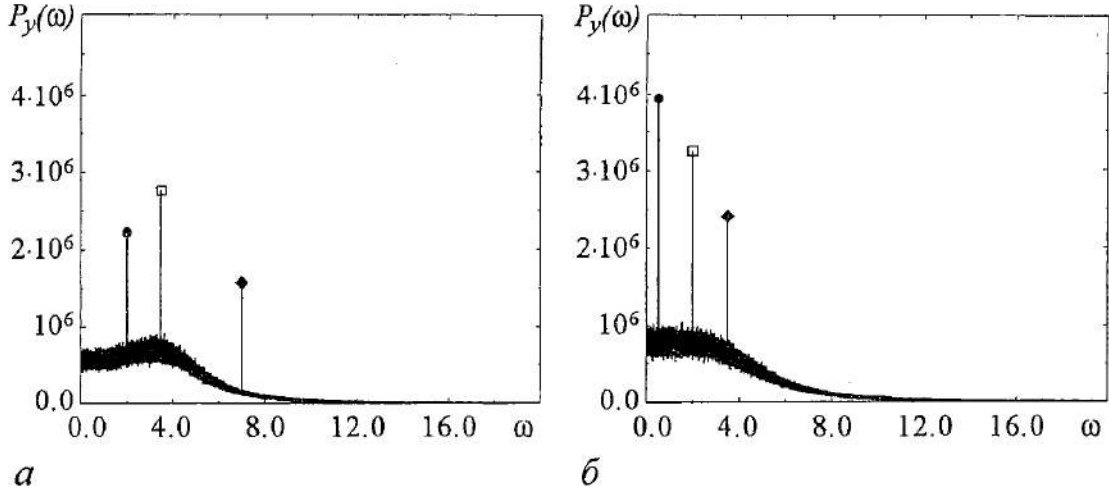


Fig. 3. Power spectrum of the variable y for three different values of the probe signal, and noise strength; (a) $\omega = 2.0, 3.5, 7.0, D=0.003$, and (b) $\omega = 0.5, 2.0, 3.5, D=0.005$. Simulations done by using the Langevin equations. Other parameters are $b_0=0.5, p=1, q=0.01$, and $\alpha=0.05$

qualitative change in the powerspectrum and in the dynamics of the system, which can be interpreted as the signature of a bifurcation.

Analytical progress by means of the Fokker-Planck equation can be made if we consider a small amplitude signal, $q=\epsilon Q$, where $\epsilon \ll 1$. The resulting FPE can then be analyzed via the method of multiple scales. Thus, Eq. (3) contains terms with two different time scales. It is then to be expected that an appropriate asymptotic method will be able to capture the long-time behavior of ρ . This may be achieved by introducing fast and slow timescales as follows:

$$\tau = t/\epsilon, \quad t = t. \quad (14)$$

We look for a distribution function satisfying the boundary condition according to the Ansatz:

$$\rho(x,y,t;\epsilon) = \sum_{n=0}^2 \rho^{(n)}(x,y,t,\tau)\epsilon^n + O(\epsilon^3). \quad (15)$$

From (15), the average of x is given by

$$\langle x \rangle = \langle x \rangle^{(0)} + \epsilon \langle x \rangle^{(1)} + O(\epsilon^2), \quad (16)$$

where

$$\langle x \rangle^{(j)} = \int_{-\infty}^{\infty} \int_{-\infty}^{\infty} dx dy x \rho^{(j)}(x,y,t). \quad (17)$$

The average of y is given by similar equations. Inserting (15) into (3), we obtain the following hierarchy of equations for $\rho^{(j)}$:

$$\partial \rho^{(0)} / \partial \tau = 0, \quad (18)$$

$$\begin{aligned} \partial \rho^{(1)} / \partial \tau = & D \partial^2 \rho^{(0)} / \partial x^2 - \partial / \partial x [(Ax^3 + Bx^2 + Cx + Hy + I)\rho^{(0)}] - \\ & - \partial / \partial y [(Ex + Fy + G_0)\rho^{(0)}] - \partial \rho^{(0)} / \partial t, \end{aligned} \quad (19)$$

$$\begin{aligned} \partial \rho^{(2)} / \partial \tau = & D \partial^2 \rho^{(1)} / \partial x^2 - \partial / \partial x [(Ax^3 + Bx^2 + Cx + Hy + I)\rho^{(1)}] - \\ & - \partial / \partial y [(Ex + Fy + G_0)\rho^{(1)}] - \partial \rho^{(1)} / \partial t - Q \sin(\omega_p t) \partial \rho^{(0)} / \partial y, \end{aligned} \quad (20)$$

where the normalization conditions

$$\int_{-\infty}^{\infty} \int_{-\infty}^{\infty} \rho^{(n)}(x,y,t) dx dy = \delta_{0n} \quad (21)$$

follows from (4). Eq. (18) implies that $\rho^{(0)}$ is independent of τ . Then, the terms in the right side of (19) which do not have τ -dependent coefficients give rise to secular terms (unbounded on the τ -time scale). The condition that no secular terms should appear is

$$\begin{aligned} D\partial^2\rho^{(0)}/\partial x^2 - \partial/\partial x[(Ax^3 + Bx^2 + Cx + Hy + I)\rho^{(0)}] - \\ - \partial/\partial y[(Ex + Fy + G_0)\rho^{(0)}] - \partial\rho^{(0)}/\partial t = 0. \end{aligned} \quad (22)$$

This equation should be solved for $\rho^{(0)}$ together with the normalization condition and initial condition data. Note that this problem is equivalent to solving the FPE (3) without the probe signal as the effects of the probe signal appear first when calculating the first-order correction, $\rho^{(1)}$.

To calculate these first-order corrections, we again impose the condition that no secular terms appear and that the right-hand side of (20) vanishes. The resulting equation is:

$$\begin{aligned} D\partial^2\rho^{(1)}/\partial x^2 - \partial/\partial x[(Ax^3 + Bx^2 + Cx + Hy + I)\rho^{(1)}] - \\ - \partial/\partial y[(Ex + Fy + G_0)\rho^{(1)}] - \partial\rho^{(1)}/\partial t - Q\sin(\omega_p t)\partial\rho^{(0)}/\partial y = 0. \end{aligned} \quad (23)$$

The analysis of the equation above can be readily accomplished in Fourier space. Fourier transforming Eq. (23), we obtain

$$i\omega\hat{\rho}^{(1)} = D\partial^2\hat{\rho}^{(1)}/\partial x^2 - \partial/\partial x[(Ax^3 + Bx^2 + Cx + Hy + I)\hat{\rho}^{(1)}] - \quad (24)$$

$$- \partial/\partial y[(Ex + Fy + G_0)\hat{\rho}^{(1)}] - i(Q/2)\partial/\partial y[\hat{\rho}^{(0)}(\omega + \omega_p) - \hat{\rho}^{(0)}(\omega - \omega_p)],$$

where

$$\hat{\rho}^{(j)}(x,y,\omega) = \int_{-\infty}^{\infty} dt e^{-i\omega t} \rho^{(j)}(x,y,t), \quad (25)$$

$$\langle \hat{x} \rangle^{(j)} = \int_{-\infty}^{\infty} \int_{-\infty}^{\infty} dx dy x \hat{\rho}^{(j)}(x,y,t), \quad (26)$$

$$j = 0, 1. \quad (27)$$

The equation (24) should be solved for $\hat{\rho}^{(1)}$ together with $\int_{-\infty}^{\infty} \int_{-\infty}^{\infty} dx dy \hat{\rho}^{(1)} = 0$. Since $\rho^{(0)}$ evolves to a stationary solution for long-time (i.e. $\hat{\rho}^{(0)} = \delta(\omega) f(\delta_1, \delta_2)$), we find that $\hat{\rho}^{(1)} = 0$ is the only solution of (24), unless $\omega = \pm\omega_p$. Then, (24), (27) imply that

$$\hat{\rho}^{(1)} = \eta^+(x,y)\delta(\omega - \omega_p) + \eta^-(x,y)\delta(\omega + \omega_p). \quad (28)$$

Inserting (28) in Eq. (24), we obtain two uncoupled equations for η^+ , and η^- . These can be solved, by expanding η^\pm in Hermite polynomials,

$$\eta^\pm(x,y) = \sum_{n=0}^{\infty} \sum_{m=0}^{\infty} (T^\pm)_n^m H_n(x) H_m(y) e^{-x^2} e^{-y^2}, \quad (29)$$

and solving the corresponding nonlinear systems of equations for the coefficients $(T^\pm)_n^m$. Once we obtain $(T^\pm)_n^m$, we can calculate $\langle \hat{x} \rangle^{(1)}$ from Eq. (27). Notice that $\hat{\rho}^{(1)}(+\omega_p) = \hat{\rho}^{(1)*}(-\omega_p)$, by taking the complex conjugate in (24), and (27). Then it follows from (28), and (29) that $(T^+)_n^m = ((T^-)_{-n}^{-m})^*$. Therefore we conclude that $\langle \hat{x} \rangle^{(1)}(-\omega_p) = (\langle \hat{x} \rangle^{(1)})^*(+\omega_p)$, and the

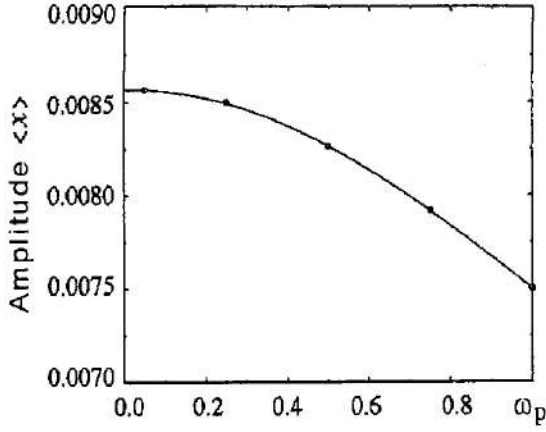


Fig. 4. Comparison between the theoretical results and the numerical simulations, marked by symbols. Parameters are $D=0.05$, $b_0=0.3$, $p=1$, $q=0.01$, and $\alpha=0.05$

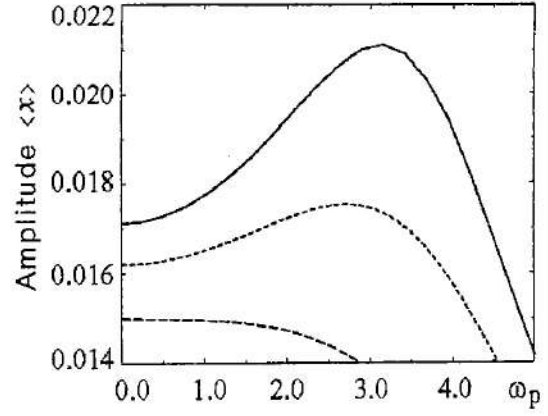


Fig. 5. $\langle x \rangle$ versus the frequency of the probe signal for different values of the noise strength: $D=0.002$ (solid line); 0.003 (dot line); 0.005 (dashed). Results obtained by means of the theory for a single FHN. Parameters are $b_0=0.5$, $p=1$, $q=0.01$, and $\alpha=0.05$

inverse Fourier transform yields

$$\langle x \rangle^{(1)}(t) = 2\text{Re}(\langle \hat{x} \rangle^{(1)}(\omega_p)) \cos(\omega_p t) - 2\text{Im}(\langle \hat{x} \rangle^{(1)}(\omega_p)) \sin(\omega_p t). \quad (30)$$

Knowing $\langle x \rangle^{(1)}(t)$, its amplitude can be readily computed, and the result is

$$A_{\langle x \rangle} = 2[\langle \hat{x} \rangle^{(1)}(\langle \hat{x} \rangle^{(1)})^*]^{1/2} + O(\epsilon^2). \quad (31)$$

In Fig. 4, we plotted the numerical solution and the theoretical approximation (31), showing a remarkable agreement with the theoretical results corresponding to the first-order expansion. It should be noticed, however, that the amplitude of the probe signal considered here is small, $q=0.01$. For increasing strength of the amplitude, higher orders in the expansion may be required. Once $\rho^{(1)}$ is known, it is also straightforward to find the successive terms in the expansion. Without entering into a detailed study, some general features can easily be drawn from the hierarchy of equations for $\rho^{(j)}$. Similarly to the analysis for $\hat{\rho}^{(1)}$, and by taking into account that $\hat{\rho}^{(1)}$ is a function exclusively of $\omega \pm \omega_p$, it

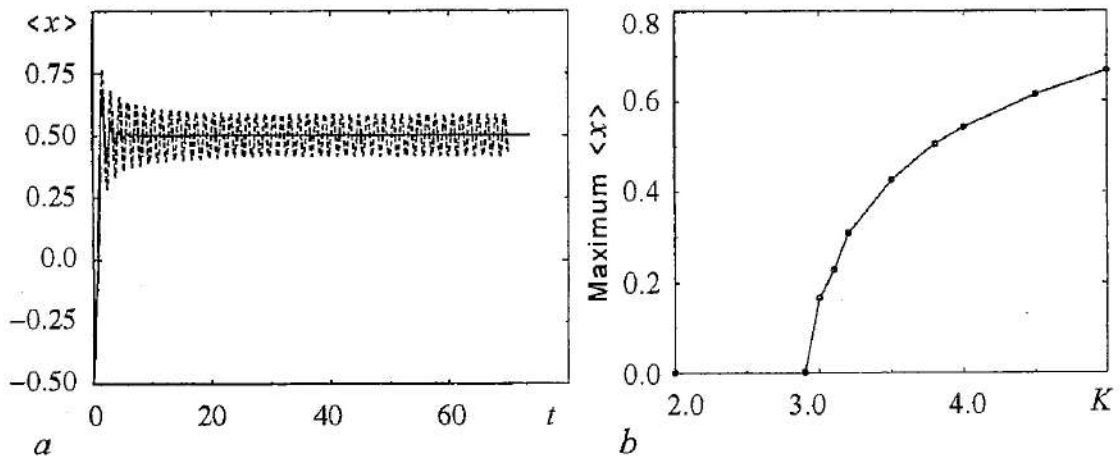


Fig. 6. (a) $\langle x \rangle$ versus time for two different values of the coupling $K=2$ (solid line) and $K=3$ (dot line), showing a clear bifurcation. (b) Amplitude of $\langle x \rangle$ vs coupling for a fixed level of noise. Parameters are as in Fig. 5

straightforward to prove that $\hat{\rho}^{(2)}=0$ is the only solution unless $\omega=0;\pm 2\omega_p$. In general, successive terms will depend on higher harmonics of the main frequency ω_p .

By applying the theory above, we were able to obtain the amplitude of $\langle x \rangle$ as function of the frequency of the probe signal, shown in Fig. 5. It should be noticed that for increasing noise levels, the peak moves to smaller values of ω and then disappears. This was already observed in Fig. 3 and can be interpreted as a sign of a stochastic bifurcation.

We now investigate the case of coupled FHN elements for which the dynamical response exhibits bifurcations, even in the absence of a probe signal. The bifurcation, of the Hopf-type, is shown in Fig. 6 where we have plotted the amplitude of $\langle x \rangle$ vs coupling for a fixed level of noise. Below some critical coupling strength, the system is not synchronized and the solution of the FPE is stationary. On the other hand, above this critical coupling strength, the system synchronizes and exhibits a time-dependent behavior.

The inclusion of a probe signal will elicit a time-dependent solution of the FPE, even when the system *without* the probe signal has a stationary solution. The amplitude of the response ($\langle x \rangle$) depends critically on the frequency of the probe signal as is shown in Fig. 7. In contrast to similar coupled systems (see e.g. [10]), increasing the coupling does not lead to the «death» of the oscillatory region and the optimal frequency actually increases as the coupling is increased. The position and amplitude of the peak in Fig. 7 depends on the coupling strength. For $K=0$ the response curve does not exhibit a peak showing that there is no underlying frequency in the problem. Increasing K produces an underlying frequency which appears as a peak in the curve. Notice that for $K>2.9$ the system will synchronize in the absence of a probe signal. This, then, leads to a response that has two principal frequencies: the frequency arising from the Hopf bifurcation and the probe frequency.

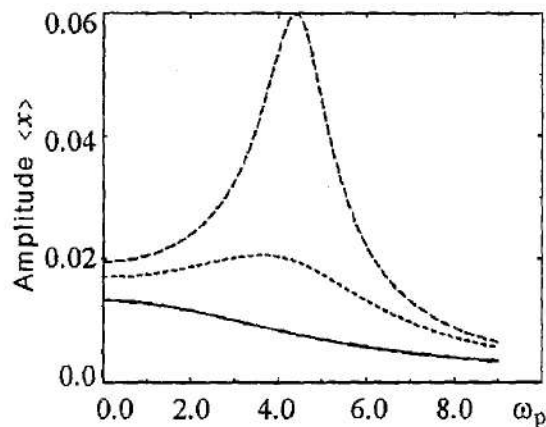


Fig. 7. Amplitude of $\langle x \rangle$ versus the frequency of the probe signal for three different values of the coupling strength $K=0$ (solid line) and $K=1$ (dot line), $K=2$ (dashed line). Parameters are as in Fig. 5

4. Summary

In this paper, we have investigated the single and globally coupled FHN model in the presence of noise and an injection signal. We have derived a FPE for the system and have shown that we can solve this FPE efficiently by using a suitably chosen expansion. We find that there is a classical resonance effect when the frequency of the probe signal approaches the one of the underlying system. We also characterize this resonance by separating the fast and slow time scales in the problem and find that, for small driving amplitudes, the agreement between numerical and analytical results is excellent. Finally, we reveal the existence of a stochastic bifurcation (see Fig. 1 and Fig. 3), manifested by the qualitative change of the peak location in the curves of $A_{\langle x \rangle}$ vs ω_p .

Future work will include the further characterization of the bifurcation we observed. Note that the bifurcation we found is different from the one found in earlier work [14]. We plan to address these differences in a future publication. In addition, we plan to investigate further the response of the globally coupled system to a probe signal. Particular attention will be paid to the possibility that, upon inclusion of an input signal, a

population can become synchronized and can produce a large output signal. By varying the intrinsic parameters, including the coupling constant, the response can thus be «tuned» at different frequencies. Whether or not real neurons make use of this mechanism remains to be seen.

This work has been supported by the Office of Naval Research (Code 331). We also thank the National Partnership for Advanced Computational Infrastructure at the San Diego Supercomputer Center for computing resources.

References

1. Hodgkin A.L. and Huxley A.F. // *J. Physiol.* (London). 1952. Vol. 117. P. 500.
2. See, e.g., Keener J. and Sneyd J. *Mathematical Physiology*. Springer-Verlag, Berlin, 1998.
3. Longtin A. // *Chaos, Soliton, Fractal*. 2000. Vol. 11. P. 1835.
4. Massanés S.R. and Pérez Vicente C.J. // *Int. J. Bif. Chaos*. 1999. Vol. 9. P. 2295; *Phys. Rev. E*. 1999. Vol. 59. P. 4490.
5. Lindner B., and Schimansky-Geier L. // *Phys. Rev. E*. 1999. Vol. 60. P. 7270.
6. Pikovsky A.S., and Kurths J. // *Phys. Rev. Lett.* 1997. Vol. 78. P. 775.
7. Kurrer C. and Schulten K. // *Phys. Rev. E*. 1995. Vol. 51. P. 6213.
8. Winfree A.T. // *Chaos*. 1991. Vol. 1. P. 303.
9. Hagberg A. and Meron E. // *Nonlinearity*. 1994. Vol. 7. P. 805.
10. Acebrón J.A., Bulsara A.R., Rappel W.-J., submitted for publication.
11. Risken H. *The Fokker-Planck equation: Methods of Solution and Applications*. Springer Verlag, Berlin, 1996.
12. Desai R.C., and Zwanzing R. // *J. Stat. Phys.* 1978. Vol. 19. P. 1.
13. Shiino M. // *Phys. Lett. A*. 1985. Vol. 112A. P. 302; *Phys. Rev. A*. 1987. Vol. 36. P. 2393.
14. Tanabe S., and Pakdaman K. // *Phys. Rev. E*. 2001. Vol. 63. 031911.

*Department of Physics
University of California, San Diego, USA
SPA WAR Systems Center,
San Diego, USA*

Received 28.08.2003

УДК 532.517: 517.9: 621.373

ДИНАМИКА ГЛОБАЛЬНО СВЯЗАННЫХ НЕЙРОННЫХ ЭЛЕМЕНТОВ ФИТЦХЬЮ - НАГУМО В ПРИСУТСТВИИ ШУМА

J.A. Acebrón, A.R. Bulsara, W.-J. Rappel

Мы изучаем модель ФитцХью - Нагумо при наличии шума и внешнего синусоидального воздействия. Записываем уравнение Фоккера - Планка для отдельного элемента и для глобально связанной системы. Представляем эффективный способ численного решения этого уравнения Фоккера - Планка и показываем, что внешнее воздействие приводит к классическому резонансу, при котором его частота совпадает с собственной частотой системы. Этот резонанс также исследуется аналитически путем использования различных временных

масштабов. В задаче наблюдается хорошее соответствие между аналитическими и численными результатами и обнаружено существование стохастической бифуркации.

J.A. Acebrón is a scientific worker of SPAWAR Systems Center Code D363, 49590 Lassing Road, RM A341 San Diego, CA 92152-6147, USA.



Dr. Bulsara is one of the leading scientists at the US Navy's Space and Naval Warfare Systems Center (SPAWAR) laboratory in San Diego, California. His major field of interest is applications of stochastic cooperative phenomena in coupled nonlinear systems.

E-mail: bulsara@spawar.navy.mil

W.-J. Rappel is a scientific worker of SPAWAR Systems Center Code D363, 49590 Lassing Road, RM A341 San Diego, CA 92152-6147, USA.



INDICES OF CARDIORESPIRATORY SYNCHRONIZATION FROM RAT BLOOD PRESSURE DATA

*N.B. Janson, N.B. Igosheva, A.G. Balanov, O. Glushkovskaya-Semyachkina,
T.G. Anishchenko, P.V.E. McClintock*

A recently developed method for the detection of phase synchronization between several oscillatory processes from one-dimensional signals has been extended to allow estimation of synchronization indices. It has been applied to blood pressure signals from freely moving rats. Each rat underwent four stages: 1) healthy; 2) healthy but challenged by beta-blockers; 3) with stress-induced myocardial injuries; 4) with the stress-induced injuries challenged by beta-blockers. It is shown that cardiorespiratory synchronization plays an essential role at each of these stages.

1. Introduction

Synchronization is one of the most fundamental phenomena in the physics of oscillations. This effect can occur between self-sustained oscillators, i.e. in systems that are nonlinear, dissipative, and able to produce undamped oscillations, given an external energy supply. Note that the timescale of the oscillations is not equal to that of the energy supply (which would make the oscillations forced rather than self-sustained). The motion in such systems can be periodic, quasiperiodic, chaotic or induced by noise [1]. The oscillators can be coupled mutually or uni-directionally. In general, synchronization means the adjustment of basic oscillatory timescale(s) due to coupling. Several manifestations of this effect have been identified, and they may be substantially different in chaotic systems [2-6]. In systems whose dynamics is periodic albeit perhaps noise-influenced, however, the varieties of synchronization are reduced to frequency, or phase synchronization [7]. Phase synchronization seems to be the most general effect. It can arise in all known kinds of oscillating system. Introducing individual phases $\phi_i(t)$, $i=1,2$ for each pair of systems involved in interaction, we may consider the generalized phase difference $\Delta\phi(t)$, with due account of the inferred order of synchronization $n:m$, where n and m are integers [8]:

$$\Delta\phi(t) = (n/m) \phi_1(t) - \phi_2(t). \quad (1)$$

It is said that $n:m$ phase synchronization occurs if $\Delta\phi(t)$ has plateaus of sufficiently long duration. Phase synchronization between the main heart rhythm and spontaneous respiration in humans in the relaxed state was established in [9]. It has recently been shown that cardiorespiratory synchronization can serve as a diagnostic criterion in

humans [10] and dogs [11], and that the order of synchronization can serve as a measure of depth of anaesthesia in rats [12].

A commonly used method for the detection of $n:m$ phase synchronization is to record signals from each of the interacting systems, compute phases from each signal, and then compare them using Eq. (1) [13]. This approach has been applied to the detection of cardiorespiratory synchronization [9,12,14]. However, it often happens that several processes with different timescales interact within a larger system, and that only a single signal is available at the output, e.g. only an electrocardiogram (ECG) without a respiration signal. Recently, a general approach was suggested for tackling such situations [15-17]. In this paper we apply it to the detection of phase synchronization, or its absence, between respiration and cardiac rhythm in rats, using the blood pressure signal alone. We extend the method reported previously in order to compute the synchronization index first introduced in [18]. We create an algorithm that allows us to find automatically the synchronization order $n:m$ for which the synchronization index is largest. By analysis of data from 7 male and 6 female rats, in four different states, we show that synchronization plays an essential role in cardiorespiratory interaction in rats, both in the healthy state and when under the influence of drugs or stress.

2. Experimental data

Experiments were performed on 13 adult Sprague-Dawley rats, 7 males and 6 females. Each animal was instrumented with an intra-arterial catheter for direct blood pressure recording. We note that in freely-moving rats it is difficult to make reliable measurements of respiration because the conventional transducers cannot safely be kept in the same position.

A series of experiments has been carried out in order to characterize blood pressure dynamics at rest, and also to observe slow transient processes induced by the intravenous injection of a nonselective beta-adrenoreceptors blocker, propranolol. All measurements were made on conscious, freely-moving, rats, and each animal underwent four stages of data acquisition:

- (I) «healthy state» at rest (90 minutes);
- (II) «healthy state», immediately after a propranolol injection (90 minutes);
- (III) «unhealthy state», immediately after being subjected to stress that induced myocardial injuries (30 minutes);
- (IV) «unhealthy state», immediately after propranolol injection, that was made 30 minutes after stress termination (90 minutes).

Stages (I) and (II) of the measurements took place one day after surgery to implant the catheter, with stages (III) and (IV) the following day after. By «healthy state» we mean the one with no sign of cardiovascular disease. By «unhealthy state» we denote significant but reversible structural and microcirculatory alterations in the myocardium, revealed by hystological analysis and resembling those observed at the initial stage of myocardial ischemia. These injuries were induced by combination of immobilization and intermittent sound stimuli during two hours. Injection of the beta-blocker propranolol (concentration 1mg/kg) simulated slow, monotonic, change in some internal parameters influencing the system. Namely, the concentration of beta-blocker in the blood influences the average heart rate and its dynamics in time. The rate of decrease of propranolol content in blood is much smaller than average heart rate, except for the very first minutes after injection. Its variation in time is known from pharmacokinetics to be approximately exponential. Thus, by studying how the dynamics of cardiovascular system changes in time, we can do a certain extent study how it depends on the concentration of propranolol.

3. Detecting synchronization: finding the order $n:m$ and index

The blood pressure signals were typically of the shape shown in Fig. 1, *a*, and in more detail in Fig. 1, *b*. Here and in what follows values of the continuous blood pressure signal $x(t)$ and its local maxima x^{\max} and minima x^{\min} are given in mm of Hg. Typically, the Fourier spectrum of the blood pressure signal (Fig. 1, *c*) contains a sharp peak at the frequency f_{AHR} of the average heart rate (AHR), a well-defined peak at the average respiration frequency f_{resp} , their combinations and, possibly, some lower-frequency components. We are interested in interactions between the cardiac and respiratory processes. To find out whether they are synchronous, or not, using just the blood-pressure signal, we exploit the approach recently developed in [15,16] and applied to human heart rate variability data in [17,19]. To quantify the degree of synchronization, if any, we extend this approach so as to be able to use synchronization index introduced in [18]. In this paper we describe the technical issues of the approach used, and for theoretical background refer the reader to [15,16]. Data-processing took place in the following sequential steps.

Step 1. Extracting discrete data. The first step is to extract from the continuous-time signal some discrete variables associated with a Poincaré map defined for the system under study. Typical discrete variables can be threshold-crossing interspike intervals, or return times T_i , which are the time intervals between successive crossings of the signal over some threshold level in one direction; successive local minima x_i^{\min} or local maxima x_i^{\max} (Fig. 1, *b*, *d*). The clinical significance of these variables is that: T_i are heart rate variability data; x_i^{\min} is the diastolic, and x_i^{\max} is the systolic, pressure during one heart beat. We can apply the approach developed to any kind of discrete data, but we note (see Fig. 1, *b*, *d*) that the amplitude variables x_i^{\min} and x_i^{\max} often display more stability compared to the temporal variable T_i . In this paper we will seek possible phase synchronization between heart rate and respiration through a study of x_i^{\min} .

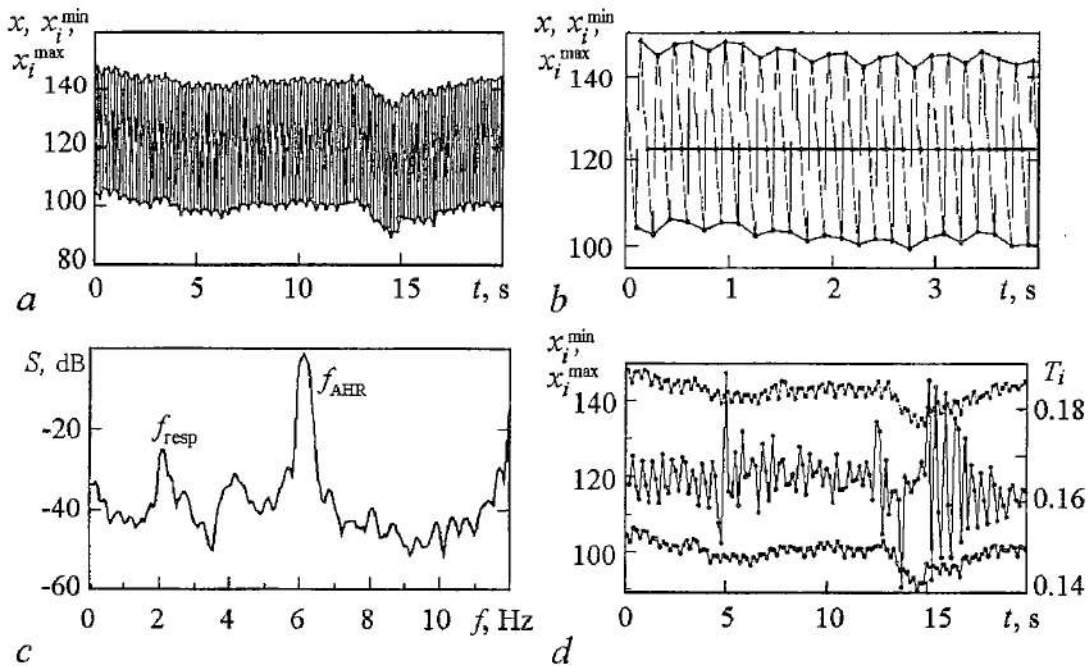


Fig. 1. (a), (b) Blood pressure signal of a rat in mmHg. Filled circles show the positions of extrema which are instantaneous systolic (maxima) and diastolic (minima) pressures: (a) Interval 20 sec; (b) Interval 4 sec. (c) Fourier power spectrum of signal shown. f_{AHR} and f_{resp} are average heart rate and respiration frequency, respectively. (d) Discrete variables extracted from signal shown in (a): x_i^{\min} (lower curve), x_i^{\max} (upper curve), T_i in seconds (middle curve)

Step 2. Filtering. Next, the low-frequency floating of average level from discrete data was reduced in order to concentrate on two higher-frequency processes: the main heart rhythm and respiration. We use two methods here. The first of these consists of computing the analogue of the second derivative of the original discrete time series $x(i)$:

$$x_{\text{der}}(i) = 1/2 [x(i+1) + x(i-1) - 2x(i)]. \quad (2)$$

Let us refer to this method as to the *method of derivatives*. How it works as applied to x^{min}_i is illustrated in Fig. 2, *a*, where the line 1 indicates original data, and the line 2 those after filtration and addition of the average value x_{av} .

The second method is an extension of the well-known detrending technique. A local average is defined within a temporal window moving along the dataset, which is then subtracted from each datapoint. The only distinction of our method is that the size of the temporal window is not constant along the dataset. Namely, one window includes all points between two successive extrema (maximum and minimum, etc.) of a discrete signal, including extrema themselves. After the local average is computed within each window, its value is attributed to the time moment of window beginning. All such averages are then connected by straight lines by means of linear interpolation. Finally, from each original datapoint the value of the resultant graph is subtracted. In Fig. 3, *a* the line 1 shows original data, the thin black line shows the local average, and the line 2 shows the filtered data, to which total average value x_{av} is added for the convenience of comparison.

Step 3. Delay embedding is then applied, and the set of points is plotted in the plane x_{i+1} vs x_i . In Fig. 2, *b* and Fig. 3, *b* the delay plots are shown for the same dataset that had undergone two types of filtering. In both cases, three clouds of points can be observed in the phase portrait, hinting at 1:3 synchronization.

Step 4. Extracting angles φ_i On the delay plot (Fig. 2, *b* and Fig. 3, *b*) one defines an angle φ_i between each phase point and the abscissa axis. The resultant time dependences of angles are shown in Fig. 2, *c* and Fig. 3, *c*. The plots of successive angle versus the previous one are given in Fig. 2, *d* and Fig. 3, *d*. Here, the line 3 shows the return function of the angles map derived in [15,17]:

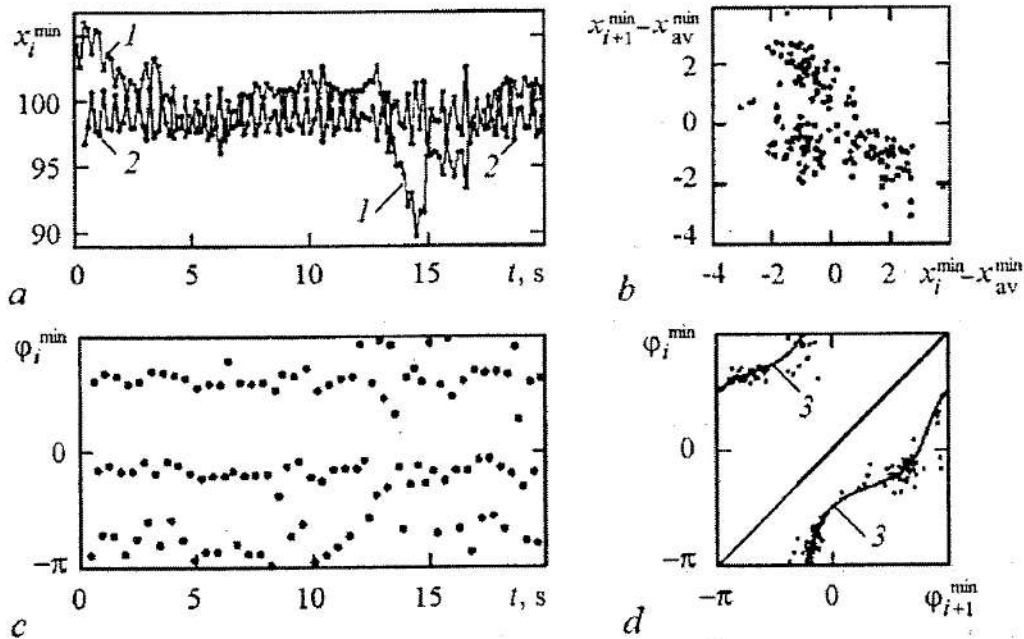


Fig. 2. Illustration of the first filtering technique: derivatives method. (a) Position of original minima x^{min}_i (curve 1) and filtered data with added average value (curve 2); (b) map of filtered x^{min}_i ; (c) angles of the map in (b) versus time; (d) map of angles. Curve 3 in (d) shows the return function of map (3) for $\xi=1/3$

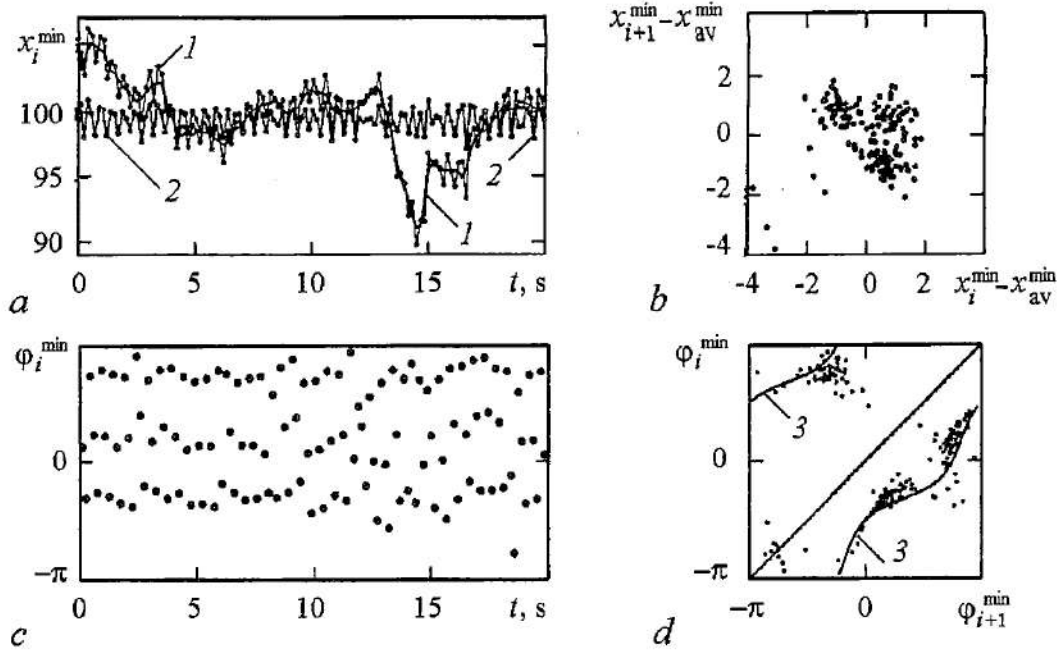


Fig. 3. Illustration of the second filtering technique: differences method. (a) Position of original minima x^{\min} (curve 1) and filtered data with added average value (curve 2); (b) map of filtered x^{\min} ; (c) angles of the map in (b) versus time; (d) map of angles. Curve 3 in (d) shows the return function of map (3) for $\xi=1/3$

$$\phi_i = \arctan(2\cos 2\pi\xi - \cot\phi_{i-1}), \quad (3)$$

for the rotation number $\xi=n:m=1:3$.

Step 5. Transforming angles ϕ_i into relative phase Ψ_i . This step is optional, but it can be used to ensure the rigour of the physical meaning of the obtained synchronization index. In [16] a relationship was established between angles ϕ_i of return times map or of the reconstructed Poincaré map, and the relative phase Ψ_i introduced in [13]:

$$\tan\phi_i = \cos(\Psi_i + 3\Theta/2) / \cos(\Psi_i + \Theta/2) = \cos\Theta - \tan(\Psi_i + \Theta/2)\sin\Theta, \quad \Theta = 2\pi\xi, \quad (4)$$

where ξ is rotation number. Note, that Eq. (4) is valid only if the coupling between the processes under study can be treated as vanishingly small. Knowledge of ϕ_i allows one to use Eq. (4) to extract relative phase Ψ_i , provided that the rotation number ξ , equal to $n:m$ in the case of synchronization, is known. Thus, one should find the suspected order of synchronization $n:m$. This can be done e.g. by computing the Fourier spectrum for the given sample of data and locating the highest peaks, namely, presumed to be those derived from heart rate and respiration, as in Fig. 1, c. The closest rational approximation to the ratio $f_{\text{resp}}/f_{\text{AHR}}$ can provide one with a guess at the suspected synchronization order $n:m$. Note that Eq. (4) cannot be used for $\xi=1:2$ because the latter produces a singularity. Fig. 4, a shows the angles ϕ_i that are transformed into the relative phase Ψ_i , which is shown in Fig. 4, b, with $\xi=1:3$.

Step 6. Unwrapping the relative phase or angles to obtain $n:m$ phase difference. The angles ϕ_i , or relative phase Ψ_i , fall by construction in the range $[-\pi; \pi]$. We need to unwrap these variables into the natural interval $]-\infty; \infty[$ in order to obtain the conventional phase difference at the time moment t_i to which the original discrete variable like x^{\min} is attributed. The proposed algorithm is as follows. We introduce an integer k , starting with $k=0$, that increases (decreases) by 1 with each phase jump in negative (positive) direction. To detect a phase jump, we consider two consecutive values, say Ψ_{i-1} and Ψ_i , and at each step i estimate the difference between them. If the absolute value of this difference is larger than $\pi/2$, this counts as a phase jump and the value of k is adjusted

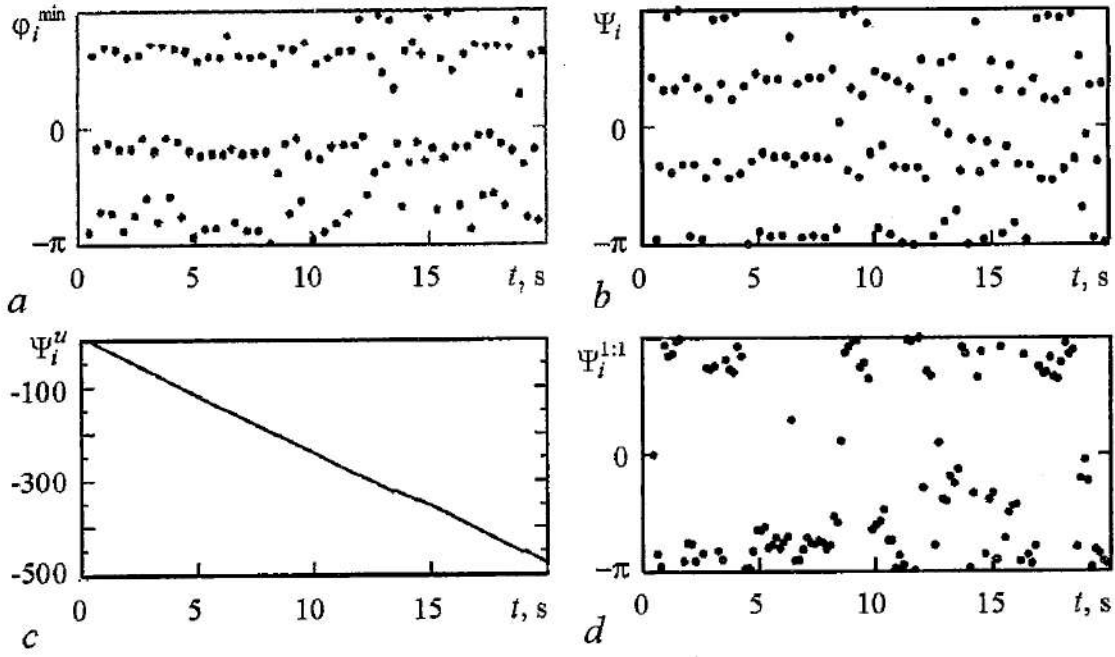


Fig. 4. Illustration of how the angles φ_i are transformed into the form suitable for computation of synchronization index. (a) angles φ_i of map of x^{\min} filtered by derivatives (the same as Fig. 2, c); (b) relative phase Ψ_i reconstructed from angles by means of Eq. (4); (c) unwrapped relative phase Ψ_i^u ; (d) phase difference $\Psi_i^{1:1}$ wrapped into $[-\pi; \pi]$

accordingly. The unwrapped variable is set to be $\Psi_i^u = \Psi_i + 2\pi k$. In Fig. 4, c the 1:3 phase difference is shown that was obtained from relative phase in Fig. 4, b.

Step 7. Transforming the $n:m$ phase difference into a 1:1 phase difference by setting $\Psi_i^{1:1} = \Psi_i^u m - 2\pi i$.

Step 8. Wrapping of 1:1 phase difference into the interval $[-\pi; \pi]$ can easily be effected by repeatedly subtracting 2π from each value of $\Psi_i^{1:1}$, until the latter falls within the required interval. Fig. 4, d illustrates this final step of data transformation and shows the 1:1 phase difference wrapped into the interval $[-\pi; \pi]$.

Step 9. Computation of synchronization index by application of the algorithm introduced in [18] to the value of $\Psi_i^{1:1}$. We introduce a temporal window of length L and move it along the data in steps of a chosen size. Inside the window, for its starting point number i , the value of ρ is estimated as:

$$\rho_c = 1/L \sum_{j=1}^L \cos \Psi_{i+j-1}^{1:1} \quad (5)$$

$$\rho_s = 1/L \sum_{j=1}^L \sin \Psi_{i+j-1}^{1:1}, \quad \rho = (\rho_c^2 + \rho_s^2)^{1/2},$$

ρ being the index of synchronization sought. It is obvious that ρ can vary between 0 and 1, the former meaning absence of synchronization, the latter perfect synchronization, and values in between implying various intermediate degrees of synchronization. For the noisy processes that we deal with in real life ρ can never reach 1.

Note, that **steps 5-7** require a reliable estimate of the synchronization order $n:m$. One usually wants to make computations automatically, but a proper guess of $n:m$ often requires some manual selection of spectral peaks (although this could also be rendered automatic in principle). To simplify the situation, we form a set of most frequently encountered synchronization orders with reasonably small numerators and denominators, and repeat **steps 5-7** for all of them. We thus obtain a synchronization index for each synchronization order from each data set.

4. Synchronization indices for rat data

A set of the following rotation numbers was tried for each blood pressure signal:

$$\xi_j: 1:2, 1:3, 1:4, 1:5, 1:6, 2:5. \quad (6)$$

The above numbers are rational approximations of the most frequent ratios of respiration frequency f_{resp} to average heart rate f_{AHR} estimated from Fourier spectra of the blood pressure signal. A temporal window of length $L=500$ was selected by trial and error. It is small enough to reflect a ρ close to instantaneous one, and large enough to provide good averaging for ρ . ρ_j was estimated within one window for all ξ_j indicated in Eq. (6), and the largest ρ^{max} was selected.

In Figs 5-8 the horizontal axis is equivalent time. The data for each stage of the experiment (I), (II), (III) and (IV) are placed sequentially. For additional clarity, the different stages are separated by vertical dashed lines. Note, that the time is in fact not continuous here, since there could be substantial time gap between stages (I) and (II), (II) and (III). The letters «f» and «m» to the right of the plots denote female or male rats respectively, and the numbers label different animals.

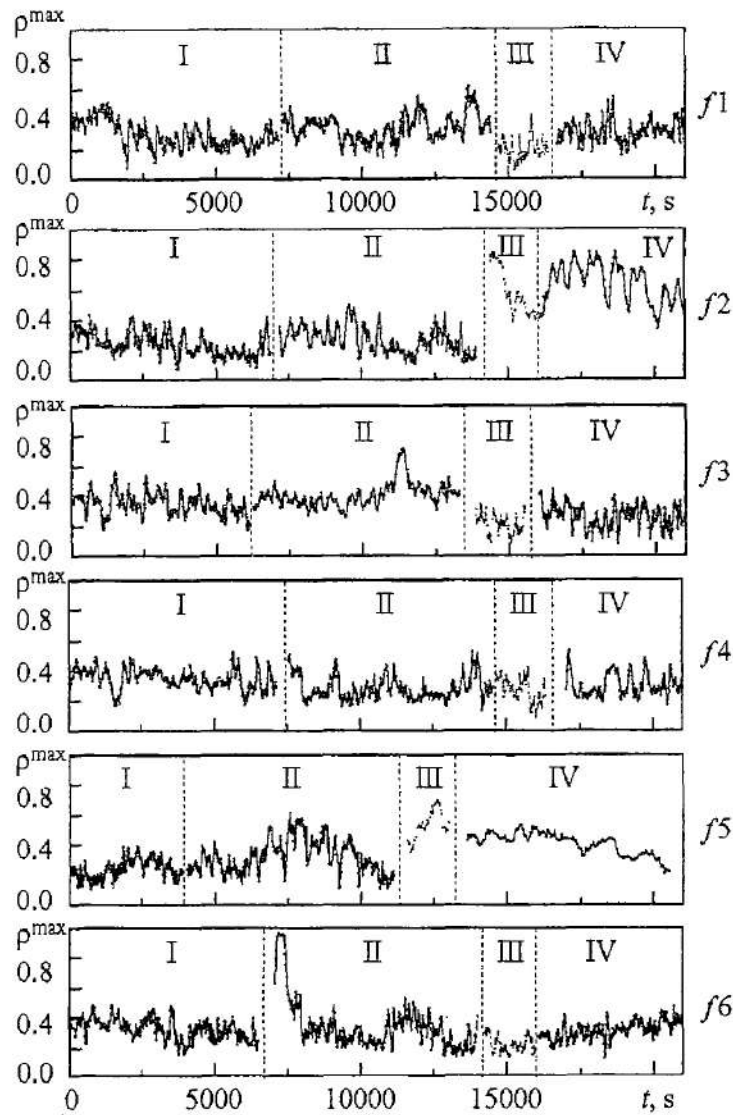


Fig. 5. Largest synchronization index versus time for female rats. Details in text

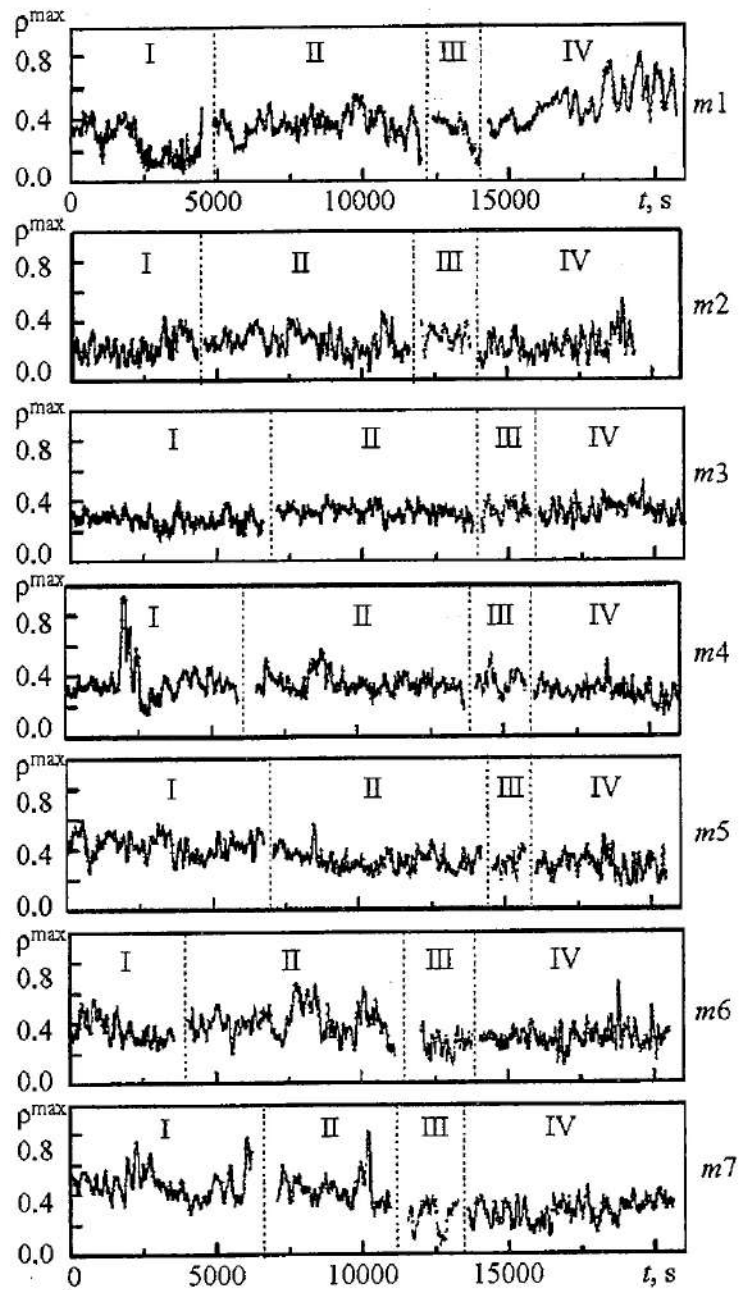


Fig. 6. Largest synchronization index versus time for male rats. Details in text

In Figs 5 and 6 the largest synchronization indices ρ^{\max} are shown for each rat dataset. In Figs 7 and 8 the rotation numbers corresponding to the ρ^{\max} are given. One can see that the synchronization index is generally small, indicating a low degree of synchronism between heart rate and respiration in rats. An interesting observation is that in conscious freely-moving rats 1:2 synchronization is quite often encountered in the states considered, contrary to observations made on humans, for which such a regime is very unnatural. Namely, at stage (I) order 1:2 prevailed in 5 of 7 male rats, and in 3 of 6 female rats.

In 7 of the 13 animals (4 female and 3 male), development of stress-induced myocardium alterations was accompanied by a decrease in synchronization index. Propranolol administered after stress restored the synchronization index to basal values in female rats, but not in the males.

It should be noted that although in most rats stress-induced alterations in the

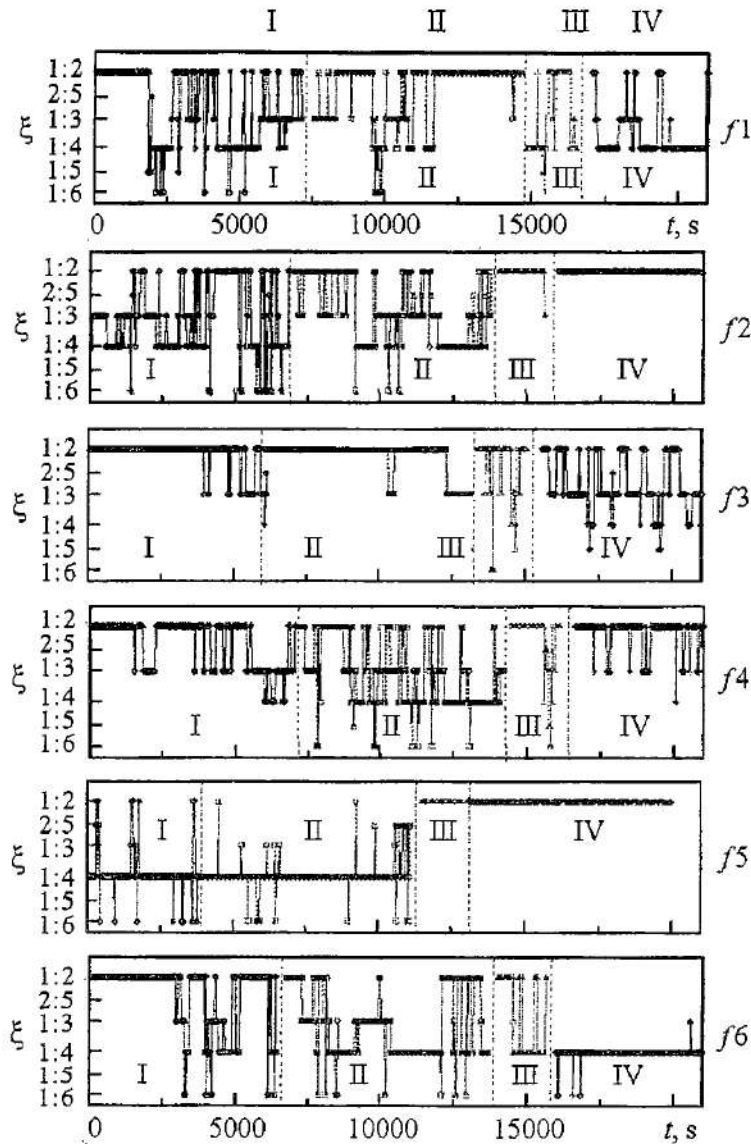


Fig. 7. Rotation number for largest synchronization index versus time for female rats. Vertical axis is in logarithmic scale. Details in text

myocardium were reversible, there were three animals in which stress induced irreversible injuries resulting in a near-death state: those marked «f2», «f5» and «m1». In these animals stress caused the synchronization order to be 1:2 most of the time; injection of propranolol that was intended to cure them in a certain sense, did not change it. In contrast, for female rats the synchronization index was markedly increased.

5. Conclusions

A method for detecting phase synchronization from one-dimensional data was applied to the blood pressure signals of conscious freely-moving rats in different states. It allowed us to detect the presence or absence of synchronization between the cardiac and respiratory processes. The method was further developed in order to automatically estimate the synchronization index from the experimental data.

13 animals of both genders were studied, in each of four different states, in order to reveal how the order and strength of cardiorespiratory synchronization are dependant on the state of cardiovascular system. There were two steady states: «healthy» and

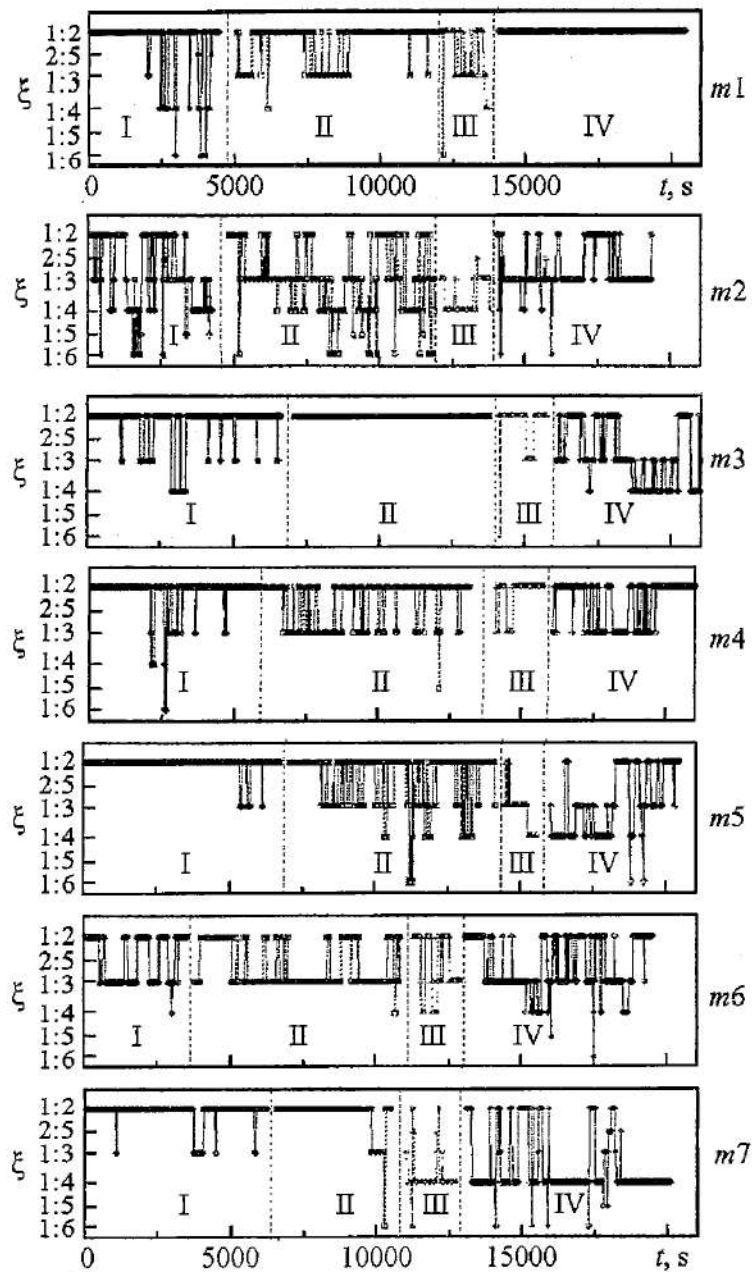


Fig. 8. Rotation number for largest synchronization index versus time for male rats. Vertical axis is in logarithmic scale. Details in text

«unhealthy», and two long slow transient processes induced by injection of a beta-blocker into a rat in each of these basic states. It was found out that, in common with humans, cardiorespiratory synchronization in rats is generally not very strong. However, the typical synchronization orders seem to be higher than in humans. In particular, 1:2 synchronization - which is untypical in healthy humans at rest - was often encountered in conscious rats at all stages including rest. It seems that no unique response to stress and/or drugs could be revealed in rats in terms either of the order $n:m$, or of the index ρ of cardiorespiratory synchronization. Rather, each animal responded individually to external influence.

The work was supported by the Engineering and Physical Sciences Research Council (UK), the Leverhulme Trust (UK), the CRDF (REC-006), and INTAS.

References

1. *Gang H., Ditzinger T., Ning C.N. and Haken H.* Stochastic resonance without external periodic force // *Phys. Rev. Lett.* 1993. Vol. 71. Pp. 807-810.
2. *Fujisaka H., Yamada Y.* Stability theory of synchronized motion in coupled-oscillator systems // *Progr. Theor. Phys.* 1983. Vol. 69. P. 32.
3. *Rosenblum M.G., Pikovsky A.S., and Kurths J.* From phase to lag synchronization in coupled chaotic oscillators // *Phys. Rev. Lett.* 1997. Vol. 78. P. 4193.
4. *Rulkov N.F., Sushchik M., Tsimring L.S., and Abarbanel H.D.I.* Generalized synchronization of chaos in directionally coupled chaotic systems // *Phys. Rev. E.* 1995. Vol. 51. P. 980.
5. *Anishchenko V.S., Vadivasova T.E., Postnov D.E., Safonova M.A.* Forced and mutual synchronization of chaos // *Radiotehn. Elektron (Moscow)*. 1991. Vol. 36. P. 338; *Int. J. of Bifurcation and Chaos Appl. Sci. Eng.* 1992. Vol. 2. P. 633.
6. *Rosenblum M., Pikovsky A., Kurths J.* Phase synchronization of chaotic oscillators // *Phys. Rev. Lett.* 1996. Vol. 76. P. 1804.
7. *Stratonovich R.L.* Topics in the theory of random noise. Gordon & Breach, 1963.
8. *Pikovsky A., Rosenblum M. and Kurths J.* Synchronization. A Universal Concept in Nonlinear Science. Cambridge University press, 2001.
9. *Schäfer C., Rosenblum M.G., Kurths J., Abel H.H.* Heartbeat synchronized with ventilation // *Nature*. 1998. Vol. 392. P. 239.
10. *Mrowka R., Patzak A., and Rosenblum M.G.* Quantitative analysis of cardiorespiratory synchronization in infants // *Int. J. of Bif. and Chaos*. 2000. Vol. 10 (11). P. 2479.
11. *Seidel H., Herzog H.* Bifurcations in a nonlinear model of the baroreceptor-cardiac reflex // *Physica D*. Vol. 115. P. 145.
12. *Stefanovska A., Haken H., McClintock P.V.E., Hožič M., Bajrović F., and Ribarić S.* Reversible transitions between synchronization states of the cardiorespiratory system // *Phys. Rev. Lett.* 2000. Vol. 85. P. 4831.
13. *Schäfer C., Rosenblum M.G., Abel H.-H., Kurths J.* Synchronization in the human cardiorespiratory system // *Phys. Rev. E.* 1999. Vol. 60 (1). Pp. 857-870.
14. *Rzeczinski S., Janson N.B., Balanov A.G., McClintock P.V.E.* Regions of cardiorespiratory synchronization in humans under paced respiration // *Phys. Rev. E.* 2002. Vol. 66. 051909.
15. *Janson N.B., Balanov A.G., Anishchenko V.S., and McClintock P.V.E.* Phase synchronization between several interacting processes from univariate data // *Phys. Rev. Lett.* 2001. Vol. 86. P. 1749.
16. *Janson N.B., Balanov A.G., Anishchenko V.S., and McClintock P.V.E.* Phase relationships between two or more interacting processes from one-dimensional time series. I. Basic theory // *Phys. Rev. E.* 2002. Vol. 65. 036211.
17. *Janson N.B., Balanov A.G., Anishchenko V.S., and McClintock P.V.E.* Phase relationships between two or more interacting processes from one-dimensional time series. II. Application to heart-rate-variability data // *Phys. Rev. E.* 2002. Vol. 65. 036212.
18. *Tass P., Rosenblum M.G., Weule J., Kurths J., Pikovsky A.S., Volkmann J., Schnitzler A., and Freund H.-J.* Detection of n:m phase locking from noisy data: application to magnetoencephalography // *Phys. Rev. Lett.* 1998. Vol. 81. P. 3291.
19. *Janson N.B., Balanov A.G., Anishchenko V.S., and McClintock P.V.E.* Modelling the dynamics of angles of human R-R intervals // *Physiol. Meas.* 2001. Vol. 22. P. 565.

*Department of Physics, Lancaster
University, Lancaster, UK
Department of Biology, Saratov State
University, Saratov, Russia*

Received 01.08.03

ИНДЕКСЫ КАРДИОРЕСПИРАТОРНОЙ СИНХРОНИЗАЦИИ ИЗ ДАННЫХ ДАВЛЕНИЯ КРОВИ КРЫС

*Н.Б. Янсон, Н.Б. Игошева, А.Г. Баланов, О.В. Глушкова-Семьякина,
Т.Г. Анищенко, P.V.E. McClintock*

Недавно разработанный метод определения фазовой синхронизации между несколькими колебательными процессами по одномерным сигналам был усовершенствован с целью позволить оценить индексы синхронизации. Он был применен к сигналам давления крови свободно двигающихся крыс. Каждая крыса исследовалась на четырех этапах: 1) здоровая; 2) здоровая, но с введенными бета-блокаторами; 3) с повреждениями миокарда, индуцированными стрессом; 4) с индуцированными стрессом повреждениями и введенными бета-блокаторами. Показано, что кардиореспираторная синхронизация играет важную роль на каждом из этих этапов.



Natalia Janson in 1993 graduated from Saratov State University and started her postgraduate course under the supervision of Prof. Vadim S. Anishchenko. In 1997 she became a candidate in physical and mathematical sciences. In 1997-2000 she worked as a Professor Assistant at the Radiophysics and Nonlinear Dynamics Chair., and in 2000-2003 as a Research Associate in Lancaster University (UK). At the moment she is a lecturer in applied mathematics in Loughborough University (UK). Her scientific interests are theory of oscillations, time series analysis, and application of nonlinear dynamics in biology and medicine. In this area she has more than 40 scientific publications.

E-mail: n.janson@lancaster.ac.uk



Natalia Borisovna Igosheva has finished Saratov State University (1990), Subdivision of Biology, Department of human and animals physiology, Candidate of Biological Sciences on the basis of thesis «Sex differences in stress-reactivity and stress resistance in rats» (1997). Her principle research interests - gender and individual differences in cardiovascular and neuroendocrine effects of stress: implications for stress-related disorders, applications of methods derived from nonlinear dynamics to analysis of cardiovascular effects of stress. She has 43 articles and thesis published in Russian and International journals and books. She attended 11 International and Russian conferences. She participates in 5 International and Russian scientific projects during last 5 years.

E-mail: igosheva@chaos.ssu.runnet.ru



Alexander Balanov: graduated from Saratov State University in 1995; since 1995 until 2000 he worked there as an engineer in the Laboratory of Nonlinear Dynamics; in 2000 he got his degree of candidate in physical and mathematical sciences from Saratov State University; since 2000 he is a Research Associate in the Department of Physics in Lancaster University (UK). The area of his scientific interests is nonlinear dynamics and its applications in biology and engineering. He is an author of about 40 scientific publications.

E-mail: a.balanov@lancaster.ac.uk



Oksana Valerievna Glushkovskaya-Semyachkina has finished Saratov State University in 1999 year with first-class diploma. In 2002 she has received a Candidate degree of the biological sciences. She works as assistant of professor at the Subdivision of biology, Department of human and animals physiology. She has 47 science works. She was awarded by 20 International and Russian Grants. She has participated in 6 International and 5 Russian conferences. Her principle research interests - the investigation of the mechanisms of sex particularities in cardiovascular adaptation to stress using physiological and nonlinear dynamics methods.

E-mail: glushkovskya@mail.ru



Tatjana Grigorievna Anishchenko has finished the Subdivision of Biology, Saratov State University (1964), Doctor of Sciences, on the basis of the thesis «Gender aspects of stress and adaptation problem» (1993), Professor of Biology, the Head of human and animals physiology chair, Saratov State University. Her list of publications includes 135 articles and thesis. She works in the field of research of mechanisms underlying gender differences in cardiovascular stress-resistance and of application of nonlinear dynamics methods in biology and medicine.

E-mail: oksana@chaos.ssu.runnet.ru



Izv. VUZ «AND», vol.11, № 3, 2003

SYNCHRONIZATION PHENOMENA IN MULTIMODE DYNAMICS OF COUPLED NEPHRONS

O.V. Sosnovtseva, A.N. Pavlov, E. Mosekilde, N.-H. Holstein-Rathlou

The individual functional unit of the kidney (the nephron) displays oscillations in its regulation of the incoming blood flow at two different time scales: fast oscillations associated with a myogenic dynamics of the afferent arteriole, and slower oscillations arising from a delay in the tubuloglomerular feedback. The paper investigates the intra- and inter-nephron interactions of these two modes. Besides full synchronization, both wavelet analyses of experimental data and numerical simulations of a detailed physiological model reveal the occurrence of a partial entrainment in which neighboring nephrons attain a state of synchronization with respect to their slow dynamics, but the fast dynamics remain desynchronized.

Introduction

The concept of homeostasis [1], i.e. the ability of the body to maintain a nearly constant internal milieu despite changes in the external conditions, plays an essential role in the description of physiological control systems. It is sometimes assumed that homeostasis implies that the physiological variables are kept near a stable steady state by means of effective feedback regulation. While this may be the case in certain situations, biological systems in general should be considered as open dissipative systems that are maintained under far-from-equilibrium conditions [2]. Regular and irregular oscillations associated with various forms of instability are common features of behavior that can be observed during normal functioning or arise in connection with particular states of disease [3].

The kidneys play an important role in regulating the blood pressure and maintaining a proper environment for the cells of the body. It is well-established that renal autoregulation is mediated by at least two mechanisms, the tubuloglomerular feedback (TGF) and the myogenic response of the afferent arteriole [4]. The TGF mechanism produces a negative feedback control that regulates the nephronal blood flow and, hence, the single-nephron glomerular filtration rate and the tubular flow rate in dependence of the NaCl concentration of the fluid that leaves the nephron. Experiments by Leyssac and Holstein-Rathlou [5,6] have demonstrated that this feedback regulation can become unstable and generate self-sustained oscillations in the proximal intratubular pressure with a typical period of 30-40 s. With different amplitudes and phases the same oscillations are manifest in the distal intratubular pressure and in the chloride concentration near the terminal part of the loop of Henle [7]. While for normal rats the

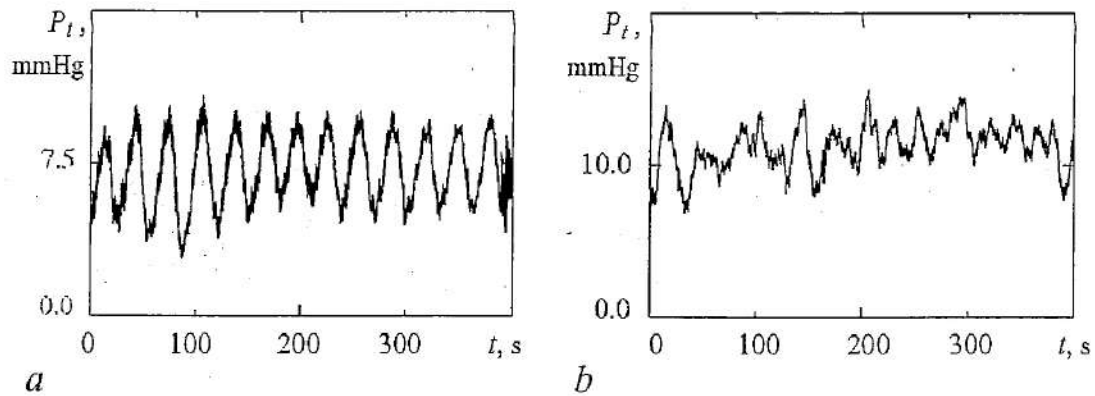


Fig. 1. Regular tubular pressure oscillations from a normotensive rat (*a*) and irregular pressure variations from a spontaneously hypertensive rat (*b*)

oscillations have the appearance of a limit cycle with a sharply peaked power spectrum (Fig. 1, *a*), highly irregular oscillations are observed for spontaneously hypertensive rats (Fig. 1, *b*) [5].

The myogenic mechanism represents the intrinsic response of the smooth muscle cells in the the vascular wall to changes in the TGF-signal as well as to other stimuli. This mechanism operates at 0.1-0.2 Hz. An increase of the transmural pressure elicits a contraction of the vascular smooth muscle causing a vasoconstriction and an increase in the resistance of the afferent arteriole. Since both mechanisms act on the afferent arteriole to control its hemodynamic resistance, the activation of one of the mechanisms modifies the response of the other [4].

Different forms of entrainment between the tubular pressure variations in adjacent nephrons were described in a couple of recent publications [8,9]. Observation of both in-phase and anti-phase synchronization was reported for the regular pressure oscillations in normal rats while spontaneously hypertensive rats revealed signs of chaotic phase synchronization.

Entrainment phenomena are of considerable interest from a physiological point of view. It is known, for instance, that epileptic seizures are related with the synchronization of larger groups of cells in the brain [10]. In their normal physiological states, waves of cytoplasmic calcium are known to propagate across cell assemblies such as, for instance, smooth muscle cells and β -cells. For the kidney, the aggregate response of the ensemble of nephrons is expected to depend on their state of synchronization. While entrainment of single-mode deterministic or stochastic oscillations is well understood, the dynamics of systems with several oscillatory modes is less studied. Living systems often exhibit oscillations with different time scales. The thalamocortical relay neurons, for instance, can generate either spindle or delta oscillations [11]. It was recently found [12] that the electroreceptors in paddlefish can be biperiodic. In the present paper we describe the individual nephron as a two-mode oscillator demonstrating relatively fast oscillations associated with the myogenic regulation of the arteriolar diameter and slower oscillations related with the delay in the tubuloglomerular feedback. We study numerically as well as experimentally the entrainment between these time scales both within the individual nephron and between neighboring nephrons. We apply the wavelet-based techniques to describe features of entrainment in nonstationary dynamics of coupled nephrons.

1. Nephron autoregulation

1.1. Mathematical model. Over the years significant efforts have been made to develop mathematical models that can account for the observed regular and irregular pressure variations and describe the physiological processes that occur along the tubular

system [13,14]. A particular aspect of this research has been to show that the transition from regular oscillations to irregular variations in the tubular pressure can be explained in terms of parameter changes within the framework of well-established physiological mechanisms. A review of the work may be found in the recent contribution by Andersen *et al.* [15]. Here, a model of nephron-nephron interaction was developed and it was shown that this model can produce a variety of different synchronization phenomena. Autoregulation of the pressures and flows in the individual nephron may be described by the following model [14]:

$$\begin{aligned}
 \dot{P}_t &= (1/C_{tub})\{F_f(P_t, r) - F_{reab} - (P_t - P_d)/R_H\}, \\
 \dot{r} &= v_r, \\
 \dot{v}_r &= (1/\omega)\{P_{av}(P_t, r) - P_{eq}(r, \Psi(X_3, \alpha), T) - \omega dv_r\}, \\
 \dot{X}_1 &= (P_t - P_d)/R_H - 3X_1/T, \\
 \dot{X}_2 &= (3/T)(X_1 - X_2), \\
 \dot{X}_3 &= (3/T)(X_2 - X_3).
 \end{aligned} \tag{1}$$

The first equation represents the pressure variations in the proximal tubule in terms of the in- and outgoing fluid flows. Here, F_f is the single-nephron glomerular filtration rate and C_{tub} is the elastic compliance of the tubule. The flow into the loop of Henle is determined by the difference $(P_t - P_d)$ between the proximal and the distal tubular pressures and by the flow resistance R_H . The reabsorption in the proximal tubule F_{reab} is assumed to be constant.

The following two equations describe the dynamics associated with the flow control in the afferent arteriole. Here, r represents the radius of the active part of the vessel and v_r is its rate of increase. d is a characteristic time constant describing the damping of the oscillations, ω is a measure of the mass relative to the elastic compliance of the arteriolar wall, and P_{av} denotes the average pressure in the active part of the arteriole. P_{eq} is the value of this pressure for which the arteriole is in equilibrium with its present radius and muscular activation Ψ . The expressions for F_f , P_{av} and P_{eq} involve a number of algebraic equations that must be solved along with the integration of Eq.(1).

The remaining equations in the single-nephron model describe the delay T in the TGF regulation. This delay arises both from the transit time through the loop of Henle and from the cascaded enzymatic processes between the macula densa cells and the smooth muscle cells that control the contractions of the afferent arteriole. The feedback delay, which typically assumes a value of 12-18 sec, will be considered a bifurcation parameter in our analysis. Another important parameter is the strength α of the feedback regulation. This parameter takes a value of about 12 for normotensive rats, increasing to about 18 for hypertensive rats [16]. For a more detailed explanation of the model and the parameters, see Ref. [15].

Considering the model equations (1) we can identify the two time scales in terms of (i) a low-frequency (TGF-mediated) oscillation with a period $T_h \approx 2.2T$ arising from the delay in the tubuloglomerular feedback, and (ii) somewhat faster oscillations with a period $T_v \approx T_h/5$ associated with the inherent myogenic adjustment.

To determine T_h and T_v in our numerical simulations we have used the mean return times of the trajectory to appropriately chosen Poincaré sections

$$T_v = \langle T_{ret} | \dot{v}_r = 0 \rangle, \quad T_h = \langle T_{ret} | \dot{X}_2 = 0 \rangle. \tag{2}$$

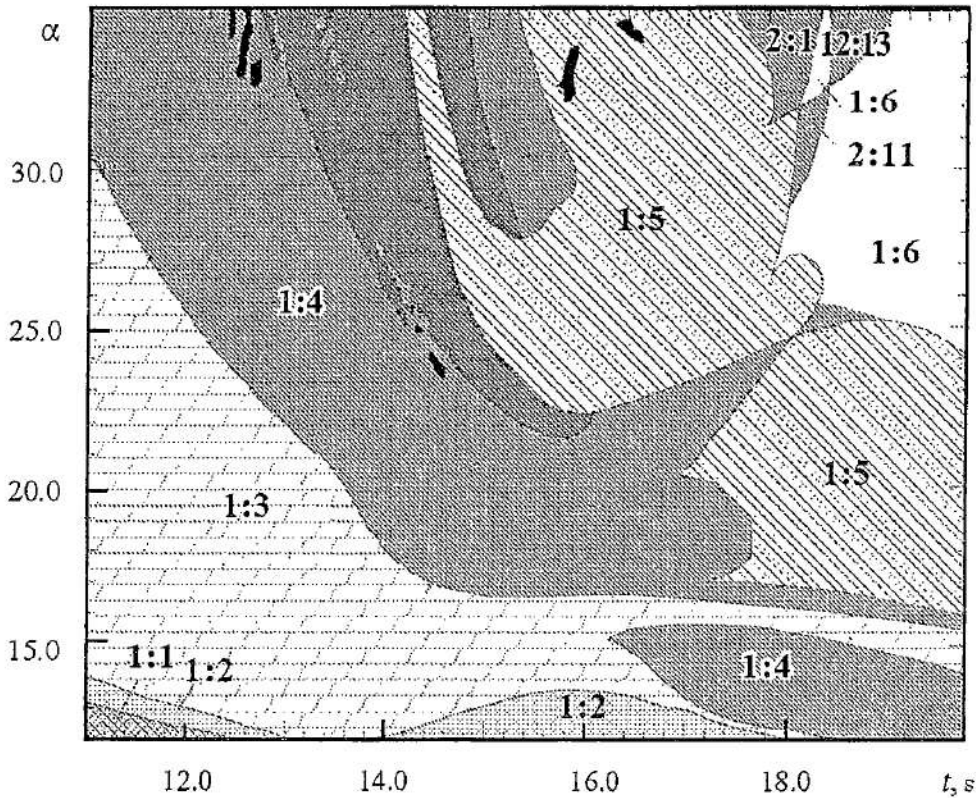


Fig. 2. Two-mode oscillatory behavior in the single nephron model. Black colored regions correspond to a chaotic solution

Here, $T_{rer} |_{\dot{v}_v=0}$ denotes the time between two subsequent crossings (from the same side) of the trajectory through the plane $\dot{v}_v=0$.

From these return times it is easy to calculate the intra-nephron rotation number (i.e., the rotation number associated with the two-mode behavior of the individual nephron)

$$r_{vh} = T_v / T_h. \quad (3)$$

With varying feedback delay T and varying slope α of the open loop feedback curve, Fig. 2 shows how the two oscillatory modes can adjust their dynamics and attain states with different rational relations ($n:m$) between the periods. The regions of high resonances (1:4, 1:5, and 1:6) are seen to exist in the physiologically interesting range of the delay time $T \in [12 \text{ sec}, 20 \text{ sec}]$. However, some of these regions are relatively small, and there are neighboring regions with 2:11, 2:13, and chaotic dynamics. While the transitions between the different locking regimes always involve bifurcations, bifurcations may also occur within the individual regime. A period-doubling transition, for instance, does not necessarily change r_{vh} , and the intra-nephron rotation number may remain constant through a complete period-doubling cascade and into the chaotic regime [9].

1.2. Experimental data analysis. Physiological signals are generated by complex, self-regulating systems and may be extremely inhomogeneous and nonstationary. Processing of data series of this type by means of conventional techniques such as correlation and/or Fourier analysis can lead to misinterpretations of the results. That is why special techniques based on wavelet analysis become of a high interest [17]. Wavelets provide us with the possibility of searching hidden periodicities in short, nonstationary data and follow the temporal evolution of different rhythmic components in the case of noisy multimode dynamics.

The wavelet transform of a signal $x(u)$ can be written as:

$$T_x(a,t) = a^{-1/2} \int_{-\infty}^{\infty} x(u) \psi^*((u-t)/a) du. \quad (4)$$

Here ψ is a «mother» function that in general can have an arbitrary shape provided it is soliton-like with zero average. $T_x(a,t)$ are the wavelet coefficients, a being a time scaling and t a time displacement parameter. To investigate the presence of various rhythmic components, the *Morlet* wavelet is particularly useful. The given function consists of two terms, however, in practice one of them is small enough and can be ignored. One typically uses the following simplified expression for the Morlet function:

$$\psi(\tau) = \pi^{-1/4} \exp(-j2\pi k_0 \tau) \exp[-\tau^2/2]. \quad (5)$$

This wavelet represents a harmonic oscillation with frequency $f=k_0/a$ and with an amplitude that is modified in time by Gaussian factor describing how the wave arises and decays. For the frequency range being of interest in the dynamics of nephrons we can take $k_0=1$ ¹. In such a case the frequency f is the simple inversion of time scale a , and the expression for the wavelet transform can be rewritten as follows:

$$T_x(f,t) = f^{1/2} \int_{-\infty}^{\infty} x(u) \psi^*(\tau) du, \quad \tau = f(u-t). \quad (6)$$

The wavelet transform $T_x(f,t)$ measures the spectral contribution near the frequency f at time t of the observed signal.

Some authors [18] prefer to consider other complex wavelet functions because of possible spurious effects (especially for time series with nonzero mean). To avoid such problems we have transformed all time series to zero mean value before applying the wavelet technique.

In addition to the wavelet transform coefficients $T_x(f,t)$ we can estimate the energy density $E_x(f,t)=|T_x(f,t)|^2$. As the result there is a surface in a 3-dimensional space $E_x(f,t)$. Sections of this surface at fixed time moments $t=t_0$ correspond to the local energy spectrum. To simplify the visualization of the two-dimensional spectrum $E_x(f,t)$ we can consider only the dynamics of the local maxima of $E_x(f,t_0)$, i.e., the peaks of the local spectra.

Fig. 3 shows the different components detected in the time series of Fig. 1. (Here, aiming to illustrate the complex nonstationary dynamics of real nephrons, we demonstrate all maxima of $E_x(f,t_0)$ independently of their magnitudes). Inspection of the figure reveals that the slow oscillations, whether they are periodic or chaotic, maintain a nearly constant

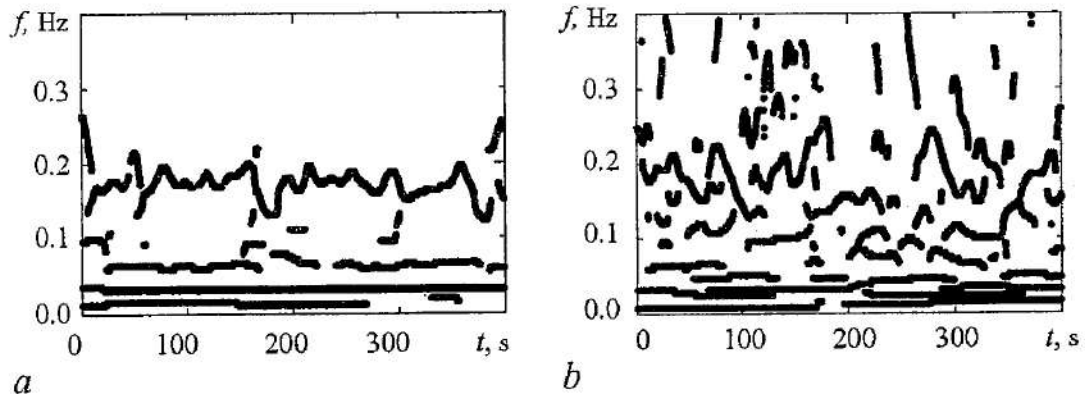


Fig. 3. Wavelet analysis of the two time-series presented in Fig.1

¹The value k_0 allows to search some compromise between localization of the wavelet function in both, time domain and frequency domain.

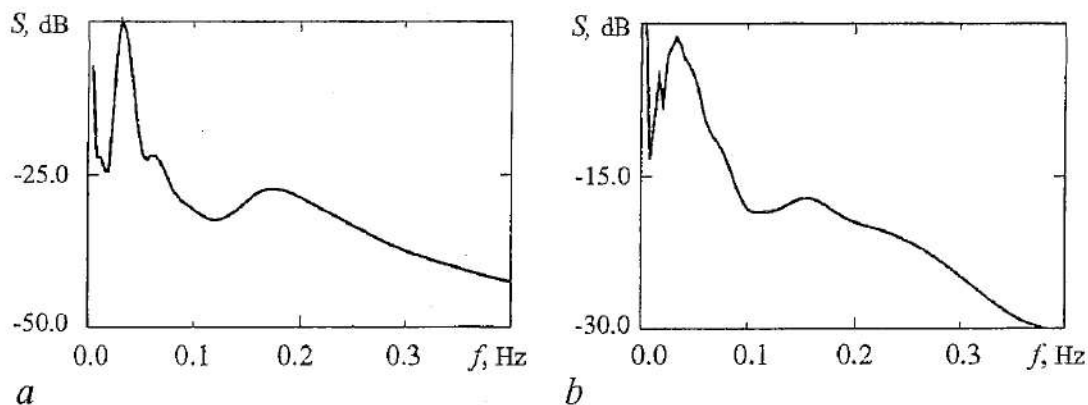


Fig. 4. Power spectrum obtained from the wavelet analysis for the two time-series presented in Fig.1. Two peaks, representing the fast myogenic oscillations and the slower tubuloglomerular oscillations, are well-distinguished

frequency through the observation time. The fast oscillations, on the other hand, fluctuate significantly, particularly for the hypertensive rat. This may be related to a complex modulation of the fast oscillations by the slow dynamics or to the influence of noise (since the fast oscillations are small in amplitude, they are more sensitive to fluctuations).

The presentation in Fig. 3 does not provide information about the dominant spectral components. This information can be obtained, for example, from a so-called *scalogram*, i.e., a time averaged power spectrum, being an analogue to the Fourier power spectrum. Such a scalogram is illustrated in Fig. 4 where a well-pronounced peak around 0.03 Hz, corresponding to the slow TGF-mediated mode, is distinguishable. The other peak at 0.15-0.2 Hz derives from the fast myogenic dynamics. It is interesting to note how clearly these oscillations can be detected from the tubular pressure variations. Since both the above frequency components are of physiological interest we extract them from the original wavelet transformation for further analysis of their coherence properties. Fig. 5 displays the relation between fast and slow oscillations in a single nephron. For the periodic oscillations observed for normotensive rats (Fig. 5, *a*), the fast and slow components adjust their periods in accordance to one another to maintain a 1:5 entrainment during the observation time. For the chaotic oscillations observed for hypertensive rats (Fig. 5, *b*), the ratio changes more randomly in time.

We conclude that besides being regular or chaotic, the self-sustained pressure variations in the individual nephron can be classified as being synchronous or asynchronous with respect to the ratio between the two time scales that characterize the fast (arteriolar) mode and the slow (TGF mediated) mode, respectively. As we shall see, this complexity in behavior may play an essential role in the synchronization between a pair of interacting nephrons.

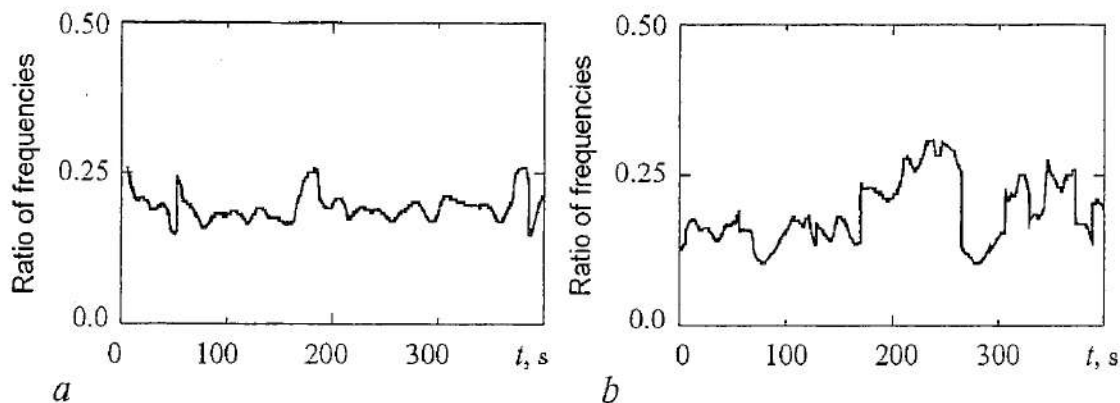


Fig. 5. Ratio of the internal time-scales for a normotensive rat (*a*) and for a hypertensive rat (*b*)

2. Entrainment of oscillatory modes for interacting nephrons

2.1. Simulation results. Neighboring nephrons can influence each other's blood supply either through vascularly propagated electrical (or electrochemical) signals or through a hemodynamic coupling arising via a direct redistribution of the blood flow between the coupled nephrons. While the hemodynamic coupling depends mainly on the flow resistances in the arteriolar network, the vascularly propagated coupling is associated with signal transmission between smooth muscle cells. The result is that only nephrons situated close to one another can interact via the vascularly propagated coupling. Nephrons situated farther apart but sharing a common piece of interlobular artery may interact via the hemodynamic coupling.

In the present work we shall focus our attention on the vascularly propagated coupling, assuming the hemodynamic coupling to be negligible. In the single-nephron model the equilibrium pressure in the afferent arteriole depends on the current radius r and on the activation level Ψ of the smooth muscles surrounding the arteriole and controlling its diameter. The muscular activation arises at the juxtaglomerular apparatus and travels upstream along the afferent arteriole in a damped fashion. When it reaches the branching point with the arteriole from the neighboring nephron, part of the signal may propagate down that arteriole and start to contribute to its TGF response. The coupling is considered nearly instantaneous since the time it takes for the vascular signal to reach the other nephron is very small relative to the period of the TGF-oscillations. It has been observed [19] that the signal decreases nearly exponentially as it propagates. Thus only a fraction, $\gamma = e^{-l/l_0} < 1$, of the original activation level reaches the vascular smooth muscles close to macula densa of the neighboring nephron. In the expression for the vascular coupling parameter γ , l is the propagation length of the coupling signal, and $l_0 \approx 500 \mu\text{m}$ is the characteristic length scale of the exponential decay. In the model, the vascularly propagated coupling is represented by adding a contribution of the activation level in one nephron to the activation level in the neighboring nephron:

$$\Psi_{1,2}^* = \Psi_{1,2} + \gamma \Psi_{2,1} \quad (7)$$

with γ being the coupling parameter and $\Psi_{1,2}$ the uncoupled activation levels of the two nephrons as determined by their respective Henle flows. In view of the characteristic propagation length for the signal and of measured distances between neighboring nephrons along the arteriolar network, a typical value of γ is considered to be 0.1-0.2 [19]. By virtue of the two-mode dynamics of the individual nephron, a number of new and interesting results appear.

The individual oscillatory system has two modes that can be locked with each other. However, an interaction between functional units can break their mutual adjustment. It is also plausible that a coupling can act in different manners on the fast and slow oscillations. For the interacting systems we introduce two rotation numbers as follows:

$$r_v = T_{v1}/T_{v2}, \quad r_h = T_{h1}/T_{h2}. \quad (8)$$

To provide more information, the variation of the phase difference is calculated separately for the slow h and for the fast v oscillations.

Let us consider the case of $\alpha=30.0$ corresponding to a weakly developed chaotic attractor in the individual nephron. The coupling strength γ and delay time T_2 in the second nephron are varied. Two different chaotic states can be recognized as asynchronous and synchronous (Fig. 6). For asynchronous behavior the rotation numbers r_h and r_v change continuously with T_2 while inside the synchronization region two cases can be distinguished. To the left, the rotation numbers r_h and r_v are both equal to unity

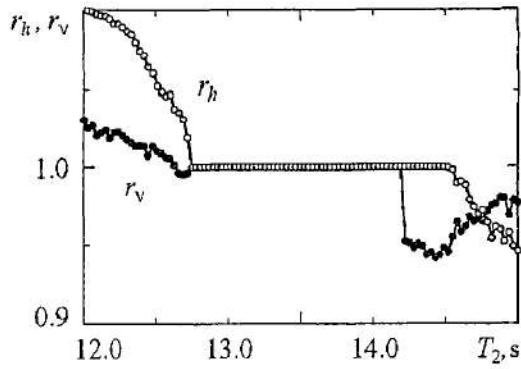


Fig. 6. Full and partial synchronization of fast and slow motions; $T_1=13.5$ sec, $\alpha=30.0$ and $\gamma=0.06$

since both slow and fast oscillations are synchronized. To the right ($T_2 > 14.2$ sec), while the slow h -mode of the chaotic oscillations remain locked, the fast v -mode drifts randomly. In this case the synchronization condition is fulfilled only for one of oscillatory modes.

2.2. Experimental results: frequency adjustments. Using anatomical criteria, neighboring nephrons having a high likelihood of deriving their afferent arterioles from the same interlobular artery were identified [19]. In these nephrons 29 out of 33 pairs (i.e., 80%) were found to have synchronized oscillations. In contrast, nephron pairs not fulfilling these criteria only showed synchronous oscillations in one case out of 23 investigated pairs (i.e., 4%). This observation shows that synchronized oscillations are preferentially found in nephrons originating from the same interlobular artery. Fig. 7 displays the tubular pressure variations in pairs of neighboring nephrons for a normotensive rat (a) and for hypertensive rats (b)-(d). The oscillations presented in (b), (c) and (d) are significantly more irregular than the oscillations displayed in (a). One can visually observe a certain degree of synchronization between the interacting nephrons. It is difficult, though, to separately estimate the degree of adjustment for the myogenic oscillations and for the TGF mediated oscillations without special tools.

To study interactive dynamics in coupled systems the newly developed wavelet

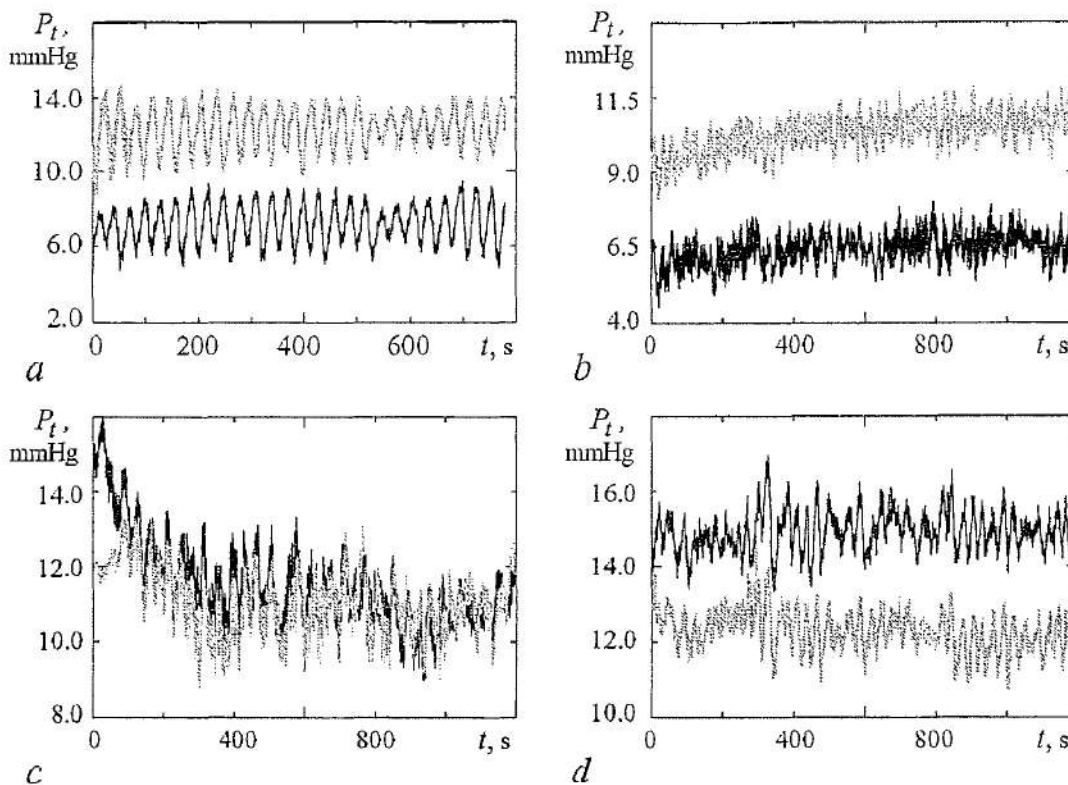


Fig. 7. Examples of the tubular pressure variation that one can observe in adjacent nephrons (a) for normotensive and (b)-(d) for hypertensive rats

based coherence measures can be successfully used [20]. In the present paper, we modify the approach proposed by Lachaux *et al.* [20] and introduce a coherence measure that is more appropriate for the purpose of our analysis. Fig. 8 shows two examples where the slow oscillations remain quite stationary while the frequencies of the fast oscillations vary significantly with time (they may be non-synchronous similar to Fig. 8, *a*, but they may be also synchronous for neighboring nephrons!- see Fig. 8, *b*). To analyze such situations we introduce a formalism where we can adjust the control frequency of the wavelet function rather than assuming some fixed value defined a priori [21]. This approach resembles to well-known sliding window analysis [22]. However, within the framework of the wavelet technique the window size is varied depending on the frequency: We need a small window to study high-frequency changes of the time series with good precision and a large window to study low-frequency spectral information. To examine entrainment phenomena between two rhythms in coupled biological oscillators (e.g., between the slow TGF-mediated motions or between the fast motions in neighboring nephrons) we have to follow the temporal evolution of rhythmic components (i.e., maxima of local spectra associated with these modes) and their coherence. Because such peaks (instantaneous frequencies of rhythmic components) may show large fluctuations relative to the mean value, we consider a coherence measure for two interacting modes that depends on both time and frequency.

Let $E_{xx}(f,t)$ and $E_{yy}(f,t)$ be the energy densities of signals $x(t)$ and $y(t)$. Let also in some range of frequencies Δ each of the processes $x(t)$ and $y(t)$ has a clearly expressed rhythm (e.g., range of slow or fast oscillations for the two nephrons). In this case synchronization means that the corresponding frequencies for $x(t)$ and $y(t)$ will be locked (coincide). Such a situation corresponds to the value $\Gamma_{\Delta}=1$ for the function:

$$\Gamma_{\Delta}^2(t) = \max_{f \in \Delta} [E_{xy}(f,t)]^2 / \{ \max_{f \in \Delta} [E_{xx}(f,t)] \cdot \max_{f \in \Delta} [E_{yy}(f,t)] \}. \quad (9)$$

Here, $E_{xy}(f,t)$ is the mutual energy density $E_{xy}(f,t) = |T_{xy}(f,t)T_{yx}^*(f,t)|$. $\Gamma_{\Delta}(t)$ is a function of time that allows us to follow the evolution of the interactive dynamics of the two processes in the chosen frequency range Δ . The more synchronous the rhythms of these processes are the closer $\Gamma_{\Delta}(t)$ will be to 1.

In general when two frequencies are coincide we can speak about the property of coherence. To prove the presence of synchronization the phenomenon of phase or frequency locking should be studied. The advantage of nonstationary dynamics consists in the following. Because the frequency associated to one rhythm changes in time, using wavelets we can clearly see whether the second frequency follow these changes or not. That is why we can speak about the synchronization phenomena besides the coherence properties.

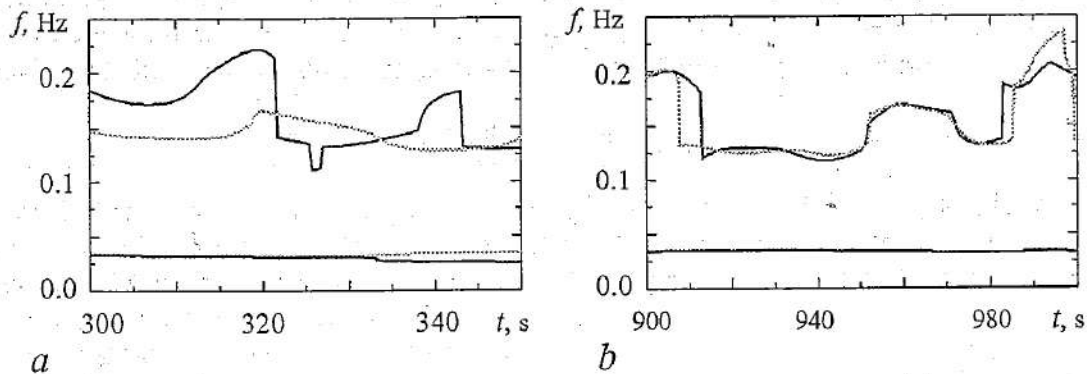


Fig. 8. Examples of nonstationary non-synchronous (*a*) and nonstationary synchronous (*b*) dynamics of the fast oscillatory modes. In both cases slow modes demonstrate stationary synchronous state

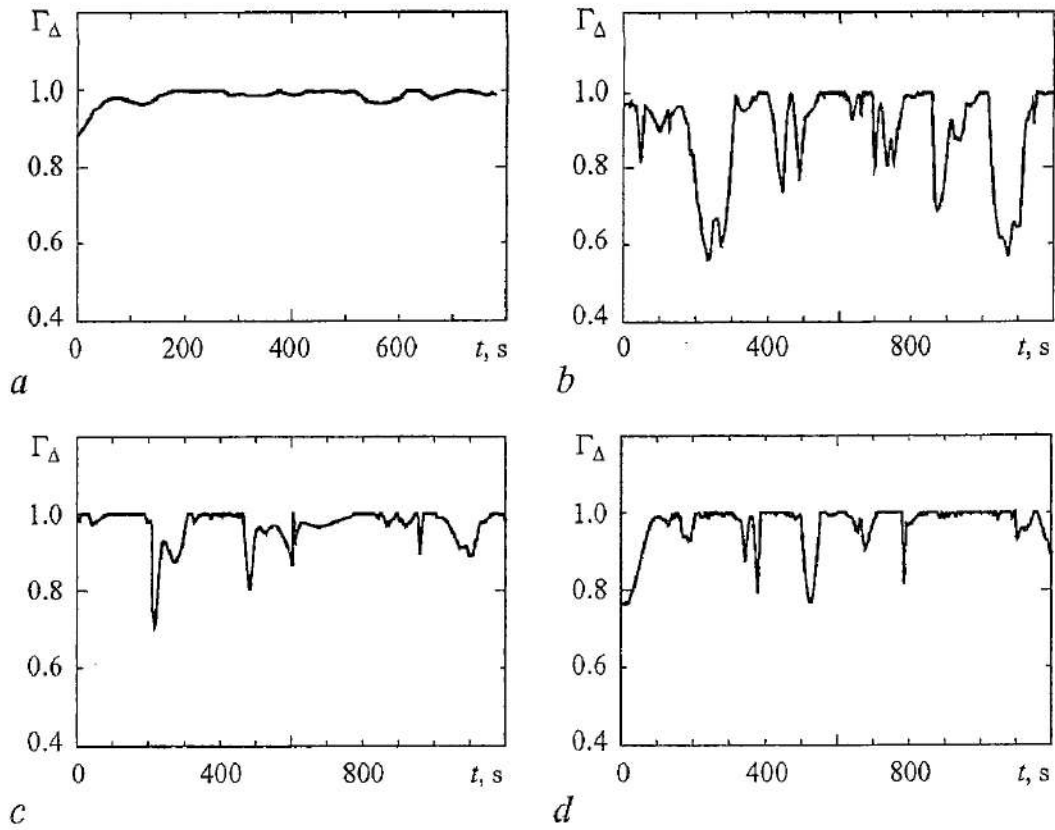


Fig. 9. Mutual wavelet analysis for the slow oscillations of the two time-series presented in Fig.7: (a) synchronous behavior, (b) nonsynchronous dynamics, (c) and (d) synchronous behavior but during limited time intervals

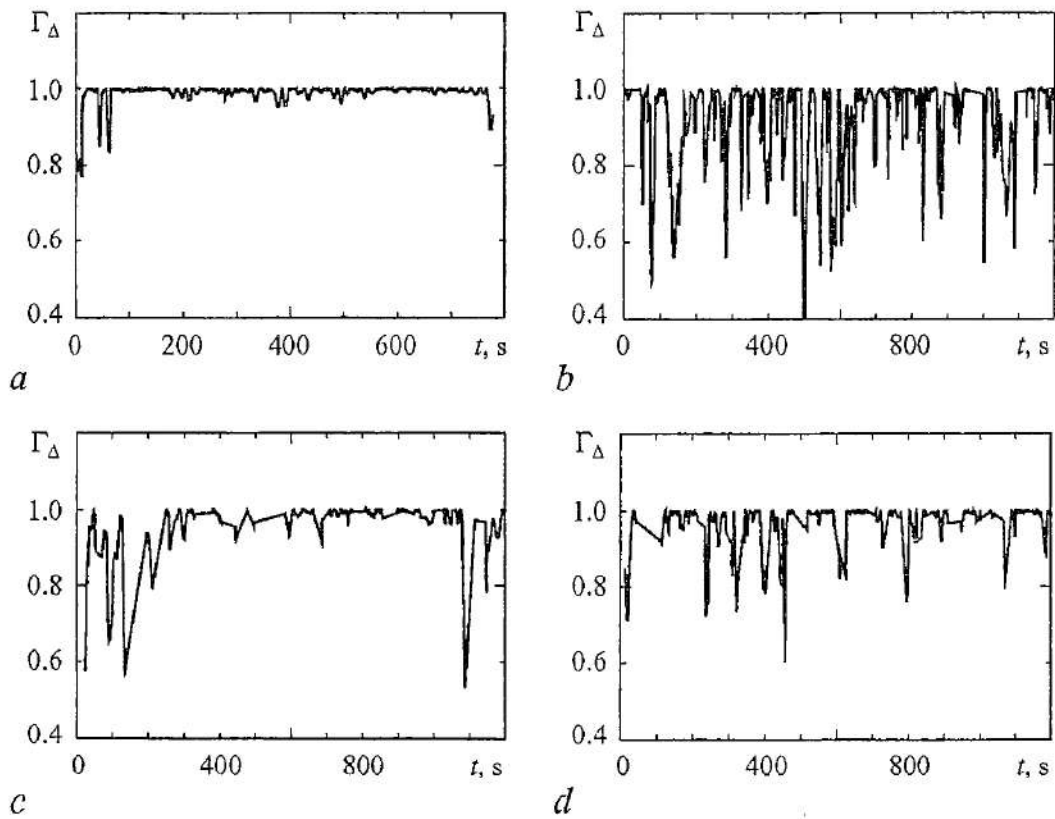


Fig. 10. Mutual wavelet analysis for the fast oscillations extracted from time-series presented in Fig. 7. (a) and (c) illustrate synchronous behavior, (b) and (d) nonsynchronous dynamics

Fig. 9 and 10 demonstrate different degrees of coherence for the considered modes. For periodic oscillations (Fig. 9, *a* and Fig. 10, *a*), both the slow and fast modes of the interacting nephrons are perfectly locked during the observation time. For a system with complex oscillations subjected to noise one can speak about a certain degree of synchronization if the periods of locking are large compared with the characteristic periods of oscillations [23]. Fully incoherent behavior with respect to both oscillatory modes can be observed in Fig. 9, *b* and Fig. 10, *b*. In many cases we can diagnose synchronization of the slow motions (Fig. 9, *c, d*) for relatively long time intervals where the frequencies remain almost equal. The fast motions, on the other hand, can demonstrate different coherence properties between nephrons. The oscillations can be locked during long periods of time together with the slow oscillations (Fig. 10, *c*). We define this type of synchronization as full synchronization since all time scales of the system are locked. Another case, illustrated in Fig. 9, *d* and Fig. 10, *d*, is when the fast oscillations are incoherent while the slow oscillations are synchronized during the considered time interval. We refer to this phenomenon as partial synchronization.

2.3. Experimental results: phase entrainments. As discussed above neighboring nephrons influence each other's blood supply either through electrical signals that activate the vascular smooth muscle cells or through a hemodynamic coupling. The two mechanisms depend very differently on the precise structure of the arteriolar network. Hence, variations of this structure may determine which of the mechanisms is the more important. This could be of considerable biological interest, because the effects produced by the two mechanisms tend to be shifted in phase, and their influence on the overall behavior of the nephron system may be very different.

In an earlier paper [8], we studied phase relations between two signals using a Hilbert transformation. This approach works perfectly as long as we are not interested in the separated dynamics of different rhythmic activities in the oscillatory process. In our case, the multimode process has one dominant rhythm while the other rhythm is small in amplitude. To account for this situation we introduce phases via wavelet-transform coefficients:

$$T_x(f,t) = |T_x(f,t)| \cdot \exp[i\varphi_x(f,t)], \quad (10)$$

where the phase function $\varphi_x(f,t)$ depends on the considered mode. As it was discussed in [18,20], we can calculate the wavelet coefficients for the chosen central frequency f_0 of the wavelet function. The corresponding phases $\varphi_x(f_0,t)$ are closely related to the phases introduced via Hilbert transform of the band-pass filtered signal [18]. An approach of band-pass filtration with the further definition of instantaneous phase was successfully used in [22]. The process of filtration can cause some technical problems in the case of nonstationary dynamics especially if two modes are close enough in the frequency domain. Such problems can be solved using sliding window analysis [22] or, alternatively, different aspects of multimode phase dynamics can be studied with wavelets.

In general, as a result of wavelet transform we obtain two-dimensional arrays of modulus $|T_x(f,t)|$ and phases $\varphi_x(f,t)$. The latter means that the notion of phase is defined for each frequency f at any fixed time moment t . When considering two processes $x(t)$ and $y(t)$ the wavelet transform allows us to calculate the phase differences $\varphi_x(f,t) - \varphi_y(f,t)$ and various synchronization factors [18]. In the case of clearly expressed rhythmic dynamics we don't need to know the complete two-dimensional phase spectrum $\varphi_x(f,t)$ because we are interesting only in phases related to the rhythmic contributions. In the case when instantaneous frequencies of modes demonstrate large fluctuations relative to the mean value (similar to Fig. 8), it seems to be useful adjust the central frequency of wavelet function according to these fluctuations. Hence, in this work we shall follow the

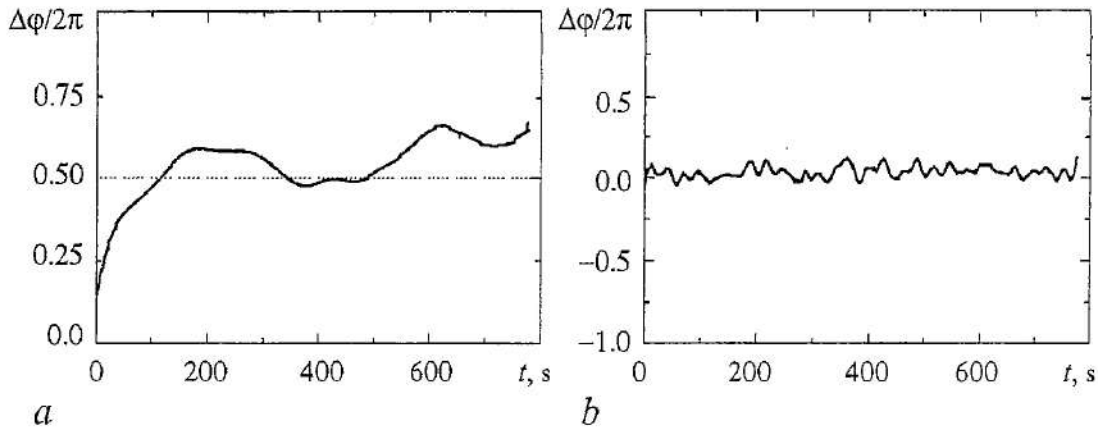


Fig. 11. Phase differences for the slow (*a*) and fast (*b*) oscillations of the coupled nephrons. The given results are obtained for the time series presented in Fig. 7, *a* (normotensive rat)

time evolution of each mode in the frequency domain and at fixed moments of time t_0 extract the phases related to the local peaks of the power spectrum $E_x(f, t_0)$ (or $|T_x(f, t_0)|$). For coupled nephrons this allows us to introduce phases for the slow and fast dynamics separately. To study synchronization phenomena in bivariate data it is possible to calculate the phase difference or the distribution of the cyclic relative phase [22].

Fig. 11 shows an example of the (normalized) phase difference for the regular pressure variations in a normotensive rat. One clearly observes in-phase ($\Delta\varphi=0$) synchronization for fast mode and anti-phase ($\Delta\varphi\approx\pi$) synchronization for slow oscillations in nephrons branching from different arterioles. Note, that fast oscillation in our analysis were always locked in phase, but there may be characteristic phase slips of $2\pi k$ because of the noisy conditions under which the nephrons operate. The case of anti-phase synchronization for slow mode occurred rather seldom. More typical situation was when both the slow and fast oscillations were synchronized in-phase. (This situation takes place for nephrons branching from the same arteriole.)

Let us consider now how our phase approach is applied to chaotic dynamics as one typically observes for hypertensive rats. Fig. 12 illustrates examples of phase dynamics for time series presented in Fig. 7, *b, c*. The phase differences indicate synchronous dynamics in Fig. 12, *a* and nonsynchronous in Fig. 12, *b*. The results for phase entrainment correspond to the results for frequency adjustments. In the case of synchronization for hypertensive rats we observed for all experimental data the in-phase regime ($\Delta\varphi=0$).

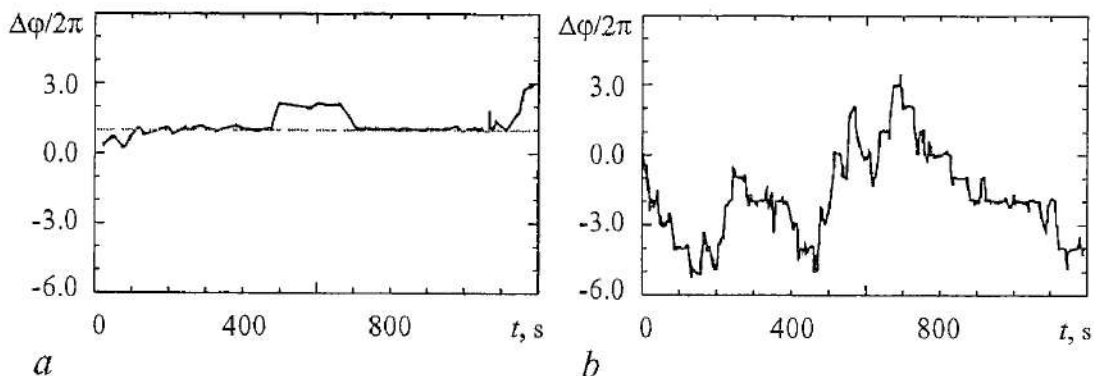


Fig. 12. Phase differences for the fast synchronous (*a*) and for the fast non-synchronous dynamics (*b*). The given examples are obtained for the time series of hypertensive rats shown in Fig. 7, *c* and *b*, respectively

Conclusions

Based on the analysis of experimental results we showed that the vascular dynamics and the tubuloglomerular feedback mechanism are responsible for two time scales associated with a fast and a slow oscillatory mode in the individual nephron. Both for periodic oscillations observed in normotensive rats and for the chaotic oscillations in hypertensive rats the two modes exhibit resonant behavior as well as nonsynchronous dynamics.

To investigate different types of internephron mode entrainment we developed an approach based on a mutual wavelet transformation that allows us to easily analyze frequency and phase adjustments between different time scales from nonstationary data. We observed simultaneous (full) locking for the slow and fast oscillations both for normotensive and for hypertensive rats. We also identified a state of partial synchronization where the slow oscillations are synchronized while the fast motion demonstrates noncoherent behavior. Such a situation is typical for hypertensive rats.

Numerical simulations for coupled nephron models demonstrate similar behavior. With varying time delay in the tubuloglomerular feedback and varying strength of the vascular coupling the experimentally observed forms of synchronous behavior were recovered.

The research described in this publication was made possible in part by Award N. SR-006-X1 of the U.S. Civilian Research & Development Foundation for the Independent States of the Former Soviet Union (CRDF). A.P. acknowledges support from RF Minobr and CRDF (grant Y1-P-06-06). This work was also partly supported by INTAS grant (01-2061) and RFBR (01-02-16709).

References

1. Cannon W.B. Organization for physiological homeostasis // *Physiol. Rev.* 1929. Vol. 9. P. 399.
2. Nicolis C. and Prigogine I. *Self-Organization in Nonequilibrium Systems.* Wiley, New York, 1977.
3. Glass L. and Mackey M.C. *From Clocks to Chaos: The Rhythms of Life.* Princeton University Press, Princeton, 1988.
4. Holstein-Rathlou N.-H., Wagner A.W. and Marsh D.J. Tubuloglomerular feedback dynamics and renal blood flow autoregulation in rats // *Am. J. Physiol.* 1991. Vol. 260. P. F53; Chou K.H., Yu-Ming Chen, Mardarelis V.Z., Marsh D.J. and Holstein-Rathlou N.-H. Detection of interaction between myogenic and TGF mechanisms using nonlinear analysis // *Am. J. Physiol.* 1994. Vol. 267. P. F160; Feldberg R., Colding-Jorgensen M. and Holstein-Rathlou N.-H. Analysis of interaction between TGF and the myogenic response in renal blood flow autoregulation // *Am. J. Physiol.* 1995. Vol. 269. P. F581.
5. Holstein-Rathlou N.-H. and Leyssac P.P. TGF-mediated oscillations in the proximal intratubular pressure: Differences between spontaneously hypertensive rats and Wistar-Kyoto rats // *Acta Physiol. Scand.* 1986. Vol. 126. P. 333.
6. Leyssac P.P. and Holstein-Rathlou N.-H. Effects of various transport inhibitors on oscillating TGF pressure response in the rat // *Pflügers Archiv.* 1986. Vol. 407. P. 285.
7. Holstein-Rathlou N.-H. and Marsh D.J. Renal blood flow regulation and arterial pressure fluctuations: A case study in nonlinear dynamics // *Physiol. Rev.* 1994. Vol. 74. P. 637.
8. Holstein-Rathlou N.-H., Yip K.-P., Sosnovtseva O.V. and Mosekilde E. Synchronization phenomena in nephron-nephron interaction // *Chaos.* 2001. Vol. 11. P. 417.
9. Postnov D.E., Sosnovtseva O.V., Mosekilde E. and Holstein-Rathlou N.-H. Cooperative phase dynamics in coupled nephrons // *Int. J. Modern Physics B.* 2001. Vol. 15. P. 3079.

10. *Mormann F., Lehnertz K., David P., and Elger C.E.* Mean phase coherence as a measure of phase synchronization and its application to the EEG of epileptic patients // *Physica D.* 2000. Vol. 144. P. 358.
11. *Wang X.-J.* Multiple dynamical modes of thalamic relay neurons: Rhythmic bursting and intermittent phase-locking // *Neuroscience.* 1994. Vol. 59. P. 21.
12. *Neiman A. and Russell D.F.* Stochastic biperiodic oscillations in the electroreceptors of paddlefish // *Phys. Rev. Lett.* 2001. Vol. 86. P. 3443.
13. *Jensen K.S., Mosekilde E. and Holstein-Rathlou N.-H.* Selfsustained oscillations and chaotic behaviour in kidney pressure regulation // *Mondes Develop.* 1986. Vol. 54/55. P. 91; *Holstein-Rathlou N.-H. and Marsh D.J.* A dynamic model of the tubuloglomerular feedback mechanism // *Am. J. Physiol.* 1990. Vol. 258. P. F1448; *Holstein-Rathlou N.-H. and Marsh D.J.* A dynamic model of renal blood flow autoregulation // *Bull. Math. Biol.* 1994. Vol. 56. P. 441.
14. *Mosekilde E.* Topics in Nonlinear Dynamics: Applications to Physics, Biology and Economic Systems. World Scientific, Singapore, 1996; *Barfred M., Mosekilde E., and Holstein-Rathlou N.-H.* Bifurcation analysis of nephron pressure and flow regulation // *Chaos.* 1996. Vol. 6. P. 280.
15. *Andersen M.D., Carlson N., Mosekilde E. and Holstein-Rathlou N.-H.* Dynamic model of nephron-nephron interaction // in *Membrane Transport and Renal Physiology* / eds H. Layton and A. Weinstein. Springer-Verlag, New York, 2001.
16. *Leyssac P.P. and Holstein-Rathlou N.-H.* Tubulo-glomerular feedback response: Enhancement in adult spontaneously hypertensive rats and effects of anaesthetics // *Pflügers Arch.* 1989. Vol. 413. P. 267.
17. *Grossmann A., Morlet J.* Decomposition of hardy functions into square integrable wavelets of constant shape // *S.I.A.M. J. Math. Anal.* 1984. Vol. 15. P. 723; *Daubechies I.* Ten Lectures on Wavelets. S.I.A.M., Philadelphia, 1992; *Ivanov P.Ch., Amaral L.A.N., Goldberger A.L., Havlin S., Rosenblum M.G., Struzik Z.R., Stanley H.E.* Multifractality in human heartbeat dynamics // *Nature.* 1999. Vol. 399. P. 461.
18. *Quiroga R.Q., Kraskov A., Kreuz T., Grassberger P.* Performance of different synchronization measures in real data: A case study on electroencephalographic signals // *Phys. Rev. E.* 2002. Vol. 65. P. 041903.
19. *Chen Y.-M., Yip K.-P., Marsh D.J., and Holstein-Rathlou N.-H.* Magnitude of TGF-initiated nephron-nephron interactions is increased in SHR // *Am. J. Physiol.* 1995. Vol. 269. P. F198.
20. *Lachaux J.P., Rodriguez E., Le Van Quyen M., Lutz A., Martinerie J., Varela F.J.* Studying single-trials of phase synchronous activity in the brain // *Int.J. Bifurcation Chaos.* 2000. Vol. 10. P. 2429.
21. *Sosnovtseva O.V., Pavlov A.N., Mosekilde E., Holstein-Rathlou N.-H.* Bimodal oscillations in nephron autoregulation // *Phys. Rev. E.* 2002. Vol. 66. P. 061909.
22. *Tass P., Rosenblum M.G., Weule J., Kurths J., Pikovsky A., Volkmann J., Schnitzler A., Freund H.-J.* Detection of n:m phase locking from noisy data: application to magnetoencephalography // *Phys. Rev. Lett.* 1998. Vol. 81. P. 3291.
23. *Stratonovich L.R.* Topics in the Theory of Random Noise. Gordon and Breach, New York, 1963.

*Department of Physics,
Saratov State University, Russia
Department of Physics,
Technical University of Denmark
Department of Medical Physiology,
Panum Institute, University
of Copenhagen, Denmark*

Received 05.09.03

ЭФФЕКТЫ СИНХРОНИЗАЦИИ В МНОГОМОДОВОЙ ДИНАМИКЕ СВЯЗАННЫХ НЕФРОНОВ

О.В. Сосновцева, А.Н. Павлов, Е. Mosekilde, N.-H. Holstein-Rathlou

Индивидуальная функциональная единица почек (нефрон) демонстрирует колебания в регуляции входящего потока крови с двумя различными временными масштабами: быстрые колебания, связанные с миогенной динамикой приносящей артериолы, и медленные колебания, обусловленные задержкой в канальцево-гломерулярной обратной связи. В данной работе исследуются взаимодействия этих двух мод в пределах одного нефрона и между нефронами. Помимо полной синхронизации, вейвлет-анализ экспериментальных данных и численные исследования детальной физиологической модели позволяют обнаружить существование частичной синхронизации, при которой соседние нефроны демонстрируют синхронное поведение по отношению к их медленной динамике, однако быстрая динамика остается несинхронной.



Olga Sosnovtseva received the M.Sc. from Saratov State University, Russia in 1989, and the Ph.D. degree in Physics and Mathematics in 1996, also from Saratov State University. Since 2001 she has been a postdoctoral fellow at The Technical University of Denmark. She is co-author of 40 scientific papers. Her current interests are within the field of nonlinear dynamics and modelling of biological systems. E-mail: olga@fysik.dtu.dk



Alexey Pavlov received the M.Sc. from Saratov State University, Russia in 1995, and the Ph.D. degree in Physics and Mathematics in 1998, also from Saratov State University. Since 2002 he has been an Associate Professor at Radiophysics and Nonlinear Dynamics Chair, Saratov State University. He is co-author of 35 scientific papers. His main interests are within the field of time series analysis and dynamics of nonlinear systems. E-mail: pavlov@chaos.ssu.runnet.ru



Erik Mosekilde received the M.Sc. in electrical engineering from the Technical University of Denmark (DTU) in 1966, the Ph.D. in solid state physics from DTU in 1968, and the Dr.Sc. in semiconductor instabilities from the University of Copenhagen in 1977. In 1970 he was a postdoctoral fellow at IBM Watson Research Center in Yorktown Heights, New York. He has been a visiting scientist at a number of different universities in Europe and North America. He is co-author of 190 scientific papers and of several books, including two recent books on «Topics in Nonlinear Dynamics» and «Chaotic Synchronization». His main interests are modeling of complex systems and applications of nonlinear dynamics. He is a Professor in nonlinear dynamics and Head of the Department of Physics at DTU, Denmark.

Niels H. Holstein-Rathlou received the M.D. degree from the University of Copenhagen, Denmark, in 1983, and the Ph.D. degree in physiology in 1992, also from University of Copenhagen. He was an Associate Professor of Physiology and Biophysics at the University of Southern California, Los Angeles, from 1986 to 1993. Since 1993, he has been a Professor of Medical Physiology at the University of Copenhagen. His current research interests are within the field of renal physiology and hypertension, and includes the application of the theory of nonlinear dynamical systems to physiological problems.



Izv. VUZ «AND», vol.11, № 3, 2003

SELF-CONSISTENT PARTICLE DYNAMICS IN THE GEOTAIL MAGNETIC FIELD REVERSAL

B.V. Shulgin, S.C. Chapman, V.M. Nakariakov

Dynamics of ions in the geotail magnetic field reversal plasmas is modelled with a hybrid code. Poincaré maps are calculated for stationary and for adiabatically changing field configurations starting from an anisotropic pressure self-consistent equilibrium. It is shown that the essential dynamics as found previously for single particle in prescribed fields persists in the hybrid code simulations of self-consistent fields. The possible interplay of dynamical processes in the Earth's magnetosphere and in the solar wind is discussed.

The Earth magnetosphere (Fig. 1) has the long magnetotail directed outwards of the sun. The magnetotail is thought to operate as a storage of the energy accumulated from the solar wind, i.e. from the inflow of the space plasma coming from the Sun. The consequent releases of the stored energy can cause magnetic substorms which have impact on the Earth inhabitants. One of the mechanisms connected with the origin of the energy releases is thought to be the changes in the complex dynamics of charged particles in the magnetosphere. We simulate particle dynamics with a hybrid code and calculate Poincaré maps for the particle trajectories in a self-consistent, adiabatically changing field.

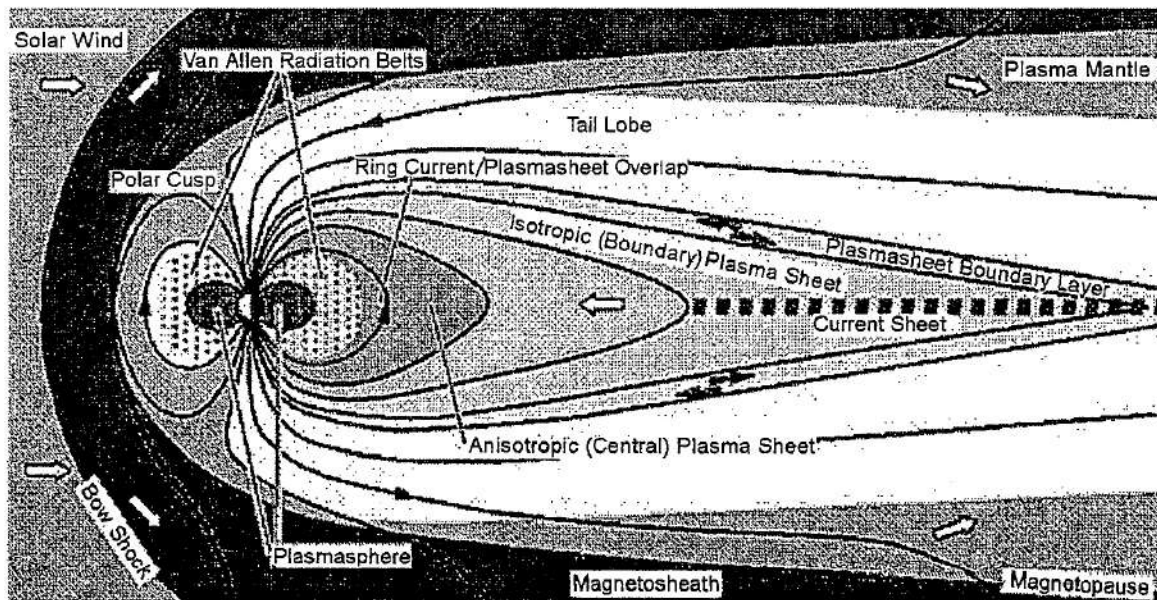


Fig. 1. Earth magnetosphere [1]

1. Method

In the magnetohydrodynamics (MHD) the plasma particle distribution function is Maxwellian and it defines its density n , and the first and the second moments (bulk velocity and pressure), \mathbf{U} , p . The MHD equations can be obtained by integration of the Vlasov equation [2,3]. But the MHD approach can not be used if the plasma distribution function can be essentially non-Maxwellian. Then other approaches allowing for an arbitrary distribution function could be used, such as the hybrid, particles-in-cell and Vlasov codes. The MHD approach also cannot be used if the time and space scales of the problem are of the order of the ion-gyromotion scales, because of appearing time dependence in the distribution function on the scales of averaging.

In the hybrid code [4-6] the ions are considered as particles with an arbitrary distribution function while the electrons are still considered as a massless fluid with the Maxwell distribution function. This approach is computationally efficient, as it allows us do not resolve the small time scales of the electron gyromotion. The particles (ions) move accordingly to the equation of motion:

$$d\mathbf{v}/dt = q/m(\mathbf{E} + \mathbf{v} \times \mathbf{B}), \quad (1)$$

and the field can be found from the Maxwell equations in the low frequency limit,

$$\partial \mathbf{B} / \partial t = -\nabla \times \mathbf{E}, \quad \nabla \times \mathbf{B} = \mathbf{J}, \quad \nabla \cdot \mathbf{B} = 0 \quad (2)$$

$$\mathbf{E} = -\mathbf{U} \times \mathbf{B} + (\nabla \times \mathbf{B} \times \mathbf{B} - \nabla P_e) / nq \quad (3)$$

$$\mathbf{U}_e = \mathbf{J} / nq - \mathbf{U}, \quad (4)$$

where \mathbf{U} is the ion bulk velocity and \mathbf{U}_e is the electron bulk velocity. The electron density is equal to the ion density, n , because of the plasma quasi-neutrality, and the electron pressure, P_e can be found from the electron fluid equation,

$$\partial P_e / \partial t = -\mathbf{U}_e \nabla P_e - \gamma P_e \nabla \cdot \mathbf{U}_e.$$

The moments of the ion distribution function: the density n and the bulk velocity \mathbf{U} , can be obtained by averaging:

$$n(\mathbf{x}, t) = \int_{\mathbf{v}} f(\mathbf{v}, \mathbf{x}, t) d\mathbf{v} + \xi_n, \quad \mathbf{U}(\mathbf{x}, t) = (1/n(\mathbf{x}, t)) \int_{\mathbf{v}} \mathbf{v} f(\mathbf{v}, \mathbf{x}, t) d\mathbf{v} + \xi_U. \quad (5)$$

The limited number of ions, N , on the computational grid leads to appearing of statistical errors of averaging, ξ_n , ξ_U , which makes the code noisy. The noise intensity is inversely proportional to $N^{1/2}$, and proportional to the temperature. The statistical noise sources ξ_n , and ξ_U can be considered as internal noise sources of the plasma. Because the considered space plasma is collisionless with zero diffusion, it is necessary to introduce the numerical diffusion to stabilize the code.

2. A self-consistent magnetic field reversal

A simple one-dimensional ($\partial/\partial x = \partial/\partial y = 0$) model for the magnetotail is the modified Harris field reversal (Fig. 2):

$$\mathbf{B}(z) = B_0 \tanh(z/L) \hat{\mathbf{x}} + B_n \hat{\mathbf{z}}. \quad (6)$$

We will study the self-consistent field of form (6) created by the motion of charged particles in that field. In order to get the reversal varying on timescale much slower than that of the particles we want to set the reversal into initial equilibrium: $\partial p / \partial t = 0$, $\partial \mathbf{U} / \partial t = 0$, $\partial \mathbf{B} / \partial t = 0$. Using (2), (3), and (6), we obtain from the condition $\partial \mathbf{B} / \partial t = 0$ that

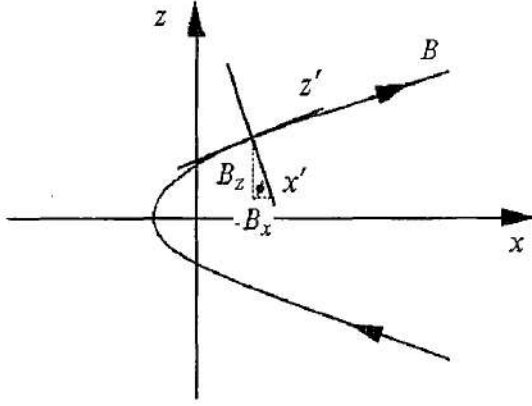


Fig. 2. Harris field reversal and axes of rotated distribution function

$$\mathbf{U} = ((1/\rho)\partial B_x/\partial z + C_U)\hat{\mathbf{y}}, \quad (7)$$

and $\partial\rho/\partial t = -\nabla(\rho, \mathbf{U}) = 0$. From $\partial\mathbf{U}/\partial t = 0$ using (7) and the MHD equation of conservation of the momentum one gets the *pressure balance equation*:

$$\mathbf{J} \times \mathbf{B} = \nabla P + \nabla P_e \quad (8)$$

which in the one-dimensional case considered is: $\nabla P = \hat{x}\partial P_{xx}/\partial z + \hat{y}\partial P_{yy}/\partial z + \hat{z}\partial P_{zz}/\partial z$ [7]. It is known that in the one-dimensional case (6) the pressure balance can not be satisfied with the isotropic pressure tensor [8]. In

order to obtain an anisotropic pressure tensor one can use the bi-Maxwellian distribution function with different temperatures in the directions perpendicular and parallel to the magnetic field [3]

$$f(\mathbf{x}, \mathbf{v}, t) = n/(T_\perp T_\parallel^{1/2}) [m/(2\pi k_B)^{3/2}] \times \exp[2(mv_\perp - U_\perp)^2/(2k_B T_\perp) - (mv_\parallel - U_\parallel)^2/(2k_B T_\parallel)]. \quad (9)$$

The pressure tensor corresponding to the bi-Maxwellian distribution function is diagonal in the local field-aligned coordinates,

$$p_\parallel = n(\mathbf{x}, t) k_B T_\parallel, \quad p_\perp = n(\mathbf{x}, t) k_B T_\perp. \quad (10)$$

It is convenient to use the cartesian coordinates rotated to the angle $\varphi(z) = \arctan(-B_x(z)/B_z)$ (Fig. 2) as the local coordinates. The tensor components in these Cartesian coordinates are:

$$P_{ij}(z) = mn \int (v'_i - U_i)(v'_j - U_j) f(z, \mathbf{v}') dv_i dv_j, \quad (11)$$

where $f(z, \mathbf{v}', t)$ is the local (rotated) ion distribution function,

$$f(z, \mathbf{v}', t) = n/(2\pi k_B)^{3/2} [m/(T_x T_y T_z)^{1/2}] \exp(-m/(2k_B)) \times \exp[(v'_x - U_x)^2/T_x - (v'_y - U_y)^2/T_y - (v'_z - U_z)^2/T_z], \quad (12)$$

where v'_x and v'_z are the velocity vector components in the local coordinates. Substituting (12) into (11) and integrating, one can obtain:

$$P_{xx}(z) = \sin 2\varphi(z)/(2m)(n(z)k_B T_\parallel(z) - n(z)k_B T_\perp(z)), \quad P_{yy}(z) = 0, \quad (13)$$

$$P_{zz}(z) = 1/m(n(z)k_B T_\parallel(z)\cos^2\varphi(z) + n(z)k_B T_\perp(z)\sin^2\varphi(z)).$$

Substituting (13) into (8), integrating and using (10), one can get the components of the equilibrium anisotropic pressure tensor:

$$p_\perp(z) = P_{m0} - P_m + \text{const}, \quad p_\parallel(z) = P_{m0} + P_m + \text{const}, \quad (14)$$

where $P_m = B^2/(2\mu_0)$ is the magnetic pressure and $P_{m0} = (B_0^2 + B_n^2)/(2\mu_0)$ is the maximum magnetic pressure.

The equation of state for the plasma with anisotropic pressure tensor aligned with directions parallel and perpendicular to the \mathbf{B} field may be obtained in the CGL theory [8]:

$$(\partial/\partial t + \mathbf{U}\nabla)(p_{\perp}^2 p_{\parallel}/\rho^3) = 0. \quad (15)$$

From (15) the equilibrium number density is:

$$n(z) = (p_{\perp}^2(z)p_{\parallel}(z))^{1/3}. \quad (16)$$

The obtained self-consistent equilibrium given by the functions (6), (7), (10), (14), and (16) is stable to the local mirror-mode perturbation: $(P_{\perp}/P_{\parallel})(P_{\perp}-P_{\parallel}) < B^2/(2\mu_0)$, and neutrally stable to the local firehose-mode perturbations: $P_{\parallel}-P_{\perp} = B^2/\mu_0$.

To study the long-time stability of this magnetic reversal, we simulated its dynamics with the hybrid code described above. The simulation showed that the self-consistent equilibrium is stable for a relatively long time, $t > 100P_g$, where P_g is the ion gyroperiod, and it slowly diffuses later due to the numerical diffusion introduced into the code. The numerical diffusion can be taken into account in the pressure balance equation (8)

$$\mathbf{J} \times \mathbf{B} = \nabla P + \nabla P_e - D_n \nabla^2 \mathbf{B}. \quad (17)$$

It leads to the appearance of an additional component of the bulk velocity,

$$U_x = -D_n/B_z (\partial B_x / \partial z), \quad (18)$$

where the diffusion coefficient is $D_n = \Delta x^2/(4\Delta t)$, where Δt and Δx are the time and space steps of the grid. Then the diffusion of the equilibrium gradually decreases.

3. The Poincaré maps

The Poincaré surface of section can be used to study the nonlinear particle dynamics [9,10]. In the map, each crossing of a chosen surface of section in the phase space by the phase trajectory in a chosen direction corresponds to a point. The ensemble of these points defines a Poincaré map. In this approach, a periodical trajectory corresponds to a finite number of points, ergodic tori correspond to a closed curves and chaotic motion corresponds to chaotic set of points.

In general, the equation of motion for a single particle defines a six-dimensional phase space. In the one-dimensional case (6), the equations are:

$$dX/dt = v, \quad dv/dt = f(z, v), \quad X, v \in \mathbb{R}^3. \quad (19)$$

One could see that in (19) there is a partial subsystem of four equations which are independent of the other two. That subsystem is four-dimensional. For a chosen constant energy, $H = mv^2/2$ and a chosen direction of the crossings, e.g. $dv/dt > 0$, set (19) corresponds to a two-dimensional map in the surface of section. There is also a transformation of variables based on the existence of constants of the motion P_y , and C_x [11]:

$$\begin{aligned} x' &= (x - P_y/(m\omega_n))/(B_n L), \\ y' &= (y + C_x/(m\omega_n))/(B_n L), \quad z' = z/(B_n L), \end{aligned} \quad (20)$$

where B_n and L are as in (6), and $\omega_n = qB_n/m$. The transformation (20) reduces the system (19) to a four-dimensional system with the two-dimensional map on the surface of section $z=0$. If the magnetic field is prescribed, the Poincaré map can be calculated from the particle equation of motion (19) [12]. The Poincaré maps for different energies corresponding to different layers in the distribution function are presented in Fig. 3. In the figure, one can observe periodic and ergodic tori, chaotic trajectories and transient (Speiser) trajectories carrying the currents (empty areas).

In order to calculate the Poincaré maps for the self-consistent field one should take into account the following problems. The fields created by the particles are affected by the statistical noise (5), that makes the maps noisy and gives them some width in the appearing third dimension (since the energy is no longer conserved). Affected by the noise, the particles can move into different areas of the phase space changing the behaviour of their motion. The diffusion of the field reversals increases the particles energy and makes the maps time-dependent. The noise and diffusion lead to development of a small B_y component that rotates and transforms [12] the Poincaré maps. The noise intensity can be reduced by the increase of number of particles in the grid. The Poincaré maps which were calculated for the self-consistent reversal are presented in Fig. 3. The Poincaré maps shown that the essential dynamics of single particles in prescribed fields [11] persists in the hybrid code simulations of self-consistent fields.

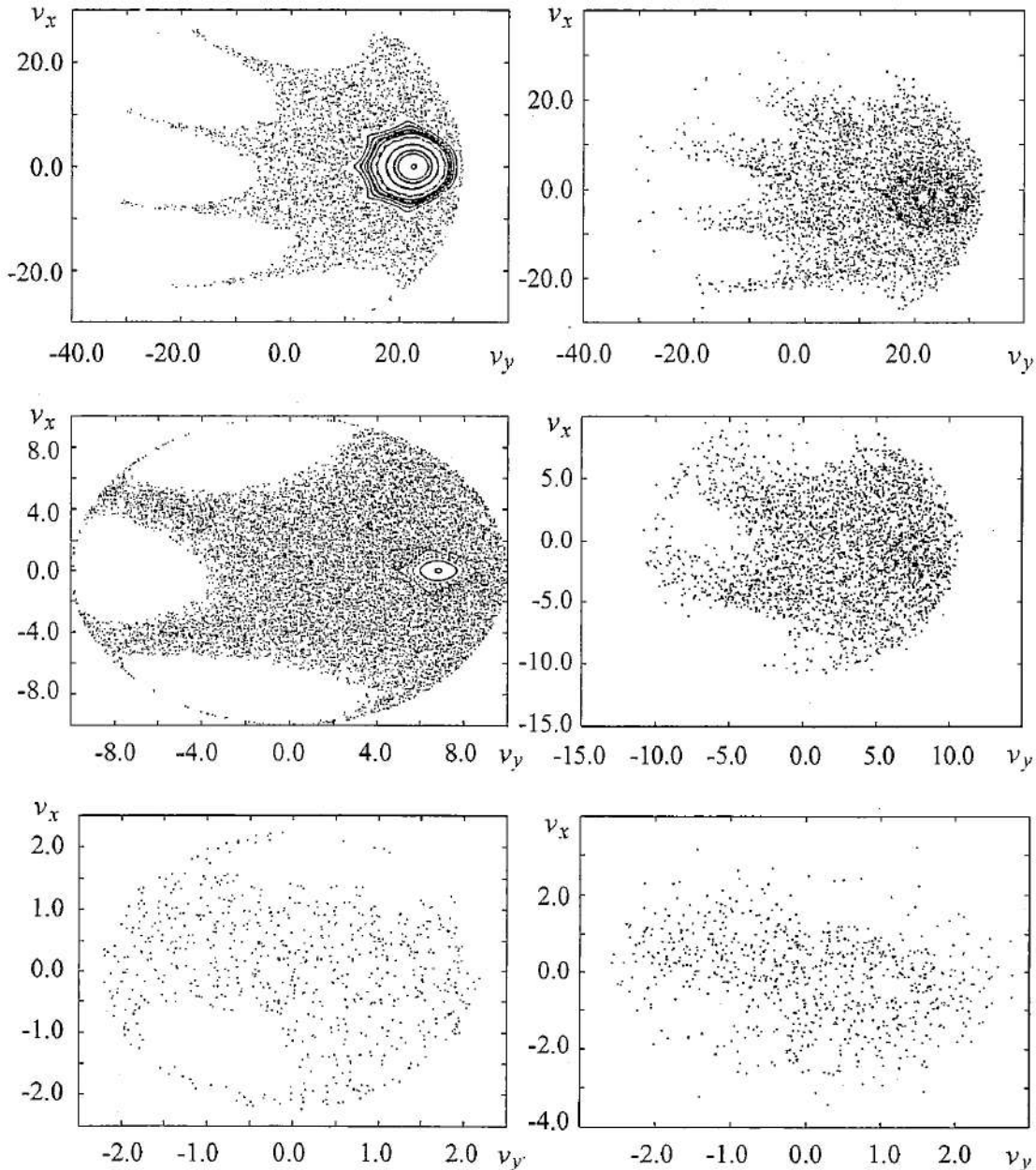


Fig. 3. Poincaré maps for prescribed magnetic field (left column) and for self-consistent magnetic field (right column). Dimensionless energy H is 500; 50; 2.5 from top to bottom

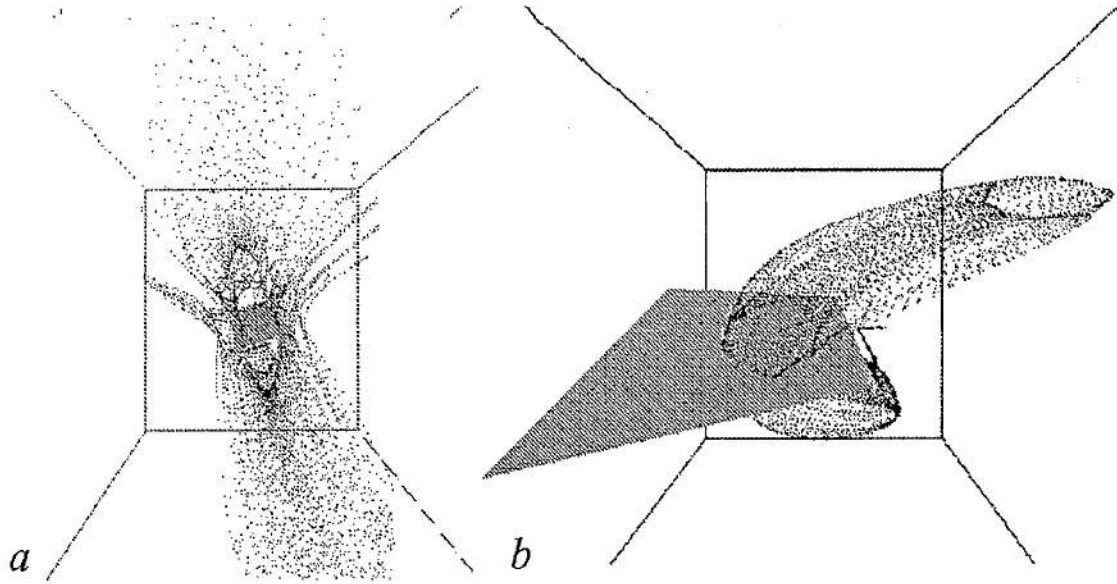


Fig. 4. Screen-shots of the virtual reality representation of particle trajectories in the phase space (v_y, v_x, z) . *a*) Chaotic particle trajectory, *b*) quasiperiodic trajectory lying on a three-dimensional projection of a four-dimensional ergodic torus and its surface of section

The virtual reality set at Warwick space and Astrophysics group provides us with a useful tool for studying complex particle trajectories. The 3D semi-immersive environment creates the effect of presence of studied objects flying in the air in the dark room with the observers. The objects could be interactively stirred (arbitrary scaled, moved or rotated) which allows us to analyse the geometry of the complex particles trajectories and corresponding Poincaré maps in details as shown in Fig. 4.

4. Time dependent field reversal

During magnetic substorms the geometry of the Earth field reversal changes in time, interacting with the charged particles. As a simple model of a time dependent field reversal, the time dependence appearing in the reversal due to instability of the equilibrium caused by noise and numerical diffusion was chosen. Hybrid simulations showed that the time dependence could be well approximated by the following expressions:

$$B_x = B_0 \tanh(z/L(t)), \quad L(t) = L_0 + t/\tau, \quad (21)$$

where the value of τ depends on the initial energy of particles. Chapman et al., [13,14] showed that it is possible to introduce two dimensionless parameters: the parameter of adiabaticity of the system α , and the phase of the process, αt [13],

$$\alpha = (B_x/B_z)(\rho_z/L)(\Omega_f/\Omega_z),$$

where ρ_z is the gyroradius, and $\Omega_f = 1/\tau$. The changes in the behaviour of particles motion and time of the changes are defined by parameters α and αt . These parameters define the dynamics of the particles moving in the slowly changing magnetic field reversal. The detailed comparison of the self-consistent simulations with the predictions of the prescribed field theory [13] is the aim of the further studies.

5. Discussion

A sudden destruction of the geotail magnetic reversal because of the field slow

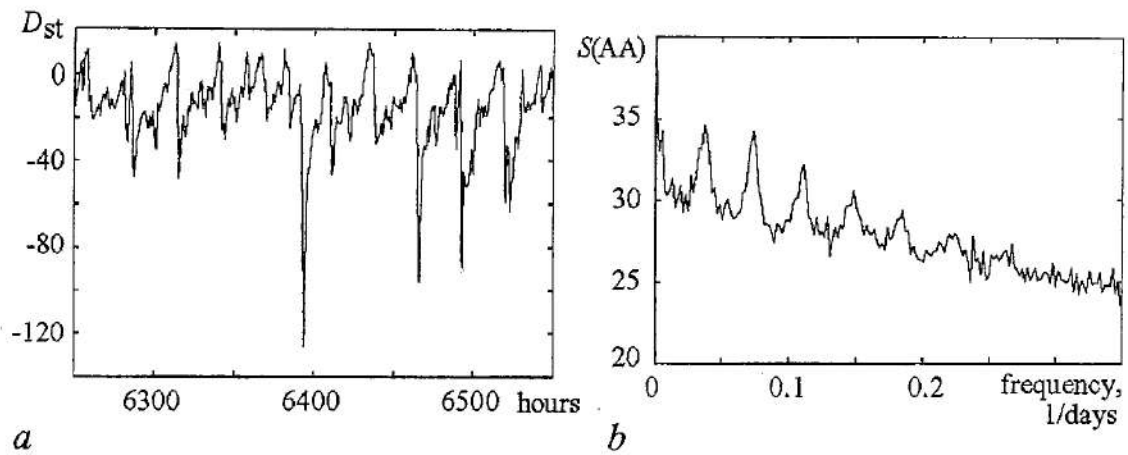


Fig. 5. a) D_{st} geomagnetic index, large negative drops correspond to magnetic substorms; b) power spectrum density of AA geomagnetic index averaged for 30 years

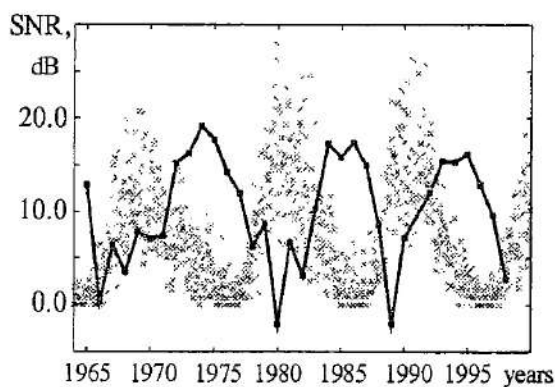


Fig. 6. Signal-to-noise ratio (SNR) in AA power spectrum (bold line), and Sun spot number, SSN (dots) divided by 10

There is also periodicity in the solar wind inflow caused by the rotation of the sun around its axes with the period of approximately 27 days [15]. That periodicity can also be seen as the first peak in the power spectra which we calculated for the Earth geomagnetic index as shown in Fig. 5, b. The strength of the periodic component is not constant but correlates with the phase of the solar cycle (the number of the sun spots or solar activity) as presented in Fig. 6. Such a behaviour may be associated with the phenomenon of stochastic resonance [17,16] and needs to be studied.

This research was supported by PPARC. B.S. thanks A.P. Nikitin and A.G. Balanov for useful discussions. The authors cordial greet Prof. Vadim Semenovich Anishchenko on the jubilee with the best wishes.

References

1. Hill T. The Rice University Electromagnetic Field Model, Rice University.
2. Klimontovich Yu.L. Statistical theory of open systems. Vol. 1. Kluwer Academic Publisher, Dordrecht, 1991; Vol. 2. Moscow. Janus-K, 1999.
3. Baumjohann W., Treumann R. Basics Space Plasma Physics. Imperial College Press, 1996.
4. Terasawa T. and Hoshino M. // JGR. 1986. Vol. 91, 4171.

5. Richardson A. and Chapman S.C. // Adv. Space Res. 1993. Vol. 13, (4) 253.
6. Richardson A. and Chapman S.C. // JGR. 1994. Vol. 99, 17391.
7. Holland D.L., Chen J. // GRL. 1993. Vol. 20, 1775.
8. Bittencourt J. Fundamentals of Plasma Physics. Pergamon press, 1986.
9. Lichtenberg A.J., Lieberman M.A. Regular and Stochastic Motion. Springer-Verlag, 1983.
10. Anishchenko V.S., Astakhov V.V., Neiman A.B., Vadivasova T.E., Schimansky-Geier L. Nonlinear Dynamics of Chaotic and Stochastic Systems. Springer, Berlin, Heidelberg 2002.
11. Chen J. // JGR. 1992. Vol. 97, 15011.
12. Ynnerman A., Chapman S.C., Tsalas M., Rowlands G. // Physica D. 2000. Vol. 139. P. 217.
13. Chapman S.C. // Ann. Geophysicae. 1993. Vol. 11. P. 239.
14. Chapman S.C. and Watkins N.W. // JGR. 1993. Vol. 98. P. 165.
15. Lockwood M., Stamper R., Wild M.N. // Nature. 1999. Vol. 399, 437.
16. Gammaitoni L., Hänggi P., Jung P., Marchesoni F. // Rev.Mod.Phys. 1998. Vol. 70, 223.
17. Anishchenko V.S., Neiman A.B., Moss F., Schimansky-Geier L.R. Stochastic Resonance: Noise-enhanced order, Physics - Uspekhi, 1999. Vol. 42(1), 7.

Department of Mathematics,
Space and Astrophysics Group,
Department of Physics,
Warwick University, Coventry, UK

Received 2.08.2003

УДК 537.5

САМОСОГЛАСОВАННАЯ ДИНАМИКА ЧАСТИЦ В РАЗВОРОТЕ ПОЛЯ ГЕОМАГНИТНОГО ХВОСТА

Б.В. Шульгин, S.C. Chapman, В.М. Накаряков

Динамика ионов в плазме геомагнитного хвоста моделируется с помощью гибридного кода. В случаях заданного и самосогласованного равновесия с медленно меняющимся магнитным полем вычисляются отображения Пуанкаре. Показано, что в рассматриваемом случае самосогласованного равновесия сохраняются основные свойства динамики заряженных частиц в заданных полях. Обсуждается возможная связь между рассматриваемыми динамическими процессами в Земной магнитосфере и в солнечном ветре.



Boris Shulgin graduated in 1992 from the Physics Department of Saratov State University. In 1987-1996 he was doing research in nonlinear dynamics at the Laboratory of Nonlinear Dynamics and Radiophysics chair of Saratov State University under supervision of Professor Vadim Semenovich Anishchenko, and got PhD degree in 1996. Since 1999 he has been working as a research fellow at University of Warwick, UK.



Professor Sandra Chapman is the head of the Space and Astrophysics Group of University of Warwick, UK. She has got PhD from Imperial College, London, in 1985. Her works was recognised with the COSPAR Zeldovich Medal and the EGS Young Scientists Medal. Her research interests includes self-consistent plasmas, wave-particle interactions, plasma acceleration at astrophysical shocks, cometary dynamics, application of nonlinear models to solar system and laboratory plasmas, time series analysis of astrophysical and space plasma data, scaling in intermittent turbulence. She has published over 60 research papers and a textbook on Electrodynamics. <http://www.astro.warwick.ac.uk/sandra.html>



Valery Nakariakov graduated from the Radiophysics Department of Nizhny Novgorod State University in 1989 and got his candidate of science degree (PhD) at the Applied Physics Institute of RAS, Nizhny Novgorod, in 1993. In 1989-1995 he worked as an assistant and then associate professor at the Applied Mathematics Department of Nizhny Novgorod State Technical University. In 1995-1999 he was a research fellow at the University of St. Andrews, UK. Since 1999 Valery Nakariakov is a Lecturer, then Senior Lecturer at the Physics Department of the University of Warwick, UK. He is the leader of the MHD waves research group and the author of more than 55 research papers. His research interests are connected with Solar Physics, Nonlinear Waves and Plasma Physics.

[Http://www.astro.warwick.ac.uk/~valery/](http://www.astro.warwick.ac.uk/~valery/)



СОГЛАСОВАННАЯ ФИЛЬТРАЦИЯ ХАОТИЧЕСКИХ СИГНАЛОВ

А.С. Дмитриев, Г.А. Касьян, Л.В. Кузьмин

В статье предлагается подход к очистке хаотических сигналов от шума (фильтрации хаотических сигналов), основанный на использовании того факта, что хаотическим сигналам, в отличие от случайных процессов, соответствуют в фазовом пространстве динамических систем предельные множества (аттракторы) относительно низкой размерности.

Введение

Очистке хаотических сигналов от шума (фильтрации хаотических сигналов) уделяется большое внимание в литературе (см., например, книги [1, 2] и ссылки в них). Хорошо известно, что проблема очистки хаотических сигналов от шума значительно отличается от очистки регулярных сигналов в силу неустойчивости фазовых траекторий хаотических систем. В частности, на примере одномерных и двумерных отображений было показано существование некоторого порогового значения шума, ниже которого очистка хаотического сигнала возможна с любой степенью точности, а выше - значительное снижение уровня шума не представляется возможным [3-5].

Большинство результатов по фильтрации хаотических сигналов относятся к малоразмерным системам. В данной работе мы рассматриваем дополнительные возможности, которые связаны с тем, что размерность фазового пространства динамической системы может быть, значительно больше размерности хаотического аттрактора.

Идея фильтрации заключается в использовании следующего факта. Пусть имеется высокоразмерная динамическая система

$$\dot{x} = F(x), \quad x \in R^n, \quad (1)$$

обладающая относительно низкоразмерным хаотическим аттрактором A

$$A \in R^{n_0}, \quad n_0 \ll n, \quad (2)$$

где R^{n_0} - линейное подпространство в R^n ; $n_0 \ll n$ в силу низкой размерности A .

Пусть на систему (1) воздействует внешний шум $\eta(t)$. Какова будет реакция системы на этот шум (при малой, для определенности, интенсивности шума)? Поскольку все траектории автономной системы «втягиваются» в то

подпространство, где лежит хаотический аттрактор, трансверсальные по отношению к подпространству аттрактора возмущения, создаваемые шумом, будут подавляться. С другой стороны, проекции возмущения на аттрактор могут усиливаться. Последнее обстоятельство затрудняет очистку хаотических сигналов от шума в маломерных системах. Однако первое обстоятельство способствует такой очистке и задача данной работы это продемонстрировать.

1. Модель фильтрации

Ниже под фазовым пространством понимаем как «естественное» фазовое пространство, в котором координатами являются переменные динамической системы, так и «искусственное» фазовое пространство, для которого искусственные переменные получаются из одного компонента процесса путем применения процедуры, основанной на взятии задержанных значений одной из фазовых переменных [6]. Заметим, что для одной и той же динамической системы размерность искусственного фазового пространства (пространства вложения) может значительно превышать размерность естественного фазового пространства. На использовании этой разницы и основан рассматриваемый подход к фильтрации. Пусть m' - размерность некоторого пространства вложения $R^{m'}$ и пусть d - корреляционная размерность аттрактора. Как было показано теоретически [7] и подтверждено численным моделированием, m' должно удовлетворять следующему неравенству

$$m' \geq 2d + 1. \quad (3)$$

Векторы пространства вложения формируются путем взятия отсчетов хаотической траектории через интервалы времени Δt (Δt выбирается по определенным правилам). Первый вектор в m' -мерном пространстве образован из m' подряд идущих элементов хаотической последовательности (с 1-го по m' -й), второй вектор образован путем сдвига на один элемент, то есть используются отсчеты со 2-го по $(m'+1)$ -й и т.д.

Пусть m - минимальная размерность пространства вложения

$$m' > m \geq 2d + 1. \quad (4)$$

Рассмотрим m -мерное пространство вложения R^m и обозначим через $m_0 \leq m$ - минимальное подпространство R^{m_0} , в котором аттрактор может быть аппроксимирован с некоторой заданной точностью ϵ .

Рассмотрим также пространство вложения $R^{m'}$ с размерностью m' и обозначим через m'_0 - минимальную размерность его подпространства, в котором аттрактор может быть аппроксимирован с той же точностью ϵ .

В дальнейшем предполагаем, что m'_0 слабо зависит от m' , то есть $m'_0 \approx m_0$.

Этим обстоятельством можно воспользоваться для фильтрации хаотического сигнала от шума. Действительно, пусть имеется хаотическая последовательность

$$x_1, x_2, \dots, x_{m'_0}, x_{m'_0+1}, \dots, x_N \dots \quad (5)$$

Построим систему векторов

$$\begin{aligned} X_1 &= (x_1 \dots x_{m'}), \\ X_2 &= (x_2 \dots x_{m'+1}), \\ &\vdots \\ X_N &= (x_N \dots x_{m'+N+1}). \end{aligned} \quad (6)$$

Если аттрактор динамической системы принадлежит подпространству размерности m_0 , то из m' компонент каждого из этих векторов лишь m_0 должны быть линейно независимы. Один из вариантов выбора системы m_0 базисных векторов предложен в [8].

Рассмотрим матрицу

$$B = N^{-1/2}(X_1 \dots X_N)', \quad (7)$$

ее ранг равен m_0 . Следовательно, ранг матрицы $B'B$ также равен m_0 . Матрица $B'B$ симметрична и обладает ортогональным базисом из собственных векторов. Обозначим эти векторы как b_i и отсортируем их в порядке убывания соответствующих этим векторам собственных значений λ_i матрицы $B'B$.

Поясним смысл этой процедуры. Разложим каждый из векторов X_i по базису b_j

$$X_i = \sum_{j=1}^{m'} \alpha_{ij} b_j \quad (8)$$

Тогда средняя энергия на вектор составляет

$$E = \langle X_i^2 \rangle = 1/N \sum_{i=1}^N \sum_{j=1}^{m'} \alpha_{ij}^2 = 1/N \sum_{j=1}^{m'} \sum_{i=1}^N \alpha_{ij}^2 = \text{tr}(B'B). \quad (9)$$

Поскольку b_i является базисом из собственных векторов матрицы $B'B$, то в этом базисе эта матрица является диагональной, так что $(B'B)_{ii} = \lambda_i$, следовательно

$$E = \text{tr}(B'B) = \sum_{j=1}^{m'} \lambda_j = \sum_{j=1}^{m_0} \lambda_j + \sum_{j=m_0+1}^{m'} \lambda_j. \quad (10)$$

Если, как было сказано выше, аттрактор лежит в подпространстве размерности m_0 и ранг матрицы равен также m_0 , то лишь первые m_0 собственных значений отличны от нуля, так что вторая сумма в (10) равна нулю.

При численных расчетах собственные числа λ_i для $i > m_0$ не равны 0, но стремятся к нулю с ростом i . Поэтому возникает проблема оценки m_0 по наблюдаемому спектру собственных значений λ_i . Число m_0 выбирается таким, чтобы часть мощности, приходящаяся согласно формуле (10) на $(m' - m_0)$ векторов с малыми λ_i , была достаточно малой, так что первые m_0 векторов дадут необходимую нам аппроксимацию аттрактора динамической системы.

Выбрав m_0 , мы получим набор из m_0 ортонормированных базисных векторов b_i

$$(b_i, b_j) = \begin{cases} 1, & \text{если } i = j, \\ 0, & \text{если } i \neq j. \end{cases} \quad (11)$$

И каждый из векторов X_i может быть представлен в виде разложения по указанной линейно независимой системе

$$X_i' = \sum_{i=1}^{m_0} \alpha_{ii} b_i. \quad (12)$$

Пусть теперь на хаотический сигнал в канале воздействует гауссов шум η_i

$$y_i = x_i + \eta_i, \quad (13)$$

где y_i - отсчеты, принимаемые приемником. Введем систему векторов

$$Y_i = X_i + N_i, \quad (14)$$

где $N_i = (\eta_i \dots \eta_{i+m'-1})$.

В отличие от векторов X_i , которые принадлежат пространству R^{m_0} размерности m_0 , векторы N_i принадлежат пространству $R^{m'}$ размерности m' , поскольку компоненты в них - независимые случайные величины.

Разложим векторы Y_l по базису (ортонормированной системе векторов) $b_i, i \in 1 \dots m_0$.

$$\beta_{il} = (b_i, Y_l) = (b_i, X_l + N_l) = (b_i, X_l) + (b_i, N_l) = \alpha_{il} + \delta_{il}. \quad (15)$$

Обозначим через Y_l' проекцию вектора Y_l на подпространство R^{m_0}

$$Y_l' = \sum_{i=1}^{m_0} \beta_{il} b_i = \sum_{i=1}^{m_0} (\alpha_{il} + \delta_{il}) b_i. \quad (16)$$

Эта проекция используется как сигнал-оценка исходного сигнала, то есть

$$\hat{X}_l = Y_l'. \quad (17)$$

Сравним векторы X_l и Y_l' , X_l и \hat{X}_l

$$\|Y_l' - X_l\| = (N_l, N_l) = \sum_{i=1}^{m'} \delta_{il}^2, \quad (18)$$

где $\|\cdot\|$ означает квадратичную норму.

Поступая аналогично выводу формулы (10) и снова воспользовавшись тем, что в базисе векторов b_i выполнено $(B'B)_{ii} = \lambda_i$, получим

$$\|\hat{X}_l - X_l\| = \|Y_l' - X_l\| = \|\sum_{i=1}^{m_0} (\alpha_{il} + \delta_{il}) b_i - \sum_{i=1}^{m'} \alpha_{il} b_i\| = \sum_{i=1}^{m_0} \delta_{il}^2 + \sum_{i=m_0+1}^{m'} \lambda_{il}^2. \quad (19)$$

Таким образом, если уровень шума достаточно высок, так что мы можем пренебречь вторым членом в сумме (19), то мощность шума в сигнале после фильтрации ниже, чем мощность исходного шума (18).

Обозначим отношение сигнал/шум на входе фильтра как $C/\Pi_{\text{вх}}$ и на выходе фильтра как $C/\Pi_{\text{вых}}$. Если шум распределен равномерно между ортогональными компонентами, то выигрыш в уровне шума составит

$$K = (C/\Pi_{\text{вх}})/(C/\Pi_{\text{вых}}) = m'/m_0. \quad (20)$$

Величину K будем называть коэффициентом очистки сигнала от шума.

Представленное в децибелах, это выражение принимает вид:

$$K_{(\text{dB})} = (C/\Pi_{\text{вых}} - C/\Pi_{\text{вх}})_{\text{dB}} = 10 \lg(m'/m_0). \quad (21)$$

Таким образом, выигрыш в подавлении шума пропорционален длине вектора m' и обратно пропорционален минимальной размерности пространства вложения m_0 , а следовательно, размерности аттрактора.

2. Компьютерное моделирование

Апробация алгоритма была проведена на примерах системы Ресслера

$$\begin{aligned} \dot{X} &= -Y - Z, \\ \dot{Y} &= X + aY, \\ \dot{Z} &= b + (X - c)Z \end{aligned} \quad (22)$$

при значениях параметров $a=0.15, b=0.2, c=10$ и для кольцевого генератора с 2.5 степенями свободы [9], описываемого системой уравнений

$$\begin{aligned}
T\dot{X} + X &= mF(Z_2) \\
\ddot{Z}_1 + \alpha_1 \dot{Z}_1 + \omega_1^2 Z_1 &= \omega_2^2 X_1 \\
\ddot{Z}_2 + \alpha_2 \dot{Z}_2 + \omega_2^2 Z_2 &= \omega_2^2 Z_1
\end{aligned}
\quad (23)$$

при значениях параметров $\alpha_1=0.06$, $\alpha_2=0.28$, $\omega_1=1$, $\omega_2=0.421$, $T=0.8$, $m=3.3$ и нелинейности $F(Z)$ вида

$$F(Z) = |Z+e_1| - |Z-e_1| + 0.5|Z-e_2| - 0.5|Z+e_2|. \quad (24)$$

Результаты численного моделирования представлены на рис. 1-3.

На рис. 1 показаны спектры собственных значений ковариационной матрицы $V'V$ для систем (22) и (23).

Из рис. 1 видно, что величина собственных значений λ_i быстро спадает с ростом i . Поэтому разложение по первым 5-10 собственным векторам позволяет получить достаточно точную аппроксимацию аттрактора системы.

На рис. 2, 3 представлен результат применения алгоритма фильтрации (при размерностях $m_0=10$ и $m'=40$) к сигналу, генерируемому системами (22) и (23), подвергнутому воздействию аддитивного гауссова шума. Кривые на рис. 2 показывают зависимость отношения сигнал/шум после применения процедуры фильтрации от отношения сигнал/шум до фильтрации. На рис. 3 представлен коэффициент очистки, полученный в результате фильтрации.

Отношение сигнал/шум на выходе фильтра определяется двумя факторами. Во-первых, точностью аппроксимации сигнала при его разложении по нескольким векторам базиса. Это шум аппроксимации. Во-вторых, шумами в канале, поступающими вместе с сигналом. Алгоритм фильтрации добавляет к сигналу шум аппроксимации и осуществляет очистку сигнала от шумов в канале. Пусть S - мощность хаотического сигнала, N_k - мощность шума в канале, N_Q - мощность шума ошибок аппроксимации. Тогда отношение сигнал/шум на входе фильтра равно

$$C/Ш_{\text{вх}} = S/N_k. \quad (25)$$

Отношение сигнал/шум на выходе фильтра при отсутствии шума в канале или при полной очистке от него сигнала равно

$$C/Ш_{\text{вых}} = S/N_Q. \quad (26)$$

В общем случае уровень шума на выходе фильтра будет функцией от уровня шума в канале и уровня шума аппроксимации

$$N_{\text{вых}}(N_k, N_Q): \quad (27)$$

Как видно из рис. 2, отношение сигнал/шум на входе фильтра при уменьшении уровня шума в канале стремится к фиксированной величине, которая определяется уровнем шума аппроксимации. При малом уровне шумов в канале коэффициент очистки падает и может стать отрицательным (рис. 3).

Это можно объяснить следующим образом. Работа алгоритма фильтрации основана на том факте, что $m_0 \ll m'$ и это позволяет снизить уровень шума

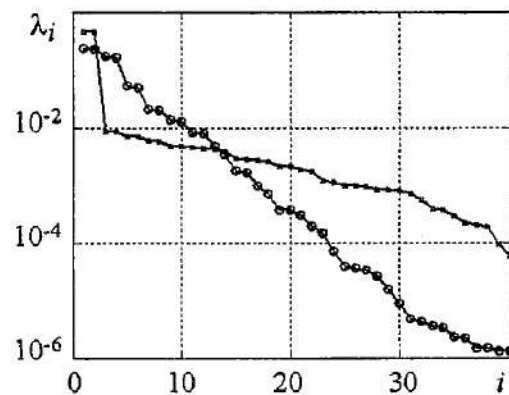


Рис. 1. Зависимость величины собственного значения λ_i от его номера i

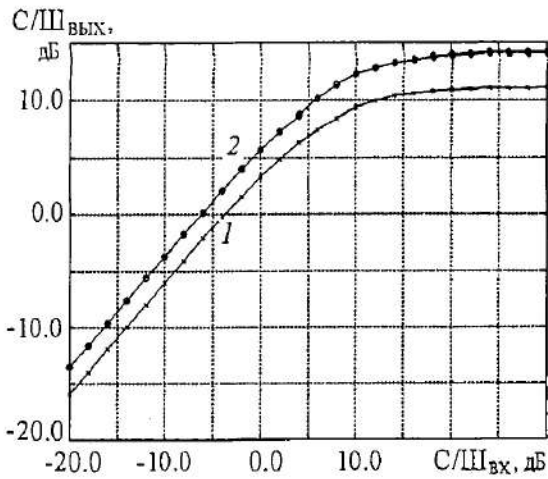


Рис. 2. Зависимость отношения C/Π после применения алгоритма фильтрации от отношения C/Π в канале. 1 - кольцевая система с 2.5 степенями свободы, 2 - система Рёсслера

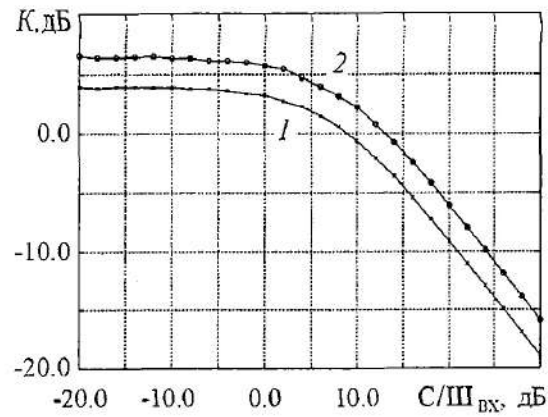


Рис. 3. Зависимость коэффициента очистки от отношения C/Π в канале. 1 - кольцевая система с 2.5 степенями свободы, 2 - система Рёсслера

приблизительно в m'/m_0 раз, практически не влияя на мощность сигнала. Однако при этом при применении фильтра используется аппроксимация сигнала его проекцией на некоторый базис, приводящая к возникновению ошибки (шуму) аппроксимации. Если эта ошибка становится сравнимой с величиной ошибки, вносимой шумом, то отношение сигнал/шум будет определяться не уровнем шума в канале, а уровнем ошибки аппроксимации, вносимой при проецировании траектории на m_0 -мерное подпространство.

Поэтому при высоких отношениях сигнал/шум требуется более высокая степень аппроксимации, которая, в принципе, может быть достигнута путем искусственного завышения размерности m_0 , то есть выбором большего количества векторов в качестве базисных. Однако в этом случае снижается эффективность фильтрации, поскольку, уменьшая отношение m'/m_0 , мы уменьшаем возможности для снижения уровня шума (см. также (18)). Заметим, что в соответствии с формулой (21) максимальный выигрыш в отношении сигнал/шум, получаемый при $m'=40$ и $m_0=10$ должен быть около 6 дБ. На рис. 2 можно видеть, что при больших шумах это значение практически достигается для обеих систем. С понижением уровня шума в канале выигрыш уменьшается.

Заключение

Проблеме фильтрации хаотических сигналов уделяется значительное внимание в литературе. Однако развитые методы, как правило, предназначены для обработки либо записанных данных, либо медленных потоков данных. Поэтому их сложно применить в телекоммуникационных системах. Подход, рассмотренный в настоящей статье, принадлежит к классу субоптимальных подходов. Его основным преимуществом является то, что он может быть применен в ситуациях, когда скорость фильтруемого сигнала высока. Концептуально этот подход близок к схеме обработки данных при помощи фильтров в коммуникационных системах.

Заметим, что, хотя данный алгоритм и похож на алгоритмы, рассмотренные в [8, 10], результаты их применения существенно различаются. В предложенном алгоритме проецирование осуществляется на заранее подготовленный базис, полученный благодаря нашему знанию динамики системы, в то время как в статьях [8] и [10] базис получается на основе наблюдаемых значений реализации. Поэтому, в отличие от методов, рассмотренных в [8, 10], наш подход, благодаря знанию

чистой фазовой траектории система, применим в ситуациях, когда уровень шума превышает уровень сигнала.

Библиографический список

1. *Abarbanel H.D.I.* Analysis of observed Chaotic Data. Berlin. Springer, 1997.
2. *Kantz H., Schreiber T.* Nonlinear Time Series Analysis. Cambridge University Press, 1997.
3. *Stojanovski T., Kocarev L., Herris K.* Application of symbolic dynamics to chaos synchronization // IEEE Trans. Circuit and Systems. 1997. Vol. CAS-44, № 10. P. 1014.
4. *Rosa E., Hayes S., Grebogi C.* Noise filtering in communications with chaos // Phys. Rev. Lett. 1997. Vol. 78, № 7. P. 1247.
5. *Dmitriev A.S., Kassian G., Khilinsky A.* Limit efficiency of chaotic signal clearing off noise // Proc. NDES'99. Ronne. Denmark. 1999. P. 187.
6. *Takens F.* // Lect. Notes in Math, Berlin; Heidelberg; New York: Springer, 1981. Vol. 898. P. 366.
7. *Mane R.* // Lect. Notes in Math. Berlin; Heidelberg; New York: Springer, 1981. Vol. 898. P. 230.
8. *Broomhead D.S., King G.P.* // Physica D. 1986. Vol. 20. P. 217.
9. *Dmitriev A.S., Panas A.I., Starkov S.O.* Ring oscillating systems and their application to the synthesis of chaos generators // Int. J. of Bif. and Chaos, 1996. Vol. 6. № 5. P. 851.
10. *Ланда П.С., Розенблюм М.Г.* // ЖТФ. 1989. Т. 59. С. 13.

Институт радиотехники
и электроники РАН,
Москва, Россия

Поступила в редакцию 02.08.03

MATCHED FILTRATION OF CHAOTIC SIGNALS

A.S. Dmitriev, G.A. Kassian, L.V. Kuzmin

In this paper an approach to cleaning chaotic signals from noise (filtration of chaotic signals) is proposed that is based on the fact that, in contrast to random processes, chaotic signals are related in the phase space to limit sets (attractors) of relatively low dimension.



Дмитриев Александр Сергеевич - родился в 1948 году, доктор физико-математических наук, профессор, заведующий отделом Института радиотехники и электроники РАН. Область научных интересов: теория динамических хаотических систем, информационные технологии с использованием динамического хаоса.

E-mail: chaos@mail.cplire.ru.



Касьян Геннадий Александрович - родился в 1978 году, аспирант МФТИ. Область научных интересов: динамический хаос и его приложения в радиофизических системах, обработка информации с использованием динамического хаоса.

E-mail: chaos@mail.cplire.ru.



Кузьмин Лев Викторович - родился в 1974 году, кандидат физико-математических наук, научный сотрудник Института радиотехники и электроники РАН. Область научных интересов: хаотическая динамика и ее использование в информационных технологиях.

E-mail: chaos@mail.cplire.ru.



THREE SUBPROBLEMS OF GLOBAL MODEL RECONSTRUCTION FROM TIME SERIES AND THEIR PECULIARITIES

T. Dikanev, D. Smirnov, V. Ponomarenko, and B. Bezruchko

We consider three main subproblems of global reconstruction of dynamical models from time series: selection of dynamical variables, selection of model function, and estimation of model parameters. Special techniques for their solution are presented. Their applications and prospects of the further development of empiric modeling methods are discussed. The approaches are illustrated in numerical and acoustic experiments.

1. Introduction

A traditional way of obtaining a mathematical model of a complex phenomenon from the first principles cannot often be realized in practice. Then, experimental data may become the main source of information about a system under investigation and problem of an *empiric* model construction may arise. Since observations of real-world processes are presented, as a rule, in the form of time series (discrete ordered sequences of observable values), the problem is called *modeling from time series*. It is important in physics, meteorology, medicine and physiology, etc. Since 1980s various methods for constructing deterministic low-dimensional models in the form of difference equations (maps) [1-3] and ordinary differential equations (ODEs) [4-16] have appeared in the framework of nonlinear dynamics. In particular, significant contribution to this field has been made by V.S. Anishchenko and his team [8-11].

In general, the problem of modeling from time series can be formulated as follows.

- There is a system of our interest («an object»).
- One picks out some quantities η_1, \dots, η_k , which characterize the processes occurring in the system and which can be measured experimentally (they are called observables).
- A time series of these quantities (i.e. the finite sequence $\{\vec{\eta}(t_i)\}_{i=1}^N$, where $\vec{\eta}(t_i) = (\eta_1(t_i), \eta_2(t_i), \dots, \eta_k(t_i))$, $t_i = i\Delta t$, Δt is a sampling interval) is measured.
- It is known that the object possesses a set of properties $\{P_1, \dots, P_M\}$.

Based on the time series, it is necessary to construct a dynamical model capable of reproducing this time series and as many of the properties $\{P_1, \dots, P_M\}$ as possible. Models are constructed in the form of differential equations (1) or discrete maps (2):

$$dx/dt = F(x(t), c), \quad (1)$$

$$\mathbf{x}_{n+1} = \mathbf{F}(\mathbf{x}_n, \mathbf{c}), \quad (2)$$

where $\mathbf{x}=(x_1, \dots, x_D) \in \mathbb{R}^D$ is a state vector of the model, \mathbf{F} is a smooth function, $\mathbf{c} \in \mathbb{R}^P$ is a parameter vector, t is continuous time, n is discrete time. If the function \mathbf{F} is expressed analytically in terms of elementary functions (in a closed form) for the entire phase space, then the model is called global. Further we consider only *global* models.

The success of modeling depends on several factors. It is exceedingly important to select properly a *model structure* that involves the choice of dynamical variables x_k (that is the relations between dynamical variables x_k and observables η_j) and choice of the form of the function \mathbf{F} .

So, the first subproblem of time series modeling is selection of dynamical variables and reconstruction of their time courses from the observed time series data. If there are too many observables then one should specify a subset of them to be used as model variables. If the number of observables is not sufficient for model construction or they cannot be used directly, then different combinations of available data are employed. Very popular methods are sequential derivatives and time delays ([5] and [6], respectively), both of them rest upon the celebrated Takens' results and their generalizations [17]. However, different ways of obtaining dynamical variables realizations, which are based on a priori information about the system under investigation or some peculiarities of its dynamics [8], may prove to be more appropriate for modeling. In Section 2 we present a technique for the selection of the best set of dynamical variables for modeling, which allows simultaneous convenient testing for nonlinearity.

The second subproblem is to specify the form of function \mathbf{F} . Algebraic polynomial is a standard recommendation [6], even though often inefficient [13]. To make polynomial more feasible different methods for spurious terms detection and exclusion were suggested which work well for a special situations [2,14,18-20]. In Section 3 we present a new method for spurious terms detection.

Third subproblem is technological: to estimate model parameters \mathbf{c} (usually the least-squares routine is used). Finally, an obtained model should be validated. But even if the model is not sufficiently adequate, model coefficients may have their own value and serve for the characterization of the system. In Section 4 we consider such a situation where coefficients of a model map describing phase dynamics are used to solve an important problem of coupling characterization [21] and suggest extension of the known technique for the case of short and noisy time series.

2. Selection of dynamical variables

As it has been already mentioned, to construct model equations in the form $\mathbf{y}(t)=\mathbf{F}(\mathbf{x}(t))$ from a time series $\{\vec{\eta}(t_i)\}$, one forms, first of all, the series of state vectors $\{\mathbf{x}(t_i)\}$. Then, the time series of quantities to enter the left-hand side of model equations $\{\mathbf{y}(t_i)\}$ is obtained from the time series $\{\mathbf{x}(t_i)\}$ according to the chosen model type:

- via numerical differentiation of $\{\mathbf{x}(t_i)\}$ for ODEs, since $\mathbf{y}(t)=d\mathbf{x}(t)/dt$;
- via the shift of $\{\mathbf{x}(t_i)\}$ along the time axis for discrete maps, since $\mathbf{y}(t_i)=\mathbf{x}(t_{i+1})$.

Finally, the form of the function \mathbf{F} is specified and its parameters are estimated.

Voluntary dynamical variables selection can make approximation of the dependencies $y_j(\mathbf{x})$ with a smooth function extremely problematic [22,23] or even make these dependencies many-valued. Here, we describe the method for assessing suitability and convenience of the selected variables x_1, \dots, x_D for constructing a global dynamical model. It is based on testing the time series $\{\mathbf{y}(t_i)\}$ and $\{\mathbf{x}(t_i)\}$ for single-valuedness and continuity of each dependency $y_j(\mathbf{x})$ in the entire region of an observed motion. It is crucial here that we use local characteristics rather than the averaged ones as in [24].

2.1. Description of technique. If a dependency $y(\mathbf{x})$ is single-valued and continuous in a domain V , then the difference $|y(\mathbf{x})-y(\mathbf{x}_0)|$ tends to zero when $\|\mathbf{x}-\mathbf{x}_0\|\rightarrow 0$ for each $\mathbf{x}_0\in V$. In practice, violation of this condition may be viewed as a sign of many-valuedness or discontinuity of the dependency $y(\mathbf{x})$. Since the length of an observable time series is finite, the above-mentioned limit cannot, strictly speaking, be found. However, it is possible to trace a tendency in variations of the quantity $|y(t_i)-y(t_j)|$ when the vectors $\mathbf{x}(t_i)$ and $\mathbf{x}(t_j)$ are made closer and closer, down to a certain *finite* distance. Given sufficiently large amount of data N , high accuracy of measurements, and low noise level, the distance $\|\mathbf{x}(t_i)-\mathbf{x}(t_j)\|$ can be made sufficiently small for each local region of observed motion.

The technique of testing consists in the following (Fig. 1, a). The domain V containing the set of vectors $\{\mathbf{x}(t_i)\}_{i=1}^{N_0}$ is partitioned into identical hypercubic boxes of the size δ . All boxes containing at least two vectors are selected. Let us denote them s_1, s_2, \dots, s_M . The difference between the largest and the smallest values of y inside a box s_k is called *local variation* $\epsilon_k = \max_{\mathbf{x}\in s_k} y(\mathbf{x}) - \min_{\mathbf{x}\in s_k} y(\mathbf{x})$. The largest local variation $\epsilon_{\max} = \max_{1\leq k\leq M} \epsilon_k$ and its graph $\epsilon_{\max}(\delta)$ are used as the main characteristics of the investigated dependency. Suitability of the considered quantities \mathbf{x} and y for global modeling is assessed using the following considerations [25].

- If a dependency $y(\mathbf{x})$ is single-valued and continuous, ϵ_{\max} is sufficiently small for small δ and tends to zero for $\delta\rightarrow 0$ (Fig. 1, b, filled circles). The following statement is often correct: the less the slope of the graph $\epsilon_{\max}(\delta)$, the better are the dynamical variables for modeling.

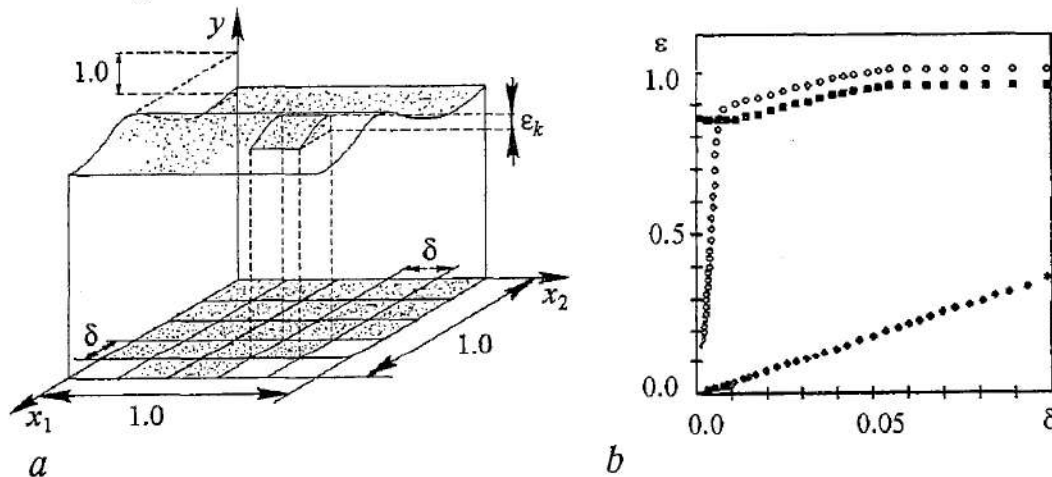


Fig. 1. (a) Illustration for a technique of testing a dependency $y(\mathbf{x})$ for single-valuedness and continuity in the case $D=2$. (b) Possible appearance of plots $\epsilon_{\max}(\delta)$ for different variants of dynamical variables

- If a single-valued and continuous dependency has a region of very steep slope (a «jump»), then ϵ_{\max} remains rather big even for sufficiently small δ . However, further decrease in δ leads to decrease in ϵ_{\max} and the graph $\epsilon_{\max}(\delta)$ exhibits a «kink» at the value of δ roughly equal to the size of the steep slope region (e.g., Fig.1,b, white circles). In such a case, the dependency $y(\mathbf{x})$ is difficult to approximate with a smooth function.

- If ϵ_{\max} remains large and does not diminish for $\delta\rightarrow 0$ (Fig. 1, b, filled squares) then the considered variables are not appropriate for global modeling. Such situation may be related both to nonuniqueness of the dependency and high noise level.

2.2. Numerical example, refinement of technique and testing for nonlinearity.

The above technique was already published and sufficiently illustrated previously [25]. Here, we describe briefly an approach to refinement of the technique and its use for assessment of nonlinearity of a dependence $y(\mathbf{x})$. Besides, we present the application of the refined technique to the analysis of a biological time series.

The procedure described in Section 2.1 is a technique with a *fixed-location* set of nonoverlapping boxes (independent of the distribution of data points). It has the disadvantage that a vector \mathbf{x} lying near a box boundary is *never* compared to the close vectors from the neighboring boxes, but it *may* be compared to more distant vectors from its own box. It can lead to intensive oscillations in the $\epsilon_{\max}(\delta)$ for small δ in the presence of noise. The nonmonotony makes the assessment of the considered dynamical variables more difficult. An example of such situation is illustrated in Fig. 2, *c*, where the results of testing are presented for chaotic regime of the logistic map $x_{n+1} = \lambda x_n^2$ at $\lambda=2.0$. The observable is $\eta_n = x_n + \xi_n$, where ξ_n is a sequence of independent identically uniformly distributed random values. We test the dependencies corresponding to the first iterate $\eta_{n+1}(\eta_n)$, to the second one $\eta_{n+2}(\eta_n)$, and to the third one $\eta_{n+3}(\eta_n)$ using the time series containing 1000 data points (see Figs 2, *a, b* for noise-free data).

The disadvantage of the technique may be obviated by using the set of overlapping boxes centered at the vectors of the time series (data-dependent location) instead of the fixed-location set of boxes. In other words, for each vector $\mathbf{x}(t_i)$ one should consider all its δ -neighbors, i.e. to calculate local variation of y in the box with the side 2δ centered at $\mathbf{x}(t_i)$. The number of considered boxes is then equal to the number of vectors N_0 . The largest value of local variation obtained in such a way (let us denote it ϵ_{\max}') monotonically decreases with decrease in δ . This advantage of the modified procedure is illustrated in Fig. 2, *c, d* for the above mentioned case of the logistic map.

Due to this advantage, the plot $\epsilon_{\max}'(\delta)$ is more reliable and informative. Note also, that the plot $\epsilon_{\max}'(\delta)$ is a straight line if the system under investigation is linear. Therefore the plot $\epsilon_{\max}'(\delta)$ can serve as a test for linearity. Its concavity indicates nonlinearity of the system under investigation (Fig. 2, *d*). As an example of the proposed techniques application to a complex real-world system, let us briefly consider testing of an acoustic time series. This is a digitized recording of the human voice (in fact, air pressure variations), which was done when a man was pronouncing the sound [a:]. Sampling frequency is 44.1 kHz. The recording length is 10000 data points. A dependence

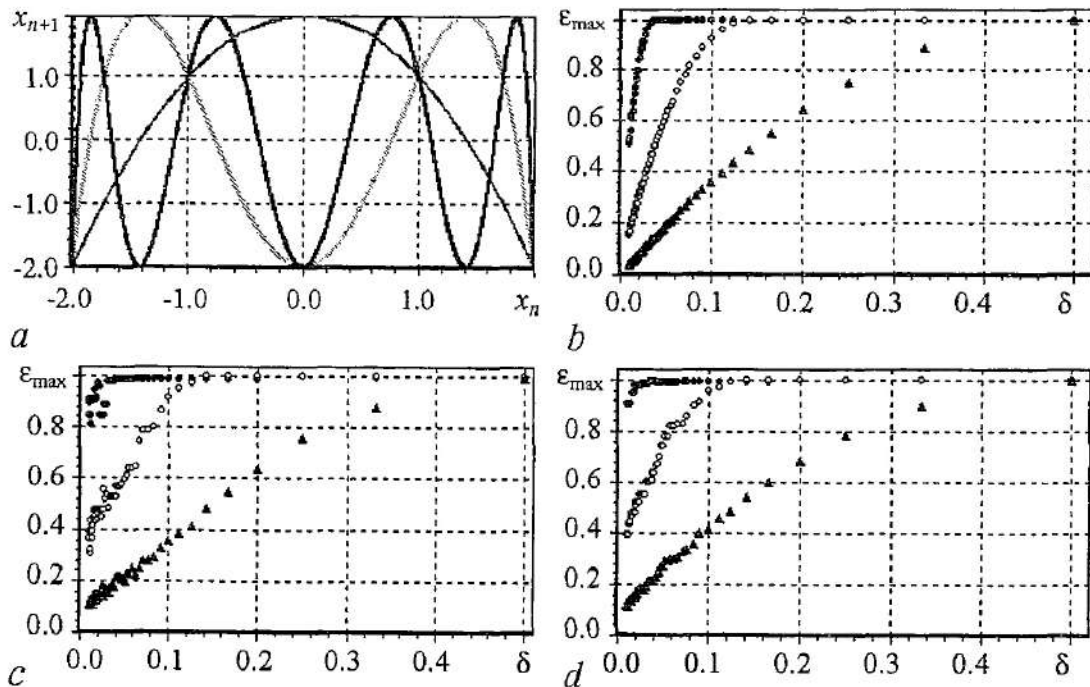


Fig. 2. Comparison of testing techniques in a numerical experiment. (a) The first, the second, and the third iterations of the chaotic logistic map. (b), (c) Results of testing with the fixed-set-of-boxes technique from noise-free and noisy data, respectively. (d) Results of testing with the modified technique from noisy data

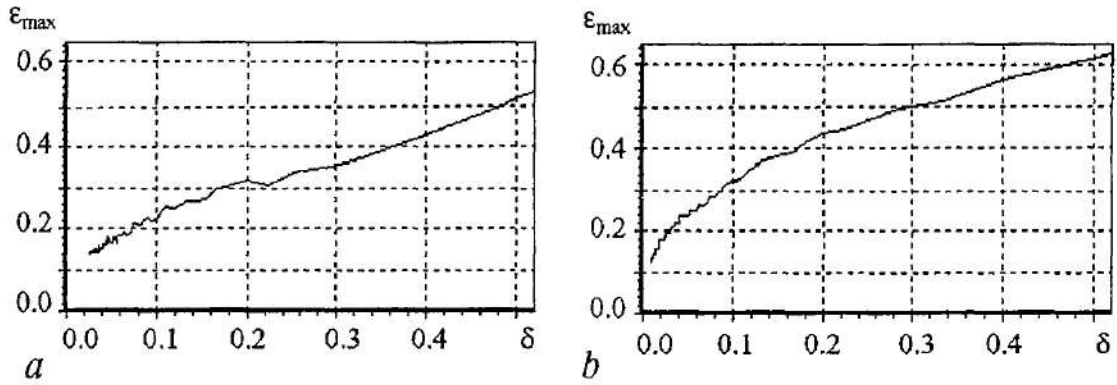


Fig. 3. Testing vocal time series described in Section 2.2. (a) The fixed-location set of boxes technique indicates many-valuedness. (b) The modified techniques indicates also nonlinearity

$\eta_{i+2}(\eta_i, \eta_{i-2}, \eta_{i-4})$ is tested. We present the plot $\epsilon_{\max}(\delta)$ in Fig. 3, a; it does not indicate single-valuedness. Other conclusions can hardly be drawn from the figure because of the above-mentioned disadvantages of the fixed-location set of boxes technique. The modified technique leads to the monotone plot $\epsilon_{\max}'(\delta)$ (Fig. 3, b). It is easily seen that the dependence $\epsilon_{\max}'(\delta)$ is significantly concave that allow a conclusion about nonlinearity of the system under investigation.

3. Detection of spurious polynomial terms

Choice of the model function F is also very important problem, which comes into play after selection of dynamical variables. In the typical case of absence of detailed a priori information about proper function form, one usually uses algebraic polynomials relying upon many rigorous mathematical results (Weierstrass' theorem). But model with polynomials are often inefficient because of their very bad extrapolation properties that are determined by the presence of «spurious» terms (basis functions).

Theoretically, polynomial terms should be regarded as spurious if «true» values of their coefficients (coefficients of the «true» function expansion in a power series) are equal to zero. Detection with subsequent exclusion of several spurious terms from the model polynomial can lead to significant refinement of the model. But, different approaches to detection of spurious terms have been suggested: small absolute values of the corresponding coefficients [2], small values of the coefficients with respect to their standard deviation (Student's criterion), intensive variation of coefficients around zero when different parts of a transient time series are used for reconstruction [14], slight change of the approximation error when the term is excluded from the model [19]. Here we develop a new (and, in our opinion, more general) approach to detection of spurious terms.

Again, theoretically, rather typical situation is such that neither of terms is spurious. If the true function is, e.g., exponential, its expansion in a power series involves nonzero coefficients at each power of a variable. In such a situation, when time series is analyzed, adding of each term to a model structure would lead to decrease of the approximation error. Nonetheless, some of the terms are undesirable (practically spurious). We state that those terms are practically spurious which affect approximation errors only in a narrow domain of the phase space. We conjecture that such terms can be detected as those terms whose coefficients depend strongly on the distribution of the data points in the phase space. (If all coefficients slightly depend on the distribution of data points, one may reasonably guess that such model function describe an object not only for the domain explored by the observed training time series, but also in its neighborhood, that is the function has good extrapolation properties.)

To determine how strongly a coefficient value depends on the distribution of training data points, consider its change under variation of the weight function $p(x_i)$ if coefficients values α_k are found by minimizing the weighted squared sum of errors

$$s^2 = \sum_{i=1}^N p(x_i) [F(x_i) - \sum_{k=1}^M \alpha_k g_k(x_i)]^2. \quad (3)$$

Here $F(x_i)$ are true (observed) values of the approximated function; $g_k(x_i)$ are basis functions (terms). Weight function $p(x_i)$ is normalized to unity $\sum_{i=1}^N p(x_i) = 1$.

If the set of basis functions is orthonormal, then coefficient values read

$$\alpha_k = \sum_{i=1}^N p(x_i) F(x_i) g_k(x_i). \quad (4)$$

Approximated function can be expressed as

$$F(t) = \sum_{k=1}^M \alpha_k g_k(x) + \tilde{F}(x), \quad (5)$$

where $\tilde{F}(t)$ is approximation error.

Let us consider now how the values of coefficients will change under slight variations of the weight function $p \rightarrow p' = p + \hat{p}$. Because of weight function normalization the variation satisfies

$$\sum_{i=1}^N \hat{p}(x_i) = 0. \quad (6)$$

Impose also the condition of smallness of variation in the form

$$\sum_{i=1}^N \hat{p}^2(x_i) = \varepsilon^2. \quad (7)$$

The change of coefficient in the linear approximation is

$$\Delta \alpha_k = \sum_{i=1}^M \hat{p}(x_i) g_k(x_i) \tilde{F}(x_i). \quad (8)$$

To estimate the intensity of coefficient variation consider $\Delta \alpha_k$ as functional of \hat{p} . For its maximum with supplementary conditions (6) and (7) we have

$$\Delta \alpha_{k_{\max}} = \varepsilon [\sum_{i=1}^N (g_k(x_i) \tilde{F}(x_i) - (1/N) \sum_{j=1}^N g_k(x_j) \tilde{F}(x_j))^2]^{1/2}. \quad (9)$$

If we suppose that at the beginning the weight function was uniform for all training time series points, that is $p(x_i) = 1/N$, then as a consequence of orthogonality of basis functions and approximation error, we have

$$\Delta \alpha_{k_{\max}} = \varepsilon [\sum_{i=1}^N (g_k(x_i) \tilde{F}(x_i))^2]^{1/2}. \quad (10)$$

As a criterion for exclusion (or inclusion) of basis function we can use the ratio between the maximum possible change of coefficient value (10) and the coefficient value itself

$$C_k = [\sum_{i=1}^M (g_k(x_i) \tilde{F}(x_i))^2]^{1/2} / [\sum_{i=1}^M g_k(x_i) F(x_i)]. \quad (11)$$

Formula (11) was derived for orthonormal basis functions. In practice this is usually not the case. However when we decide if the basis function is spurious or not we can consider only its projection orthogonal to all other basis functions $g_k'(x)$. After this we can freely use the method described above. We don't need to calculate this projection in

explicit form. Let $\tilde{F}_k(x)$ be an error of approximation in the absence of the k -th basis function, then the orthogonal projection of the k -th basis function is

$$g_k'(x) = (\tilde{F}_k(x) - \tilde{F}(x))/\alpha_k', \quad (12)$$

where α_k' is coefficient for this projection, calculated with least squares method.

After substitution of (12) into (11) for coefficient instability we have

$$C_k = [\sum_{i=1}^M (\tilde{F}_k(x_i) - \tilde{F}(x_i))^2 (\tilde{F}(x_i))^2]^{1/2} / [\sum_{i=1}^M (\tilde{F}_k(x_i) - \tilde{F}(x_i)) \tilde{F}(x_i)]. \quad (13)$$

Above we talked about exclusion of spurious terms from initially large basis, but adding the most suitable functions can also optimize the basis functions set. We can choose them using the same methodology, according to minimal value of criterion (13).

Let us illustrate proposed method on test example. The realization of x variable from Rössler system in chaotic regime is used as time series. Fig. 4, *b* shows phase trajectory of this system reconstructed with time delay method. Model is constructed in the form

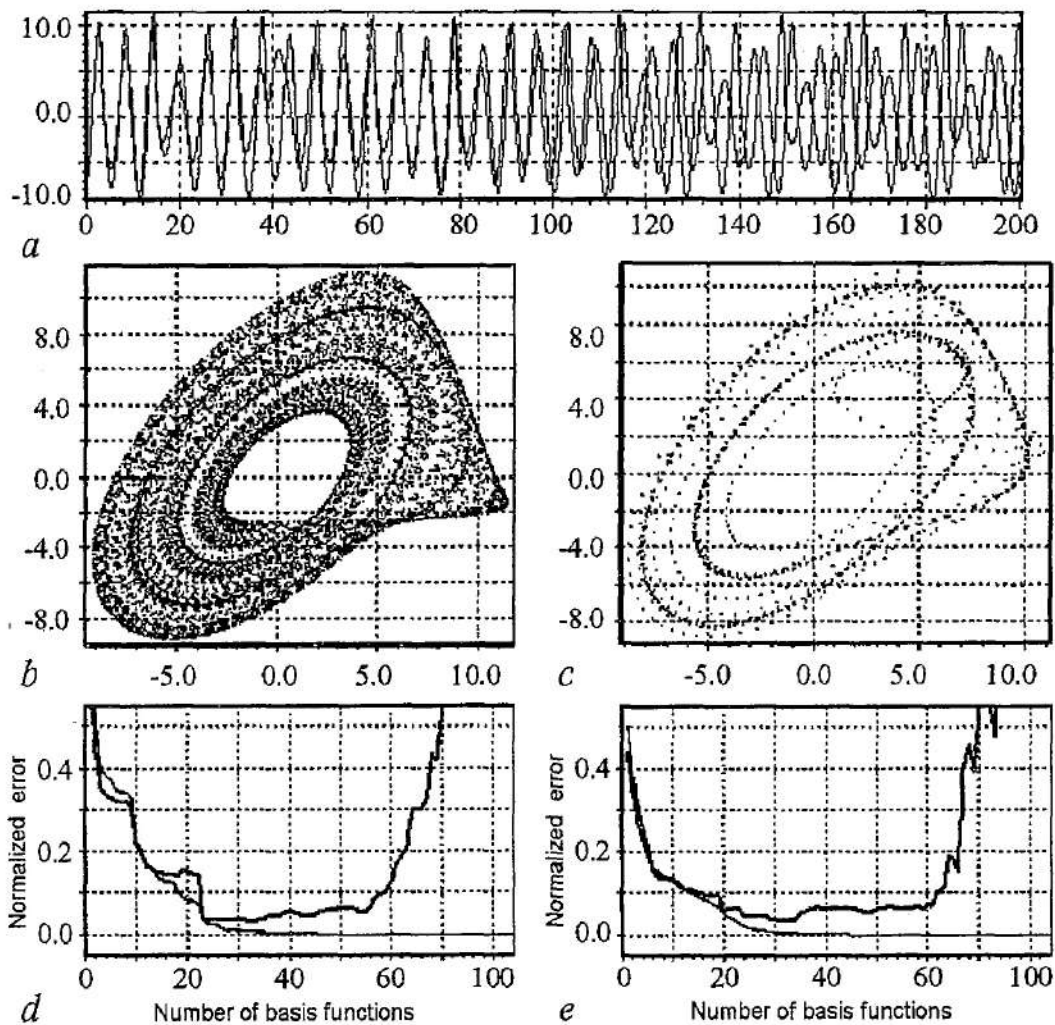


Fig. 4. (a) Comparison of test part of time series generated by Rössler system in chaotic regime with time series generated by optimized model. Good prediction for about 6 quasi-periods is observed. (b) Phase trajectory of Rössler system reconstructed with delay method from time series of x variable. (c) Phase trajectory generated by optimized model. (d) Error of approximation of training time series (thin curve) and error of test time series prediction (bold curve) as a function of basis functions number, added during process of basis functions set optimization with new method. (e) The same as (d) for old method

$$\begin{aligned}
dx_1/dt &= x_2, \\
dx_2/dt &= x_3, \\
dx_3/dt &= f(x_1, x_2, x_3).
\end{aligned}
\tag{14}$$

If we transform the Rössler equations into the form (14) we will have rational function f . We will try to construct the model in universal form using polynomial of the 6th order as function f . The short part of 200 data points (about 3 quasi-periods) is used as training time series. Let us add to initially empty basis such function for which the relative variation of coefficient (13) is minimal.

In Fig. 4, *d* the dependencies of training series approximation error (thin curve) and error of prediction of test time series (bold curve) on the number of added basis functions are shown. Errors are normalized by the standard deviation of the third derivative dx_3/dt of training time series. One can see that training series approximation error decreases monotonous, while the prediction error for test part of time series has minimum when the number of basis functions is 32 and it is equal to 0,032 (3.2% of standard deviation). At this moment the error on training series is 0.008. Before optimization (when we use full polynomial of the 6th order) the behavior of the model was divergent. After optimization the model generates stable trajectories and allows prediction of about 6th quasi-periods of test time series. In Fig. 4, *c* the phase trajectory generated by the model is shown. One can see that the trajectory is located in the same phase space domain as the trajectory of Rössler system, but the cycle of period 2 is eventually established.

In Fig. 4, *e* for comparison purposes the results of optimization of basis functions set with previously known method is shown. In this method we add to the basis such functions that allows maximal decrease of approximation error. One can see that the sequence of adding basis functions is different from proposed method. The best basis according to test series prediction error includes 33 functions. This best error is 0.034 (slightly worse than with new method), error of training time series approximation 0.006. The behavior of the optimal (from this point of view) model turns out to be divergent. So we can state that in this example new proposed method of optimization outperforms the well-known one.

4. Determining character of coupling between subsystems from time series

The problem of determining the presence and direction of interaction between two subsystems is very important in many fields, including physiology and medicine where interaction between human cardio-vascular and respiratory systems [26,27] and between different brain areas are of interest [28-30]. Thus, recently Rosenblum and Pikovsky suggested a very delicate and nice idea for characterization of weak coupling between subsystems from time series by estimating coefficients of a model map [21]. But their method works well for the case of very long time series (for «reasonable» noise level, time series should contain about $10^4 \dots 10^5$ data points). In practice, nonstationarity of processes, impossibility to collect sufficient amount of data, and significant noise often require estimation of the interaction (coupling) characteristics under conditions of short observation interval. Here, we develop an extension of Rosenblum and Pikovsky approach to the case of short* and noisy time series. For a detailed consideration see [32].

* E.g., typical quasi-stationary segments of electroencephalogram (EEG) is about 5 seconds long [31]. EEGs are recorded at typical sampling rate of 200 Hz. Then, quasi-stationary segment contains about 10^3 data points. Roughly speaking, typical length of a short time series in practice is of the order of 10^3 data points.

4.1. Evolution map approach. The technique of Rosenblum and Pikovsky is based on construction of empiric model maps, describing *phase dynamics* of the subsystems, and is called *evolution map approach*. Having an original time series $\{\eta_{1,2}(t_i)\}_{i=1}^N$, where η_1, η_2 are observables, $t_i=i\Delta t$, $i=1, \dots, N$, Δt is a sampling interval, one calculates the time realizations of phases $\{\phi_{1,2}(t_i)\}_{i=1}^{N_s}$ and construct a global model map, which characterizes the dependence of phase increments (over a time interval $\tau\Delta t$) on the phases of subsystems' oscillations, in the form

$$\Delta_{1,2}(t) = \phi_{1,2}(t+\tau\Delta t) - \phi_{1,2}(t) = F_{1,2}(\phi_{1,2}(t), \phi_{2,1}(t), \mathbf{a}_{1,2}), \quad (15)$$

where τ is positive integer; $\mathbf{a}_{1,2}$ are vectors of the coefficients of the functions $F_{1,2}$; $F_{1,2}$ are trigonometric polynomials:

$$F_1(\phi_1, \phi_2) = \sum_{i=1}^{L_1} a_{1,i} g_i(\phi_1, \phi_2), \quad (16)$$

with $g_1=1$; $g_i=\cos(m_i\phi_1+n_i\phi_2)$ for even $i\geq 2$; $g_i=\sin(m_i\phi_1+n_i\phi_2)$ for odd $i\geq 3$; L_1 is the number of terms of the polynomial F_1 . For $i\geq 2$, $m_{2i}=m_{2i+1}$ are nonnegative integer, $n_{2i}=n_{2i+1}$ are arbitrary integer, and by definition $m_1=1$, $n_1=0$.

Using the estimates of coefficients $\hat{\mathbf{a}}_{1,2}$, obtained from the time series via the least-squares routine, one computes intensities of influence of the second subsystem on the first one ($2\rightarrow 1$) \hat{c}_1 as

$$\hat{c}_1^2 = 1/(2\pi^2) \int_0^{2\pi} \int_0^{2\pi} (\partial F_1(\phi_1, \phi_2, \hat{\mathbf{a}}_1) / \partial \phi_2)^2 d\phi_1 d\phi_2 = \sum_{i=1}^{L_1} n_i^2 \hat{a}_{1,i}^2. \quad (17)$$

Everything is similar for the influence of the first subsystem on the second one ($1\rightarrow 2$) \hat{c}_2 . Directionality index is defined as $\hat{d}=(\hat{c}_2-\hat{c}_1)/(\hat{c}_2+\hat{c}_1)$. Since $\hat{c}_{1,2}\geq 0$, \hat{d} takes the values only within the interval $[-1,1]$: $\hat{d}=1$ or $\hat{d}=-1$ corresponds to unidirectional coupling ($1\rightarrow 2$ or $2\rightarrow 1$, respectively), $\hat{d}=0$ for ideally symmetric coupling.

4.2. Short time series. For very long time series ($N\rightarrow\infty$) the estimates \hat{c}_1 , \hat{c}_2 , and \hat{d} are unbiased and have practically no scattering, in other words, the method gives correct characterization of coupling. However, if the time series is short, the following important questions arise. Are the estimates $\hat{c}_{1,2}$, \hat{d} biased or not? How can statistical significance of the results be estimated? To illustrate importance of the questions, let us consider a simple *demonstrative example*, when two subsystems are uncoupled and linear, that is a system of difference equations

$$\Delta_{1,2}(t) = \phi_{1,2}(t+2\pi) - \phi_{1,2}(t) = 2\pi\omega_{1,2} + \varepsilon_{1,2}(t), \quad (18)$$

where $\varepsilon_{1,2}$ are Gaussian random processes independent of each other with variances $2\pi D_{1,2}$. Obviously, correct values of coupling should be $c_1=c_2=d=0$ in this case.

We have carried out numerical experiment in the following way. Time realizations of original equations were simulated using the generator of pseudo-random numbers realized in the subroutine DRNNOR of the library IMSL. Initial conditions for each realization are random numbers $\phi_1(0), \phi_2(0)$ distributed uniformly on the interval $[0, 2\pi]$. We obtained 1000 short time realizations (1000 pairs of scalar time series) with the length $N_\phi=10^3$. The values of estimates $\hat{c}_{1,2}$ and \hat{d} are computed for each of them. From the obtained sets of values we construct histograms.

The estimates $\hat{c}_{1,2}$ and \hat{d} appear misleading. Their distributions are shown in Fig. 5. Thus, in the case of identical subsystems ($D_1=D_2$ and $\omega_1=\omega_2$) \hat{c}_1 is always positive and

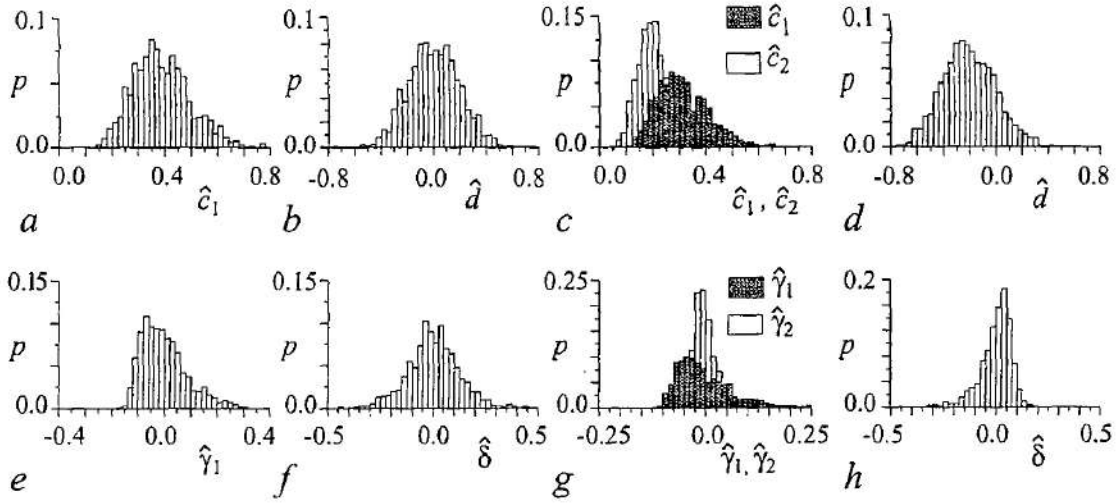


Fig. 5. Histograms for the estimates of coupling, constructed as a result of processing of 1000 time realizations of the equations (16) with $\omega_1=\omega_2=1.0$ (a), (b) \hat{c}_1 (a biased estimate) and \hat{d} for identical subsystems with $D_1=D_2=0.4$. (c), (d) \hat{c}_1, \hat{c}_2 (exhibit different biases) and \hat{d} (exhibits negative bias) for subsystems with different noise levels $D_1=0.4, D_2=0.1$. (e), (f), (g), and (h) $\hat{\gamma}_1, \hat{\gamma}_2$, and $\hat{\delta}$ (unbiased estimates) for the situations corresponding to (a), (b), (c), and (d), respectively

takes sufficiently large values (Fig. 5, a), i.e. it is a biased estimate for $c_1=0$; \hat{d} is unbiased, but exhibits quite a large scattering; even the values of $\hat{d}=\pm 0.4$ are encountered quite often (Fig. 5, b). Thus, it is very probable to get spurious indication of the presence of interaction from a single realization. The situation becomes even more complicated when subsystems are nonidentical. It is illustrated in Fig. 5, c, d for the case $D_1>D_2$, $\omega_1=\omega_2$. The estimates $\hat{c}_{1,2}$ are biased, bias in \hat{c}_1 being greater (Fig. 5, c). This leads to biasedness of \hat{d} whose values are *systematically* less than zero (Fig. 5, d). Hence, predominant influence ($2 \rightarrow 1$) is diagnosed, even though coupling is absent in reality.

4.3. Corrections to evolution map approach and novel unbiased estimates of coupling. By careful analytic consideration of the problem we found out the cause of biases and developed corrected estimates of coupling [32]. Novel unbiased estimate of c_1^2 is the quantity

$$\hat{\gamma}_1 = \hat{c}_1^2 - \sum_{i=1}^{L_1} n_i^2 \hat{\sigma}_{a_{1i}}^2, \quad (19)$$

where $\hat{\sigma}_{a_{1i}}^2$ are unbiased estimates of variances $\sigma_{a_{1i}}^2$. Derivation of $\hat{\sigma}_{a_{1i}}^2$ is not trivial. Under some simplifying assumptions (noise $\epsilon_{1,2}(t)$ are Gaussian, coupling between subsystems and their individual nonlinearities are very weak) we obtain the following analytic expression for $\hat{\sigma}_{a_{1i}}^2$:

$$\hat{\sigma}_{a_{1i}}^2 = (2\hat{\sigma}_{\epsilon_1}^2/N)[1 + 2\sum_{j=1}^{\tau-1} (1-j/\tau) \cos((m\hat{a}_{1,1} + n\hat{a}_{2,1})j/\tau) e^{-j(m\hat{\sigma}_{\epsilon_1}^2 + n\hat{\sigma}_{\epsilon_2}^2)/2\tau}], \quad i>1, \quad (20)$$

where $\hat{\sigma}_{\epsilon_{1,2}}^2$ are estimates of noise variances, their derivation is straightforward. Normalized index d is replaced by nonnormalized quantity $\delta = c_2^2 - c_1^2$, whose unbiased estimator is $\hat{\delta} = \hat{\gamma}_2 - \hat{\gamma}_1$.

To estimate reliability of numbers $\hat{\gamma}_{1,2}$ and $\hat{\delta}$ obtained from a single realization, one needs the estimate of variance of $\hat{\gamma}_1$ (we denote it as $\hat{\sigma}_{\hat{\gamma}_1}^2$). After some algebra and

experimentation, we derive a semiempiric formula [32] for $\hat{\sigma}_{\hat{\gamma}_1}^2$ in terms of estimates $\hat{a}_{1,i}$ and $\hat{\sigma}_{a_{1,i}}^2$ derived earlier, we do not present it here for the sake of brevity. Since $\hat{\gamma}_1$ has a skewed distribution for low order trigonometric polynomials $F_{1,2}$ typically used, we take asymmetric expression $[\hat{\gamma}_1 - \alpha \hat{\sigma}_{\hat{\gamma}_1}, \hat{\gamma}_1 + \beta \hat{\sigma}_{\hat{\gamma}_1}]$ as a confidence interval for c_1^2 . We found constants α and β empirically to provide necessary significance level; 95% confidence interval is obtained if $\alpha=1.6$, $\beta=1.8$. Conclusion about the presence of influence ($2 \rightarrow I$) can be drawn with probability of error 0.025 provided

$$\hat{\gamma}_1 - \alpha \hat{\sigma}_{\hat{\gamma}_1} > 0. \quad (21)$$

The degree of belief can be adjusted by changing α (and, hence, confidence interval width).

Conclusion of predominant direction of interaction can be drawn after estimation of the variance of $\hat{\delta}$. Its «good» estimate is $\hat{\sigma}_{\hat{\delta}}^2 = \hat{\sigma}_{\hat{\gamma}_1}^2 + \hat{\sigma}_{\hat{\gamma}_2}^2$. Our experiments show, that $\alpha=1.6$ also provides approximately 95% confidence interval for δ in the form $\hat{\delta} \pm \alpha \hat{\sigma}_{\hat{\delta}}$. More accurately, the values

$$\hat{\gamma}_2 - \alpha \hat{\sigma}_{\hat{\gamma}_2} > 0 \quad \text{and} \quad \hat{\delta} - \alpha \hat{\sigma}_{\hat{\delta}} > 0 \quad (22)$$

allow the statement about influence ($I \rightarrow 2$) with probability of error 0.025 (similarly for ($2 \rightarrow I$)).

Results of application of the proposed estimates $\hat{\gamma}_{1,2}$ and $\hat{\delta}$ to the above mentioned example (17) are presented in Fig. 5, e-h. Systematic errors in $\hat{\gamma}_{1,2}$ and $\hat{\delta}$ are absent. Fig. 6 demonstrates usefulness of the interval estimates to ensure reliable conclusions of coupling direction.

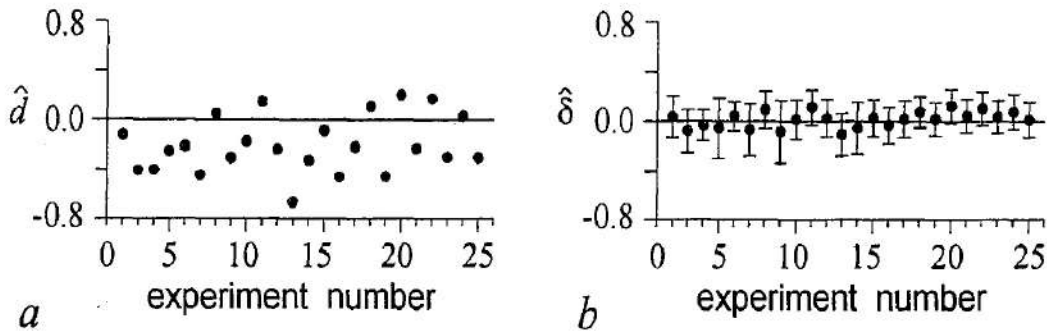


Fig. 6. Estimates of coupling for example (17), results obtained for the first 25 of the 1000 time realizations of the subsystems with different noise levels $D_1=0.4$, $D_2=0.1$. (a) \hat{d} takes predominantly negative values. (b) $\hat{\delta}$ (circles) takes negative as well as positive values, estimated confidence intervals are shown as error bars and, as a rule, include zero

5. Summary

This paper illustrates some important details of the procedure of constructing mathematical model from a time series. Namely, three main subproblems are selected and their peculiarities are shown. Special techniques for better solutions of two of them are proposed:

- preliminary testing of time series of dynamical variables, which provides the variants which are the most suitable for modeling and allows convenient testing of experimental dependencies for nonlinearity;
- a procedure of model structure optimization, which allows elimination of

spurious terms from the polynomial model, whereby model performance can be significantly refined.

Finally, we have developed an approach to estimation of intensity and directionality of coupling between two subsystems in the case of short and noisy time series. Under certain assumptions (nonlinearity of subsystems and coupling between them are weak), *unbiased* estimates of intensity and directionality of interaction *provided with confidence* intervals are derived. In our opinion, suggested estimates are applicable for wide range of real-world processes, including signals of biologic origin when it is important to analyze short time series segments due to nonstationarity.

The work was supported by the RFBR (grant №. 02-02-17578), CRDF (Award REC-006), and the Russian Ministry of education.

References

1. Crutchfield J.P. and McNamara B.S. Equations of motion from a data series // Complex Systems. 1987. Vol. 1. P. 417-452.
2. Judd K., Mees A.I. On selecting models for nonlinear time series // Physica D. 1995. Vol. 82. P. 426-444.
3. McSharry P.E. and Smith L.A. Better nonlinear models from noisy data: Attractors with maximum likelihood // Phys. Rev. Lett. 1999. Vol. 83, №. 21. P. 4285-4288.
4. Baake E., Baake M., Bock H.J., and Briggs K.M. Fitting ordinary differential equations to chaotic data // Phys. Rev. A. 1992. Vol. 45, № 8. P. 5524-5529.
5. Brown R., Rulkov N.F., and Tracy E.R. Modeling and synchronizing chaotic systems from time-series data // Phys. Rev. E. 1994. Vol. 49, № 5. P. 3784-3800.
6. Gouesbet G., Letellier C. Global vector-field approximation by using a multivariate polynomial approximation on nets // Phys. Rev. E. 1994. Vol. 49. P. 4955-4972.
7. Hegger R., Kantz H., Schmuser F., Diestelhorst M., Kapsch R.-P., and Beige H. Dynamical properties of a ferroelectric capacitors observed through nonlinear time series analysis // Chaos. 1998. Vol. 8, № 3. P. 727-754.
8. Janson N.B., Pavlov A.N., and Anishchenko V.S. One method for restoring inhomogeneous attractors // Int. J. of Bifurc. and Chaos. 1998. Vol. 8, № 4. P. 825-833.
9. Anishchenko V.S. and Pavlov A.N. Global reconstruction in application to multichannel communication // Phys. Rev. E. 1998. Vol. 57, № 2. P. 2455-2457.
10. Anishchenko V.S., Pavlov A.N., and Janson N.B. Global reconstruction in the presence of a priori information // Chaos, Solitons & Fractals. 1998. Vol. 8. P. 1267-1278.
11. Pavlov A.N., Janson N.B., and Anishchenko V.S. Reconstruction of dynamical systems // Radiotekh. i Electron. 1999. Vol. 44, № 9. P. 1075-1092.
12. Anosov O.L., Butkovskii O.Ya., and Kravtsov Yu.A. Reconstruction of dynamical systems from chaotic time series: brief review // Izv. VUZ. Applied Nonlinear Dynamics. 2000. Vol. 8, № 1. P. 29-51.
13. Bezruchko B. and Smirnov D. Constructing nonautonomous differential equations from a time series // Phys. Rev. E. 2001. Vol. 63. 016207.
14. Bezruchko B., Dikanev T., and Smirnov D. Role of transient processes for reconstruction of model equations from time series // Phys. Rev. E. 2001. Vol. 64. 036210.
15. Timmer J., Rust H., Horbelt W., and Voss H.U. Parametric, nonparametric and parametric modelling of a chaotic circuit time series // Phys. Lett. A. 2000. Vol. 274. P. 123-134.
16. Horbelt W., Timmer J., Bunner M.J., Meucci R., and Ciofini M. Identifying physical properties of a CO₂-laser by dynamical modeling of measured time series // Phys. Rev. E. 2001. Vol. 64. 016222.

17. Sauer T., Yorke J.A., and Casdagli M. Embedology // J. Stat. Phys. 1991. Vol. 65, № 3-4. P. 579-616.
18. Le Sceller L., Letellier C., and Gouesbet G. Structure selection for global vector field reconstruction by using the identification of fixed points // Phys. Rev. E. 1999. Vol. 60, № 2. P. 1600-1606.
19. Aguirre L.A., Freitas U.S., Letellier C., Maquet J. Structure-selection techniques applied to continuous-time nonlinear models // Physica D. 2001. Vol. 158. P. 1-18.
20. Small M., Judd K. and Mees A. Modeling continuous processes from data // Phys. Rev. E. 2001. Vol. 65. 046704.
21. Rosenblum M.G. and Pikovsky A.S. Detecting direction of coupling in interacting oscillators // Phys. Rev. E. 2001. Vol. 64. 045202(R).
22. Letellier C., Maquet J., Le Sceller L., Gouesbet G., and Aguirre L.A. On the non-equivalence of observables in phase space reconstructions from recorded time series // J. Phys. A: Math. Gen. 1998. Vol. 31. P. 7913-7927.
23. Letellier C., Aguirre L.A. Investigating nonlinear dynamics from time series: The influence of symmetries and the choice of observables // Chaos. 2002. Vol. 12, № 3. P. 549-558.
24. Kaplan D.T. Exceptional events as evidence for determinism // Physica D. 1994. Vol. 73. P. 738-748.
25. Smirnov D., Bezruchko B. and Seleznev Ye. Choice of dynamical variables for global reconstruction of model equations from time series // Phys. Rev. E. 2002. Vol. 65. 026205.
26. Bracic-Lotric M. and Stefanovska A. // Physica A. 2000. Vol. 283. P. 451.
27. Janson N.B., Balanov A.G., Anishchenko V.S., McClintock P.V.E. // Phys. Rev. E. 2002. Vol. 65. 036212.
28. Arnhold J., Grassberger P., Lehnertz K., and Elger C.E. // Chaos in Brain? / Eds K. Lehnertz, J. Arnhold, P. Grassberger, and C.E. Elger. World Scientific, 2000, p. 325.
29. Rodriguez E. et al. // Nature (London) 1999. Vol. 397. P. 430.
30. Andrzejak R.G., Lehnertz K., Mormann F., Rieke C., David P., and Elger C.E. // Phys. Rev. E. 2001. Vol. 64. 061907.
31. Kaplan A.Ya. // Uspekhi Fiziol. Nauk. 1998. Vol. 29(3). P. 35.
32. Smirnov D. and Bezruchko B. Estimation of interaction strength and direction from short and noisy time series // Phys. Rev. E. 2003, to be published.

Saratov State University
 Institute of RadioEngineering
 and Electronics of RAS, Saratov Branch

Received 04.09.03

УДК 517.9: 519.6

ТРИ ПОДЗАДАЧИ РЕКОНСТРУКЦИИ ГЛОБАЛЬНОЙ МОДЕЛИ ПО ВРЕМЕННЫМ РЯДАМ И ИХ ОСОБЕННОСТИ

Т. Диканев, Д. Смирнов, В. Пономаренко, Б. Безручко

Мы рассматриваем три основные подзадачи глобальной реконструкции динамических моделей по временным рядам: выбор динамических переменных, выбор функций модели и определение параметров модели. Представлены

специальные методы для их решения. Обсуждаются их приложения и перспективы дальнейшего развития методов эмпирического моделирования. Данные подходы иллюстрируются в численных и акустических экспериментах.



Smirnov Dmitry Alekseyevich was born in 1977. He studied physics in Department of Nonlinear Processes of Saratov State University (DNP SSU) and graduated in 1999. He performed his candidate dissertation work in DNP SSU and Saratov Department of Institute of Radio Engineering and Electronics of RAS (SD IRE RAS) and obtained the Ph.D. degree in 2001. He has received several international and Russian awards for young scientists. Now, he is a senior researcher in Laboratory of Nonlinear Dynamical Modeling of SD IRE RAS. His scientific interests include mathematical modeling of complex systems, time series analysis, and dynamical systems theory. He is an author of more than 45 publications including 14 papers in refereed journals.



Bezruchko Boris Petrovich was born in 1946. He graduated from Department of Physics, Saratov State University (1969). He is a doctor of Physics and Mathematics (he obtained this degree in 1995) and a professor in the Chair of Electronics, Oscillations, and Waves of Saratov State University. Field of his scientific activity involves experimental investigation of nonlinear phenomena in radiophysical and electronic systems, mathematical modeling from experimental observable time series. He published more than 100 papers in Russian and foreign journals.



Izv. VUZ «AND», vol.11, № 3, 2003

INVESTIGATING THE TRANSITION TO PHASE SYNCHRONIZATION IN EXPERIMENTAL NONLINEAR OPTICS

S. Boccaletti, E. Allaria, R. Meucci, and F.T. Arecchi

The transition route to phase synchronization in a chaotic laser with external modulation is investigated. We show evidence of the presence of a regime of periodic phase synchronization, where phase slips occur with maximal coherence in the phase difference between output signal and external modulation. We demonstrate that such a regime occurs at the crossover point between two different scaling laws of the intermittent type behavior of phase slips.

Synchronization phenomena in coupled chaotic systems has been a topic of great interest over the past decade [1-5], insofar as its relevance and ubiquitousness have been demonstrated in laboratory experiments [6], as well as in natural phenomena [7]. These processes happen when several coupled or forced chaotic units correlate with each other a given property of their motion, and they encompass behaviors ranging from a perfect locking of the chaotic trajectories [1], to the emergence of a functional relationship relating the chaotic outputs [8], to a weaker form of correlation consisting in the locking of the phases of the systems [3,4].

This latter behavior has been called phase synchronization (PS). There, a coupling or a forcing induce a phase locked regime, where the amplitudes remain chaotic and almost uncorrelated, whereas the difference between the two free running [3] phases $\Phi_{1,2}$ evolves in a bounded manner and obeys the synchronization relation

$$\Delta = |\Phi_1 - \Phi_2| < \text{const.} \quad (1)$$

PS was first demonstrated in mutually coupled [3] or periodically forced chaotic oscillators [4], and later observed in theoretical models [8] and experiments [9,10]. In particular, PS has been shown to play a crucial role in many physiological systems, such as human heartbeat and respiration [11], magnetoencephalography and electromyography of Parkinsonian patients [12], and electroencephalograms during visual stimulations [13].

Being PS the weakest stage of synchronization, a relevant issue is to understand the transition route to such a behavior from unsynchronized motion. On the border of PS, the dynamical evolution of the system is characterized by epochs of almost constant phase difference intermittently interrupted by sudden 2π jumps in Δ , which are called *phase slips*.

For coupled or forced periodic oscillators, the transition to PS corresponds to a

saddle-node bifurcation, and the average duration τ between successive phase slips obeys a type-I intermittency scaling law [14] $\tau \sim |P - P_c|^{-1/2}$, P being the relevant parameter of the transition (either the coupling strength or the external frequency), and P_c denoting its transitional value to PS.

A different scenario emerges for chaotic systems. If one considers a forced chaotic oscillator, and supposes that the system is phase synchronized for $\nu < \nu_c$, at forcing frequencies $\nu \geq \nu_c$, one observes another transition point $\nu_r > \nu_c$, such that for $\nu > \nu_r$, the scaling law for τ is the same as the classical case ($\tau \sim |\nu - \nu_c|^{-1/2}$), while for $\nu_c < \nu < \nu_r$, the intermittency shifts from type-I to that of superlong laminar periods described by $\ln(1/\tau) \sim -|\nu - \nu_c|^{-1/2}$. The theoretical picture of this transition has been described as a boundary crisis mediated by an unstable-unstable pair bifurcation [15], and the two above scaling behaviors have been numerically reported for coupled chaotic model systems [16].

Another important feature of such transition is that it can be identified by inspection of the Lyapunov spectrum. Precisely, PS is set around the passage to a negative value of a Lyapunov exponent that was zero in the uncoupled or unforced regime [3]. More recently, it has been demonstrated that the transition from no synchronization to PS is mediated by a regime, called *periodic phase synchronization* (PPS), where the time intervals between successive phase slips are almost equal to one another [17].

In this communication, we review the main features of the entire transition route from no synchronization to PS, that were firstly observed by us in Ref. [18]. The experimental setup is sketched in Fig. 1, *a* and consists of a CO₂ laser tube, pumped by an electric discharge current of 6 mA and inserted within an optical cavity closed by a totally reflecting mirror and a partially reflecting one. The detected laser output intensity suitably amplified drives an intracavity electro-optic modulator that controls the cavity losses. The feedback loop is realized by the voltage exiting a HgCdTe fast infrared diode detector, conveyed into an amplifier together with a bias voltage B_0 , and driving the electro-optic modulating crystal. Under these conditions, and in the absence of any further modulation, the output intensity consists of a train of homoclinic spikes repeating at chaotic times and interconnected by minor oscillations [10] (see Fig. 1; *b*). This sequence of homoclinic

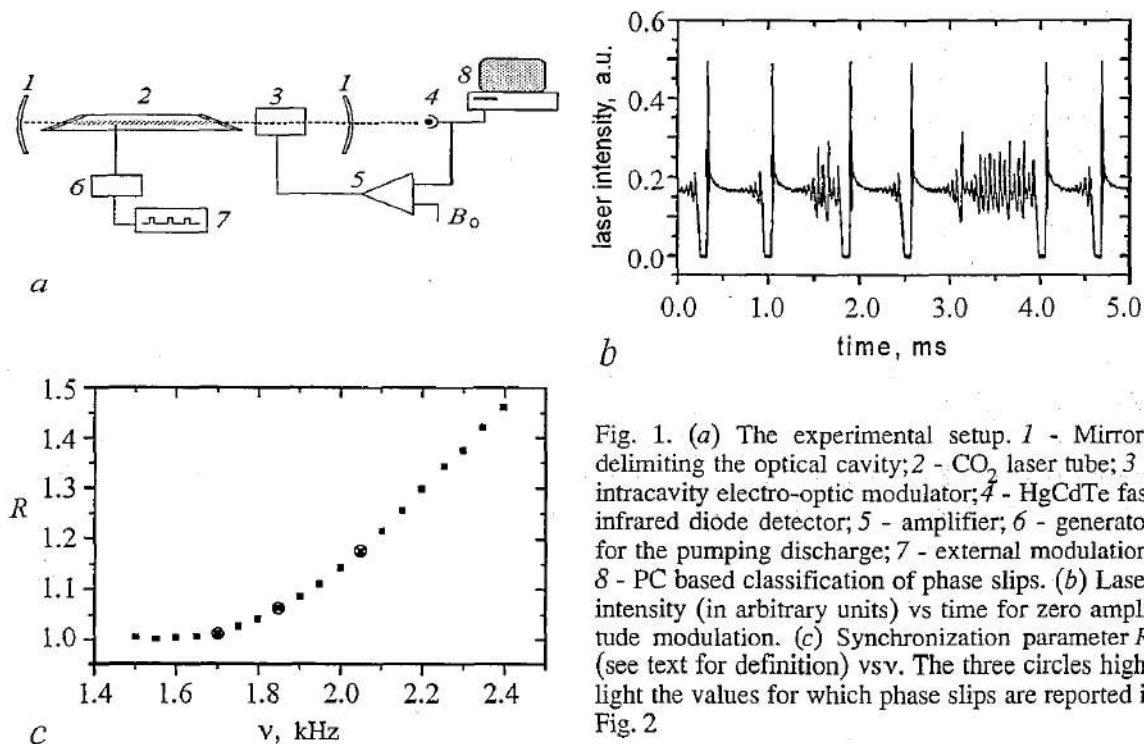


Fig. 1. (a) The experimental setup. 1 - Mirrors delimiting the optical cavity; 2 - CO₂ laser tube; 3 - intracavity electro-optic modulator; 4 - HgCdTe fast infrared diode detector; 5 - amplifier; 6 - generator for the pumping discharge; 7 - external modulation; 8 - PC based classification of phase slips. (b) Laser intensity (in arbitrary units) vs time for zero amplitude modulation. (c) Synchronization parameter R (see text for definition) vs ν . The three circles highlight the values for which phase slips are reported in Fig. 2

spikes can be phase entrained by an external sinusoidal modulation [10]. By adding a square signal modulation in the pumping discharge whose amplitude provides a 2% perturbation in the electric discharge current, one enters a regime of PS. The modulation is applied on a control unit of the generator (element 6 in Fig. 1, a). As for phases, the phase Φ_e of the external modulation evolves linearly in time ($\Phi_e = 2\pi\nu t$), and the phase Φ_s of the chaotic signal is calculated by linear interpolation between successive spiking times following the rule $\Phi_s = 2\pi k + 2\pi(t - T_k)/(T_{k+1} - T_k)$, $T_k \leq t < T_{k+1}$, where T_k denotes the time at which the k^{th} spike is produced. We call R the ratio between the number of maxima in the input modulation and the number of output spikes, and report in Fig. 1, c the route toward PS ($R=1$) as ν approaches $\nu_c \approx 1.62$ kHz.

We record sequences of more than 150 000 interspike intervals and study the occurrence of phase slips in the proximity of the transition to PS. Figure 2 reports the temporal evolution of $\Delta = |\Phi_e - \Phi_s|$ for (a) $\nu = 2.05$ kHz, (b) $\nu = 1.85$ kHz, and (c) $\nu = 1.70$ kHz. A sequence of 2π phase slips characterizes the evolution of Δ , whose occurrence becomes rarer and rarer as ν approaches ν_c . We furthermore calculate the distribution of interslip time intervals (ITI) and monitor its coherence factor $C = \tau/\sigma^2$ as a function of ν , where τ represents the average interslip time interval, and σ the standard deviation of the ITI distribution. According to [17], one should expect a value $\nu_{\text{PPS}} > \nu_c$ where phase slips occur periodically in Δ , reflected by a maximum in the coherence factor C close to the transition point for PS.

This is reported in Fig. 3, where a maximum of $C(\nu)$ is apparent at $\nu_{\text{PPS}} \approx 1.84$ kHz. The further growth of C beyond $\nu \sim 2.1$ kHz is due to the approaching of a new locking regime, namely, 2:1 rather than 1:1. The temporal evolution of Δ at ν_{PPS} is shown in Fig. 2, b, where one can see that phase slips are almost equispaced in time.

A further question concerns how the occurrence of PPS is related to the cross-over between the two scaling behaviors of phase slips. These scaling properties can be explained as follows. The type-I intermittency behavior describes the classical case of periodic systems, and it characterizes the intermittent phase slip duration just outside the border of PS.

For chaotic systems, the PS region corresponds to the overlap of all the phase-locking regions of the unstable periodic orbits (UPO) embedded in the chaotic attractor [19]. Each locked UPO is associated with an attractor and a repeller in the

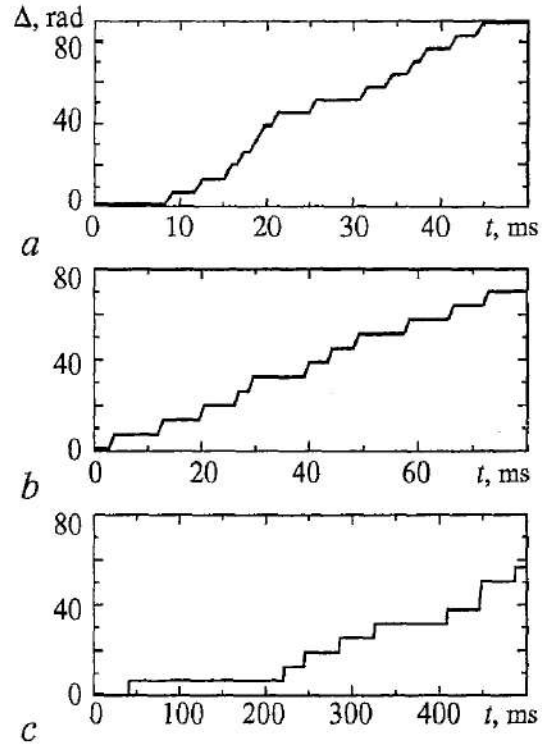


Fig. 2. Temporal evolution of $\Delta = |\Phi_e - \Phi_s|$ for: (a) $\nu = 2.05$ kHz, (b) $\nu = 1.85$ kHz, and (c) $\nu = 1.70$ kHz

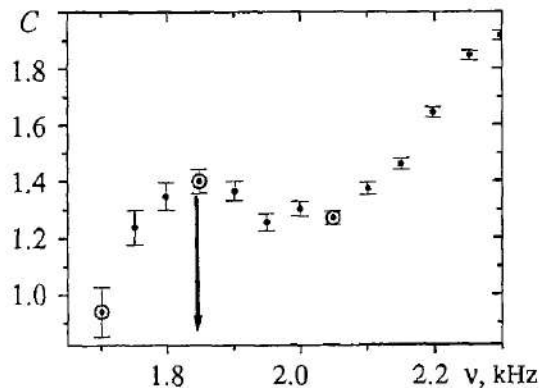


Fig. 3. Coherence factor C (see text for definition) vs ν . The arrow at $\nu_{\text{PPS}} = 1.84$ kHz indicates the frequency value for which phase slips are maximally coherent. The circles surround the three points for which measurements of $\Delta(t)$ are reported in Fig. 2

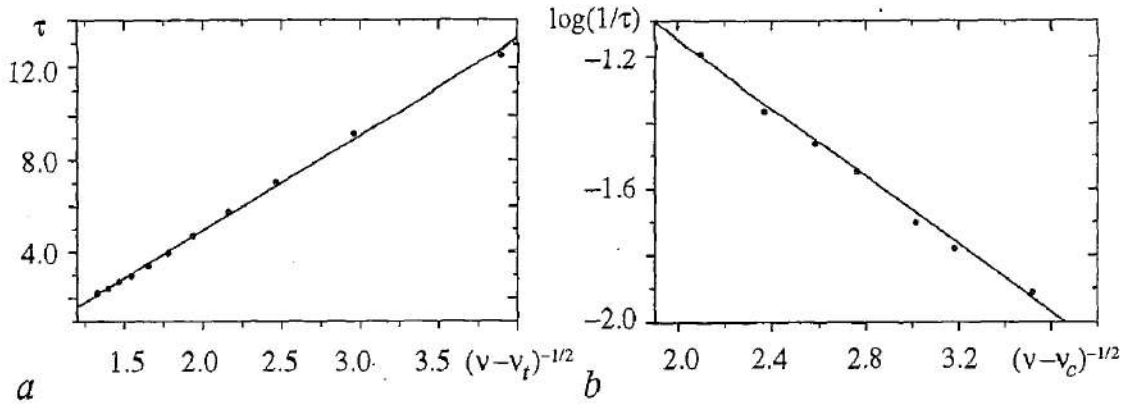


Fig. 4. Type-I intermittency scaling behavior (a) and superlong laminar scaling behavior (b) of interslip time intervals. Dots indicate the experimental measurements. Lines are the best fits: (a) $\tau = -3.4 + 4.2|\nu - \nu_i|^{-1/2}$, $\nu_i = 1.84$ kHz; (b) $\log(1/\tau) = -0.13 - 0.51|\nu - \nu_c|^{-1/2}$, $\nu_c = 1.62$ kHz. The crossover point for the two scaling laws is located at $\nu = \nu_i = 1.84$ kHz, that corresponds exactly to the value ν_{PPS} of maximal coherence (periodic phase synchronization) in the phase slip occurrence

direction of the phase. The repellers are periodic orbits on the basin boundary of the attractors. As we approach the PS bifurcation point, the attractor and the repeller of each of a few UPOs approach, coalesce, and annihilate through a saddle-node bifurcation [15]. As a consequence, these UPOs are unlocked to the external force and phase slips occur. Just beyond the transition point, most UPOs are still attractive, and phase slips can develop only when the trajectory of the system stays for a sufficiently long time τ_1 in a close vicinity of the unlocked UPO. Due to ergodicity, the probability for a trajectory to visit a particular UPO for a duration τ_1 is proportional to $e^{-\lambda\tau_1}$ (λ being the largest Lyapunov exponent). The average interslip interval (the inverse of this probability) will be given by $\tau \sim e^{(\lambda|\nu - \nu_c|^{-1/2})}$, where τ_1 has been substituted with its type-I intermittent scaling behavior, hence the expression for the superlong laminar behavior. Such a scaling behavior was also verified by numerical simulation of maps [20], and by direct simulation of the chaotic Roessler oscillator driven by external forcing [15,19].

In summary, one expects a type-I intermittent scaling law only for frequencies $\nu > \nu_i$, where ν_i denotes the value for which all UPOs are in the unlocked regime, and a superlong laminar behavior for $\nu_c < \nu < \nu_i$.

These expectations have been demonstrated by us, by making use of a series of measurements at different values of ν , obtaining the results shown in Fig. 4. The best fits yield $\nu_c = 1.62$ kHz and $\nu_i = 1.84$ kHz. Fig. 4 confirms the existence of two different scaling behaviors, and shows that the crossover point for the two scaling laws coincides with ν_{PPS} of Fig. 3, thus indicating that the coherence between successive phase slips mediates the transition from the two scaling behaviors.

We take the occasion to gratefully acknowledge the many illuminating discussions with V. Anishchenko on the whole issue of phase synchronization of chaotic oscillators, which have stimulated and inspired the present research, and continue stimulating our main experimental efforts in the field. Work supported by EU Contract HPRN-CT-2000-00158 (COSYC of SENS).

References

1. Fujisaka H. and Yamada T. // Prog. Theor. Phys. 1983. Vol. 69. P. 32; Afraimovich V.S., Verichev N.N., and Rabinovich M.I. // Izv. Vyssh. Uchebn. Zaved. Radiofiz. 1986. Vol. 29. P. 1050; Pecora L.M. and Carroll T.L. // Phys. Rev. Lett. 1990. Vol. 64. P. 821.

2. Rulkov N.F., Sushchik M.M., Tsimring L.S., and Abarbanel H.D.I. // Phys. Rev. E. 1995. Vol. 51. P. 980; Kocarev L. and Parlitz U. // Phys. Rev. Lett. 1996. Vol. 76. P. 1816.
3. Rosenblum M.G., Pikovsky A.S., and Kurths J. // Phys. Rev. Lett. 1996. Vol. 76. P. 1804.
4. Pikovsky A.S., Rosenblum M., Osipov G.V., Zaks M., and Kurths J. // Physica D (Amsterdam). 1997. Vol. 104. P. 219.
5. Boccaletti S., Kurths J., Osipov G., Valladares D.L., and Zhou C.S. // Phys. Rep. 2002. Vol. 366. P. 1.
6. Van Wiggeren G.D. and Roy R. // Science. 1998. Vol. 279. P. 1198; Neiman A., Pei X., Russell D., Wojtenek W., Wilkens L., Moss F., Braun H.A., Huber M.T., and Voigt K. // Phys. Rev. Lett. 1999. Vol. 82. P. 660.
7. Duane G.S. and Tribbia J.J. // Phys. Rev. Lett. 2001. Vol. 86. P. 4298.
8. Blasius B., Huppert A., and Stone L. // Nature (London). 1999. Vol. 399. P. 354; Josic K. and Mar D.J. // Phys. Rev. E. 2001. Vol. 64. 056234.
9. Ticos C.M., Rosa E., Jr., Pardo W.B., Walkenstein J.A., and Monti M. // Phys. Rev. Lett. 2000. Vol. 85. P. 2929; Maza D., Vallone A., Mancini H., and Boccaletti S. // Phys. Rev. Lett. 2000. Vol. 85. P. 5567; DeShazer D.J., Breban R., Ott E., and Roy R. // Phys. Rev. Lett. 2001. Vol. 87. 044101.
10. Allaria E., Arecchi F.T., Di Garbo A., and Meucci R. // Phys. Rev. Lett. 2001. Vol. 86. P. 791.
11. Schäfer C., Rosenblum M.G., Weule J., Kurths J., and Abel H.H. // Nature (London). 1998. Vol. 392. P. 239.
12. Tass P., Rosenblum M.G., Weule J., Kurths J., Pikovsky A., Volkmann J., Schnitzler A., and Freund H.-J. // Phys. Rev. Lett. 1998. Vol. 81. P. 3291.
13. Rodriguez E., George N., Lachaux J., Martinerie J., Renault B., and Varela F. // Nature (London). 1999. Vol. 397. P. 430.
14. Manneville P., and Pomeau Y. // Physica D (Amsterdam). 1980. Vol. 1. P. 219.
15. Rosa E., Ott E., and Hess M.H. // Phys. Rev. Lett. 1998. Vol. 80. P. 1642.
16. Lee K.J., Kwak Y., and Lim T.K. // Phys. Rev. Lett. 1998. Vol. 81. P. 321.
17. Kye W.-H., Lee D.-S., Rim S., and Kim C.-M. // Phys. Rev. Lett. (to be published).
18. Boccaletti S., Allaria E., Meucci R., and Arecchi F.T. // Phys. Rev. Lett. 2002. Vol. 89. 194101.
19. Pikovsky A.S., Zaks M., Rosenblum M., Osipov G., and Kurths J. // Chaos. 1997. Vol. 7. P. 680.
20. Pikovsky A., Osipov G., Rosenblum M., Zaks M., and Kurths J. // Phys. Rev. Lett. 1997. Vol. 79. P. 47.

*Instituto Nazionale di Ottica Applicata,
Florence, Italy
Department of Physics, University of Florence, Italy*

Received 28.08.03

УДК 621.373

ИССЛЕДОВАНИЕ ПЕРЕХОДОВ К ФАЗОВОЙ СИНХРОНИЗАЦИИ В ЭКСПЕРИМЕНТАЛЬНОЙ НЕЛИНЕЙНОЙ ОПТИКЕ

S. Boccaletti, E. Allaria, R. Meucci, F.T. Arecchi

Исследуется путь перехода к фазовой синхронизации в лазере с хаотической динамикой при наличии внешней модуляции. Приводится доказательство наличия режима периодической фазовой синхронизации, когда фазовые сбои случаются с

максимальной когерентностью, проявляющейся в фазовом различии между выходным сигналом и внешней модуляцией. Показано, что такой режим возникает в переходной точке между двумя различными скейлинговыми законами, описывающими режим перемежаемости в поведении фазовых сбоев.



Stefano Boccaletti graduated in Physics *summa cum laude* in 1992 and was awarded the Ph.D. in Physics in 1995. His major studies concerned the theoretical modeling of pattern formation and competition and the study of chaos recognition, control and synchronization.

Boccaletti is Referee of major physical journals, Member of the Advisory board of the AIP Journal CHAOS, Member of the Editorial Board of the Journal «Dynamical Systems: Chaos and Complexity Letters», and Associate Editor of the «Journal of Mathematical Biosciences and Engineering» of the American Institute of Mathematical Sciences. Boccaletti coauthored 97 research papers published on the major peer-review physical Journals. He was member elected of the Florence City Council from 1995 to 1999.



Enrico Allaria graduated in Physics at the University of Florence in 2000. He received its Specialization on Optics at the University of Florence with the support of the European Contract «Control Synchronization and Characterization of Spatially Extended Nonlinear Systems» on 2002. His research activity is focused mainly on nonlinear dynamics effects in optics with experiments on «Control and synchronization of chaos», «Models for the nonlinear dynamics in isotropic lasers» and «Optical measurements in the infrared». Allaria coauthored 20 research papers published on the major peer-review physical and optical Journals. Actually he is collaborating with the University of Florence and he is searching for a permanent position.



Riccardo Meucci graduated in Physics on December 20 1982 and was awarded the Ph.D. He received its Specialization on Optics at the University of Florence on March 13 1987. He received a position of researcher at Istituto di Cibernetica of the Italian National Research Council (CNR) on March 1984. He joined the Istituto Nazionale di Ottica (INO) now transformed into Istituto Nazionale di Ottica Applicata (INOA). At the present time he is a senior research charged with the division of Experimental Quantum Optics at INOA. His main scientific contribution are in the field of Chaotic instabilities in single mode lasers, Laser transients, Dynamical models for the CO₂ laser, Control and Synchronization of chaos, Spatio-temporal instabilities and delayed systems. Actually he carries out didactic activity as contract professor at the University of Florence. Meucci is referee of major physical and optical journals and is coauthor of about 100 papers.



Fortunato Tito Arcacchi started his scientific activity in 1957 as Researcher at CISE, Milano. Since 1970 he is Chair of Physics in the Italian University (Pavia 1970-77, Firenze since 1977). Between 1975 and 2000 he was President of Istituto Nazionale di Ottica (INO), later transformed into Istituto Nazionale di Ottica Applicata (INOA). Since 2001 he is Scientific Responsible of INOA.

He is member of the Italian Physical Society, the Academie Internationale de Philosophie des Sciences, the Academia Europea and Fellow of Optical Society of America (OSA). He was Max Born Medal of OSA in 1995.

He is Editor of many scientific journals. His main scientific contributions are in the following areas: Cooperative effects in quantum optics, Photon statistics and laser fluctuations, Deterministic chaos in optics, Pattern formation in extended media, Complex phenomena and cognitive processes.

He is coauthor of more than 350 scientific papers and several books.



Izv. VUZ «AND», vol.11, № 3, 2003

RIDDLING IN THE PRESENCE OF SMALL PARAMETER MISMATCH

Serhiy Yanchuk and Tomasz Kapitaniak

Riddling bifurcation leads to the loss of chaos synchronization in coupled identical systems. We discuss here the manifestation of the riddling bifurcation for the case of a small parameter mismatch between coupled systems. We show that for slightly nonidentical coupled systems, the transverse growth of the synchronous attractor is mediated by transverse bifurcations of unstable periodic orbits embedded into the attractor.

Introduction

Consider two symmetrically coupled identical systems $dx/dt=f(x)$ and $dy/dt=f(y)$ and $x, y \in \mathbb{R}^n$ which evolve on an asymptotically stable bounded chaotic attractor A ,

$$dx/dt = f(x) + C(y-x), \quad dy/dt = f(y) + C(x-y). \quad (1)$$

Complete synchronization occurs when the coupled systems asymptotically exhibit identical behaviour, i.e., $|x(t)-y(t)| \rightarrow 0$ as $t \rightarrow \infty$. The synchronous behaviour takes place on the synchronization manifold $x=y$, which is invariant in the phase space of the coupled system (1) and has half the dimension of the full system. The synchronization loss in system (1) is initiated with the riddling bifurcation [1] when the first unstable periodic orbit (UPO) embedded into chaotic attractor A loses its transverse stability. In this paper we discuss the manifestation of the riddling bifurcation for the case of a small parameter mismatch between coupled systems. We give evidence that for slightly nonidentical coupled systems, the transverse growth of the synchronous attractor is mediated by transverse bifurcations of unstable periodic orbits embedded into the attractor. The desynchronization mechanism is shown to be similar to the bifurcation of chaos-hyperchaos transition [2]. We also note that the parameter mismatch leads to the increase of transverse instabilities after the riddling bifurcation.

Model

Without loss of generality, a small difference between coupled systems can be incorporated in (1) as

$$dx/dt = f(x) + \alpha(x) + C(y-x), \quad dy/dt = f(y) + C(x-y), \quad (2)$$

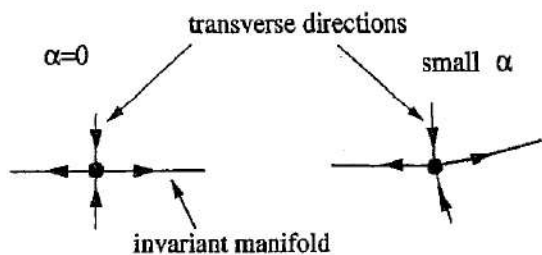


Fig. 1. Small parameter mismatch implies small perturbation of stable and unstable manifolds of saddle periodic orbits embedded in an attractor

where $\alpha(x)$ describes parameter mismatch. For sufficiently small α the evolution of the system (2) can be considered as the perturbed evolution of the system (1), so the motion of the system can be asymptotically close to the synchronization manifold $|x-y| < \epsilon$ with small ϵ .¹ In these cases, the attractor of the system (2) is located in the neighborhood of the invariant manifold $x=y$ of system (1). For sufficiently small α , transverse stability of orbits embedded in A is also preserved in

system (2).

It is also meaningful to speak about transverse and longitudinal stability of saddle periodic orbits embedded in the attractor A since a sufficiently small mismatch will cause only small perturbation of the local unstable and stable manifolds and will not affect stability properties of the UPOs, as sketched in Fig. 1.

Therefore, the moment of riddling bifurcation will correspond to the loss of transverse stability of some orbit embedded in the attractor. Here, of course, the situation may arise when the above mentioned orbit leaves the attractor before its transverse destabilization as it was described in [5]. In this situation, we may consider the remaining orbits that lose transverse stability with decrease of a coupling coefficient. In general, for nonidentical systems, we are dealing with a chaotic attractor which is no longer located in low-dimensional synchronization manifold but remains in the neighborhood of it. Moreover, periodic orbits embedded into this attractor are proved to lose transverse stability with the decrease of coupling [6]. Therefore, we have the same situation as for chaos-hyperchaos transition [2,4] where the growth of the attractor is mediated by doubly unstable orbits embedded in it. It was shown in [2] that this growth can be either smooth or abrupt depending on the type of «riddling» bifurcation.

In the following as the numerical example, we consider two coupled Rössler systems

$$\begin{aligned} dx/dt &= f(x) + \bar{\alpha} + C(d)(y-x), \\ dy/dt &= f(y) + C(d)(x-y), \end{aligned} \quad (3)$$

where $C(d) = \text{diag}\{d-0.6, 1.0, -3.1d+0.7\}$, $\bar{\alpha} = (0, 0, \alpha)$,

$$f(x) = (-x_2 - x_3, x_1 + 0.42x_2, 2+x_3(x_1-4))^T.$$

The mismatch is introduced via parameter α .

It was shown in [8] that the corresponding system of identical coupled oscillators, i.e. for $\alpha=0$ loses complete synchronization with the decrease of parameter d . In particular, the riddling bifurcation occurs at $d=0.241$ when the embedded period-1 cycle becomes transversely unstable via supercritical transverse period-doubling bifurcation. At $d=0.192$ the blowout bifurcation takes place when transverse Lyapunov exponent of the synchronous attractor becomes negative. Note also, that using numerical simulation of coupled identical systems we were unable to detect bursts from the synchronization manifold for the parameter values $d \in (0.22, 0.24)$, i.e. where synchronous attractor has already lost its transverse stability but is still weakly stable.

¹ This is the case, for example, when the synchronous object in system (1) is normally a hyperbolic torus or a saddle periodic orbit embedded into the attractor. Some generic cases where such estimation holds are also described in [3].

In the case for systems with the mismatch the above mentioned transverse period-doubling bifurcation persists and for $\alpha=0.003$ it takes place at $d=0.24$. Numerically computed Lyapunov exponents for the system (3) are shown in Fig. 2. In the interval I the chaotic attractor A is located in the neighborhood of the manifold $x=y$. We observe the growth of the second Lyapunov exponent what is connected with the riddling bifurcation at $d=0.24$ and initiation of the chaos-hyperchaos transition. As it was shown in [2], this transition is mediated by the transverse destabilization of UPOs embedded in the chaotic attractor A . In the interval II, the system (3) has the stable hyperchaotic attractor with two positive Lyapunov exponents. At $d \approx 0.21$ chaotic attractor A becomes unstable and disappears. The evolution of the system (3) switches to the limit cycle (interval IIIa) and torus (interval IIIb). Fig. 3 shows the behavior of the synchronization error $x_1(t) - y_1(t)$ for different values of d . We can observe transverse bursts for the parameter values after the moment of riddling bifurcation (Fig. 3, b, c). More detailed information about the transverse size of the attractor can be seen in Fig. 4, where the maximum amplitude of bursts detected during time interval $T=200000$ versus coupling coefficient d is shown. It

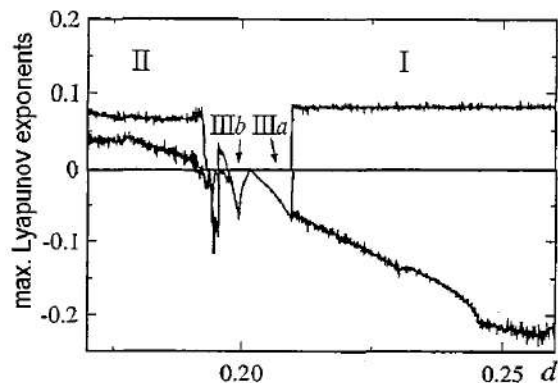


Fig. 2. Lyapunov exponents of system (3) versus d ; $\alpha=0.003$: I - interval in which chaotic attractor A is located in the neighborhood of the manifold $x=y$, II - interval in which hyperchaotic attractor exists, III - interval where the chaotic attractor A loses stability and solution switches into stable limit cycle (IIIa) and torus (IIIb)

At $d \approx 0.21$ chaotic attractor A becomes unstable and disappears. The evolution of the system (3) switches to the limit cycle (interval IIIa) and torus (interval IIIb). Fig. 3 shows the behavior of the synchronization error $x_1(t) - y_1(t)$ for different values of d . We can observe transverse bursts for the parameter values after the moment of riddling bifurcation (Fig. 3, b, c). More detailed information about the transverse size of the attractor can be seen in Fig. 4, where the maximum amplitude of bursts detected during time interval $T=200000$ versus coupling coefficient d is shown. It

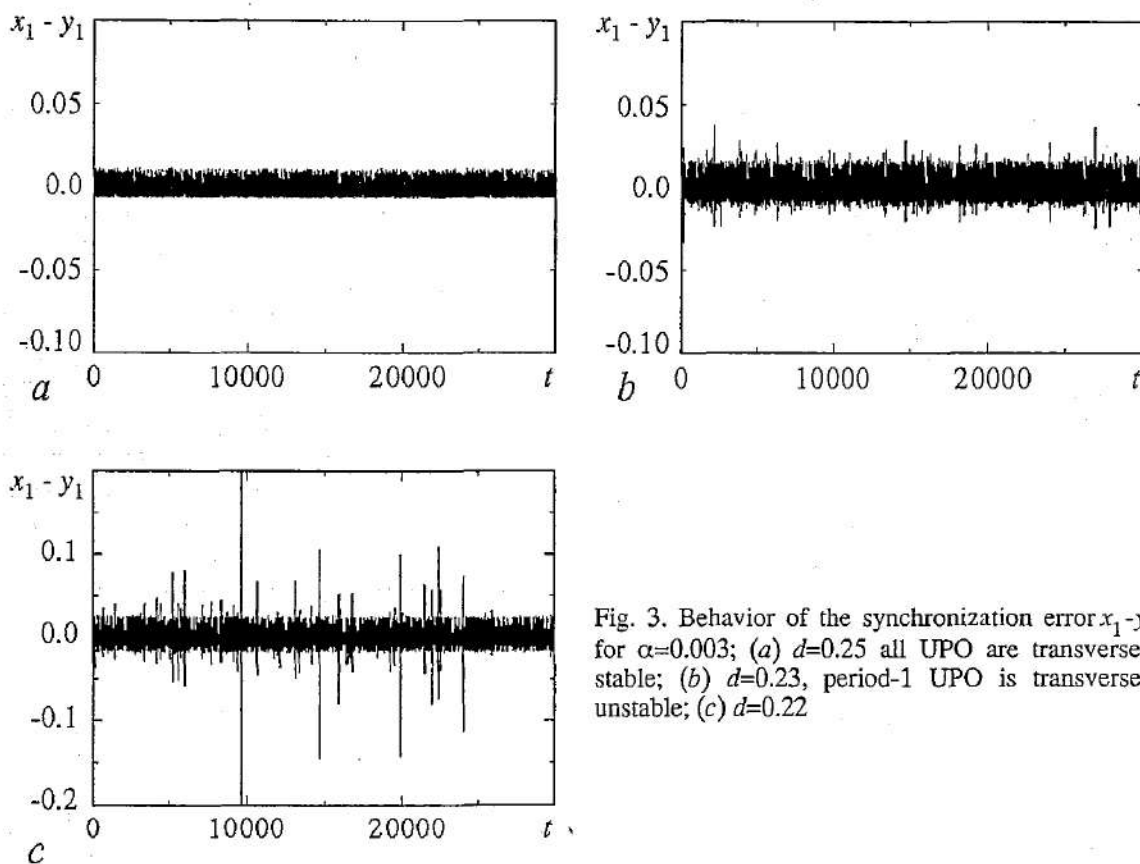


Fig. 3. Behavior of the synchronization error $x_1 - y_1$ for $\alpha=0.003$; (a) $d=0.25$ all UPO are transversely stable; (b) $d=0.23$, period-1 UPO is transversely unstable; (c) $d=0.22$

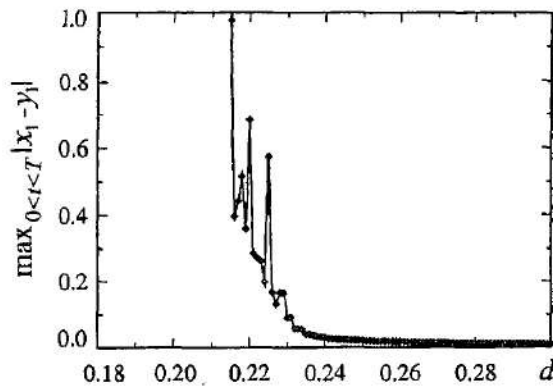


Fig. 4. Transverse growth of the attractor with decreasing of d ; $\alpha=0.003$

iterations be diverted back to A . If there is neighborhood U of A such that in any neighborhood V of any point in U , there is a set of points of positive measure which leaves U and goes to the other attractor (attractors), then the basin of A is *globally riddled*.

can be seen that the attractor grows rapidly in transverse direction already after the riddling bifurcation.

In the case of the ideal coupled systems the chaotic attractor A located at the invariant manifold $x=y$ can have locally or globally riddled basins of attraction. A is an attractor² with *locally riddled* basin if there is neighborhood U of A such that in any neighborhood V of any point in A , there is a set of points in $V \cap U$ of positive measure which leaves U in a finite time. The trajectories which leave neighborhood U can either go to the other attractor (attractors) or after a finite number of

Conclusions

In conclusion, we investigated the effect of riddling bifurcation on the chaotic attractor of the coupled systems with the parameter mismatch. After the onset of bifurcation, the system trajectory shows intermittency-like behavior with bursts away from the manifold $x=y$. These bursts grow rapidly resulting in the growth in size of the chaotic attractor. Contrary to the case of the coupled ideal systems we have not observed globally riddled basins of the chaotic attractor located in the neighborhood of the manifold $x=y$.

References

1. Lai Y.-Ch., Grebogi C., Yorke J.A., and Venkataramani S.C. // Phys. Rev. Lett. 1996. Vol. 77. P. 5361; Astakhov V., Shabunin A., Kapitaniak T., Anishchenko V.S. // Phys. Rev. Lett. 1997. Vol. 79. P. 1014.
2. Kapitaniak T., and Steeb W.-H. // Phys. Lett. A. 1991. Vol. 152. P. 33; Kapitaniak T. // Phys. Rev. E. 1993. Vol. 47. P. R2975; Stefanski K. // Chaos, Solitons and Fractals. 1998. Vol. 9. P. 83; Harrison M.A. and Lai Y.-Ch. // Phys. Rev. E. 1999. Vol. 59. P. R3799; Kapitaniak T., Maistrenko Yu., Popovich S. // Phys. Rev. E. 2000. Vol. 62. P. 1972; Yanchuk S. and Kapitaniak T. // Phys. Lett. A. 2001. Vol. 290, № 3-4. P. 139.
3. Johnson G., Mar D., Carroll T., Pecola L. // Phys. Rev. E. 1998. Vol. 80. P. 3956; Yanchuk S., Maistrenko Yu., Lading B., Mosekilde E. // Int. J. Bifurcation and Chaos. 2000. Vol. 10. P. 2629.
4. Yanchuk S. and Kapitaniak T. // Phys. Rev. E. 2001. 056235.
5. Astakhov V., Kapitaniak T., Shabunin A., Anishchenko V. // Phys. Lett. A. 1999. Vol. 258. P. 99.

² Here we assume the attractor in the sense of Milnor [9].

6. Nagai Y. and Lai Y.-Ch. // Phys. Rev. E. 1997. Vol. 55. P. R1251; Nagai Y. and Lai Y.-Ch. // Phys. Rev. E. 1997. Vol. 56. P. 4031.
7. Lai Y.-Ch. // Phys. Rev. E. 1997. Vol. 56. P. 1407.
8. Yanchuk S., Maistrenko Yu., Mosekilde E. // Physica D. 2001. Vol. 154. P. 26.
9. Milnor J. // Commun. Math. Phys. 1985. Vol. 99. P. 177.

*Institute of Mathematics,
Academy of Sciences of Ukraine
Division of Dynamics,
Technical University of Lodz, Poland*

Received 08.08.03

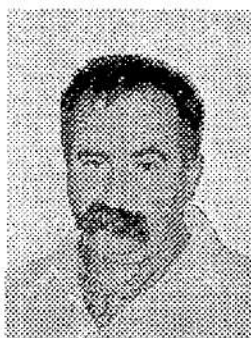
УДК 534.015

РИДЛИНГ В ПРИСУТСТВИИ МАЛОЙ РАССТРОЙКИ ПО ПАРАМЕТРУ

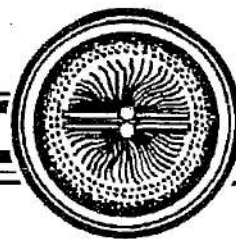
С. Янчук, Т. Капитаниак

Ридлинг-бифуркация приводит к потере синхронизации хаоса в связанных идентичных системах. В статье обсуждается проявление ридлинг-бифуркации для случая малой расстройки по параметру между связанными системами. Показано, что для немного неидентичных связанных систем уширение синхронного аттрактора обуславливается трансверсальной бифуркацией неустойчивых периодических орбит, встроенных в аттрактор.

*Serhiy Yanchuk - Institute of Mathematics, Academy of Sciences of Ukraine, 3 Tereshchenkivska st.,
01601 Kyiv, 252601 Ukraine*



*Tomasz Kapitaniak - Division of Dynamics, Technical University of Lodz,
Stefanowskiego 1/15, 90-924 Lodz, Poland
E-mail: tomaszka@p.lodz.pl*



НЕЛИНЕЙНЫЕ ЭФФЕКТЫ В ХАОТИЧЕСКИХ И СТОХАСТИЧЕСКИХ СИСТЕМАХ

*В.С. Анищенко, В.В. Астахов, Т.Е. Вадивасова, А.Б. Нейман,
Г.И. Стрелкова, Л. Шиманский-Гайер*

© Институт компьютерных исследований, 2003
© В.С. Анищенко, 2003

Москва - Ижевск: Институт компьютерных исследований, 2003. 544 с.
ISBN 5-93972-289-X

Настоящая книга представляет собой фундаментальный труд по основам нелинейной динамики хаотических и стохастических систем. Книга включает исчерпывающее введение в теорию динамических и стохастических систем и детальный анализ современных результатов, в основном полученных авторами. Каждая из глав книги построена таким образом, что может изучаться независимо от других. В частности, каждая глава имеет свой собственный список литературы. Все это позволяет использовать предлагаемую книгу в качестве учебника для студентов и аспирантов физико-математических специальностей (глава 1), а также специалистам в области нелинейной динамики детерминированных (глава 2) и стохастических (глава 3) систем.

*Нашим учителям и друзьям
Werner Ebeling,
Ю.И. Климонтович,
Frank Moss*

Предисловие редактора перевода

Читателю предлагается доработанный и расширенный перевод книги V.S. Anishchenko, V.V. Astakhov, A.B. Neiman, T.E. Vadivasova, L. Schimansky-Geier «Nonlinear Dynamics of Chaotic and Stochastic Systems»*, опубликованной в 2002 году издательством Springer. Книга посвящена современным проблемам нелинейной динамики хаотических и стохастических систем и ориентирована как на молодых ученых, так и специалистов в области исследования нелинейных колебаний и волн. Настоящее издание в своей основе соответствует оригиналу.

* V.S. Anishchenko, V.V. Astakhov, A.B. Neiman, T.E. Vadivasova, L. Schimansky-Geier. Nonlinear dynamics of chaotic and stochastic systems: Tutorial and modern developments. Springer-Verlag, Berlin, Heidelberg, New York, 2002. 374 p.

При переводе авторами внесены в текст некоторые уточнения и исправлены опечатки в ряде формул. Во вторую главу книги добавлены три новых раздела: «Корреляционный анализ режимов детерминированного и зашумленного хаоса», «Эффекты синхронизации в цепочках связанных осцилляторов» и «Синхронизация в живых системах». Включение этих разделов естественным образом вписывается в материал второй главы и отражает наиболее интересные результаты авторов, полученные после выхода английского издания.

Мы надеемся, что книга будет с интересом воспринята широкой аудиторией читателей, интересующихся современными проблемами теории нелинейных колебаний и волн, динамическим хаосом, теорией синхронизации и индуцированными внешним шумом явлениями. Мы будем благодарны за любые замечания, которые можно направлять в адрес издательства.

Профессор В.С. Анищенко

Предисловие

Эта книга посвящена классическим основам и современным результатам нелинейной динамики детерминированных и стохастических систем. Значительное внимание в ней уделяется индуцированным шумом переходам и влиянию флуктуаций на характеристики нелинейных динамических систем в различных колебательных режимах.

С одной стороны существует обширная литература по нелинейной динамике и хаосу, представленная замечательными книгами; с другой стороны, имеется немало великолепных монографий и учебников по статистической физике неравновесных и стохастических процессов. В данной же книге предпринята попытка сочетать подход нелинейной динамики, основанный на детерминированных эволюционных уравнениях, с подходом статистической физики, базирующемся на стохастических или кинетических уравнениях. Данная работа нацелена главным образом на то, чтобы показать, какую важную роль играет шум в формировании свойств динамических режимов функционирования нелинейных диссипативных систем.

В рамках этой книги освещается определенный, ограниченный круг вопросов, относящихся к интересной, продолжающей развиваться области нелинейной динамики. В настоящее время существует огромное количество разноплановых задач, связанных с детерминированными и стохастическими динамическими системами. С целью обстоятельного и полного представления материала при написании этой книги мы руководствовались следующими тремя критериями: во-первых, динамическая модель должна быть минимальной, т.е. оптимально прозрачной в физическом и математическом смысле; во-вторых, модель должна быть простейшей, но вместе с тем четко демонстрировать наиболее важные стороны рассматриваемого явления; наконец, в-третьих, основное внимание уделяется тем моделям и явлениям, исследуя которые, авторы накопили за последние годы определенный опыт.

Книга состоит из трех глав. *Первая глава* служит кратким введением и содержит фундаментальные положения теории нелинейных детерминированных и стохастических систем и классической теории синхронизации периодических колебаний. Сюда вошли все основные понятия и определения, необходимые для того, чтобы изучать последующие главы, не обращаясь к специальной литературе.

Вторая глава посвящена детерминированному хаосу. В ней мы рассматриваем различные сценарии возникновения хаоса, включая проблему

разрушения двух- и трехчастотного квазипериодического движения. Кроме того, в этой главе обсуждаются различные аспекты синхронизации и управления хаосом, а также методы реконструкции аттракторов и динамических систем по экспериментальным временным рядам.

В *третьей главе* особое внимание уделяется стохастическим системам, динамика которых в значительной мере определяется влиянием шума. Здесь обсуждаются некоторые явления нелинейного характера, такие как стохастический резонанс в динамической системе под воздействием гармонических и сложных сигналов и шума, стохастическая синхронизация и стохастический рэчет, представляющие собой индуцированный шумом упорядоченный и направленный перенос броуновских частиц, движущихся в бистабильных и периодических потенциалах. Особое внимание уделено роли шума в динамике возбудимых систем и сред.

Книга ориентирована на широкий круг читателей, интересующихся естественными науками. Первая глава будет полезна студентам и аспирантам, изучающим физику, химию, биологию и экономику, а также преподавателям этих предметов, проявляющих интерес к современным проблемам нелинейной динамики. Специалисты по нелинейной динамике могут использовать этот раздел в качестве расширенного справочного пособия. Вторая и третья главы предназначены для специалистов в области математического моделирования сложной динамики нелинейных систем, в том числе в присутствии шума.

Мы постарались составить книгу таким образом, чтобы любая из трех глав могла быть воспринята читателем преимущественно независимо от других. В частности, к каждой главе прилагается отдельный список литературы. Такое решение продиктовано желанием сделать книгу еще более полезной для читателя. Однако представленную нами библиографию, без сомнения, нельзя назвать исчерпывающей, поскольку существует огромное количество публикаций, посвященных вопросам, рассматриваемым в данной книге.

Эта книга явилась результатом продолжительного сотрудничества лаборатории нелинейной динамики Саратовского государственного университета с исследовательской группой по изучению прикладных стохастических процессов в Гумбольдтском университете в Берлине, а также с центром нейродинамики в Университете Миссури в Сент-Луисе.

Мы выражаем глубокую благодарность W. Ebeling, Ю.Л. Климонтовичу и F. Moss за поддержку, обмен научной информацией и постоянный интерес к нашей работе. Мы также благодарны за плодотворные дискуссии С. van den Broek, P. Hänggi, J. Kurths, A. Longtin, A. Pikovski и Ю.М. Романовскому. Книга приобрела много ценного благодаря участию наших соавторов по предыдущим работам. Мы признательны А. Баланову, R. Bartussek, V. Bucholtz, И. Дикштейну, J.A. Freund, J. Garcia-Ojalvo, M. Hasler, Н. Янсон, Т. Kapitaniak, И. Хованову, M. Kostur, П.С. Ланде, В. Lindner, P. McClintock, E. Mosekilde, А. Павлову, Т. Pöschel, Д. Постнову, P. Reimann, R. Rozenfeld, P. Ruzsyczynsky, А. Шабунину, Б. Шульгину, U. Siewert, А. Сильченко, О. Сосновцевой, А. Заикину и С. Zülicke за совместные работы, частые плодотворные дискуссии, ценные замечания и критику, позволившие нам глубже проникнуть в изучаемые проблемы.

Мы благодарим редактора этой серии Н. Naken за полезные советы по рукописи, а также P. Talkner, J. Freund и В. Lindner за полезные замечания при правке корректуры.

Особую благодарность хотелось бы выразить Галине Стрелковой за огромную работу по подготовке рукописи и перевод многих разделов этой книги на английский язык, а также А. Климшину за оказание технической помощи.

Кроме того, В. Анищенко, Т. Вадивасова и В. Астахов благодарят

Американский Фонд гражданских исследований и развития (CRDF, грант REC-006) и Российский Фонд фундаментальных исследований (гранты № 00-02-17512, № 99-02-17732). В.С. Анищенко также благодарит за поддержку Международный Фонд им. Александра фон Гумбольдта. А. Нейман выражает благодарность Институту Фитцера и физическому отделению Военно-морского управления США. Л. Шиманский-Гайер благодарит за оказание поддержки Deutsche Forschungsgemeinschaft (Sfb 555 и GK 268).

*В. Анищенко, А. Нейман, Т. Вадивасова,
В. Астахов, Л. Шиманский-Гайер*

Оглавление

1. Основы динамического и статистического описания эволюционных процессов

1.1. Динамические системы.

Введение. Динамическая система и ее математическая модель. Устойчивость (линейное приближение). Бифуркации динамических систем, катастрофы. Аттракторы динамических систем. Детерминированный хаос. Заключение.

1.2. Флуктуации в динамических системах.

Введение. Основные концепции теории случайных процессов. Шум в динамических системах. Уравнение Фоккера - Планка. Стохастические осцилляторы. Задача о выходе из ограниченной области. Заключение.

1.3. Синхронизация периодических систем. Введение. Синхронизация генератора Ван дер Поля. Синхронизация в присутствии шума. Эффективная синхронизация. Фазовое описание. Заключение.

Литература

2. Хаотические и сложные колебания динамических систем

2.1. Бифуркационные механизмы перехода к хаосу.

Введение. Переход к хаосу через последовательность бифуркаций удвоения периода. Универсальность Фейгенбаума. Жесткие переходы к хаосу. Кризис и перемежаемость. Переход к хаосу через разрушение двухчастотных колебаний. Переход к хаосу через трехмерный тор. Хаос на трёхмерном торе. Хаотические нестранные аттракторы. Переход к хаосу через разрушение эргодического тора. Странные нехаотические аттракторы. Заключение.

2.2. Корреляционный анализ режимов детерминированного и зашумленного хаоса.

Введение. Гармонический шум и телеграфный сигнал. Корреляционно-спектральный анализ спирального хаоса. Автокорреляционные функции и спектры мощности в режиме винтового хаоса. Корреляционно-спектральные характеристики хаотических автоколебаний переключающего типа в режиме квазигиперболического аттрактора Лоренца. Заключение.

2.3. Синхронизация хаоса.

Введение. Классический подход к синхронизации хаоса. Особенности взаимодействия осцилляторов с фейгенбаумовским сценарием развития хаоса. Фазовая мультистабильность в области синхронизации. Бифуркационные механизмы разрушения полной и частичной синхронизации хаоса. Заключение.

2.4. Эффекты синхронизации в цепочках связанных генераторов.

Введение. Образование частотных кластеров в неоднородных цепочках генераторов. Влияние шума на режимы кластерной синхронизации в цепочке квазигармонических генераторов. Вынужденная синхронизация цепочки хаотических автоколебательных систем. Синхронизация и мультистабильность в кольце генераторов с удвоениями периода. Заключение.

2.5. Синхронизация в живых системах.

Введение. Стохастическая синхронизация электрорецепторов веслоноса. Синхронизация кардиоритма. Заключение.

2.6 Управление хаосом.

Введение. Управляемая противофазная синхронизация хаоса в связанных кубических отображениях. Управление и синхронизация хаоса в системе взаимно связанных осцилляторов. Управляемая синхронизация хаоса методом периодических параметрических возмущений. Стабилизация пространственно-однородных движений посредством параметрического воздействия. Управление хаосом в решетках связанных отображений. Заключение.

2.7 Реконструкция динамических систем.

Введение. Реконструкция аттракторов по временным рядам. Глобальная реконструкция ДС. Реконструкция по данным биологических экспериментов. Метод реконструкции в приложении к задаче защиты передаваемой информации. Заключение.

Литература

3. Стохастическая динамика

3.1 Стохастический резонанс.

Введение. Физические основы эффекта СР. Характеристики эффекта СР. Отклик на слабый сигнал. Теоретические подходы. Теория двух состояний. Усиленный массивом стохастический резонанс. Удвоенный стохастический резонанс в системах с индуцированным фазовым переходом. Стохастический резонанс для сигналов сложного спектрального состава. Стохастический резонанс в хаотических системах с сосуществующими аттракторами. Физический эксперимент. Заключение.

3.2 Синхронизация стохастических систем.

Введение. Синхронизация и стохастический резонанс. Внешняя стохастическая синхронизация триггера Шмитта. Взаимная стохастическая синхронизация связанных бистабильных систем. Внешняя и взаимная синхронизация переключений в хаотических системах. Стохастическая синхронизация ансамблей стохастических резонаторов. Стохастическая синхронизация как индуцированный шумом порядок. Заключение.

3.3 Конструктивная роль шума в возбудимых системах.

Когерентный резонанс вблизи бифуркаций периодических решений динамической системы. Когерентный резонанс в возбудимой динамике. Усиленная шумом синхронизация связанных возбуждаемых систем. Заключение.

3.4 Индуцированный шумом транспорт.

Введение. Мигающие и качающиеся рэтчет потенциалы. Адиабатическое приближение. Передемпфированный коррелированный рэтчет. Сортировка частиц в рэтчет потенциале под действием цветного шума. Двумерный рэтчет. Дискретный рэтчет. Среды с пилообразной зависимостью потенциала. Формирование пространственных структур с помощью рэтчет потенциала. Заключение.

Литература



СИНХРОНИЗАЦИЯ. ФУНДАМЕНТАЛЬНОЕ НЕЛИНЕЙНОЕ ЯВЛЕНИЕ

А. Пиковский, М. Розенблюм, Ю. Куртс

Original english language edition
Published by Cambridge University Press
© All Rights Reserved, 2002
Перевод на русский язык,
оригинал-макет, оформление
© ЗАО РИЦ «Техносфера», 2003

Москва: Техносфера, 2003. 496с.
ISBN 5-94836-020-2

Явление синхронизации широко распространено в науке, природе, технике и обществе. Тенденция к синхронному поведению наблюдается в столь различных системах, как часы, стрекочущие кузнечики, водители ритма сердца, генерирующие потенциалы действия нейроны и аплодирующие зрители. Такие эффекты универсальны, их можно объяснить в рамках единого подхода, основанного на современных достижениях нелинейной динамики.

Приведены как классические результаты по синхронизации периодических автоколебаний, так и последние достижения в исследовании хаотических систем, больших ансамблей и колебательных сред. Монография адресована широкой аудитории - от студентов до квалифицированных исследователей в области физики, прикладной математики, инженерных и естественных наук.

*Моему отцу Самуилу АП
Соне МР
Моему отцу Герберту ЮК*

Предисловие к русскому изданию

Мы рады, что наша книга выходит в свет на родном для нас языке и становится доступной русскоязычному читателю. Мы взяли за перевод по совету ряда наших друзей и коллег, которые, ознакомившись с английским изданием, сочли, что книга была бы полезной для широкого круга читателей - студентов, аспирантов, научных работников разных специальностей - в странах СНГ. Мы благодарим Ю.А. Данилова и Л.Ф. Соловейчика, непосредственно подтолкнувших нас к работе над переводом. Мы хотели бы выразить свою особую признательность Е.М. Розенблюму и С.А. Розенблюм за неоценимую помощь в наборе и корректуре русского текста.

А.С. Пиковский, М.Г. Розенблюм

Предисловие к английскому изданию

Слово «синхронный» часто встречается как в научной, так и в обыденной речи. Происходя от греческих слов $\chi\rho\nu\nu\omicron\varsigma$, (хронос - время) и $\sigma\acute{\upsilon}\nu$ (син - тот же самый, общий), в прямом переводе «синхронный» означает «разделяющий общее время», «происходящий в то же самое время». Этот термин, как и родственные слова «синхронизация» и «синхронизованный», относится ко множеству явлений, встречающихся почти во всех областях естественных наук, техники и социальной жизни, явлений, которые кажутся совершенно различными, но, тем не менее, подчиняются универсальным закономерностям.

Если в какой-либо научной базе данных ввести запрос на поиск статей, содержащих в заголовке слово с корнем «синхро», то мы получим список из сотен (если не тысяч) публикаций. Изначально эффект синхронизации был обнаружен и изучен в различных устройствах, от маятниковых часов до музыкальных инструментов, электронных генераторов, силовых электрических установок и лазеров; ему было найдено множество практических применений в инженерном деле. В наши дни «центр тяжести» исследований сместился в сторону изучения биологических систем, где синхронизация встречается на самом различном уровне. Синхронное изменение клеточных ядер, синхронная генерация потенциалов действия нейронами, подстройка сердечного ритма к дыханию и/или локомоторным ритмам, различные формы коллективного поведения насекомых, животных и даже человеческих сообществ - все это лишь некоторые примеры фундаментального явления природы, которое и является предметом данной книги.

В нашем окружении сплошь и рядом встречаются осциллирующие объекты. Системы радиосвязи и электрическое оборудование, скрипки в оркестре, светлячки, испускающие последовательности световых импульсов, стрекочущие сверчки, птицы, машущие крыльями, химические системы, демонстрирующие колебательное изменение концентрации реагентов, нервные центры, управляющие сокращением сердца человека, и само сердце, центр патологической активности, вызывающей непроизвольное дрожание конечностей вследствие болезни Паркинсона, - эти и многие другие системы имеют общее свойство: они генерируют ритмы. Обычно эти объекты не отделены от своего окружения, а, наоборот, взаимодействуют с другими объектами; иными словами, они являются открытыми системами. Действительно, биологические часы, управляющие ритмами суточной активности (циркадными ритмами), подвержены влиянию суточного и сезонного изменения освещенности и температуры, скрипач слышит своего коллегу по оркестру, на светлячка воздействует световое излучение всей популяции, различные центры ритмической активности мозга воздействуют друг на друга, и так далее. Такое взаимодействие может быть очень слабым, иногда едва заметным, но, тем не менее, оно часто приводит к качественному изменению состояния: объект подстраивает свой ритм, согласуя его с ритмами других объектов. В результате, скрипачи играют в унисон, насекомые в популяции генерируют световые или акустические импульсы с общей частотой, птицы в стае одновременно машут крыльями, сердце быстро галопирующей лошади сокращается один раз за каждый локомоторный цикл.

Такая подстройка ритмов за счет взаимодействия и является сущностью синхронизации, явления, которое систематически исследуется в этой книге.

Книга рассчитана на широкую аудиторию: физиков, химиков, биологов, инженеров, а также на других специалистов, занимающихся исследованиями на стыке различных областей¹; она рассчитана как на теоретиков, так и на

¹ Так как авторы - физики, то акцент неизбежно делается на физическом подходе к описанию естественных явлений.

экспериментаторов. Поэтому изложение экспериментальных фактов, основных принципов и математических методов в разных главах неоднородно, и иногда повторяется. Разнообразие предполагаемой аудитории отражено в структуре книги.

Первая часть книги, «Синхронизация без формул», рассчитана на читателя с минимальной математической подготовкой (знание математического анализа не требуется), по крайней мере, книга писалась с таким намерением. Хотя часть I практически не содержит уравнений, в ней описываются и объясняются на качественном уровне все основные идеи и эффекты². Здесь мы иллюстрируем синхронизацию экспериментами и наблюдениями из различных областей. Часть I может быть пропущена физиками-теоретиками, специалистами в нелинейной динамике, или же она может быть использована как источник примеров и приложений.

Части II и III охватывают тот же круг идей, но на уровне количественного описания; предполагается, что читатель этих частей знаком с основами нелинейной динамики. Мы надеемся, что основная часть материала будет понятна студентам старших курсов. В этих частях мы приводим обзор классических результатов по синхронизации периодических осцилляторов, как без учета, так и с учетом влияния шумов; рассматриваем явление синхронизации в ансамблях осцилляторов и в распределенных системах; представляем различные эффекты взаимодействия хаотических систем; приводим обширную библиографию.

Мы надеемся, что эта книга заполнит пробел в литературе. Действительно, хотя почти каждая книга по теории колебаний (или, в современных терминах, по нелинейной динамике) рассматривает синхронизацию в числе других нелинейных эффектов, только монографии И.И. Блехмана [1971; 1981], написанные в «дохаотическую» эру, специально посвящены этой теме. В них главным образом рассматриваются механические и электромеханические системы, но они также содержат подробный обзор теории, природных явлений и приложений в различных областях. При написании нашей книги мы пытались совместить описание классической теории с детальным обзором недавних результатов, делая упор на междисциплинарные приложения.

В процессе исследований по синхронизации мы с радостью сотрудничали и обсуждали результаты с В.С. Афраймовичем, В.С. Анищенко, В. Blasius, И.И. Блехманом, Н. Chate, U. Feudel, P. Glendinning, P. Grassberger, C. Grebogi, J. Hudson, С.П. Кузнецовым, П.С. Ланда, А. Lichtenberg, R. Livi, Ph. Marcq, Ю. Майстренко, E. Mosekilde, F. Moss, А.Б. Нейманом, Г.В. Осиповым, Е.-Н. Park, U. Parlitz, К. Piragas, А. Politi, А. Поповичем, R. Roy, O. Rudzick, S. Ruffo, Н.Ф. Рульковым, С. Schafer, L. Schimansky-Geier, L. Stone, Н. Swinney, P. Tass, E. Toledo и А.А. Заикиным.

Мы высоко ценим комментарии А.А. Непомнящего, А.А. Пиковского, А. Politi и С. Ziehmann, которые частично прочли рукопись.

О. Футер, Н.Б. Игошева и R. Mrowka терпеливо отвечали на наши многочисленные вопросы, касающиеся медицинских и биологических проблем.

Мы хотели бы выразить свою особую благодарность Михаилу Александровичу Заксу, который поддерживал нас на всех стадиях реализации этого проекта.

Мы также благодарим Philips International B.V., Company Archives (Эйндховен, Нидерланды) за присланные фотографию и биографию Балтазара Ван дер Поля и А. Kurths за ее помощь в подготовке библиографии.

² Для упрощения изложения мы опускаем в первой части ссылки на оригинальные работы, где эти идеи были высказаны; ссылки могут быть найдены в библиографическом разделе Введения, а также в библиографических заметках к частям II и III.

В заключение мы хотим отметить доброжелательное отношение сотрудников Cambridge University Press. Мы в особенности благодарны S. Capelin за его поддержку и терпение и F. Charman за ее превосходную работу по улучшению рукописи.

Интернет-страничка книги. Мы просим всех, кто желает высказать свои комментарии по поводу книги, прислать электронную почту по адресам:

pikovsky@stat.physik.um-potsdam.de;

mros@agnld.uni-potsdam.de;

jkurths@agnld.uni-potsdam.de.

Все опечатки и ошибки будут отмечены на интернет-страничке (URL: <http://www.agnld.uni-potsdam.de/~syn-book/>).

Электронная почта издательства: knigi@technosphere.ru;

Телефон (095) 234-01-10

Содержание

Предисловие к русскому изданию

Предисловие к английскому изданию

Часть I. Синхронизация без формул

Глава 1. Введение

- 1.1. Синхронизация в исторической перспективе.
- 1.2. Синхронизация: краткое описание явления.
Что такое синхронизация? Что не является синхронизацией.
- 1.3. Синхронизация: обзор различных случаев.
Терминологические замечания.
- 1.4. Основная библиография.

Глава 2. Основные понятия: автоколебательная система и ее фаза

- 2.1. Автоколебательные системы: математические модели естественных осцилляторов.
Автоколебательные системы типичны в природе. Геометрический образ периодических автоколебаний: предельный цикл.
- 2.2. Фаза: определение и свойства.
Фаза и амплитуда квазилинейного осциллятора. Амплитуда устойчива, фаза свободна. Общий случай: предельный цикл произвольной формы.
- 2.3. Автоколебательная система: основные свойства.
Диссипация, устойчивость и нелинейность. Автономные системы и системы под действием силы: фаза вынужденных колебаний не свободна!
- 2.4. Автоколебательные системы: дополнительные примеры и обсуждение.
Типичная автоколебательная система с контуром обратной связи. Релаксационные автоколебательные системы

Глава 3. Синхронизация периодических автоколебаний внешней силой

- 3.1. Слабое воздействие на квазилинейные автоколебания.
Автономные автоколебания и сила во вращающейся системе координат. Захват фазы и частоты. Переход к синхронизации. Пример: захват частоты дыхания механической вентиляцией.
- 3.2. Синхронизация внешней силой: более общий подход.
Стробоскопический метод. Пример: периодическая стимуляция светлячка. Захват последовательностью импульсов. Синхронизация высшего порядка. Языки Арнольда. Пример: периодическая стимуляция пейсмекерных клеток. Захват фазы и частоты: общий подход. Пример: синхронизация лазера.
- 3.3. Особенности синхронизации релаксационных автоколебаний.
Сброс внешним импульсом. Пример: кардиостимулятор. Электрическая модель сердца по Ван дер Полю и Ван дер Марку. Вариация порога. Пример: электронный релаксационный

автогенератор. Изменение собственной частоты. Модуляция и синхронизация. Пример: синхронизация песен сверчков.

- 3.4. Синхронизация в присутствии шума.
Диффузия фазы в автоколебаниях с шумом. Автоколебания с шумом и внешней силой. Проскоки фазы. Пример: захват дыхания при механической вентиляции. Пример: захват сердечного ритма слабым внешним стимулом.
- 3.5. Различные примеры.
Циркадные ритмы. Менструальный цикл. Захват периодических колебаний уровня инсулина периодическими инъекциями глюкозы. Синхронизация плазмодия миксомицета *Physarum*.
- 3.6. Явления, близкие к синхронизации.
Явления при большой внешней силе. Воздействие на возбудимые системы. Стохастический резонанс с точки зрения синхронизации. Захват нескольких осцилляторов общей силой.

Глава 4. Синхронизация двух и многих осцилляторов

- 4.1. Взаимная синхронизация автоколебательных систем.
Два взаимодействующих осциллятора. Пример: синхронизация триодных генераторов. Пример: частота дыхания и частота взмаха крыльев свободно летящих уток. Пример: переход между состояниями с синфазными и противофазными движениями. Заключительные замечания и связанные с синхронизацией эффекты. Релаксационные осцилляторы. Пример: клетки истинного и латентного водителей ритма синоатриального узла. Синхронизация в присутствии шума. Пример: активность мозга и мышц при болезни Паркинсона. Синхронизация ротаторов. Пример: контакты Джозефсона. Несколько осцилляторов.
- 4.2. Цепочки, решетки и колебательные среды.
Синхронизация в цепочке. Пример: цепочка лазеров. Образование кластеров. Пример: электрическая активность кишечника млекопитающих. Кластеры и биения в среде: подробное рассмотрение. Колебательная среда под периодическим воздействием. Пример: воздействие на реакцию Белоусова - Жаботинского.
- 4.3. Глобально связанные осцилляторы.
Самосинхронизация в ансамбле: переход Курамото. Пример: синхронизация менструальных циклов. Пример: синхронизация гликолитических колебаний в популяции дрожжевых клеток. Экспериментальное изучение ритмических аплодисментов.
- 4.4. Различные примеры.
Бег и дыхание у млекопитающих. Синхронизация двух осцилляторов «соль - вода». Захват колебаний тубулярного давления в нефронах. Клеточные популяции. Синхронизация колебаний систем хищник - жертва. Синхронизация в нейронных системах.

Глава 5. Синхронизация хаотических систем

- 5.1. Хаотические колебания.
Пример: модель Лоренца. Чувствительность к начальным условиям.
- 5.2. Фазовая синхронизация хаотических автоколебаний.
Фаза и средняя частота хаотических автоколебаний. Захват частоты внешней силой. Пример: хаотический разряд в газе.
- 5.3. Полная синхронизация хаотических систем.
Полная синхронизация идентичных систем. Пример: синхронизация двух лазеров. Синхронизация неидентичных систем. Полная синхронизация в общем контексте. Пример: синхронизация и кластеры в глобально связанных электрохимических осцилляторах. Синхронизация путем подавления хаоса.

Глава 6. Экспериментальное исследование синхронизации

- 6.1. Оценка фазы и частоты по сигналу.
Фаза импульсной последовательности. Пример: электрокардиограмма. Фаза узкополосного сигнала. Пример: дыхание. Несколько практических замечаний.
- 6.2. Анализ данных в «активном» и «пассивном» эксперименте.
«Активный» эксперимент. «Пассивный» эксперимент
- 6.3. Анализ взаимоотношения между фазами.
Непосредственный анализ разности фаз. Пример: регуляция позы человека. Высокий уровень шума. Стробоскопический метод. Фазовый стробоскоп в случае. Пример: взаимодействие сердечно-сосудистой и дыхательной систем. Фазовые соотношения при сильной модуляции. Пример: генерация потенциалов действия электрорецепторами веслоноса.
- 6.4. Заключение и библиографические заметки.
Несколько заметок о «пассивных» экспериментах. Количественное оценивание фазовых соотношений и его статистическая значимость. Некоторые полезные ссылки.

Часть II. Захват фазы и частоты

Глава 7. Синхронизация периодических автоколебаний периодическим внешним воздействием

7.1. Фазовая динамика.

Предельный цикл и фаза автоколебаний. Малые возмущения и изохроны. Пример: уравнение для комплексной амплитуды. Уравнение фазовой динамики. Пример: неавтономное уравнение для комплексной амплитуды. Медленная динамика фазы. Медленная динамика фазы: захват фазы и область синхронизации. Итоги рассмотрения фазовой динамики.

7.2. Слабо нелинейные автоколебания.

Амплитудное уравнение. Свойства синхронизации: изохронный случай. Свойства синхронизации в случае неизохронных автоколебаний.

7.3. Отображения окружности и кольца.

Отображение окружности: вывод и примеры. Свойства отображения окружности. Отображение кольца. Большая сила и переход к хаосу.

7.4. Синхронизация роторов и контактов Джозефсона.

Динамика роторов и контактов Джозефсона. Передемпфированный ротор во внешнем поле.

7.5. Системы фазовой автоподстройки.

7.6. Библиографические заметки.

Глава 8. Взаимная синхронизация двух взаимодействующих периодических осцилляторов

8.1. Фазовая динамика.

Усредненные фазовые уравнения. Отображение окружности.

8.2. Слабонелинейные осцилляторы.

Общие уравнения. Вымирание (гашение) колебаний. Притягивающее и отталкивающее взаимодействие.

8.3. Релаксационные колебания

8.4. Библиографические заметки

Глава 9. Синхронизация в системах с шумом

9.1. Автоколебания в присутствии шума

9.2. Синхронизация в присутствии шума.

Качественная картина ланжевеновской динамики. Количественное описание в случае белого шума. Синхронизация квазигармонической флуктуирующей силой. Взаимная синхронизация автоколебаний с шумом.

9.3. Библиографические заметки

Глава 10. Фазовая синхронизация хаотических систем

10.1. Фаза хаотического осциллятора.

Понятие фазы. Фазовая динамика хаотических осцилляторов

10.2. Синхронизация хаотических осцилляторов.

Фазовая синхронизация внешней силой. Косвенное описание синхронизации. Синхронизация в терминах неустойчивых периодических орбит. Взаимная синхронизация двух связанных осцилляторов.

10.3. Библиографические заметки.

Глава 11. Синхронизация в осциллирующих средах

11.1. Цепочки осцилляторов

11.2. Непрерывное по пространству распределение фазы.

Плоские волны и мишени. Влияние шума: шероховатость против синхронизации.

11.3. Слабо нелинейная колебательная среда.

Комплексное уравнение Гинзбурга - Ландау. Внешнее воздействие на колебательную среду.

11.4. Библиографические заметки

Глава 12. Ансамбли глобально связанных осцилляторов

12.1. Переход Курамото.

12.2. Осцилляторы с шумом.

12.3. Обобщения.

Модели, основанные на фазовом приближении. Глобально связанные слабонелинейные осцилляторы. Связанные релаксационные осцилляторы. Связанные контакты Джозефсона. Эффекты конечности числа элементов ансамбля. Ансамбль хаотических осцилляторов.

12.4. Библиографические заметки

Часть III. Синхронизация хаотических систем

Глава 13. Полная синхронизация I: основные свойства

- 13.1. Простейшая модель: два связанных отображения
- 13.2. Устойчивость синхронного режима
- 13.3. Статистическая теория перехода к синхронизации.
Возмущение как случайное блуждание. Диффузия определяется статистикой локальных по времени ляпуновских показателей. Модуляционная перемежаемость: степенные распределения. Модуляционная перемежаемость: корреляционные свойства.
- 13.4. Переход к синхронизации: геометрическое рассмотрение.
Поперечные бифуркации периодических траекторий. Слабая и сильная синхронизация. Локальный и глобальный риддинг.
- 13.5. Библиографические заметки

Глава 14. Полная синхронизация II: обобщения и сложные системы

- 14.1. Идентичные отображения, связь общего вида.
Однонаправленная связь. Асимметричная локальная связь. Глобальная связь (через среднее поле).
- 14.2. Системы с непрерывным временем
- 14.3. Распределенные системы.
Пространственно однородный хаос. Поперечная синхронизация пространственно-временного хаоса. Синхронизация в связанных клеточных автоматах.
- 14.4. Синхронизация как симметричное состояние общего вида.
Копированные системы.
- 14.5. Библиографические заметки

Глава 15. Синхронизация сложной динамики внешним воздействием

- 15.1. Синхронизация периодической силой
- 15.2. Синхронизация шумовым воздействием.
Периодические колебания под действием шума. Синхронизация хаотических колебаний внешним шумом.
- 15.3. Синхронизация хаотических колебаний хаотической силой.
Полная синхронизация. Обобщенная синхронизация. Обобщенная синхронизация квазипериодической силой.
- 15.4. Библиографические заметки

Приложение 1. Открытие синхронизации Христианом Гюйгенсом

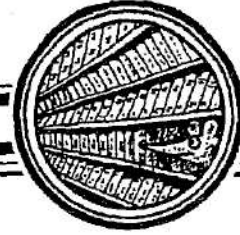
- П1.1. Письмо Христиана Гюйгенса его отцу, Константину Гюйгенсу
- П1.2. Морские часы (симпатия часов). Часть V

Приложение 2. Мгновенные фаза и частота сигнала

- П2.1. Аналитический сигнал и преобразование Гильберта
- П2.2. Примеры
- П2.3. Численные проблемы и практические рекомендации
- П2.4. Вычисление мгновенной частоты

Список литературы

Предметный указатель



FLUCTUATION AND NOISE LETTERS
**An Interdisciplinary Scientific Journal on Random Processes in Physical,
Biological and Technological Systems**

© World Scientific Publishing Company

Vol. 3, No. 2 (2003) C1

Vadim S. Anishchenko
Issue Editor

**SYNCHRONIZATION OF CHAOTIC
AND STOCHASTIC OSCILLATIONS AND ITS APPLICATIONS**

The field «Nonlinear Dynamics of Complex Systems in the Presence of Fluctuations» is one of the hottest topics of today's physical and biological research. It is very intriguing to see and to research the rules how a deterministic process becomes stochastic or how a stochastic process becomes synchronized to a deterministic process when certain parameters evolve.

This is a strongly interdisciplinary field of science. Originally, only mathematicians and theoretical physicists dealt with these phenomena but nowadays a wide range of scientists, including experimental physicists, biophysicists, information scientists, engineers, biomedical scientists, etc. devote their efforts to this field.

The International scientific conference «Synchronization of Chaotic and Stochastic Oscillations; Applications in Physics, Chemistry, Biology and Medicine» (SYNCHRO-2002) took place in September, 22-28, 2002, in Saratov (Russia). The conference was organized by the Laboratory of Nonlinear Dynamics of Saratov State University and the Research-Educational Center of Nonlinear Dynamics and the Biophysics of SSU (REC-006). The conference SYNCHRO-2002 was sponsored by the U.S. Civilian Research and Development Foundation, the Russian Federation Ministry of Education, the Russian Foundation for Basic Research, the Alexander von Humboldt Foundation and Project SFB 555 (Germany).

About hundred scientists coming from fourteen countries of Europe, Asia and America attended the meeting. Twenty-eight invited talks were held by recognized leaders in scientific fields related to stochastic nonlinear dynamical systems.

The focus topics of the conference were synchronization phenomena and related fundamental issues in nonlinear systems and the practical applications of the results.

The conference proceedings is published in a special issue of the Journal «Applied Nonlinear Dynamics» (in Russian)* and a special selection of invited papers in the Journal «Fluctuation and Noise Letters».

You have that special selection in your hands. We wish you an inspiring reading.

Laboratory of Nonlinear Dynamics,
Physics Department, Saratov State University
Astrakhanskya str. 83, 410012 Saratov, Russia
vadim@chaos.ssu.runnet.ru
igor@chaos.ssu.runnet.ru

Vadim S. Anishchenko
Chairman of organizing committee
of the conference, Director of
Scientific and Educational
Center «Nonlinear dynamics
and biophysics SSU», professor
Igor A. Khovanov, PhD

CONTENTS

Current Opinions

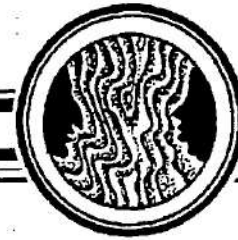
- Synchronization of Chaotic and Stochastic Oscillations and its Applications.
Vadim S. Anishchenko and Igor A. Khovanov C1

Letters

- Relaxation Times in Systems with Zero and Non-Zero Stationary Flow.
N.V. Agudov and A. V. Safonov L107
- Coherence Resonance of the Noise-Induced Motion on the Way to Breakdown
of Synchronization in Chaotic Systems. *A.G. Balanov, N.B. Janson and*
P.V.E. McClintock L113
- An Experimental Study of Stochastic Phase Synchronization in Vertical Cavity
Lasers. *Sylvain Barbay, Giovanni Giacomelli, Stefano Lepri and*
Alessandro Zavatta L121
- Entrainment of Optical Low-Frequency Fluctuations is Enhanced by Coupling.
J.M. Buldú, J. Garcia-Ojalvo, M.C. Torrent, Raúl Vicente, Toni Pérez
and Claudio R. Mirasso L127
- Synchronization of Stochastic Motions in Swarms of Active Brownian Particles
with Global Coupling. *Werner Ebeling* L137
- Collective Motion of Brownian Particles with Hydrodynamic Interactions. *Udo*
Erdmann and Werner Ebeling L145
- Stationary Probability Distributions for Fitzhugh-Nagumo Systems. *Marcin*
Kostur, Xaver Sailer and Lutz Schimansky-Geier L155
- Interactions and Synchronization in the Cardiovascular System. *Peter*
V.E. McClintock and Aneta Stefanovska L167
- Noise Induced Phenomena in Lotka-Volterra Systems. *B. Spagnolo, A. Fiasco-*
naro and D. Valenti L177
- Using Synchronization to Detect Chaotic Response in Externally Forced
Dynamical Systems. *Andrzej Stefanski, Tomasz Kapitaniak and*
Przemyslaw Szuminski L187
- Noise-Induced Phase Synchronization: Theoretical and Experimental Results.
Jan A. Freund, Sylvain Barbay, Stefano Lepri, Alessandro Zavatta and
Giovanni Giacomelli L195

* The best reports of young scientists were awarded by prize of the organizing committee and recommended for publishing. Now they have been recently published in the journal «Izv. VUZ. Applied Nonlinear Dynamics», 2003, vol. 11, № 2.

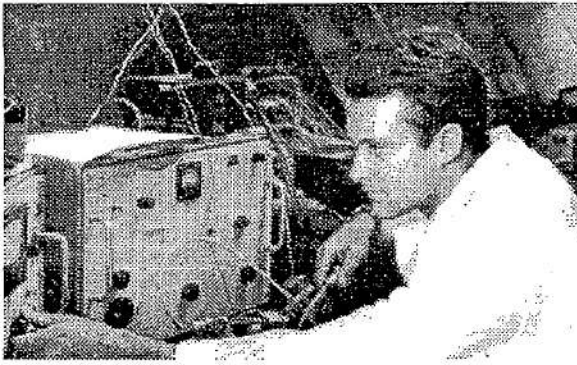
A Model of Oscillations of Macromolecule with Anomalous Quality Factor. <i>O. Chichigina, A. Netrebko and Yu. Romanovsky</i>	L205
Spectral and Correlation Analysis of Spiral Chaos. <i>Vadim S. Anishchenko, Tatjana E. Vadivasova, Andrey S. Kopeikin, Galina I. Strelkova and Jürgen Kurths</i>	L213
Sociodynamics - A Systematic Approach to Mathematical Modelling in the Social Sciences. <i>Wolfgang Weidlich</i>	L223
Segregation of Particles Using Chaotic Ratchets. <i>Jose L. Mateos</i>	L233
Fluctuation-Induced Local Oscillations and Fractal Patterns in the Lattice Limit Cycle Model. <i>A. Provata, G.A. Tsekouras, F. Diakonos, D. Frantzes- kakis, F. Baras, A.V. Shabunin and V. Astakhov</i>	L241
Renormalization in Quasiperiodically Forced Systems. <i>A.H. Osbaldestin and B.D. Mestel</i>	L251



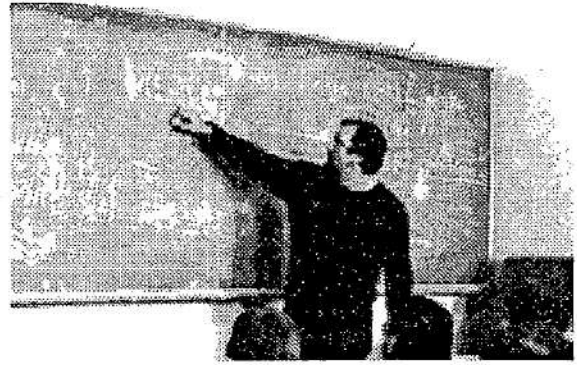
НАУЧНАЯ БИОГРАФИЯ В.С. АНИЩЕНКО

Вадим Семенович Анищенко окончил физический факультет Саратовского государственного университета в 1966 году. После окончания СГУ он работает инженером НИИМФа, учится в аспирантуре, а с 1970 года преподает на кафедре радиофизики. Еще будучи студентом он занимается исследованиями в научной группе под руководством А.И. Штырова. Круг его научных интересов в то время связан с флуктуационными явлениями в электронных СВЧ устройствах. Первая научная статья А.И. Штыров, В.С. Анищенко «Коэффициент шума ЛБВ в режиме непрерывного и равномерного токоперехвата замедляющей системы» (Радиотехника и электроника, 1967. Т. 12, № 8) вышла в свет в 1967 году. В 1970 году В.С. Анищенко защищает кандидатскую диссертацию на тему «Шумовые свойства электронных потоков СВЧ-усилителей О-типа». В те же годы он впервые на физическом факультете разрабатывает и читает общий курс лекций «Статистическая радиофизика и теория информации», создает соответствующий лабораторный практикум по статистической радиофизике. Сочетание научных интересов, лежащих в области нелинейных колебаний и случайных процессов, логически приводят доцента В.С. Анищенко к совершенно новому в то время фундаментальному научному направлению - исследованию динамического хаоса. На рубеже 70-80 годов он создает небольшую научную группу из студентов и аспирантов и начинает исследования в новой для него области. Одним из первых, но очень важных достижений В.С. Анищенко и его группы было создание базовой модели динамического хаоса - радиофизического генератора с инерционной нелинейностью, известного в настоящее время как генератор Анищенко - Астахова [1,2]. Эта простая система с 1.5 степенями свободы легла в основу теоретических и экспериментальных исследований, позволивших обнаружить и изучить ряд новых фундаментальных явлений и закономерностей. Впервые были обнаружены и исследованы такие явления, как перемежаемость типа «хаос-хаос» [3], бифуркации удвоения двумерных и трехмерных торов [4,5,6], пространственные бифуркации удвоения и пространственное «насыщение» хаоса в цепочке хаотических автогенераторов [7,8]. Впервые была показана особая роль флуктуаций в системах с негиперболическими хаотическими аттракторами [9,10]. Впервые проведен двухпараметрический экспериментальный анализ разрушения двухчастотных квазипериодических колебаний, приводящий к возникновению хаоса [4,11]. Впервые численно и экспериментально обнаружено и исследовано явление частотной синхронизации хаоса, состоящее в захвате или подавлении базовых частот, выделяющихся в спектре хаотических колебаний [12,13].

Научные результаты 1980-1984 годов составили материал монографии В.С. Анищенко «Стохастические колебания в радиофизических системах» (Изд-во Саратов. ун-та, 1985, часть 1; 1986, часть 2). Это была первая в России и одна из

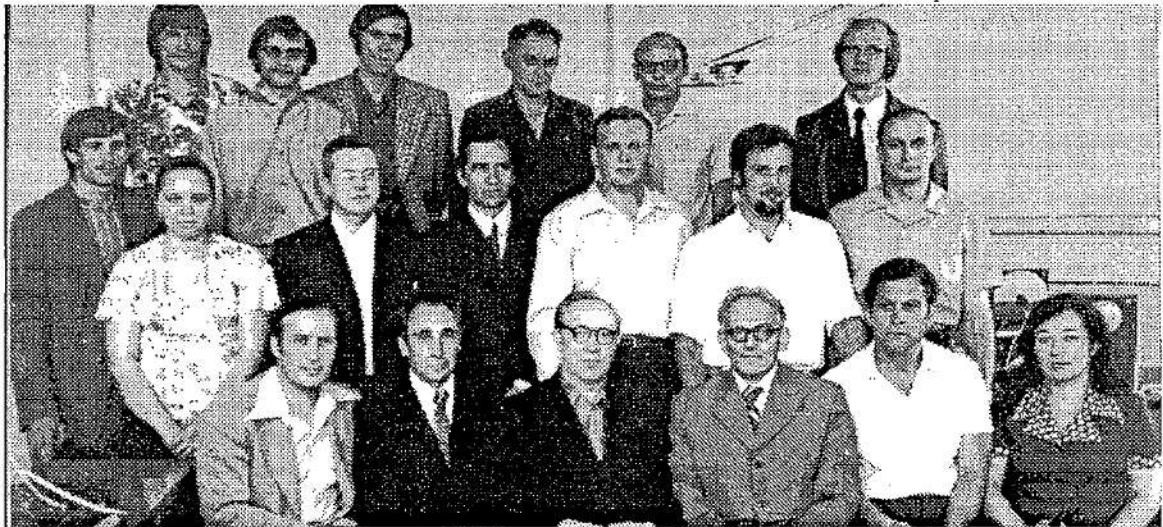


В научной лаборатории, 1967 год
Архив В.С.Анищенко



Лекция доцента В.С.Анищенко по статистической радиофизике, 1972/73 уч. год

Архив О.Н.Соколов



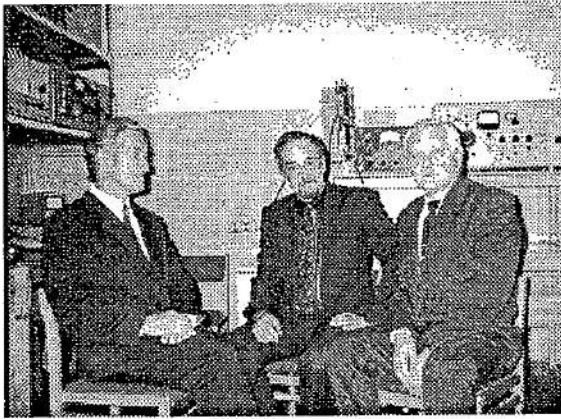
Кафедре радиофизики 25 лет. В первом ряду слева направо: доцент В.С. Ильин, ст. преподаватель Ю.П. Науменко, доцент В.А. Седин, зав. кафедрой Г.М. Герштейн, доцент А.В. Штыров, ст. преподаватель Е.А. Родионова. Во втором ряду слева направо: лаборант Семеняка (вторая), доценты О.Н. Соколов, Г.Н. Коростелев, И.Н. Салий, В.С. Анищенко, ассистент А.С. Листов. В третьем ряду слева направо: инженеры А.В. Розанов (второй), Н.Ф. Демидов (четвертый), ст. преподаватель В.Д. Лучинин, нач. лаборатории В.Н. Сорокин. 1976 год

Архив кафедры

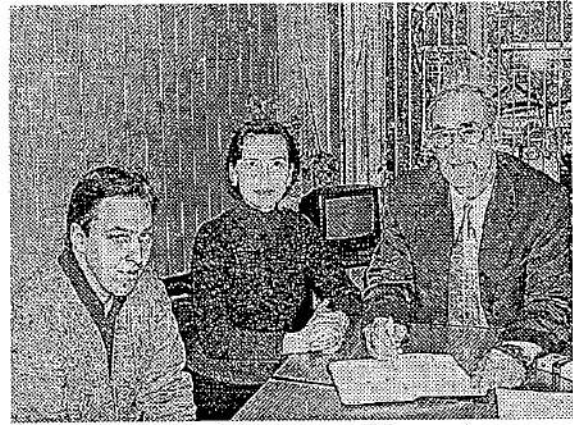


В общежитии МГУ с профессором Ю.Л. Климонтовичем и его аспирантами, второй слева М. Бонц (ныне профессор Ростокского университета, Германия). ФПК 1980 года

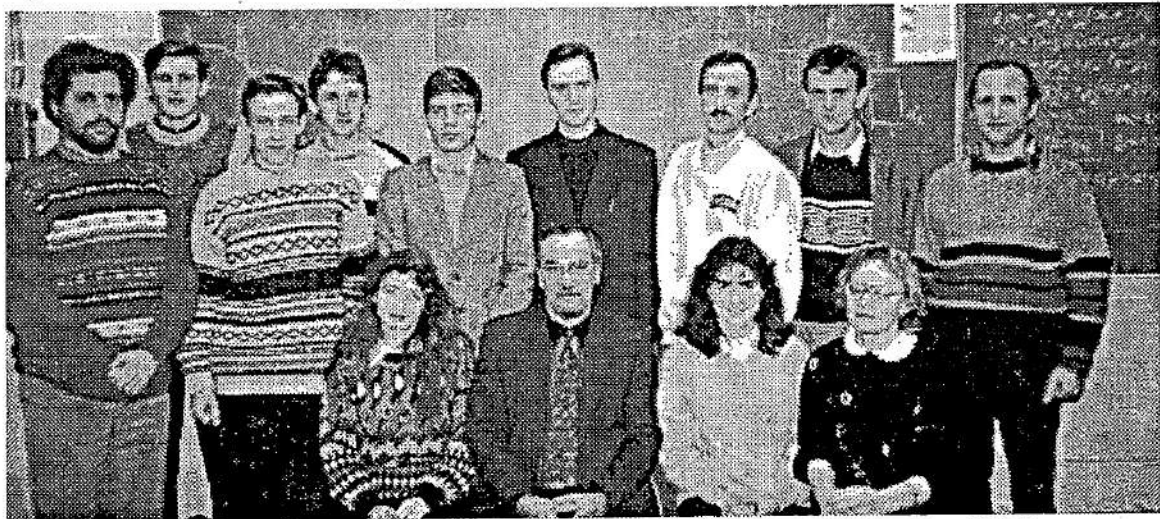
Архив В.С.Анищенко



С профессорами кафедры радиофизики: А.В. Хохлов (слева) и И.Н. Салий (справа), 1994 год
Архив кафедры



Лауреаты грантов Президента РФ, слева-направо: доцент А.Н. Павлов, вед. инженер Г.И. Стрелкова, профессор В.С. Анищенко, 2004 год



Лаборатория нелинейной динамики. В первом ряду слева направо: аспирантка О.В. Сосновцева, научный руководитель В.С. Анищенко, аспирантка Н.Б. Янсон, доцент Т.Е. Вадивасова. Во втором ряду: доцент А.Б. Нейман; аспиранты И.А. Хованов, А.Н. Павлов, А.Н. Сильченко, А.П. Никитин, А.Г. Баланов, доцент Д.Э. Постнов, ст. преподаватель А.В. Шабунин, доцент В.В. Астахов. 1994 год



Сотрудники кафедры радиофизики, 1994 год.

Архив кафедры

первых в мире монографий, посвященных исследованию динамического хаоса. Годом спустя книга была издана в Германии на английском языке. В 1986 году состоялась защита докторской диссертации «Механизмы разрушения и свойства хаотических колебаний в радиофизических системах с конечным числом степеней свободы». Достижения Вадима Семеновича и его учеников находят признание у отечественных и зарубежных ученых. Успешное развитие нового научного направления привело к созданию на основе научной группы Анищенко Лаборатории нелинейной динамики СГУ.

С 1988 г. профессор В.С. Анищенко заведует кафедрой радиофизики. В связи с успехами в развитии нового научного направления она в 1997 года была преобразована в кафедру радиофизики и нелинейной динамики. Несмотря на тяжелое экономическое положение в стране в 90-е годы, возглавляемая профессором Анищенко кафедра продолжает развиваться. На кафедре разрабатываются новые лекционные курсы и практикумы. Преподаватели и сотрудники постоянно ведут научные исследования по различным направлениям нелинейной динамики и радиофизики, в которых активно участвуют аспиранты и студенты. Растет число публикаций, сотрудники кафедры участвуют в большинстве ведущих конференций по нелинейной динамике. Практически ежегодно на кафедре защищаются диссертации. Укрепляются и расширяются международные связи. На деньги, заработанные сотрудниками по научным грантам, кафедра оснащается современной вычислительной техникой и радиоизмерительной аппаратурой, создается локальная сеть с выходом в интернет, открывается дисплейный класс для студентов кафедры.

Новые технические средства проведения компьютерных и физических экспериментов открыли широкие возможности для исследований. К научным достижениям В.С. Анищенко в последние годы можно отнести следующие фундаментальные результаты:

- Открыто явление стохастического резонанса в хаотических бистабильных системах, включая эффект динамического стохастического резонанса без воздействия внешних шумов [14-16].
- Открыто явление стохастической синхронизации в бистабильных системах, представляющее собой захват средней частоты переключений внешним периодическим сигналом [17,18].
- Впервые установлен эффект синхронизации кардиоритма внешним периодическим и хаотическим сигналами [19,20].
- Экспериментально и численно показано, что мгновенная фаза хаотических автоколебаний в режиме спирального аттрактора ведет себя подобно винеровскому процессу и характеризуется конечным коэффициентом эффективной диффузии.
- Спектрально-корреляционные характеристики различных типов хаотической динамики могут быть смоделированы с помощью классических случайных процессов, таких как гармонический шум и случайный телеграфный сигнал [21-23].

В настоящее время Вадим Семенович Анищенко - один из ведущих в России и мире специалистов в области нелинейной теории колебаний и теории флуктуаций в нелинейных системах. Он автор более 350 научных работ, среди которых 9 научных монографий.

Под руководством профессора В.С. Анищенко защищено 4 докторских и 16 кандидатских диссертаций, выполнены исследования по 19 научным грантам, из которых 7 - международные. Он является одним из основных организаторов и создателей Научно-образовательного центра (НОЦ) СГУ «Нелинейная динамика и биофизика». НОЦ был организован в 2000 году в результате победы в конкурсе

грантов в рамках программы «Фундаментальные исследования и высшее образование», финансируемой МО РФ и Американским Фондом гражданских исследований и развития (CRDF). С момента создания НОЦ профессор Анищенко является его директором. В 2003 году им организован Международный институт нелинейной динамики, в работе которого, помимо сотрудников кафедры участвуют научные группы ведущих европейских университетов. В.С. Анищенко проводит активную работу по развитию международных научных связей. На сегодняшний день создано 9 международных научных групп, в которых работают аспиранты и докторанты кафедры, перенимая опыт и повышая квалификацию. Профессор Анищенко входит в состав редколлегий 2 специализированных научных журналов, принимал участие в работе оргкомитетов 6 международных научных конференций, организовал и провел 2 международных конференции по нелинейной динамике в Саратове (в 1996 и 2002 годах). Профессор Анищенко является членом координационного совета Центра исследований сложных систем при Потсдамском университете (Германия).

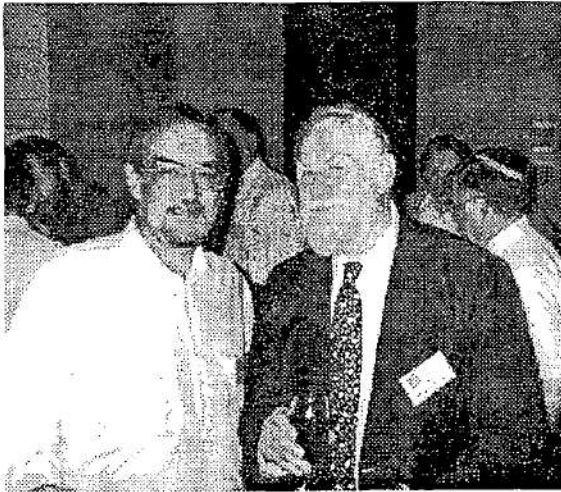
За достижения в науке и преподавательской деятельности В.С. Анищенко пять раз присуждалось звание «Соросовский профессор», он избран академиком РАЕН, ему трижды присуждалась государственная научная стипендия РАН. За выдающиеся научные достижения в области нелинейной динамики стохастических систем в 1999 году В.С. Анищенко была присуждена премия Международного научного фонда имени Александра фон Гумбольдта по физике. Коллектив, который он возглавляет, по итогам конкурса 2003 года вошел в число ведущих научно-педагогических коллективов Российской Федерации.

Scientific Carrier of Prof. Dr. Vadim S. Anishchenko

Vadim Anishchenko graduated from the Department of Physics of Saratov State University in 1966. Being a graduate student he started his scientific research in the group supervised by Dr. Alexander I. Shtyrov. After his graduation Vadim continued active research under supervision of Professor Shtyrov as an engineer at the Research Institute of Mechanics and Physics (this Research Institute belonged to the Department of Physics). Then he entered a PhD program at the Department of Physics. The main topic of Vadim Anishchenko's scientific studies was related to fluctuational phenomena in electronic microwave devices. The first paper written by A.I. Shtyrov and V.S. Anishchenko, «Noise coefficient of a traveling wave tube in the regime of continuous and uniform current interception of a decelerating system» was published in 1967 in the journal «Radiotekhnika i Elektronika», published by the Soviet Academy of Sciences. In 1970 Vadim Anishchenko defended his candidate of science thesis (an equivalent of PhD) on the topic «Noisy properties of electronic flows of microwave amplifiers of the *O*-type».

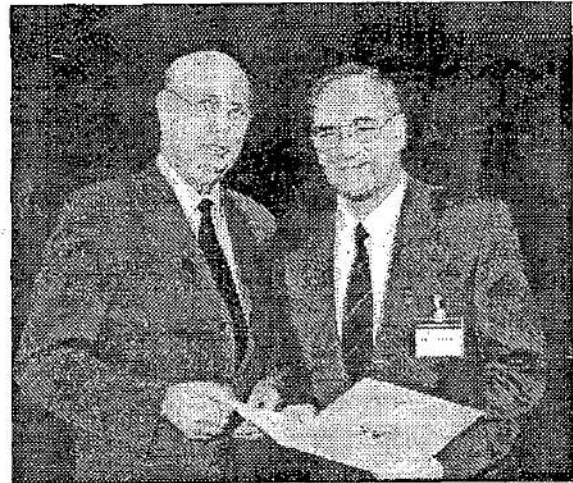
Since 1970 Vadim Anishchenko has been teaching at the Radiophysics Chair. He developed and delivered a lecture course on «Statistical radiophysics and the theory of information» at the Department of Physics. Additionally, he built the laboratory on statistical radiophysics.

Combination of scientific interests lying in the area of nonlinear oscillations and random processes served as a background for him to come to studies of dynamical chaos being that time an absolutely new fundamental scientific direction. In the very early 1980's Vadim Anishchenko, already Associate Professor, created a small research group with students and PhD students and started scientific investigations in the new field. The development and creation of a radiophysical generator with inertial nonlinearity becoming a basic model of dynamical chaos were one of the first and important



With the founder of synergetics Prof. H. Haken.
Conference in Beer-Sheva, Israel, 1998

Chair property



Delivery of the Humboldt Research Award. Prof.
V.S. Anishchenko with the President of the AvH
Foundation Prof. W. Frühwald, Bamberg, Germany,
2001

Chair property



With Prof. L.P. Shilnikov (in the center) and Prof. A.N. Sharkovsky at the Conference NOLTA - 93.
Honolulu Airport, USA 1993

Chair property



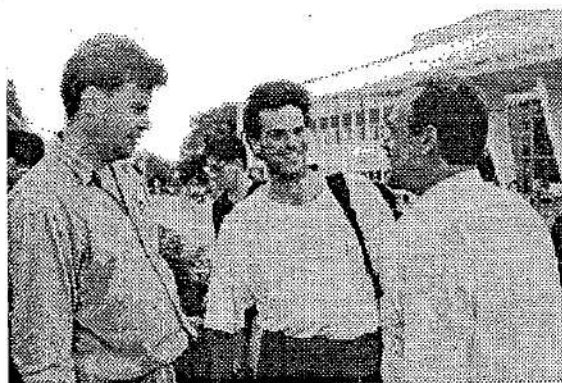
Chairmen of the Conference ICND - 96: Prof. W. Ebeling (Humboldt University, Berlin), Prof.
D.I. Trubetskov (Saratov State University), Prof. V.S. Anishchenko (Saratov State University). Saratov,
Russia, 1996

Chair property

Participants of the Conference ICND - 96



Prof. Erik Mosekilde (Technical University of Denmark)



Dr. J. Freund (Humboldt University, Germany) and Dr. R. Bartussek (University of Augsburg, Germany)



Prof. Y.L. Klimontovich (Moscow State University, Russia)



Dr. A. Feudel (Potsdam University, Germany)



Prof. P.V.E. McClintock (Lancaster University, UK)



Prof. P.S. Landa (M.S.U., Russia), Dr. M. Rosenblum and Prof. J. Kurths (Potsdam University, Germany)



Prof. M. Hasler (Swiss Federal Institute of Technology, Switzerland) and Dr. Yu. Maistrenko (National Academy of Sciences, Ukraine)



Prof. U. Feudel (Potsdam University, Germany)

achievements of Vadim Anishchenko and his group. This generator is known now as the Anishchenko-Astakhov oscillator [1,2]. This simple system with 1.5 degrees of freedom served as the basis for theoretical and experimental studies that enabled to discover and explore a number of new fundamental phenomena and regularities. Using this system, Vadim Anishchenko and his collaborators first revealed and studied «chaos-chaos» intermittency [3], period-doubling bifurcations of two-dimensional and three-dimensional tori [4-6], spatial period-doubling bifurcations and spatial «saturation» of chaos in a chain of chaotic self-sustained oscillators [7,8]. A special role of fluctuations was first demonstrated in systems with non-hyperbolic chaotic attractors [9,10]. A two-parametric experimental analysis was first performed to study the mechanism of two-frequency quasi-periodic oscillations destruction leading to the onset of chaos [4,11]. There was first revealed and explored numerically and experimentally the phenomenon of frequency synchronization of chaos, that consists in locking or suppression of basic frequencies pronounced in the power spectrum of chaotic oscillations [12,13].

Scientific results obtained by Vadim Anishchenko and his group in 1980-1984 were put in the monograph «Stochastic Oscillations in Radiophysical Systems» published in 1985 (Part I) and 1986 (Part II) by the Saratov University Publisher. This book was one of the first in the world monographs dedicated to dynamical chaos. One year later it was translated to English and published in Germany by Teubner.

In 1986 Vadim Anishchenko defended his Doctor of Sciences thesis on the topic «Mechanisms of destruction and properties of chaotic oscillations in radiophysical systems with a finite number of degrees of freedom». Scientific achievements of Vadim Anishchenko and his research group become world wide recognized. The successful development of the new scientific direction led to the creation of the Nonlinear Dynamics Laboratory supervised by Prof. Vadim Anishchenko.

Since 1988 Prof. V.S. Anishchenko is the Head of the Radiophysics Chair. The study of dynamical chaos becomes one of the leading scientific directions at the Chair and in 1997 it was renamed as the Radiophysics and Nonlinear Dynamics Chair.

In spite of a quite difficult economic situation in Russia in 1990's the Chair supervised by Vadim Anishchenko continued developing. New lecture courses and practical laboratories were established. The professors and research fellows continuously carried out cutting edge researches on various topics and directions of nonlinear dynamics and radiophysics, where students and PhD students participate actively.

The number of publications has grown significantly in 1990's and the laboratory members have attended numerous International and local Conferences on nonlinear dynamics. These years of intensive research and of many different scientific projects created a constant flow of PhD dissertations coming from the laboratory almost every year. All this gained local and international recognition of the laboratory and allowed to extend international scientific collaboration. Vadim Anishchenko and his laboratory have organized several international conferences with proceedings published in leading international journals.

The laboratory leading by Vadim Anishchenko has brought significant funds to the Chair which allowed to build modern research and educational environment as well as modern computer facilities, including a recently established parallel computer cluster. It also allowed to bring world leading scientists in the area of nonlinear dynamics to give lectures and seminars at Saratov State University.

Among very recent scientific achievements of Vadim Anishchenko the following fundamental results are worth to be emphasized especially.

- The effect of stochastic resonance in chaotic bistable systems was discovered including the effect of dynamical stochastic resonance without external noise sources [14-16].
- The phenomenon of stochastic synchronization in bistable systems was first

revealed that represents the mean switching frequency locking by an external periodic signal [17,18].

- The effect of synchronization of cardiorythm by external periodic and chaotic signals was first established [19,20].
- It was demonstrated experimentally and numerically that the instantaneous phase of chaotic self-sustained oscillations in the regime of a spiral attractor behaves like a Wiener process and is characterized by a finite value of the effective diffusion coefficient. Spectral and correlation characteristics of different types of chaotic dynamics can be modeled by means of classical random processes such as harmonic noise and a random telegraph signal [21-23].

Now Vadim Anishchenko is one of the leading world experts in the field of nonlinear theory of oscillations and the theory of fluctuations in nonlinear systems. He is the author of more than 350 scientific papers and 9 scientific monographs.

16 PhD dissertations were defended under supervision of Prof. Vadim Anishchenko and 4 Doctor of Sciences dissertation were defended by the members of the laboratory. He also supervised the work on more than 19 scientific research grants among which 7 projects were international. Vadim Anishchenko is one of the main organizers and founders of the Research and Educational Center (REC-006) on «Nonlinear Dynamics and Biophysics» at Saratov State University. This Center was organized in 2000 as a result of the grant competition in the framework of the Basic Research and Higher Education Program supported by the Civil Research and Development Foundation of the U.S. (CRDF) and the Russian Ministry of Education. Prof. Vadim Anishchenko is the Director of this Center. In 2003 he organized the International Institute of Nonlinear Dynamics that involves both the Chair collaborators and several research groups of the leading European Universities. Vadim Anishchenko has been leading an active work to develop and expand international scientific linkages. At the present time 9 international research groups were created where PhD students and collaborators of the Chair took an active part. Vadim Anishchenko is on the Editorial Boards of two scientific journals, namely, «Applied Nonlinear Dynamics» and «Discrete Dynamics in Nature and Society». He also participated in the work of the Organizing Committees of 6 International Scientific Conferences, organized and conducted 2 International meetings on nonlinear dynamics in Saratov (1996 and 2002). Prof. Vadim Anishchenko is a member of the Advisory Board of the Center for Complex Systems Studies at Potsdam University (Germany). For the achievements in science and teaching Prof. Vadim Anishchenko was awarded the Soros Professor title 5 times. He is an academician of the Russian Academy of Natural Sciences. He was awarded three times the State Scientific grants of the Russian Academy of Sciences. For his outstanding scientific research in the field of nonlinear dynamics of stochastic systems Prof. Vadim Anishchenko was awarded the Humboldt Research Prize in physics in 1999. The group supervised by Prof. Vadim Anishchenko won the competition in 2003 and was included into the list of the leading scientific and teaching groups of the Russian Federation.

*V. Astakhov
T. Vadivasova
G. Strelkova
A. Khokhlov
D. Postnov*

Monographs

1. *Анищенко В.С. Стохастические колебания в радиофизических системах. Часть 1. Физико-математические основы описания и исследования динамической стохастичности. Саратов: Изд-во Сарат. ун-та, 1985.*

2. Анищенко В.С. Стохастические колебания в радиофизических системах. Часть 2. Типичные бифуркации и квазиаттракторы в нелинейных системах с малым числом степеней свободы. Саратов: Изд-во Саратов. ун-та, 1986.

3. *Anishchenko V.S.* Dynamical Chaos - Basic Concepts. Leipzig: Teubner-Texte zur Physik, Bd 14, 1987.

4. *Anishchenko V.S.* Dynamical Chaos in Physical Systems: Experimental Investigation of Self-Oscillating Circuits. Leipzig: Teubner-Texte zur Physik, Bd 22, 1989.

5. Анищенко В.С. Сложные колебания в простых системах. М.: Наука, 1990.

6. *Anishchenko V.S.* Dynamical Chaos - Models and Experiments. Singapore: World Scientific, 1995.

7. Анищенко В.С., Вадивасова Т.Е., Астахов В.В. Нелинейная динамика хаотических и стохастических систем. Саратов: Изд-во Саратов. ун-та, 1999.

8. *Anishchenko V.S., Astakhov V.V., Neiman A.B., Vadivasova T.E., Schimansky-Geier L.* Nonlinear Dynamics of Chaotic and Stochastic Systems. Berlin, Heidelberg, New York, Springer, 2002.

9. Анищенко В.С., Астахов В.В., Вадивасова Т.Е., Нейман А.Б., Стрелкова Г.И., Шиманский-Гайер Л. Нелинейные эффекты в хаотических и стохастических системах. Ижевск, 2003.

Key publications

1. Анищенко В.С., Астахов В.В., Летчфорд Т.Е. Многочастотные и стохастические автоколебания в генераторе с инерционной нелинейностью // Радиотехника и электроника. 1982. Том 27, № 10. С. 1972.

Anishchenko V.S., Astakhov V.V., Letchford T.E. Multi-frequency and Stochastic Self-Sustained Oscillations in an Oscillator with Inertial Nonlinearity // Radiotechnika i Elektronika. 1982. Vol. 27, № 10. P. 1972 (in Russian).

2. Анищенко В.С., Астахов В.В., Летчфорд Т.Е. Экспериментальное исследование структуры странного аттрактора модели генератора с инерционной нелинейностью // ЖТФ. 1983. Том 53, № 1. С. 152.

Anishchenko V.S., Astakhov V.V., Letchford T.E. Experimental Study of the Structure of a Strange Attractor in the Model of an Oscillator with Inertial Nonlinearity // Sov. Tech. Phys. 1983. Vol. 28, № 1. P. 91.

3. Анищенко В.С. Взаимодействие странных аттракторов. Перемежаемость «хаос - хаос» // Письма ЖТФ. 1984. Том 10, № 10. С. 629.

Anishchenko V.S. Interaction of Strange Attractors. «Chaos - Chaos» Intermittency // Sov. Tech. Phys. Lett. 1984. Vol. 10, № 5. P. 266.

4. Анищенко В.С., Летчфорд Т.Е., Сафонова М.А. Эффекты синхронизации и бифуркации синхронных и квазипериодических колебаний в неавтономном генераторе // Радиофизика. 1985. Том 28, № 9. С. 1112.

Anishchenko V.S., Letchford T.E., Safonova M.A. Effects of Synchronization and Bifurcations of Synchronous and Quasi-periodic Oscillations in a Non-autonomous Oscillator // Izv. VUZov - Radiofizika. 1985. Vol. 28, № 9. P. 1112 (in Russian).

5. Анищенко В.С., Летчфорд Т.Е., Сафонова М.А. Критические явления при гармонической модуляции двухчастотных колебаний // Письма ЖТФ. 1985. Том 11, № 9. С. 536.

Anishchenko V.S., Letchford T.E., Safonova M.A. Critical Phenomena Under Harmonics Modulation of Two-frequency Oscillations // Sov. Tech. Phys. Lett. 1985. Vol. 11, № 5. P. 223.

6. Анищенко В.С., Летчфорд Т.Е. Разрушение трехчастотных колебаний в

генераторе при бигармоническом воздействии // Письма ЖТФ. 1986. Том 56, № 11. С. 2250.

Anishchenko V.S., Letchford T.E. Breakup of Three-frequency Oscillations and Onset of Chaos in a Biharmonically Excited Oscillator // Sov. Phys. Tech. Phys. 1986. Vol. 31, № 11. P. 1347.

7. *Анищенко В.С., Постнов Д.Э., Сафонова М.А.* Размерность и физические свойства хаотических аттракторов цепочки связанных генераторов // Письма ЖТФ. 1985. Том 12, № 24. С. 1505.

Anishchenko V.S., Postnov D.E., Safonova M.A. Dimension and Physical Properties of Chaotic Attractors in a Chain of Coupled Oscillators // Sov. Tech. Phys. Lett. 1985. Vol. 11, № 12. P.621.

8. *Анищенко В.С., Арансон И.С., Постнов Д.Э., Рабинович М.И.* Пространственная синхронизация и бифуркации развития в цепочке связанных генераторов // ДАН СССР. 1986. Т. 28, № 5. С. 1120.

Anishchenko V.S., Aranson I.S., Postnov D.E., Rabinovich M.I. Spatial Synchronization and Development Bifurcations in a Chain of Coupled Oscillators // Sov. Phys. Dokl. 1986. Vol. 31, № 2. P. 169.

9. *Анищенко В.С., Сафонова М.А.* Индуцированное шумом экспоненциальное разбегание фазовых траекторий в окрестности регулярных аттракторов // Письма ЖТФ. 1986. Том 12, № 12. С. 740.

Anishchenko V.S., Safonova M.A. Noise-Induced Exponential Dispersal of Phase Trajectories in the Neighborhood of Regular Attractors // Sov. Tech. Phys. Lett. 1986. Vol. 12, № 6. P. 305.

10. *Anishchenko V.S., Herzel H.* Noise-induced Chaos in a System with Homoclinic Points // ZAMM. 1988. Vol. 68, № 7. P. 317.

11. *Анищенко В.С.* Разрушение квазипериодических колебаний и хаос в диссипативных системах // ЖТФ. 1986. Том 56, № 2. С. 225.

Anishchenko V.S. Destruction of Quasi-periodic Oscillations and Chaos in Dissipative Systems // Sov. Phys. Tech. Phys. 1986. Vol. 31, № 2. P. 137.

12. *Анищенко В.С., Вадивасова Т.Е., Постнов Д.Э., Сафонова М.А.* Вынужденная и взаимная синхронизация хаоса // Радиотехника и электроника. 1991. Том 36, № 2. С. 338-351.

Anishchenko V.S., Vadivasova T.E., Postnov D.E., Safonova M.A. Forced and Mutual Synchronization of Chaos // Radiotekhnika i Elektronika. 1991. Vol. 36, № 2. P. 338 (in Russian).

13. *Anishchenko V.S., Vadivasova T.E., Postnov D.E., Safonova M.A.* Synchronization of chaos // Int. J. Bifurcation and Chaos. 1992. Vol. 2, № 3. P. 633.

14. *Anishchenko V.S., Safonova M.A., Chua L.O.* Stochastic resonance in Chua's circuit // Int. J. Bifurcation and Chaos. 1992. Vol. 2, № 2. P. 397.

15. *Anishchenko V.S., Neiman A.B., Safonova M.A.* Stochastic Resonance in Chaotic Systems // J. Stat. Phys. 1993. Vol. 70, № 1/2. P. 183.

16. *Анищенко В.С., Нейман А.Б., Мосс Ф., Шиманский-Гайер Л.* Стохастический резонанс как индуцированный шумом эффект увеличения степени порядка // УФН. 1999. Том 169, № 1. С. 7.

Anishchenko V.S., Neiman A.B., Moss F., Schimansky-Geier L. Stochastic Resonance: Noise Enhanced Order // Physics - Uspekhi. 1999. Vol. 42, № 1. P. 7.

17. *Shulgin B., Neiman A., Anishchenko V.* Mean Switching Frequency Locking in Stochastic Bistable Systems Driven by Periodic Force // Phys. Rev. Lett. 1995. Vol. 75. P. 4157.

18. *Anishchenko V.S., Silchenko A.N., Khovanov I.A.* Synchronization of switchings processes in coupled Lorenz systems // Phys. Rev. E. 1998. Vol. 57, № 1. P. 316.

19. *Anishchenko V.S., Janson N.B., Balanov A.G., Igosheva N.B., Bordyugov G.V.* Synchronization of cardiorhythms by weak external forcing // *Discrete Dynamics in Nature and Society*. Special issue on synchronization (ed. by Prof. V. Anishchenko). 2000. Vol. 4. P. 201.

20. *Anishchenko V.S., Janson N.B., Balanov A.G., Igosheva N.B., Bordyugov G.V.* Entrainment between Heart Rate and Weak External Forcing // *Int. J. of Bifurcation and Chaos*. Special issue on phase synchronization (ed. by Prof. J. Kurths). 2000. Vol. 10(10). P. 2339.

21. *Anishchenko V.S., Vadivasova T.E., Kopeikin A.S., Kurths J., and Strelkova G.I.* Effect of noise on the relaxation to an invariant probability measure of nonhyperbolic chaotic attractors // *Phys. Rev. Lett.* 2001. Vol. 87. 054101.

22. *Anishchenko V.S., Vadivasova T.E., Kopeikin A.S., Kurths J., and Strelkova G.* Peculiarities of the relaxation to an invariant probability measure of nonhyperbolic chaotic attractors in the presence of noise // *Phys. Rev. E.* 2002. Vol. 65(3). 036206.

23. *Anishchenko V.S., Vadivasova T.E., Okrokvertskhov G.A., Strelkova G.I.* Correlation Analysis of Dynamical Chaos // *Physica A.* 2003. Vol. 325. P. 199.

Зав. редакцией *Н.Н. Левина*
Редакторы *Л.А. Сидорова, Н.Н. Левина*
Обложка художника *Д.В. Соколова*
Оригинал-макет подготовлен *Г.А. Суминой, О.Н. Афанасьевой*
на компьютерной системе Apple Macintosh

Подписка на I полугодие 2004 года
по каталогу «Газеты и журналы», индекс 73498,
стоимость подписки на I полугодие 150 руб.

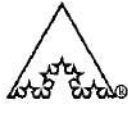
Распространение журнала по подписке и предварительным заявкам
осуществляется Государственным учебно-научным центром «Колледж»
при Саратовском государственном университете. ИНН 6452006136
Банковские реквизиты
р/с № 40603810900000000378 в ЗАО «Экономбанк» г. Саратова,
БИК 046311722, кор.счет банка 30101810100000000722

Правила подписки за рубежом на сайте: <http://www.periodicals.ru>

Сдано в набор 15.09.03. Подписано к печати 21.12.03. Формат 70x108/16
Бумага «Снегурочка». Печать трафаретная. Гарнитура Латинская
Усл. печ. л. 18,90(13,5). Уч.-изд. л. 16,70. Тираж 200. Заказ 322

Издательство ГосУНЦ «Колледж». Лицензия ЛР №020773 от 15.05.98
410012, Саратов, ул. Астраханская, 83
Тел. (845-2)523864, факс (845-2) 523864
E-mail: and@cas.ssu.runnet.ru
<http://cas.ssu.runnet.ru>

Отпечатано на ризографе GR 3750 издательства ГосУНЦ «Колледж»

© Издательство ГосУНЦ «Колледж» 
© Оформление художника Д.В. Соколова, 2003

EDITOR-IN-CHIEF

Yu.V. Gulyaev, Member of the Russian Academy of Sciences, Institute of Radioengineering and Electronics of RAS, Moscow

EDITORS

D.I. Trubetskov, Corresponding Member of the Russian Academy of Sciences, Saratov University

D.A. Usanov, Member of the International Academy of Sciences of High School, Saratov University

SECRETARY-IN-CHIEF

B.P. Bezruchko, Professor, Institute of Radioengineering and Electronics of RAS, Saratov University

EDITORIAL BOARD

V.S. Anishchenko, Professor, Saratov University

Yu.A. Danilov, Professor, Kurchatov Scientific Centre, Moscow

A.S. Dmitriev, Professor, Institute of Radioengineering and Electronics of RAS, Moscow

S.P. Kuznetsov, Professor, Institute of Radioengineering and Electronics of RAS, Saratov

P.S. Landa, Professor, Moscow University

G.G. Malinetski, Professor, Institute of Applied Mathematics of RAS, Moscow

O.V. Rudenko, Professor, Moscow University

Yu.M. Romanovsky, Professor, Moscow University

E.E. Son, Professor, Institute of Physics and Technical Dolgoprudny

V.D. Shalfeev, Corresponding Member of the Russian Academy of Engineer Sciences, Nizhny Novgorod University

V.V. Tuchin, Professor, Saratov University

V.K. Yulpatov, PhD, Institute of Applied Physics of RAS, Nizhny Novgorod

V.G. Yakhno, Professor, Institute of Applied Physics of RAS, Nizhny Novgorod